Flow, Combustion and Emissions in a Four-Valve Spark-Ignition Engine Fuelled by Compressed Natural Gas

Jongwoo Kim
B.Sc., M.Sc.

Department of Mechanical Engineering
Imperial College of Science, Technology and Medicine
University of London

Thesis submitted for the degree of Doctor of Philosophy in the University of London and for the Diploma of Membership of the Imperial College

May, 2000

ABSTRACT

Natural gas has been considered as one of the most promising alternative engine fuels for its cleanness and abundance. However, its combustion and emissions behaviour is quite different from conventional liquid fuels such as gasoline and diesel. Thus, the objective of this work was to investigate the flow and combustion characteristics as well as ways to reduce the exhaust emissions of a purpose-built, spark-ignition engine fuelled with compressed natural gas (CNG) and equipped with a four-valve cylinder head and optical access through an extended piston and windows in the liner.

The first part of the thesis presents research focussing on ways to improve the lean operating stability of a single-cylinder port injected CNG engine through use of sleeved ports to enhance the mean flow and turbulence during compression and open-valve injection to enhance the charge motion and achieve mixture stratification at the time of ignition. Results of the flow distribution obtained by means of laser Doppler and particle image velocimetry have been complemented by combustion and emission analysis. Furthermore, a baseline comparison was performed between gasoline and CNG fuels to allow conclusion to be drawn about their combustion characteristics and relative engine performance.

The second part of the thesis presents a new approach centred on direct-injection of CNG in a multi-cylinder spark ignition engine and its advantages in terms of combustion, emissions and performance relative to manifold injection engines. This study was complemented by CNG jet imaging in a constant-volume chamber using Schlierern photography for investigating the jet characteristics such as cone angle and tip penetration. Baseline testing was performed using manifold injection of CNG, by obtaining images of the propagating flame and simultaneous measurement of the in-cylinder pressure to investigate combustion characteristics and engine performance. The effect of charge stratification was examined by means of a sampling probe incorporated into the spark plug for measuring the hydrocarbon levels in the spark gap

at the time of ignition.

The results revealed that direct injection of CNG increases the volumetric efficiency of the engine and allows enhanced in-cylinder flow motion and charge stratification at the time of ignition which results in faster flame propagation and reduced cycle-to-cycle variations, thus approaching the combustion performance of gasoline-fuelled engines while offering potential for reduced NO emissions as a result of extending the engine's lean operation limit.

ACKNOWLEDGEMENTS

I would like to express my sincere gratitude to my PhD. supervisor Prof. C.Arcoumanis for his guidance and encouragement throughout the work of this thesis.

Thanks are due to many colleagues in the Internal Combustion Engines Group for their advice and assistance; especially, the help and assistance of Dr. Simon Godwin during this project is deeply appreciated. I would also like to thank Dr. H. Xu, Dr. S. Cho, Mr. Y. Choi, Dr. S. Whitelaw, Dr. H. Lee and Mr. J. Uhm for their assistance and discussions throughout the project. Further, the technical assistance of Harminda Flora and John Laker is most appreciated.

I would also like to extend my appreciation to the Daewoo Motor Company and Perkins Technology for their financial support and research project. I am grateful to Cambustion Ltd., particularly Dr. Mark Peckham, for technical support concerning the in-cylinder sampling equipment. Thanks are also due to Oxford Lasers Ltd for the PIV equipment and advice on its use.

Finally, I wish to express my gratitude to my parents and my wife for their unconditional and unwavering support and encouragement during the course of this work.

Table of Contents

List of Tables

List of Figures

List of Symbols

Greek symbols

ϕ	Equivalence ratio
η_v	Volumetric Efficiency
λ	Air-fuel ratio
ρ	Density
γ	Specific heat ratio

Roman symbols

n	Engine speed
P_i	Intake manifold pressure
P_{max}	Peak pressure in combustion chamber
T	Temperature
V_t	Tumble velocity
V_p	Mean piston speed
V_d	Displacement volume
V_c	Clearance volume

Abbreviations

A/D	Analogue to digital converter
A/F	Air-fuel ratio
aTDC	After TDC
BDC	Bottom-dead centre
BMEP	Brake mean effective pressure
bTDC	Before TDC
CA	Crank angle
CARB	California Air Resources Board
CCD	Charge coupled device (camera)
CNG	Compressed natural gas

CO	Carbon monoxide
CoV	Coefficient of variation
Cr	Compression ratio
FID	Flame ionisation detector
GDI	Gasoline direct injection
HC	Hydrocarbon
IMEP	Indicated mean effective pressure
LDV	Laser Doppler velocimetry / anemometry
LIF	Laser-induced fluorescence
MBT	Maximum brake torque
NGV	Natural Gas Vehicle
NMHC	Non-methane hydrocarbons
NMOG	Non-methane organic gases
NO	Nitrogen oxide
NO_X	Oxides of nitrogen
PIV	Particle image velocimetry
PM	Photomultiplier
ppm	Parts per million by volume
PTV	Particle tracking velocimetry
RAF	Reactivity Adjustment factor
rms	Root mean square
rpm	Revolutions per minute
SI	Spark-ignition
SNR	Signal-to-noise ratio
TDC	Top dead centre
THC	Total hydrocarbons
UHC	Unburned hydrocarbons
ULEV	Ultra low emissions vehicle
WOT	Wide open throttle

CHAPTER 1

INTRODUCTION AND LITERATURE SURVEY

1.1 Introduction

In view of the stringent Californian emission standards and the European Stage III and IV legislation for 2000 and 2005, spark-ignition engine manufacturers are intensively exploring various ways of meeting these ultra-low emission targets. Their main approach is to combine precise control of the air/fuel ratio with advanced after-treatment systems but some efforts are also devoted to modify existing engines or design new ones capable of achieving optimum performance when fuelled with alternative fuels including renewables. In addition, for increasing the fuel economy and reducing the CO_2 emissions responsible partly for the greenhouse effect, automotive engine manufacturers have been developing lean burn engines. More recently, several companies have produced gasoline direct injection (GDI) engines (Iwamoto *et.al.*, 1997; Harada *et.al.*,1997; Takaki *et.al.*, 1990) which are, in principle, capable of reducing CO_2 emissions by about 20% compared to port-injected engines through improvements in fuel consumption. However, there are still problems with the after treatment of HC and NOx emissions under lean operating conditions which are expected to be eventually solved using a combination of very low sulfur fuel and high-efficiency NOx traps.

Some of the advantages of CNG relative to other alternative fuels include its low cost, better knocking resistance, wide flammable air-fuel ratios, and significantly lower non-methane hydrocarbon (NMHC) emissions (Leming *et.al.*, 1985; Kim *et.al.*,1994). On the negative side, CNG has slow burning, lower power output and limited driving range due to its reduced calorific value.

A convenient way to improve the fuel economy and reduce the exhaust emissions of

CNG-fuelled vehicles is to operate the engine with lean air/fuel mixtures. Unfortunately, these are associated with increased cycle-to-cycle variations and hydrocarbon emissions as well as reduced flame initiation and propagation rates. The most practical approach for improving engine stability under lean mixture conditions is to shorten combustion duration through enhanced in-cylinder mean flow and turbulence combined with stratification of the local mixture near the spark plug at the time of ignition. There are a number of possible ways for enhancing the turbulence intensity in the cylinder of a reciprocating engine; the most common method is using 4-valve cylinder heads with directed ports that generate tumble in the pentroof-type combustion chamber during the induction and compression strokes (Arcoumanis *et.al.*,1990; Floch *et.al.*,1995). Alternatively, squish-induced combustion chambers can be used that are capable of enhancing turbulence near TDC of compression (Evans *et.al.*,1997). In previous work conducted in the same engine (Bae, 1993; Arcoumanis *et.al.*,1994; Arcoumanis *et.al.*,1998) flow measurements were obtained using laser Doppler velocimetry to characterise the bulk and turbulent flow generated by different intake port geometries incorporating sleeves in the intake ports, which deflect the inducted air over the intake valves, thus producing a stronger tumbling vortex in the cylinder relative to that generated by conventional non-sleeved ports.

In a production conventional port-injected spark-ignition engine, the fuel is injected towards the back of the closed intake valves. This occurs well before the valves open, so that a significant fraction of the fuel vaporises under warm engine conditions before entering the cylinder, to allow a nearly gaseous fuel to mix with air and burn more efficiently than if it was in liquid form. Since CNG is a gas at room temperature, it is possible to inject it through the open intake valves without having to consider the time required for droplet vaporisation. This mode of fuel injection can induce some degree of charge stratification in the vicinity of the spark plug at the time of ignition that allows stable operation under lean overall mixture conditions.

The rate of combustion in SI engines is strongly influenced by turbulence and charge motion; for example Arcoumanis *et.al.*,1990. Because of the much lower density of natural gas compared to gasoline, the flow through a gas injector can attain the speed of sound at the nozzle ever at moderate injection pressures. In gas direct injection type of

combustion, it is the diffusion process of the fuel that greatly influences the in-cylinder motion and mixture distribution.

The aim of the research programme presented in this thesis is to investigate the performance of 4-valve spark ignition engines fuelled by CNG in a port injection and direct injection configuration under lean mixture conditions. The first part of the investigation focuses the lean operating stability of a port injection CNG engine and on ways to improve it through the use of sleeved ports to enhance the mean flow and turbulence during compression, and an open-valve injection strategy to enhance charge motion and its stratification at the time of ignition. Results obtained with laser Doppler and particle image velocimetry were complemented by combustion and exhaust emission analysis. The second part of the investigation presents the concept of direct-injection of CNG as means for improving combustion, emissions and performance relative to manifold injection engines. This work has concentrated on a four-cylinder optical spark-ignition engine, with emphasis placed on evaluating the benefits of direct injection against the baseline arrangement where the CNG/air mixture is prepared in the intake manifold. The gas direct-injector was tested first in a constant volume chamber with various ambient and injection pressures and subsequently installed in one of the four cylinders. Measurements of engine performance with manifold and direct injection of CNG were obtained in terms of pressure analysis, flame propagation, fuel concentration at the spark plug around the time of ignition using a direct sampling probe, and exhaust emissions.

1.2 Thesis outline

The thesis consists of five chapters. Chapter 1 comprises an introduction and literature survey that summarises of previous research in CNG engines and provides some calculations quantifying the difference in performance between CNG and gasoline engines. Also included are sections on lean burn technology in port-injected and direct injection engines. The findings of past research are presented in a tabular format indicating paper authors and year, experimental apparatus and techniques used, with the final column outlining the most important conclusions.

In Chapter 2 the experimental systems and measurement techniques are described. Experimental techniques applied in this study include laser Doppler velocimetry and particle image velocimetry, which was used for the in-cylinder flow measurements, techniques for combustion analysis based on in-cylinder pressure measurements and flame visualisation using a CCD camera. For measuring the fuel concentration near the spark plug, a sampling probe incorporated into the spark plug was used. Emission analysis was performed using a flame ionization detector and a NO chemiluminescent analyser in the exhaust manifold. For investigating the injection and jet characteristics of high-pressure fuel injection systems appropriate for use in direct-injection CNG engines, Schlieren photography was used.

Chapter 3 presents results obtained in a single cylinder port injected CNG engine. Section 3.1 is an introduction. Section 3.2 describes the test engine and experimental arrangements. Section 3.3 presents the baseline comparison between gasoline and CNG through analysis of cold start characteristics, combustion characteristics and exhaust emission measurements. The effect of altering the intake port geometry is described in section 3.4. Section 3.5 describes the effect of altering injection timing. In-cylinder pressure analysis was performed. For investigation of charge stratification using an open valve injection, fuel concentration measurement was performed at the spark plug. For visualisation, flame-imaging analysis was also performed. Section 3.6 describes the effect of increasing the compression ratio from 9.0 to 11.5 to improve the engine performance by taking advantage of the high octane number of natural gas.

Chapter 4 describes results obtained in a modified multi-cylinder spark-ignition engine to allow direct-injection of CNG into the cylinder through high-pressure injectors. Comparison is made between homogenous mixture and direct injection towards the spark plug to induce charge stratification.

Finally, Chapter 5 summarises the most important findings of this research and suggests further experiments which can provide additional insight into the CNG engine development under lean mixture conditions.

1.3 Literature survey

1.3.1 Characteristics of CNG

Natural gas is generally composed of 85-95% of methane, thus the combustion characteristics of natural gas are similar to those of methane. The fuel properties are summarised in Table 1.1.

Table 1.1: Comparison of fuel properties (Goto *et. al*, 1996)

	Methane	**Gasoline**	**Light diesel**
Formula and (phase)	CH_4 (gas)	$C_nH_{1.87n}$ (liquid)	$C_nH_{1.8n}$ (liquid)
Density ratio with air	0.56	3.3	3.78
Octane number	120	92~98	------
Stoichiometric air/fuel ratio	17.2	14.7	14.5
Auto-ignition temperature (°C)	537	~257	
Lower heating value (MJ/kg)	50	44	43.2
Laminar flame speed (cm/s)	33.8	~38	

The basic characteristics of methane are its lower density compared to air, its higher octane number, a wider range of flammability, higher auto-ignition temperature and lower laminar flame speed. Due to its characteristics of much higher auto-ignition temperature and lower flame speed, the influence of CNG on the initial state of flame propagation and on the entire combustion process is more significant than other hydrocarbon fuels (Goto et al., 1996). The mixture formation process of natural gas is very different from liquid fuels such as gasoline due to its lower density compared to air.

1.3.2 Performance of CNG engines

Yamamoto *et. al.* (1994) have performed comprehensive experiments to identify the power characteristics of CNG engines. They have explained the power difference between CNG and gasoline using four different reasons that include the effect of

volumetric efficiency, the effect of heat of combustion, the increase of the molecular mass after combustion and the effect of the specific heat ratio. Each cause of power reduction for the case of CNG-fuelled engines is described in detail below.

Effect of volumetric efficiency -The most likely cause of the lower power output of CNG engines is the reduction in volumetric efficiency(η_v). Compared to gasoline which is supplied to the engine's combustion chamber in liquid form, in the case of the CNG the fuel injection system injects gas accounting for 10% of the intake air volume, thus reducing the proportional amount of inducted air into the cylinder. In addition, the volumetric efficiency can drastically change when the pressure in the intake manifold is varied by forcing gas into the cylinder.

Effect of heat of combustion- CNG has a higher heat of combustion per unit weight than gasoline. However, when considering them as a mixture introduced into the engine, the gasoline/air mixture has a higher overall heat of combustion. In this respect, the CNG/air mixture is inferior to its gasoline counterpart by approximately 10.5%; Table 1.2 summarises the comparison of calorific values between CNG (based on 100% methane) and gasoline.

Table 1.2: Comparison of calorific values between CNG and gasoline (Yamamoto *et. al.*, 1994)

Fuel	CNG (Methane)	Gasoline	CNG/Gasoline Ratio
Stoichiometric Air/Fuel ratio	17.2 :1	14.7 :1	---------
Mixture weight (g/l)	1.24	1.37	---------
Calorific value of unit weight of fuel (MJ/kg)	50	44	+ 13.6%
Calorific value of unit weight of mixture (MJ/kg)	(50/18.2) 2.74	(44/15.7) 2.80	- 2.1 %
Calorific value of unit volume of mixture (MJ/l)	(2.74x1.24/ 1000) 0.0034	(2.80x1.37/ 1000) 0.0038	- 10.5 %

The actual difference in the heat of combustion between CNG and gasoline/air mixtures is expected to be smaller since CNG contains certain amounts of ethane, propane and other hydrocarbon components.

Comparison of number of moles before and after combustion - Another cause of power reduction may be the increased number of moles due to combustion. In particular, 1 mole of CNG (methane) requires 2 mole of O_2 to burn, and in this process 8 moles of N_2 contained in the air are taken into the combustion chamber. As a result of combustion, 1 mole of CO_2 and 2 moles of H_2O are formed. Assuming that NO_x formation can be ignored because the amount is small when compared to that of CO_2, 8 moles of N_2 thus remain inactive. As a result, there are 11 moles of reactants and 11 moles of products before and after combustion which implies no change in the number of moles due to combustion.

Assuming that the typical gasoline molecule is paraffin (C_7H_{16}) whose molecular number equals 100 for ease of calculation, 11 moles of O_2 are required to burn 1 mole of gasoline and in this process, 44 moles of N_2 are taken into the combustion chamber. 7 moles of CO_2 and 8 moles of H_2O are formed during combustion, whereas 44 moles of N_2 remain unchanged. The molecular mass increases from 56 moles before combustion to 59 moles after combustion, which corresponds to an increase of 5 %. Based on the reaction occurring with the gasoline mixture, it can be argued that effects associated with the 5% molecular mass increase are absent from the CNG mixture.

Effect of specific heat ratio (κ) - Generally, the work (W) produced by adiabatic expansion due to combustion is defined by the equation given below;

$$W = \frac{P_0 V_0 (1 - \varepsilon^{-K})}{K} \quad (K = k - 1)$$

where,

P_o = Pressure at which adiabatic expansion begins to occur

V_o = Volume at which adiabatic expansion begins to occur

k = Specific heat ratio (Cp/Cv)
ε = Compression ratio

Assuming that specific heat ratios of $CNG_{(M)}$ (methane) and $gasoline_{(G)}$ are assumed to be

$k_M = 1.3$
$k_G = 1.1$

The compression ratio of the engine tested can be defined as 10.5 assuming that the p_o of both fuels is the same. Work in each case is then determined as follows;

$W_M = 1.69\ p_o v_o$
$W_G = 2.10\ p_o v_o$

Thus, for CNG the work resulting from combustion is approximately 19.5% less than that of gasoline in terms of the effect of the specific heat ratio.

To overcome all these causes of power reduction in the case of CNG, optimisation of the intake system, compression ratio and injection and ignition timings is therefore needed.

1.3.3 Combustion characteristics of CNG engines

Ignition timing characteristics- Since CNG (methane) exhibits relatively slow burning, the ignition timing for MBT should be advanced by several degrees compared to a gasoline engine. As a result of CNG's high octane rating, it is possible to set ignition timing at MBT at all engine speeds. On the other hand, gasoline engine's ignition timing must be retarded to avoid knocking, which implies that SI engines are incapable of generating the highest possible torque. Yamamoto *et. al.*(1994) have found that the effect of load variations on CNG ignition timing is rarely evident which means that CNG enables stable combustion even at small loads.

Study of combustion pressure-Yamamoto *at el.*(1994) measured the combustion pressure in both CNG and gasoline engines; Table 1.3 summarises their results. Under

the same engine condition, the maximum combustion pressure of CNG is much smaller than that of gasoline, which affects the power difference between the two. The 10 -90% burn duration confirms the slow combustion speed of CNG, however CNG has a shorter ignition delay than gasoline. Since CNG combustion pressure increases more slowly than gasoline, a high compression ratio and strong tumble are prerequisites for the development of efficient CNG engines.

Table 1.3: Comparison of combustion pressure and combustion periods (Yamamoto *et. al.*, 1994)

Fuel	CNG	Gasoline	CNG/gasoline
P max (kPa)	1098	1331	- 24%
P max standard deviation (kPa)	111.8	125.5	+11%
dP/dθ (kPa/deg)	26.5	50	-47%
Ignition Delay (deg.CA)	30.48	32.36	+5.8%
10-90% Combustion period (deg.CA)	28.98	23.61	-18.5%

Combustion stability- According to Yamamoto *et. al.* (1994), when the same engine was used, the lean limit for gasoline was λ =1.2, but was extended to λ = 1.6 for CNG. Thus, the lean limit of CNG is wider than that of conventional mass-production port fuelled lean burn engines (λ= 1.5). On the other hand, the rich limit was identified to correspond to an excess air ratio of 0.8.

1.3.4 Emission characteristics of CNG engines

According to the results of the gas chromatography analysis of THC emissions from CNG vehicles (Kim *et al.*, 1994), the methane represents 85.3%, the paraffinic group 14.5% and other miscellaneous components up to 0.2%. On the other hand, THC exhausted by a gasoline vehicle consists of 16.4% methane, 26.9% paraffins, 15.9% olefins and 40.8% aromatics. Thus, unlike gasoline vehicles, natural gas vehicles (NGV) emit neither aromatics nor olefins. Moreover, methane which constitutes most

of the emissions has a very low maximum incremental reactivity of 0.0148; the content of the paraffinic group is also fairly low at 0.25-1.04. In contrast, aromatics and olefins have a strong reactivity that is about 10 times higher than that of methane or of the paraffinic group. As a result, there is a large difference between THC emissions from NGVs and gasoline-fuelled vehicles and their effect on atmospheric pollution, i.e. ozone formation. Recently CARB (California Air Resources Board) has modified its NMOG (Non-Methane Organic Gas) emission regulation which considered in the past only the total amount of HC emissions regardless of their effect on the environment. New NMOG values are calculated by using a Reactivity Adjustment Factor (RAF) which is estimated for each hydrocarbon species based on its ability to form Ozone. CARB-set RAFs for phase 2 gasoline are 0.94 for LEV (Low Emission Vehicles) and ULEV (Ultra Low Emission Vehicles), whereas CARB proposed RAFs for NGVs for LEV and ULEV of 0.43; this low RAF value allows NGVs to meet tough California emission regulations more easily.

In term of the engine-out emissions, the emissions of HCs from natural gas fuelled engine are about 50% lower than those for gasoline at WOT and 65% at full-load condition (Evans *et. al.*, 1997). The NOx emissions are nearly the same for both fuels at WOT and close to stoichometric air/fuel ratios. The CO emissions from gasoline at WOT are double those for natural gas (Evans *et. al.*, 1997).

1.3.5 In-cylinder flow motion– *tumble*

Fluid motion within the cylinders of internal combustion engines is fundamentally affecting engine performance and emissions characteristics (Arcoumanis and Whitelaw; 1987, Heywood, 1987). Modern multi-valve spark ignition engines with four valves per cylinder exhibit favourable characteristics with regard to power output and exhaust emissions. This has been attributed to turbulence enhancement resulting from the breakdown of barrel or tumble motion which is generated during the induction stroke (Arcoumanis *et al,* 1990). As the piston approaches TDC, the large-scale tumble breaks down into smaller vortices or even nearly homogeneous small-scale turbulence due to severe vortex distortion and shear. The enhanced turbulent flow field promotes faster

burn rate, improved flame propagation and better cyclic variability even under the high dilution conditions required for emissions control.

While turbulence enhancement is required for rapid and repeatable combustion of the charge, high tumble ratios also lead to strong bulk flows which, depending on the combustion chamber geometry, can persist until well after the time of ignition (Kuwahara *et al,* 1990; Hu, 1992). An excessive bulk flow may adversely affect initiation of the flame kernel by convecting it away from the spark plug and towards a combustion chamber surface. Additional excessive turbulence intensities may lead to flame quenching due to high local strain rates (Bradley *et al,* 1988). In the design of improved combustion systems it is therefore important to understand the evolution of the large scale in-cylinder flow structures, the phasing of their breakdown and how these processes are affected by the engine geometry, so that a suitable degree of turbulence enhancement can be achieved with minimal adverse effects on flame initiation and early flame growth.

To characterise the evolution of tumble, advanced velocimetry techniques are increasingly applied to the study and development of improved internal combustion engines. Tumble evolution in motored and fired engines has been studied using hot wire anemometry (Benjamin, 1988) and laser Doppler velocimetry (Arcoumanis *et. al,* 1994; Hadded and Denbratt; 1991), and these techniques have provided much useful velocity and turbulence data at selected points within the flow field. However, since the velocity field is rather complex, unsteady and exhibits cyclic variations, whole field measurements are also required for full characterization of the in-cylinder flow. Hence whole field techniques such as particle tracking velocimetry (PTV) (Ronnback *et. al,* 1991; Kiyota *et. al,* 1992) and particle image velocimetry (PIV) (Pickering and Halliwell, 1985) are finding increasing application to the study of in-cylinder flows. These closely related techniques which are capable of providing instantaneous characterization of unsteady velocity fields are reviewed by Adrian (1991). Reeves *et. al.* (1995) used auto correlation PIV in a vertical plane to analyse the formation and breakdown of tumble in a transparent 4-valve engine with production geometry. It was found that the stable tumble in existence at BDC begins to break down into smaller vortices at about 260° aTDC. This breakdown process continues during the latter stages

of compression, but a significant mean flow seem to persist up to the ignition point, at approximately 20° bTDC. Marc *et. al.* (1997) used both PIV and LDV to characterise tumble and its breakdown into turbulence near TDC in a square-piston model engine. They found that small cyclic variations in the position of the tumble vortex produced high levels of ensemble-averaged velocity fluctuations. Church and Farrell (1998) employed PTV in a single-cylinder 2-valve symmetric engine to study the effect of intake ports of differing angle on in-cylinder tumble and its development during compression. It was found that the intake port with an approach angle of about 20° to the horizontal produced the strongest tumble, and that stronger tumble also persisted longer into the compression stroke before its breakdown into turbulence.

1.3.6 Overview of lean burn engines

Lean combustion in a SI engine has been recognised as one of the most promising methods for achieving further improvements in fuel economy. There have been, however, practical difficulties in extending the lean misfire limit low enough to realise NO_x emission levels below the mandatory level and still keep satisfactory combustion stability (Matsushita *et al.*, 1985a). Lean burn can be obtained by the homogeneous charge approach in which care is taken to distribute fuel consistently and evenly throughout the combustion chamber, while the turbulence of the charge is enhanced to counteract the slower burning rate of a lean mixture. Such an approach is unlikely to achieve flammable mixtures that are significantly leaner than 25:1 air-fuel ratios (Inoue *et. al.*, 1993). The alternative approach is to supply a stratified charge in which the mixture around the spark plug is kept close to stoichiometric, while the mixture elsewhere in the cylinder is considerably leaner. This has opened the possibility of achieving mixtures with overall air-fuel ratios of 40:1 or leaner (Ando *et. al.*, 1996) and it is now a more favoured approach than homogeneous charge lean burn. This section reviews the current state of knowledge concerning lean burn engines with conventional port fuel injection and emerging direct injection engines. These reviews provide useful background information for developing CNG lean burn engines and overcoming the refuelling problem in natural gas fuelled vehicles.

Lean burn with homogeneous mixtures

The lean flammability limit in an engine is defined in terms of an upper allowable limit on CoV of IMEP, around which burn duration and partial-burn cycles or misfires affect engine stability greatly. In order to reduce the coefficient of variation of indicated mean effective pressure (CoV of IMEP) in this region the flame speed should be increased, and in many studies this has been achieved by optimising the in-cylinder charge motion using swirl and tumble. Matsushita *et. al.* (1985) identified a misfire limit at an air-fuel ratio of 23 using a swirl control valve to increase turbulence. Arcoumanis *et. al.* (1994a) and Jeon *et. al.* (1998) measured increased stability of combustion with lean mixtures when converting from standard to a high tumble configuration in a four-valve engine. Often, increasing turbulence by enhancement of tumble or swirl requires an alteration to the intake geometry that reduces volumetric efficiency and, therefore, engine power at full load operation. On the other hand, in contrast to these methods, it has been found (for example see Le Coz, 1992) that for mixtures close to the lean limit, the stability of combustion is controlled by cyclic variations of the large-scale flow field. Thus any the variation in the charge motion needs to be reduced, which implies reducing the ensemble-averaged turbulence levels and creating more repeatable early flame convection.

A further method of improving combustion with a lean mixture is to modify the spark ignition system. It is well documented that an increase in spark energy results in significant improvement in early flame propagation, therefore contributing to enhanced combustion stability (Arcoumanis *et. al.*, 1993; Hacohen *et. al.*, 1995). An extension of this principle is to implement multiple spark sources or multiple sparking of the same source (Czekala *et. al.*, 1998), the advantage of which is two-fold. By increasing the number of ignition sites or ignition events, the likelihood of misfire is reduced, allowing for a leaner overall mixture. In addition, the overall burn duration is much reduced, reducing the cyclic variability. Such multi-spark systems have been introduced into production engines (for example Alfa Romeo's twin-spark engine), but have been limited to either two spark plugs per cylinder, or 2-3 electrodes per spark plug (Durbin & Tsai, 1983).

Lean burn with charge stratification

Charge stratification in port fuelling lean burn engines-To develop a lean burn system, a large extension of the lean limit is required so that sufficient NO_x reduction can be realised by lowering the combustion temperature. In general, the following two strategies are adopted at the same time for achieving sufficient extension of the lean limit:

- Enhancement of turbulence,
- Charge stratification around the spark plug

There are two different concepts to achieve charge stratification. The first is axial stratification and the second is barrel stratification. In axial stratification, swirl is used to enhance combustion. Fuel is introduced into the cylinder during the latter half of the intake stroke when the piston is near BDC and the rich mixture is concentrated in the upper region of the cylinder. Because the vertical velocity component is relatively small in a flow field controlled by swirl, vertically stratified charge layers can be maintained until the end of the compression stroke. Using a helical port and swirl control valve, Toyota increased their lean limit of the engine to an A/F ratio of 23 under part load conditions (Matsushita *et al.*, 1985b). Because of the shape of the swirl port, there is reduced volumetric efficiency at full load conditions. In barrel stratification, stratification of the charge is realised in the direction of the axis of the barrel-shaped tumbling vortex. This method has the following advantages over axial stratification (Kuwahara *et. al.*, 1994):

- Since it utilises the tumble generated by straight intake ports, it does not penalise full load performance
- Since it realises charge stratification using the inherent characteristics of four valve engines, no additional devices are required
- Stable charge stratification is realised over a wide range of engine operating conditions even with a pentroof-type combustion chamber which is not suitable to conserve the axially stratified layers

Kuwahara *et al.*(1994) introduced the three-layer barrel stratification. Using the two vertical partitions provided inside an intake port and a tumble control piston having a curved-top surface, they were able to extend the lean limit to an A/F ratio of 23.

Charge stratification in direct injection lean burn engines-The gasoline direct-injection engine (Harada et al., 1997; Iwamoto et al., 1997) is widely considered at present as the most promising concept for improving the fuel consumption and reducing the exhaust emission levels of next generation spark-ignition engines. At present, only Mitsubishi, Toyota and Nissan had the courage of introducing their first production GDI engines in their internal markets in Japan, but it is well known that all major automotive manufacturers are presently pursing intensive research in various versions of GDI engines which share certain common features such as swirl or reverse tumble generating intake ports, a piston-bowl cavity and a high pressure fuel injection system. In this section, the newly adopted technologies for charge stratification in GDI engines are presented.

In order to achieve the necessary combustion characteristics, the Mitsubishi GDI engine (Iwamoto *et al.*, 1997) employs a combination of a high pressure swirl injector, reverse tumble intake port , spherical piston cavity and three different air / fuel mixture preparation strategies. In the idle and partial load operating condition, a late injection strategy during the final stages of the compression stroke is applied so as to obtain stratified mixing; in this case, the air /fuel ratio is controlled within the range from 30 - 40. For medium loads early injection during the intake stroke is employed and the engine is operated under homogenous lean conditions with an air/fuel ratio between 20 and 25 so as to obtain the best economy. For higher load operating condition, fuel is also injected during the early stage of intake stroke but the mixture is either stoichiometric or slightly rich at full load in order to reduce exhaust temperatures and protect the three-way catalyst.

The above novel mixture formation concept has been used for inducing charge stratification in the Mitsubishi GDI engine (Iwamoto *et. al.*, 1997). Instead of the narrow spacing layout, used in earlier attempts of direct-injection gasoline engines, it adopts the wide spacing approach where the fuel spray is not directed towards the spark

plug but towards the piston surface where it impinges on a spherical piston cavity before being reflected towards the spark plug. By adopting this layout, the interval between the end of injection and spark ignition is long enough for promoting fuel vaporisation and adequate mixing with the surrounding air. The principal factor controlling mixing is the fuel spray or the gaseous mixture reflected on the cavity wall which depends on the fuel spray momentum. To realise adequate mixing control by the wide spacing layout, the following technologies are employed;

- Upright straight intake ports generating an intense reverse tumble
- A spherical compact piston cavity
- A high pressure swirl injector

At higher loads, the direct injection engine (Iwamoto *et. al.*, 1997) is operated by adopting the early injection strategy. In the case of conventional multi point injection (MPI) engines, the latent heat of evaporation is supplied from the surface of the intake port, intake valve or the cylinder liner. However, in the case of early direct injection, the fuel spray follows the piston, and the impingement of the liquid fuel on the surface is carefully minimised. Therefore, the latent heat is supplied by the intake air which causes efficient charge air-cooling. When proper injection timing is selected, volumetric efficiency can be increased by 5%. It can be estimated that the charge air is cooled by about 15K which the gas temperature at the end of the compression stroke is reduced by about 30K and knocking is thus suppressed (Iwamoto *et. al.*, 1997). Because of this anti-knock characteristic, GDI engines can increase their compression ratio above that of MPI engines. Throughout the engine speed range, torque can be higher than conventional MPI engines by about 10%. In the lower speed range, the primary beneficial factors are the increased volumetric efficiency and the transient spark-timing advance. In the higher speed range, the advantages include the increased volumetric efficiency, the higher compression ratio and the improved intake port flow coefficient.

Table 1.4: Summary of recent research studies

Characteristics of CNG engines

Author(s)	Experimental technique(s)	Main finding(s)
Fleming and O'Neal (1985)	• 2 valve single cylinder engine • In-cylinder pressure measurement • Engine-out emission measurement (HC, CO, NOx) • Aldehydes emission measurement using gas chromatography	♦ MBT ignition timing for natural gas was 2 to 6 degrees crank angle more advanced than that for gasoline depending on equivalence ratio ♦ Engine performance on natural gas fuel was increased from 8 to 15% depending on engine speed when compression ratio was increased from 8.4 to 15.5 ♦ At an equivalence ratio of 0.78 with natural gas as fuel, indicated thermal efficiency was increased from the baseline of 8.4 to 15.5 ♦ Total hydrocarbons and oxides of nitrogen were significantly increased when compression ratio was increased from the baseline of 8.4 to 15.5
Geiss, Burkmyre, and Lanigan (1992)	• Measurement of emission levels and engine torque, power and durability.	♦ Potential for emission levels to satisfy LEV and ULEV requirements. ♦ Power and torque reduced 13% and 11% respectively compared to gasoline version. ♦ Modified exhaust valve seat inserts and intake valve material used to counter problems of wear due to engine properties of CNG.
Jääskeläinen & Wallace (1993)	• Measurement of torque, fuel consumption and exhaust emissions in a four-cylinder CNG engine with comparison of compression ratio 10.1 and 11.5.	♦ Increase in compression ratio from 10.1 to 11.5 improves maximum torque by 3.2%. ♦ However, torque is still below gasoline engine by 10-12%. ♦ Total hydrocarbon emissions increased by 30-50% at higher compression ratio.

Author(s)	Experimental techniques	Main finding(s)
Kim et al.(1994)	• In-line 4 production engine • Measurement of CNG engine performance, in-cylinder pressure and heat release analysis • Measurement of engine-out emissions • Measurement of tail-out emissions through gas chromatography	♦ Lack of power when using CNG can be overcome by increased compression ratio, optimised spark and injection timing ♦ CNG has very low NMOG emission considering reactivity adjustment factor ♦ ULEV emission regulations can be met by using a CNG dedicated catalyst
Yamamoto et.al.(1994)	• In-line 4 production engine • Measurement of CNG engine performance • In-cylinder pressure and heat release analysis • Measurement of engine-out emission	♦ Although the engine power decreases with CNG, performance similar to a gasoline engine by optimising engine design ♦ CNG is superior to gasoline in term of its lean limit and combustion characteristics at low temperature
Anon (1995)	• Literature survey on three CNG vehicles in comparison to their gasoline equivalents.	♦ Emissions for CNG compared to gasoline: ♦ NMHC is 90% lower. ♦ Methane is 900% higher ♦ CO is 20-80% lower. ♦ NO_X is 0-80% lower. ♦ Reactivity weighted emissions is 80% lower. ♦ Fuel economy is 15-25% lower for CNG.
Lapetz, Beitler, Fulton, LeRoux, Locke, Peters, Roman, Walsh and Wolff (1995)	• Measurement of torque, power, in-cylinder pressure, emissions and catalyst efficiency in an eight-cylinder CNG engine.	♦ Compression ratio increased from 9:1 to 10:1. ♦ Torque and power reduced by 12% compared to gasoline engine. ♦ Certified ULEV vehicle with OEM warranty.

Author(s)	Experimental techniques	Main finding(s)
Goto et al.(1996)	• Single cylinder engine • In-cylinder pressure and heat release analysis • Engine-out emission analysis	♦ Non-uniform mixture states are maintained in the swirl main flow because of the low density of natural gas compared with that of air, or the relative rich mixture distribution in the swirl centre may be generated by the centrifugal force ♦ Combustion speed rises by the increase of the temperature in the cylinder and the combustion periods in higher compression ratio (Cr:11) is shorter than that in lower compression ratio (CR:9) engine ♦ THC increase rapidly by increasing air/fuel ratio because the ignition energy will not enough and misfire will take place in a large air/fuel ratio area
Matsuura, Otaka, Kato, Yamashiro & Fujii (1996)	• Measurement of performance and emissions of a CNG vehicle with increased compression ratio 12.5.	♦ Driveability similar to a gasoline engine was achieved. ♦ Range of 80% of gasoline vehicle was achieved. ♦ Potential to meet CARB's ULEV standard claimed. ♦ CO_2 emissions reduced by 23% compared to the gasoline engine.
Evans and Blaszczyk (1997)	• Comparison of performance and emissions for a single-cylinder test engine with gasoline and CNG.	♦ With CNG: ♦ BMEP reduced by 12%. ♦ 7-12% improved specific fuel consumption. ♦ HC emissions reduced by 50% at WOT, less at part load. ♦ NO_X emissions similar at WOT, reduced at lower load. ♦ CO emissions reduced by 50% at all loads. ♦ Burn duration slightly longer for CNG, except at leanest conditions and lowest loads.

Author(s)	Experimental techniques	Main finding(s)
Arcoumanis and Kim (1999)	• 4 valve port injection single cylinder optical engine • In-cylinder flow measurement by LDV and PIV • In-cylinder pressure, heat release analysis and flame imaging measurement • Measuring the local hydrocarbon levels at the time of ignition • Exhaust emission measurements (THC and NO_X)	♦ The combination of sleeved intake ports and open valve injection strategy increased the directional flow during early injection, generating a strong tumble flow during compression and higher mean velocities and turbulence levels near the spark plug at the time of ignition ♦ The enhanced tumble strength produced by the sleeved ports achieved strong convection of the flame away from the spark plug during the early flame development and faster flame propagation in the direction of the mean flow during the main combustion period. ♦ The use of sleeved intake ports with open valve fuel injection strategy led to improved by 12% combustion stability under lean mixture conditions (ϕ=0.76) due to the combination of favourable flow conditions and modest charge stratification near the spark plug at the time of ignition.

In-cylinder flow and combustion

Author(s)	Experimental techniques	Main finding(s)
Hu, Whitelaw and Vafidis (1992)	• Analysis of two intake port configurations in a single cylinder spark-ignition test engine: • Heat release analysis by measurement of in-cylinder pressure. • Flame propagation analysis by ion current measurement. • In-cylinder flow measurement by LDV.	♦ Good correlation was found between combustion duration and mean flame speed. ♦ Increased turbulence levels with high tumble configuration resulted in higher combustion rate, improving combustion stability and extension of the lean operating limit. ♦ Deflected intake ports producing higher tumble and turbulence reduced volumetric efficiency at WOT.
Kudou et al.(1992)	• 4 valve optical single cylinder engine • LLS(laser light sheet) for in-cylinder flow visualisation • Numerical simulation using KIVA code for analysis of tumble flow configuration	♦ LLS flow images well match with LDV results with a few error range ♦ Initial burn can be reduced without significant increase in main burn rate by enhancing of tumble intensity ♦ It is possible to improve the combustion stability by enhancing of tumble intensity without deterioration which are due to increasing in main burn velocity
Arcoumanis, Bae & Hu (1994a)	• LDV measurement of tumble in a steady flow rig and motored engine with a four-valve pentroof head comparing intake ports with and without sheet metal sleeves to deflect the intake flow. • LDV measurement of turbulence at the time of ignition in the motored engine.	♦ Tumble vortex ratios calculated for steady flow rig and for motored engine were found to be comparable. ♦ Turbulence levels were more than 60% higher than with a two-valve cylinder head. ♦ Sleeved intake ports increased combustion rates by 6% and allowed more stable operation with lean mixtures.

Author(s)	Experimental techniques	Main finding(s)
Kuwahara et al. (1994)	• 4 valve single cylinder engine w/ optical access and w/o optical access • In-cylinder flow observation by multi-colour laser sheet method • In-cylinder pressure analysis • Three dimensional modelling analysis with STAR-CD	♦ Enhancement of tumble is an effective way to maintain charge stratification during the compression stroke ♦ By promoting tumble distortion, eddies and turbulence are uniformly distributed in combustion chamber andsignificant lean-limit extension can be realised ♦ By providing the intake port partitions at the upstream and a tumble-control piston, charge stratification at the central layer in the combustion chamber can be realised
Arcoumanis & Bae (1995)	• Direct flame imaging and flame imaging using Mie scattering from a thin sheet of laser light, comparing intake ports with and without sheet metal sleeves to deflect the intake flow.	♦ Higher tumble produced by sleeved ports resulted in faster growth of the flame. ♦ Higher tumble also produced stronger convection of the early flame.
Reeves, Garner, Dent & Halliwell, (1995)	• Auto-correlation particle image velocimetry measurements of tumble and flow-field during compression in a single-cylinder four-valve optical engine.	♦ Tumble vortex begins to break down into smaller-scale structures after 260° aTDC. ♦ A mean bulk flow is still present at 338° aTDC, around the time of ignition.
Dai, Newman and Davies, (1996)	• Bulk flow modelling of the bulk tumble motion in a four-valve SI engine cylinder based on conservation of angular momentum. • Particle tracking velocimetry measurements of tumble in a steady flow apparatus.	♦ Qualitative validation of the tumble model. ♦ Effect of tumble on combustion rate is non-linear.

Author(s)	Experimental techniques	Main finding(s)
Meyer and Heywood (1997)	• Optical single cylinder engine • PDPA(Phase Doppler Particle Analyser) for measuring the velocity and size of liquid fuel droplets in the combustion chamber	♦ With closed valve injection, substantial wall wetting occurs in the cold intake port during start up and significant liquid fuel transport into the cylinder ♦ Due to fuel film build up in the intake port, the amount of liquid fuel entering the cylinder peaks after 15 seconds of engine operation following start ♦ After about 30 seconds of engine operation, under more warmed up conditions, substantial fuel evaporation occurs in the intake port and practically no liquid fuel enters the cylinder as droplets ♦ with open valve injection, less liquid fuel enters the cylinder at start up due to enhanced fuel atomisation through injection into the moving charge ♦ under warmed up condition, more liquid fuel than with closed valve injection is transformed into the cylinder as droplets due to injection onto the open valve
Arcoumanis, Godwin and Kim (1998)	• Single-cylinder 4-valve engine • LDV measurement in steady flow rig • Direct flame imaging and pressure analysis • Exhaust emission analysis	♦ In the steady flow rig test, sleeved intake ports increase by 80% the angular momentum of the tumbling charge compared to the non-sleeved ports ♦ In the single cylinder engine sleeved ports, that increase tumble intensity and enhance turbulence during combustion, have resulted in reduction of burn duration at part load condition ♦ With sleeved intake ports there is a consistent increase in IMEP of approximately 0.4 bar relative to the non-sleeved ports. At the same time there is a reduction in the coefficient of variation (CoV) of IMEP for the lean mixtures

Exhaust emissions

Author(s)	Experimental techniques	Main finding(s)
Jordan, Kaplan and Heywood (1991)	• Modeling the engine warm-up process to predict component temperature and hydrocarbon emissions	♦ The piston temperature increased most rapidly during the engine warm-up period ♦ Heat transfer through the piston rings to the cylinder liner was the major source of heat rejection ♦ Crevice region hydrocarbons have been shown to be a likely cause of a large fraction of cold start emissions.
Cheng et al.(1993)	• An overview of hydrocarbon emissions mechanisms in spark-ignition engine	♦ The various sources of HC in term of contribution in a warmed-up engine were: crevices about 38%, oil layers and deposits about 16% each, flame quenching about 5%, and in-cylinder liquid fuel effects about 20%, exhaust valve leakage less than 7% ♦ In an engine which had not yet warmed up, the amount of fuel escaping normal combustion was likely to be higher because the crevices and the oil layer were colder and much more liquid fuel entered the cylinder. The amount of oxidation that occurred after normal combustion ends was likely to be lower due to the lower wall and burned gas temperature.
Min, Cheng and Heywood (1994)	• Ricardo Hydra single cylinder engine • Fast FID was used for exhaust HC measurement	♦ The engine-out HCs were mostly sensitive to the piston top land crevice volume. A 10% change in the top land volume would produce a ~2% change in the engine-out HCs in the propane fuelled engine. ♦ The piston crevice outflow in the blown down process was trapped at the centre of the piston scrap-up vortex, and is therefore not likely to exit the cylinder

Lean burn engines

Author(s)	Experimental techniques	Main finding(s)
Matsushita et al.(1985)	• 2 valve single cylinder engine and 4-cylinder engine • Steady flow rig test • Engine performance measurement(Torque, BSFC and pressure analysis) • Flame image with high speed camera • In-cylinder flow velocity measurement with hot-wire anemometer	♦ The cylinder head with SCV achieved an improvement of combustion due to high swirl at partial load condition ♦ In the case of the helical port with SCV, the combustion duration reduced by 10% and lean limit and EGR tolerance were improved ♦ Under the SCV closed , rotating flow was produced in the cylinder and its axis was eccentric and rotated about cylinder axis
Horie, Nishizawa, Akazaki & Miura (1992)	• Measurement of performance and emissions in a Honda VTEC-E engine using valve deactivation and a compact combustion chamber.	♦ Axially stratified charge was realised by varying the swirl by valve deactivation and injecting fuel during the intake stroke. ♦ Stable combustion was achieved at an air fuel ratio of 22, with improved fuel consumption by 12% and reduction of NO_X emissions to meet USA standard.
Kiyota, Akishino & Ando (1992)	• Laser sheet analysis and flame imaging of combustion in a four-valve engine with charge stratification by injection through only one intake valve.	♦ Significant reduction in fuel consumption was achieved while maintaining combustion stability. ♦ Significant reduction in NO_X emissions was achieved by extending the lean operating limit of the engine.
Inoue, Matsushita, Nakanishi & Okano (1993)	• Measurement of performance and emissions in a four-valve per cylinder engine using homogeneous lean combustion controlled by a combustion pressure sensor.	♦ Lean limit control allowed continuous operation close to the lean limit. ♦ Reduction of 10% in fuel consumption and 30% in NO_X emissions was realised.

Author(s)	Experimental technique(s)	Main finding(s)
Shimotani et al.(1996)	• GDI 4 valve single cylinder engine • In-cylinder pressure measurement(IMEP, CoV of IMEP) • Fuel consumption measurement(BSFC) • Engine-out emission measurement with FID and NOx analyser	♦ Antiknock quality and volumetric efficiency are improved by optimising the fuel injection timing in DI engine ♦ The DI engine has such advantages as quick response in each cycle and low emission at cold engine and transient mode ♦ Fuel injection in the first half of compression stroke greatly improve lean limit ♦ To meet the emission regulations with lean burn DI engine, the EGR and lean NOx catalyst at around 20 at part load should be used
Arcoumanis et al. (1997)	• Single cylinder two - valve optical engine, propane fuelled • LDV, pressure , HC emission measurement	♦ Local mixture injection, at a fixed ignition timing, extended the lean limit from an A/F ratio of 24:1 to 29:1 ♦ At an A/F ratio of 24:1 the rich injected mixture increased the peak pressure by 50% compared to a 30% gain for the homogeneous injection ♦ The flame speed with mixture injection at ϕ=0.7 was similar to homogeneous fuelling at ϕ =0.9
Harada et al. (1997)	• Optical 4 -valve GDI single cylinder engine • Combustion pressure analysis and flame image analysis	♦ Toyota GDI engine with stratified ultra-lean burn mixture operation realised 22% fuel economy improvement, featuring new technologies such as involute shape concave piston, swirl intake ports and high pressure fuel injection system ♦ Smoke generation was avoided over all engine operation areas by employing three types of injection strategy ♦ Exhaust emissions satisfied Japanese standards with EGR, NO_X storage-reduction catalyst and closed coupled catalyst

Author(s)	Experimental technique(s)	Main finding(s)
Iwamoto et al.(1997)	• Optical access 4 valve GDI single cylinder engine • Simulation of in-cylinder flow motion • Air entertainment into the fuel spray with tracer particle of polymer micro-balloon • Combustion presser and emission measurement	♦ Below Fundamental technologies adopted to make Mitsubishi GDI engine; 1. Upright straight intake ports generating reverse tumble 2. A spherical compact piston cavity 3. An electromagnetic swirl injector ♦ GDI engine realise the fuel economy equivalent to diesel engine, performance superior to port injection SI engine and exhaust emission as clean as that of port injection SI engine
Ohsuga et al.(1997)	• Optical 4 -valve GDI single cylinder engine • Fuel spray characteristics taken by LIF	♦ This new method for stratified charge in a centred injection and ignition engine uses a flat type piston and offers an in-cylinder swirl air flowand low speed solid cone spray ♦ Intake manifold of this system includes an air jet passage and generated a swirl flow in the cylinder ♦ Fuel is injected at the centre of the swirl flow during the intake stroke and is kept at this position. As the piston moves upwards in the compression stroke, the mixture also moves upward and is concentrated around the spark plug, so stratified charge is achieved

CHAPTER 2

EXPERIMENTAL SYSTEM AND MEASUREMENT TECHNIQUES

2.1 Introduction

In recent years there has been a rapid increase in the use of laser diagnostic techniques as measurement and visualisation tools, in conjunction with combustion and emission analysis, to allow the study of important features of the in-cylinder flow and the subsequent combustion process and exhaust emissions. This chapter is devoted to the description of the experimental system and instrumentation used in the present project in order to provide the necessary background for the investigations described and discussed in Chapter3 and 4.

2.2 In-cylinder flow measurements

The measurement of the velocity of the charge motion inside the cylinder was performed in order to examine the effect of different intake port configurations on the flow field present around the time of ignition. The different intake configurations encompassed the standard and the sleeved intake port geometry, as well as that resulting from the injection of gaseous fuel through open intake valves compared to closed-valve injection.

Laser Doppler Velocimetry (LDV) was employed in the single-cylinder optical engine to assess the effect of tumble strength on the bulk velocity and turbulence near the spark plug during the induction and compression strokes and, in particular, around the time of ignition. In order to gain a more clear view of the breakdown of the tumbling motion inside the cylinder, Particle Image Velocimetry (PIV) was used to characterise the two-dimensional flow field during the induction and compression strokes.

2.2.1 Measurement of in-cylinder flow using LDV

The in-cylinder flow velocity measurements were obtained using an LDV system. LDV is a non-intrusive technique which is unaffected by the measurement location, temperature and pressure, and is offering directional flow information, but it does have the limitation of being a point measurement technique requiring optical access, with results that are dependent upon the seeding particles being small enough to follow the air flow in question. The principles of the technique have been well documented by Durst et al.(1981) and Drain (1980).

The system used in this project comprised an Argon-ion laser (1.3W at 514.5nm) and a rotating diffraction grating-based optical unit which delivered the laser beams into the combustion chamber through the side window in the engine liner. The seeding generator was able to generate oil droplets of up to 2.0 μm, which were introduced into the intake manifold, while the scattered light was collected by a photo-multiplier using forward scattering.

On entry into the transmitting optics unit, the monochromatic coherent laser beam was split in two. One beam passed through the rotating grating which induced a phase shift into it, while a moving fringe pattern was produced within the measurement volume at the beam intersection. When a particle passed through the measurement volume a Doppler signal was detected by the photomultiplier, with the signal frequency being directly proportional to the particle velocity component normal to the bisector of the beams.

The resulting electrical signal was processed by a TSI 1990C counter that was interfaced to a personal computer and synchronised with the shaft encoder signal to allow the velocity information to be related to a crank angle index with a resolution of 0.5 degrees, within the measurement window during the induction and compression strokes. Mean and rms velocities were estimated by ensemble averaging of the raw data within each crank angle window. The statistical accuracy of the results was dependent upon the number of data points measured and the size of the respective window. Although LDV can quantitatively resolve velocity and turbulence intensities, it is a point measurement technique and without a large number of measurement locations it can not provide a full picture of the flow pattern. The experimental set-up and measurement points for the LDV experiment in the optical engine are shown in Figures 2.1 and 2.2.

2.2.2 Measurement of in-cylinder flow using PIV

Particle image velocimetry is now considered a well-established technique for the measurement of instantaneous planar velocity fields in various flow configurations (Adrian, 1991 and Hinsch, 1993). In its simplest form, the flow is illuminated with a double pulsed light sheet and the positions of tracer particles are recorded with a photographic camera positioned normal to the plane of the sheet. The mean displacement of the particle images within each small interrogation region gives a measure of the local mean flow velocity.

In this study, the two-dimensional in-cylinder flow field in a vertical plane was characterised using cross-correlation particle image velocimetry (PIV). The measurement plane was along the symmetry plane of the cylinder head and was used to observe the tumbling vortex just below the head; unfortunately, optical access was not available into the pentroof chamber which prevented monitoring of the flow in the close proximity of the spark plug. The laser sheet was produced in a vertical plane and passed into the cylinder via a 45° mirror and piston window while the PIV image was obtained through the side windows. For flow visualisation, copolymer-type microballons were used as seeding particles; these have a 50 μm mean diameter and were introduced into the intake plenum chamber to allow time for uniform mixing. Due to the limited optical access the field of view was rather narrow, but sufficient to characterise the mean flow under the spark plug and to identify the breakdown of the tumble as the piston approaches TDC. The cross-correlation PIV technique used here is based on the recording of two successive and separate images of the flow and the subsequent cross-correlation of these images. Illumination in this case was provided by a pulsed copper-vapour laser of maximum output 15W and pulse frequency of 10kHZ, focused into a light sheet of 1mm minimum thickness through a system of two lenses and a slit. The experimental set-up for the PIV measurements in the optical engine is shown in Figure 2.3.

The flow images were taken using a Cordin Drum camera which incorporates a hollow drum rotating at speeds corresponding to around 150 Hz and an internal optical system that includes a shutter and a zoom lens (200mm) attached to the laser. On average, 70 consecutive images were recorded on the film rotating inside the drum camera. To convert negative film (Kodak - Tmax 400) into positive digital images, the developed film was scanned using a Nikon scanner directly connected to a PC. The images were further processed to obtain the vector flow fields by commercial analysis software.

2.3 Combustion analysis

2.3.1 Pressure measurements

The engine head was fitted with a threaded hole for installation of a pressure transducer (Kistler 6001 piezoelectric type), which was positioned with its sensor-face flush with the pentroof wall. The voltage signal from the transducer was connected to a Kistler type 5007 charge amplifier, giving an output of 10 bar/volt. The transducer and charge amplifier were calibrated using a hydraulic gauge, to confirm a linear relationship between pressure and output voltage signal.

The pressure data were ensemble-averaged and post-processed to characterise the peak pressure, the crank angle at which the peak pressure occurred, the maximum pressure rise and the crank angle at which this pressure rise occurred, as well as the indicated mean effective pressure (IMEP). The IMEP is a parameter used extensively in this work to represent the thermodynamic work done in each cycle per unit swept volume.

The cycle-to-cycle variations of the pressure-related parameters such as peak pressure and IMEP were calculated on the basis of cycle-resolved data, and in all cases the standard deviation (σ) and mean ($\bar{x}$) were used to calculate the coefficient of variation (COV) from which an indication of the cycle-to-cycle combustion stability could be determined.

Heat release analysis was performed using a one-zone model (Chun & Heywood, 1987) which calculates the chemical energy of the fuel-air mixture that is converted to mechanical energy from the increase in the cylinder pressure at each point in the cycle. The mass fraction burned which is normalised for each engine cycle was represented by the 0-10% and 10-80% burn duration.

2.3.2 Flame imaging

Flame images were acquired using a Proxytronic HF-1 Intensified CCD camera, by viewing vertically into the combustion chamber via the 45° mirror and quartz piston window. The camera is fitted with a 50 mm lens, and its field of view incorporates the entire diameter of the

piston window (Figure 2.4). The maximum flame size that can be visualised is, however, limited by the diameter of the piston window; a view of the pentroof head as seen from the CCD camera is presented in Figures 2.4(a) and (b), where the visible part of the cylinder head including the position of the spark plug and valves can be clearly seen. The intensifier on the camera is triggered by a 5 Volt pulse which is generated by the counter-timer card once per cycle at a crank angle position that is set using the control software. The maximum number of images acquired is 12 and thus images from 12 successive cycles at the same crank angle position can be obtained. Each of these images is a square array of 512 × 256 pixels (Figure 2.4 (c)), and has a possible greyscale value between zero (black) and 255 (white). The images are software processed in order to remove noise and calculate various parameters. In this process, a threshold greyscale value is set for each image and all pixels below this value are set to zero (black). This provides a 'clean' image of the flame (Figure 2.4 (d)) and the remaining non-zero pixels provide a measure of the 2-dimensional enflamed area. In addition, calculations of the size and position of the flame centre can be made (for example, see zur Loye & Bracco, 1987; Bates, 1991; Arcoumanis & Bae, 1995), by setting a minimum threshold greyscale value and setting to zero any pixel with a greyscale value below this threshold. These values are used as a measure of flame development and for characterising the magnitude and direction of the convection of the flame away from the spark plug.

A second imaging device was used to obtain crank-angle resolved flame images for direct observation of flame propagation within an engine cycle. The Imacon 468 Camera is of the CCD type, but contains 6 image intensifiers and a revolving prism which allows the 6 image intensifiers to be illuminated consecutively at a maximum frequency of 1 MHz. This can be used to acquire successive flame images within one engine cycle, to study the temporal development of the flame. Each of the six images is an array of 576 × 385 pixels, each of which can have a greyscale value of 0 to 255. The data are output as a single file, from which the images can be accessed and processed in the same way as those from the other CCD camera.

2.4 Fuel concentration measurements

The air-fuel ratio in the spark gap at the time of ignition is a key contributor to both the combustion and emissions of an automotive engine. This section explores the use of a sampling probe connected to a fast ionisation detector with in the spark plug to quantify any rapid changes in the cylinder hydrocarbons composition in the vicinity of the spark gap. Unlike some alternative techniques such as snatch-sampling and optical techniques, it requires no modifications to the engine and can give information on cyclic mixture variability as well as ensemble-average data in the all-important for ignition spark gap region.

2.4.1 Sampling spark plug and fast flame ionisation detector

The real time HC concentration in the vicinity of the spark plug, with a time resolution of a few degrees of crank angle, was measured using a 'Cambustion' HFR400 fast flame ionisation detector (FFID). This system is illustrated in Figures 2.5 and 2.6. The typical 1-2s response time of a FID has been reduced to less than 5ms by introducing the sample directly into the base of the hydrogen flame positioned as close as possible to the sampling point, instead of mixing the sample and hydrogen upstream of the flame. The flame was maintained under partial vacuum and the sample was drawn from the engine via a small diameter and length stainless steel tube. Pressure fluctuation effects were avoided through the use of a constant-pressure chamber and the sample line was heated to prevent any hydrocarbon condensation. A special type of offset spark plug incorporating a sampling tube (Figures 2.7 and 2.8), that was extended to 450 mm to minimise the sample gas transport delay, was used in these experiments. The pressure in the constant-pressure chamber was set at 300 mmHg to reduce the pressure fluctuations, and the chamber volume was increased to 0.4 l. Calibration was performed before and after every experimental test run in order to eliminate any errors arising from drift of the equipment. Figure 2.9 illustrates the features of a typical in-cylinder HC signal from a sampling spark plug system. The output from the FFID only becomes valid when the cylinder pressure has increased such that there is sufficient flow along the sample line. This occurs typically towards the end of the intake stroke, beginning of the compression stroke, and here the HC concentration begins to increase. The HC level continues to increase rapidly during the compression stroke until it reaches its maximum value; this maximum represents the pre-flame HC concentration at the spark plug prior to flame initiation. After

ignition, the propagating flame front entrains and burns any fuel in the vicinity of the probe and the HC concentration rapidly falls to a low level. Some time later in the cycle, the HCs are purged from the cylinder and the HC concentration increases due to the unburned fuel leaving the crevice volumes. The transport delay for the sample gas, that is the time taken between the sample entering the probe and reaching the measurement head of the FID, was calculated based on the length of the sampling tube, the in-cylinder pressure and the pressure in the FID constant pressure chamber by using the software (SATFLAP3) supplied with the Cambustion system [FFID Users Manual]. For this experimental condition, the transport delay time was estimated to be about 40° crank angle.

2.5 Engine-out emissions

2.5.1 Fast flame ionisation detector

The fast flame ionisation detector (FFID, 'Cambustion HFR400') was employed to measure the concentration of unburned hydrocarbons in the exhaust. The FFID works on the principle that combustion of hydrocarbons in air produces ions, contrary to combustion of hydrogen in air which produces no ions. In the FID, the gas to be sampled is introduced into a quiescent hydrogen-air flame and a cathode is placed adjacent to the flame to detect the extent of flame ionisation. If unburned hydrocarbons are not present in the sample, there is no ionisation, and no current to the cathode is detected. When hydrocarbon compounds are present, a current is detected which is proportional to the number of carbon atoms present in the hydrocarbon compounds. The current is converted to a voltage value, which is displayed on the FID control panel, and there is also a voltage output socket that is connected to the data acquisition system. The sample was acquired along a heated line regulated to a temperature of 180°C, from a sampling point located approximately 0.5m downstream of the exhaust valve; it was drawn into the oven for analysis and maintained at 200°C to prevent retention of any heavier hydrocarbons present in the sample. The FID was calibrated using a gas of known hydrocarbon composition, in this case propane at 800 parts per million (ppm) in inert nitrogen diluent; this carbon concentration was of the same order as the typical exhaust gases at the test conditions studied.

2.5.2 Fast NO analyser

In conjunction with the hydrocarbon measurements, the concentration of the oxides of nitrogen in the exhaust gases was measured using a fast response NO detector (Cambustion fNO_x400). The instrument bases its measurement approach upon the following chemical reaction :

$$NO + O_3 \longrightarrow NO_2 + O_2 + \text{Light emission } (h\nu)$$

When nitric oxide (NO) and ozone (O_3) react to form nitrogen dioxide (NO_2) and oxygen (O_2), a fraction of this excited NO_2 decays via chemiluminescence reaction to NO_2 and a photon. The resulting chemiluminescent reaction produces photons in the 700-1500 nm wavelength range which are detected with a photomultiplier; the linearity of this device from 0 to 4000 ppm is within 2%. The fast NO gas reaction chamber is housed in a remote sampling head so that sampling from a location close to the exhaust system can be facilitated. The light is transferred from the reaction chamber to a photomultiplier in the main control unit via a fiber-optic bundle. The main control unit also contains the power supply, electronics, ozone generator, and vacuum regulators to operate the sampling head. The 90-10% response time for the fNO_x400 is 3.0 ms which is considered sufficiently fast to measure transient NO emissions within a single engine exhaust stroke where 720° crank angle at 1,500 rpm correspond to 80ms. The analyser was calibrated using two gases of known composition: pure nitrogen was used for the zero level, and NO at 500 ppm for the calibration span. Calibration was performed before and after each experimental run in order to eliminate any errors arising from drift of the equipment.

2.6 Schlieren photography

2.6.1 Schlieren optical system

Information about flow in gases can be obtained optically when there are local changes of density since these are accompanied by changes of the refractive index; the excess of the refractive index above unity is, for a given gas, proportional to the density (Duncan et. al., 1986). This technique is mainly of value for high speed two-dimensional flow. A collimated

beam of light is passed through the gas, normal to the plane of flow, and in the simplest application of the principle a "shadow picture" is obtained on a plane white screen. The variations of density give rise to variations of brightness on the screen on account of what may be called a lens effect.

A schematic of the Schlieren system is shown in Figure 2.10. The optical components and lens positioning were chosen to produce a collimated light beam of 55 mm in diameter, which is slightly larger than the diameter of the quartz windows of the constant-volume chamber (50 mm). Since the spark light source was around 12 mm in length, it was not possible to treat the spark itself as a point source. Thus, light from the spark was collected using a bi-convex lens of 150mm focal length (f1) and focused to form an image of the spark on the surface of a pinhole having a diameter of 0.6 mm. A 50 mm diameter aperture was placed in front of the lens to reduce spherical aberration caused by light rays striking the lens surface at larger distances from the optical axis. The relative distances between the spark, lens and pinhole were chosen to produce an image of the spark on the surface of the pinhole with a magnification factor of 0.83.

Light from the pinhole, which acted as a point light source, was collimated using a plano-convex lens (f2 = 150 mm) placed with its plane side facing the pinhole to reduce the effects of spherical aberration. The collimated light beam, which had a diameter of 55 mm, passed through the test section, and was then focused by a second plano-convex lens (f3 = 450 mm) which had its plane side facing away from the pinhole. A knife-edge was placed at the focal point of the beam to produce the Schlieren effect. Light was collected by a camera lens (f4 = 200 mm) placed at a distance of 200 mm from the knife-edge. This resulted in a parallel light beam of 22 mm in diameter being imaged onto the film with a magnification factor of 0.44. Since the camera lens was being used to collimate the light beam before it was imaged onto the film surface, it proved not possible to use the camera aperture to control the amount of light reaching the film. Thus, a yellow filter (Jessop Y2) was fitted to the camera lens to enhance the contrast of the image recorded on the black-and-white film (Kodak TMax Pro 400 ASA). The focal lengths and relative positioning of the optical components are summarised in Figure 2.10.

2.6.2 Constant volume chamber

The constant-volume chamber used for imaging the CNG jet consists of a sandwich of three steel blocks, the outer two incorporating round quartz windows of 50 mm diameter set into the centre, and the middle block being hollow to generate a chamber with a diameter of 55 mm which is optically accessible though the two side windows. Two solenoid valves were connected to the central section of the chamber to enable charging and discharging of the fuel/air mixture, together with a safety valve used to allow scavenging at 25 bar. Also set into the central section of the constant-volume chamber was the gas injector. Figure 2.11 shows a photograph of the chamber with the injector installed.

The light source, a Palflash Sparklight, provided white light with duration of less than 10 μs, which necessitated accurate timing of the Sparklight and the injector. With the photography performed in a dark room, the camera shutter could be left open for over a second with no detrimental effect on the image; however, the spark-light required triggering at a known time after activation of the injector which was achieved using two pulse generators and a storage oscilloscope. The first pulse generator was used to send out one TTL signal to both the injector driver circuit, in order to activate the injector solenoid for as long as the TTL signal was present, and the second pulse generator. This second pulse generator delayed the TTL signal by a predetermined period before sending it to trigger the Sparklight. Both TTL signals were monitored using the storage oscilloscope to verify the delay period between the two. Using this system, both the spark-light and the injector could be controlled from the same button, enabling the user to operate the camera simultaneously. To provide a charge of pressurised air within the chamber, one of the two solenoid valves incorporated into the chamber were connected to a bottle of compressed air. The regulator on the bottle could be pre-set to the required air pressure and the solenoid valve opened when the air charge was required. This was performed at least 5 seconds before the image was taken to allow time for the gas to settle within the chamber. After the jet image was captured, the chamber was evacuated through the second solenoid valve and subsequently scavenged with clean air prior to obtaining the next image.

2.7 Summary

This chapter has presented the experimental equipment and measurement techniques which were employed during the research project. In this study, the in-cylinder flow was examined using LDV and PIV. Combustion was visualised by direct flame imaging using a digital image intensified CCD camera with simultaneous measurement of the in-cylinder pressure to investigate combustion characteristics and engine performance. Engine-out emissions of unburned hydrocarbons and NO were measured using a fast FID and NO analyser. For measuring the local hydrocarbon levels in the spark plug gap at the time of ignition, a sampling probe incorporated into the spark plug was used. Finally, the characteristics of the CNG jet were examined using Schlieren photography in a constant-volume chamber prior to the engine tests in order to provide insight into the jet structure, cone angle and tip penetration.

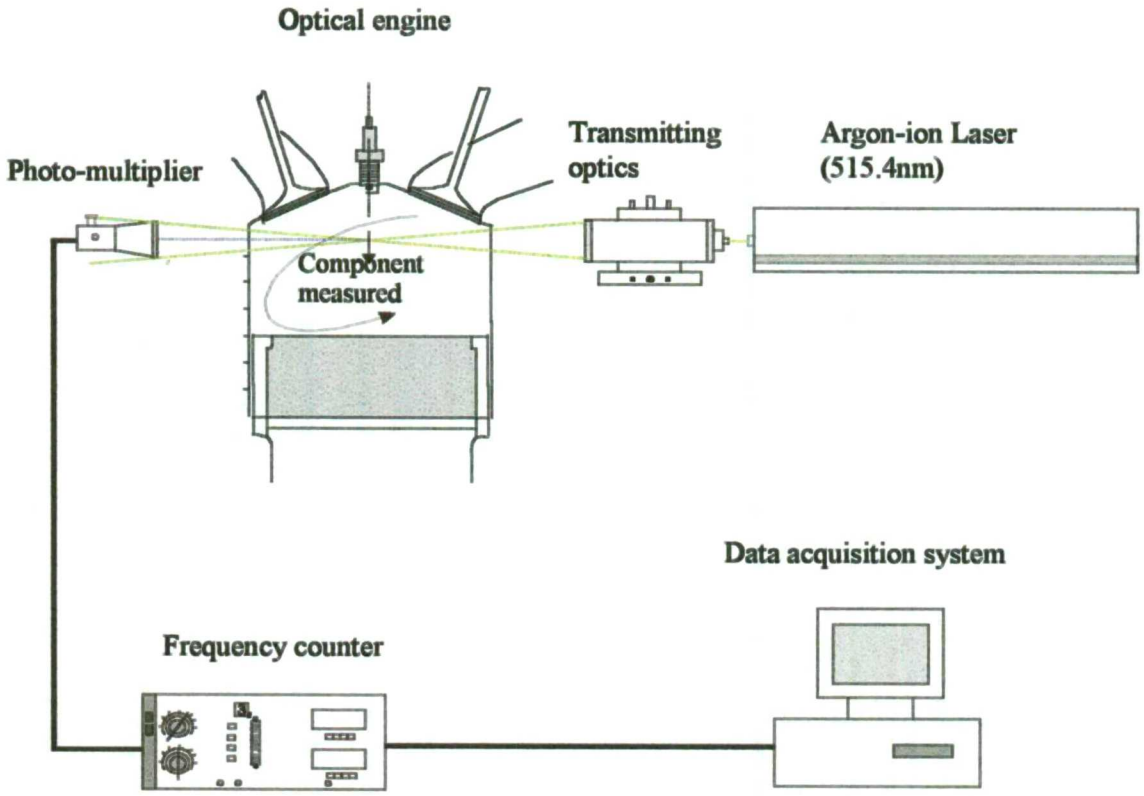

Figure 2.1: Schematic of the system arrangement for laser Doppler velocimetry

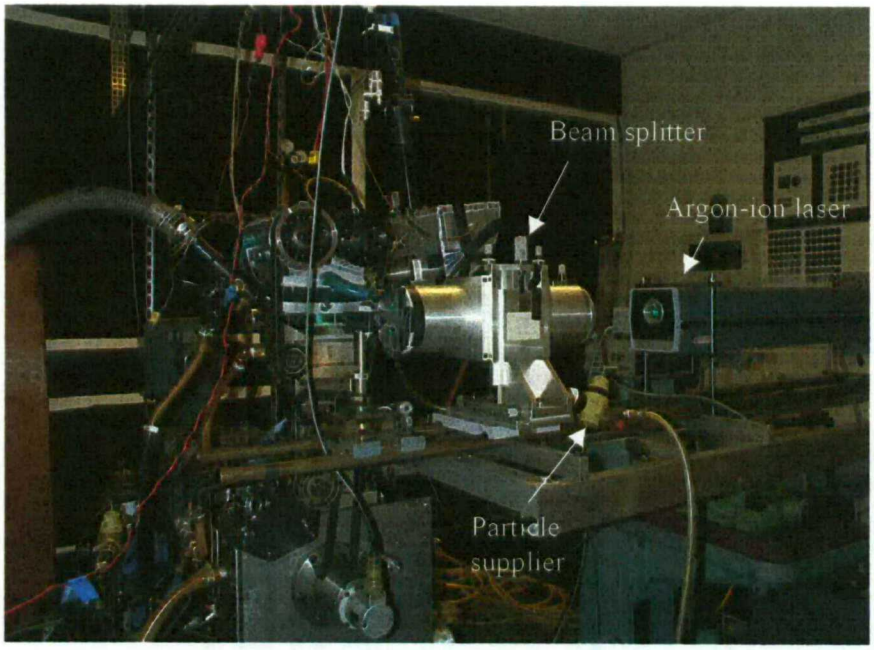

Figure 2.2: Photograph of the laser Doppler velocimeter for measurements through side window of optical engine

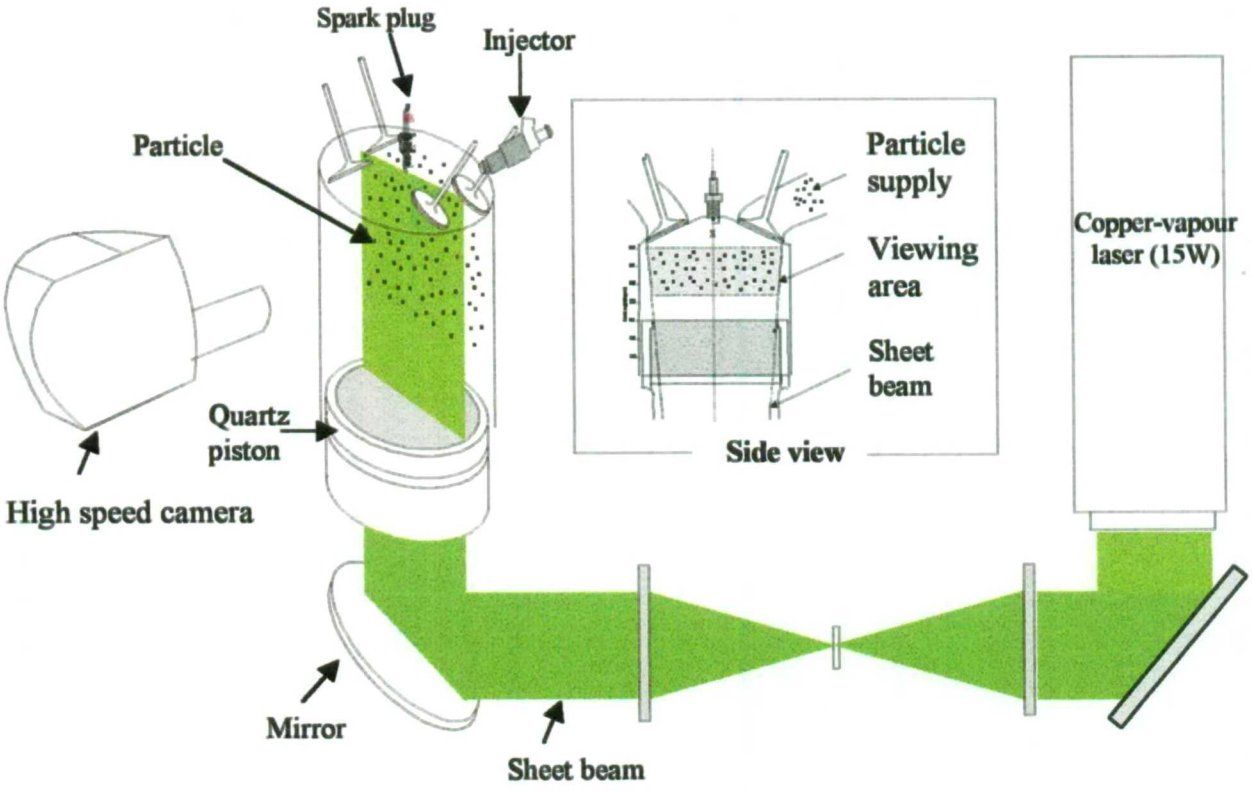

Figure 2.3: Schematic diagram of particle image velocimetry measurements in optical engine

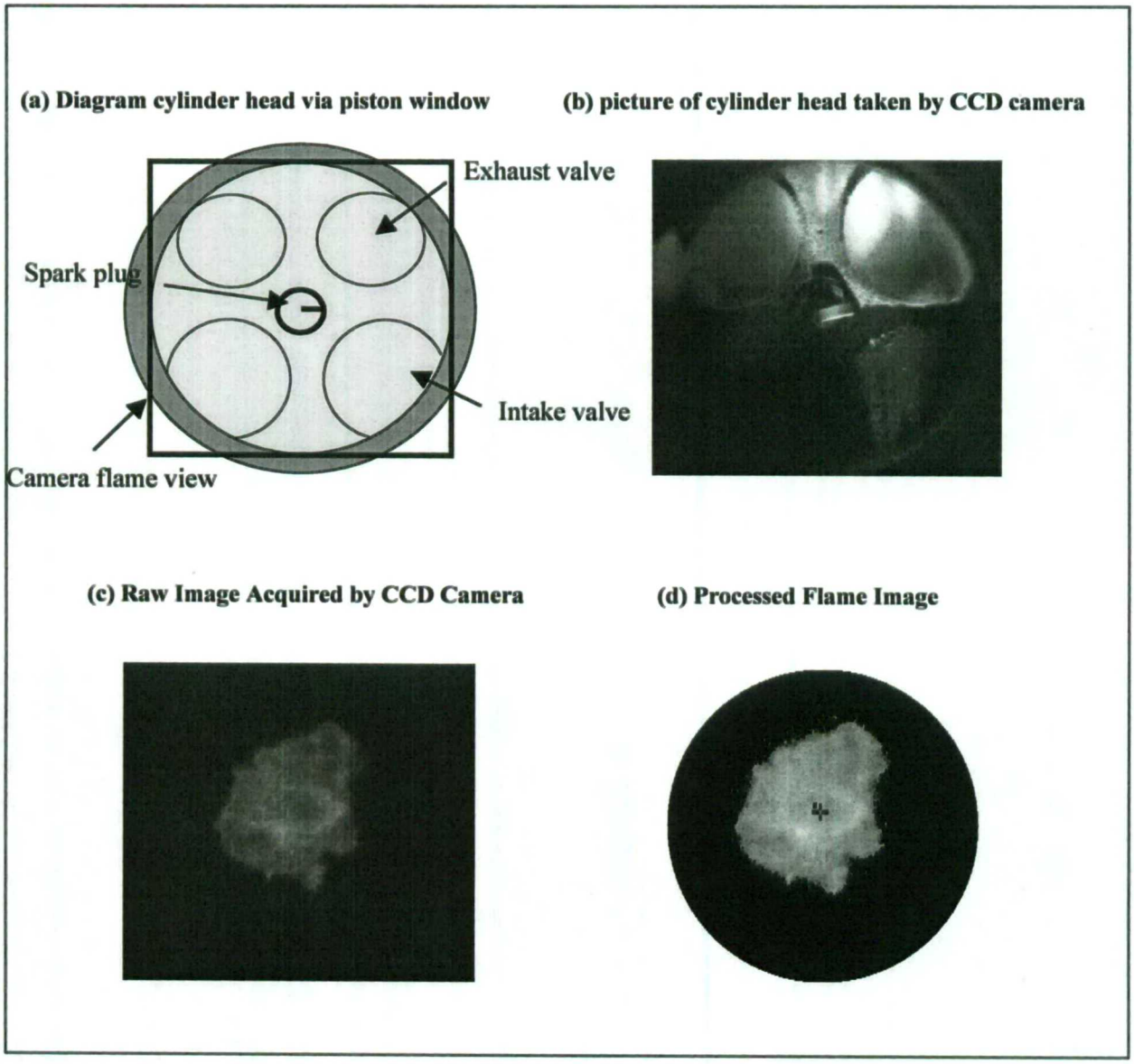

Figure 2.4: View of cylinder head and typical flame image before and after processing

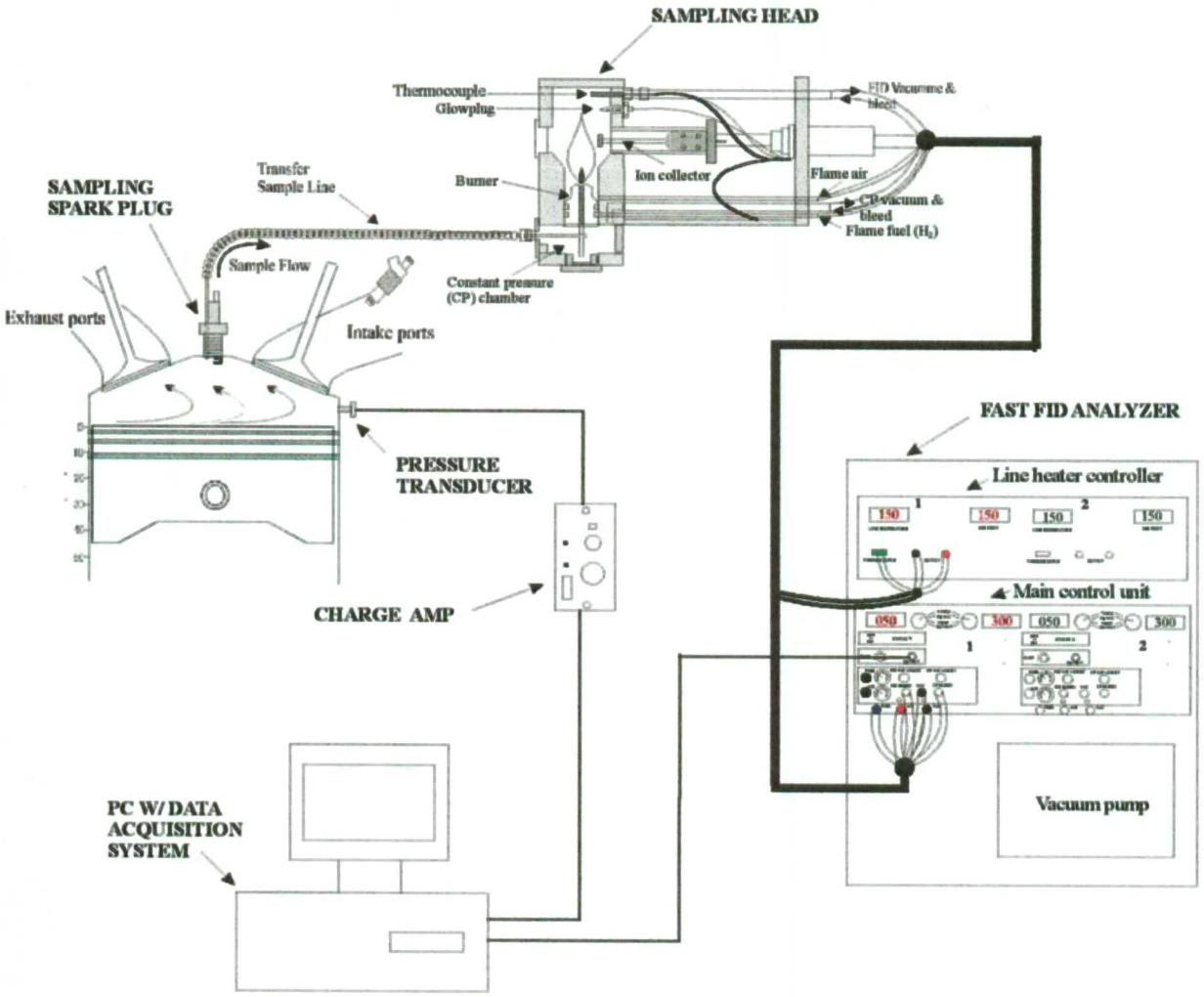

Figure 2.5: Schematic diagram of in-cylinder gas sampling system with a fast FID analyser

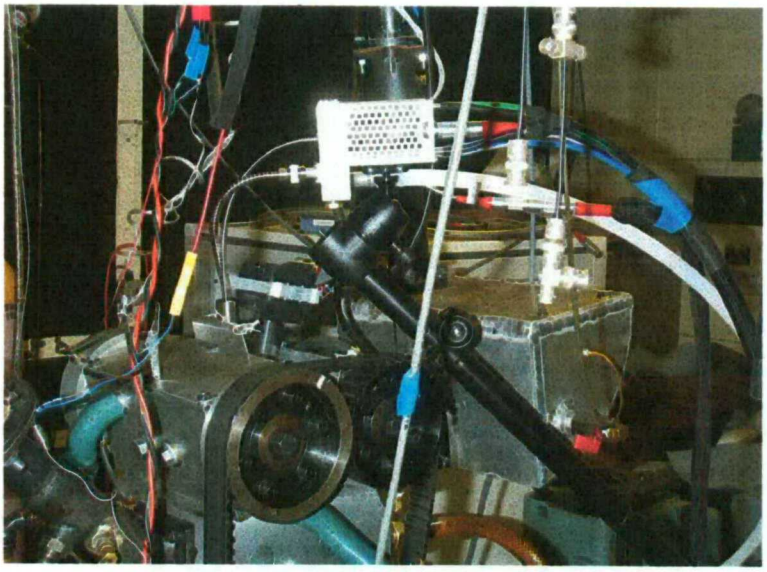

Figure 2.6: Photograph of in-cylinder gas sampling system with a fast FID analyser

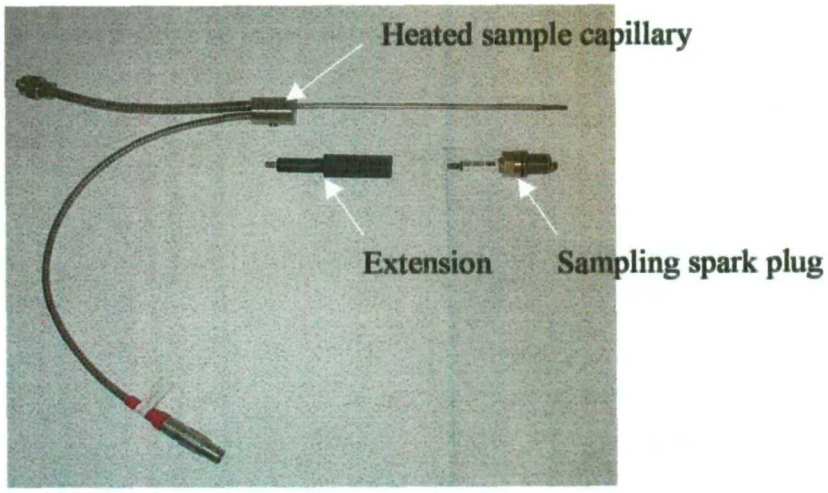

Figure 2.7: Sampling spark plug kits

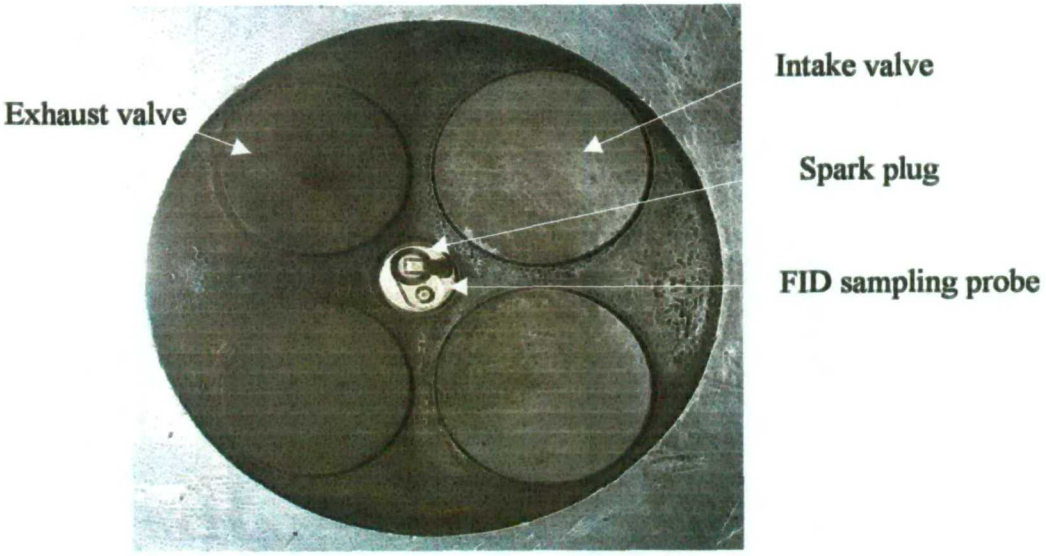

Figure 2.8: Engine head with sampling spark plug

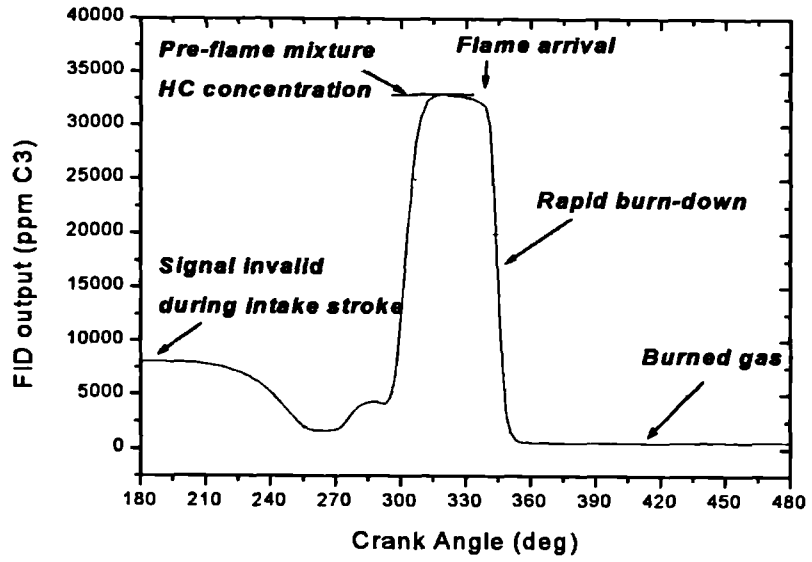

Figure 2.9: Typical in-cylinder trace of hydrocarbons concentration at the spark plug

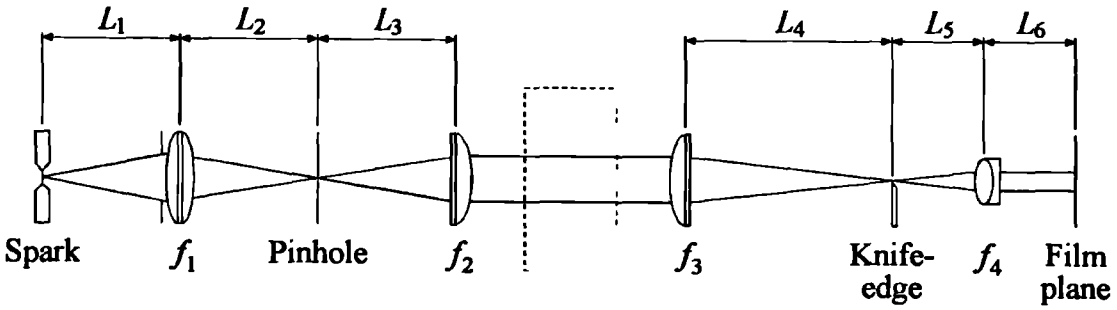

L_1	330 mm	f_1	150 mm
L_2	275 mm	f_2	150 mm
L_3	150 mm	f_3	450 mm
L_4	450 mm	f_4	200 mm
L_5	200 mm	Aperture for f_1:	50 mm
L_6	200 mm	Pinhole diameter:	0.6 mm

Figure 2.10: Diagram of the lens arrangement for the Schlieren system

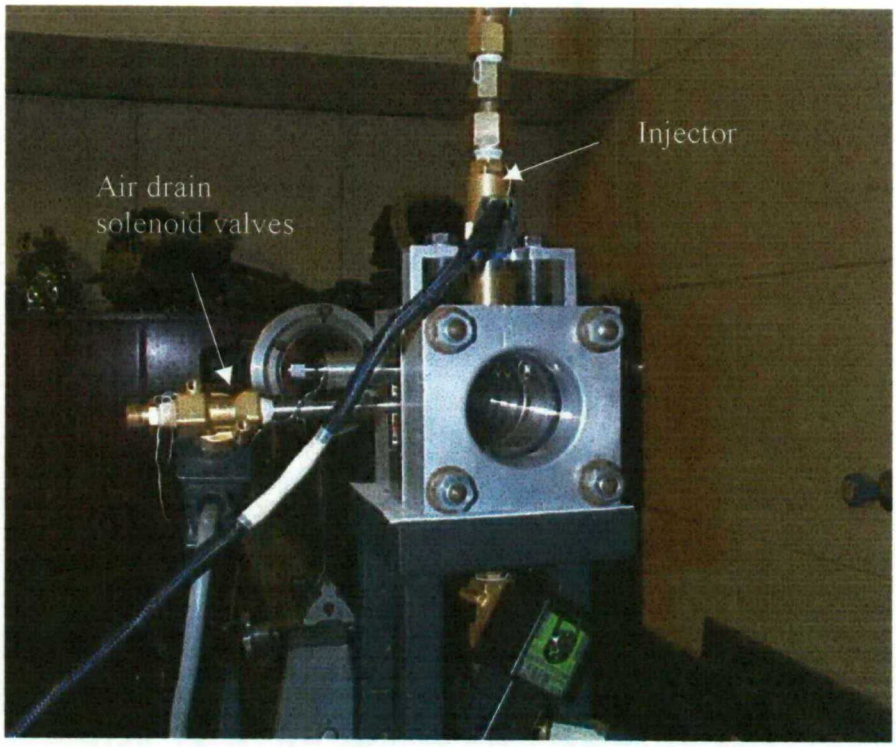

Figure 2.11: Constant volume chamber with high pressure injector installed

CHAPTER 3

PORT INJECTION CNG ENGINE

3.1 Introduction

Natural gas has been used as automotive fuel in many countries (Italy, Netherlands, New Zealand, Canada, Russia and USA) around the world. Main reason for its use until recently has been to reduce dependency on oil as a transportation fuel. But now days, to meet the stringent emission regulation in many countries, there is a strong demand for development of ultra low emission vehicle using alternative fuels. Natural gas fuel systems for vehicles consist basically of two types, mechanical (carburetted) and electronic (fuel injected). Mechanical systems have been used for many years and operate on the same principle as gasoline carburettor fuel metering systems wherein the fuel is mixed with the intake air in the throat of a converging-diverging nozzle (carburettor). Electronic systems utilise injectors to meter the fuel injected into the intake air. A precisely controlled air-fuel ratio and a high efficiency catalytic converter by three-way catalysts are necessary to reduce exhaust gas emissions. For precise control of the mixture formation in a homogeneous-charge in SI engine, the best solution is sequential injection of the fuel in each inlet port just upstream of the inlet valve instead of the air-fuel mixer used in mechanical systems. It is apparent that fuel injection offers significant improvements over carburetors or air-fuel mixers. Advantages of electronic injection over carburetted systems are precise fuel control, instant throttle response, pulse with modulated control strategy, quick start in cold weather, improved BSFC, control of fuel flow rate on deceleration, low pressure regulator not required and superior emissions control. In this study, a recently developed gaseous injector by Bosch was used to allow injection of CNG into the engine intake port.

It is well known that the in-cylinder flow motion has a dominant effect on the combustion process in spark ignition engines. Today there is a strong need for

development of high performance engines with high lean burn and EGR capabilities to meet more stringent emission and fuel economy requirements. This may be satisfied by the use of multi-valve per cylinder engines. In order to obtain satisfactory part load performance and, particular improved, combustion stability, a specific design of the inlet system is required to enhance the in-cylinder flow. Combustion stability is often improved in current port fuel injection multi-valve engines by inducing a tumble motion in the combustion chamber obtained with specific inlet port shape and arrangement. Many investigations were carried out on the effect of tumble motion, for example (Arcoumanis *et.al.*,1990; Jie *et. al.*, 1993; Kodou *et. al.*, 1992). Inlet port development is often conducted using steady flow rigs where the swirl and tumble ratio can be calculated. However, the understanding of the interaction between the in-cylinder air motion and combustion requires a better knowledge of the detailed flow field in the combustion chamber, especially the turbulence characteristics in the vicinity of the spark-plug which are believed to be closely related to the flame kernel growth and eventual combustion rate (Witze, 1982)). The use of laser-based optical techniques such as LDV and more recently PIV (Khalighi *et. al.*, 1990; Trigui *et. al.*, 1994;) have allowed significant progress in the understanding of the detailed in-cylinder flow development. In previous work conducted in the same engine (Arcoumanis *et.al.*,1994; Arcoumanis *et.al.*,1998), flow measurements were obtained using laser Doppler velocimetry to characterise the bulk and turbulent flow generated by different intake port geometries incorporating sleeves in the intake ports, which deflect the inducted air over the intake valves, thus producing a stronger tumbling vortex in the cylinder relative to that generated by non-sleeved ports.

In a conventional port-injected spark-ignition engine, the fuel is injected towards the back of the closed intake valves. This occurs well before the valves open, so that a significant fraction of the fuel vaporises under warm engine conditions before entering the cylinder, to allow a nearly gaseous fuel to mix and burn with air more efficiently than if it was in liquid form. Since CNG is a gas at room temperature, it is possible to inject it through the open intake valves without having to consider the time required for droplet vaporisation. This mode of fuel injection can induce some degree of charge stratification in the vicinity of the spark plug at the time of ignition that promotes stable operation under overall lean mixture conditions.

The aim of this chapter is to investigate the performance of a single-cylinder 4-valve spark ignition engine fuelled by CNG using a port-fuelled injection system under lean mixture conditions and employing, on the one hand, sleeved ports to enhance the mean flow and turbulence during compression and, on the other, open-valve fuel injection strategy to enhance charge motion and its stratification at the time of ignition. Finally, a compression ratio investigation was carried out to improve the engine performance by taking advantage of the high octane number of natural gas. It may be worth mentioning that the work presented in this Chapter represents an extension of the investigation described previously by Godwin (1998) in that special emphasis is given here to the flow diagnostics (LDV, PIV), the fuel concentration at the spark plug around the time of ignition and the measurement of the engine-out emissions (HC, NO) under a more extended range of engine operating conditions.

3.2 Research engine and experimental arrangement

3.2.1 Research engine

The single cylinder optical research engine is based on a Ricardo-Hydra and was modified to accommodate a Jaguar cylinder head of four-valve pent-roof geometry. Figure 3.1 and 3.2 illustrate characteristics of the optical engine used in these experiments. The cylinder head is mounted on an extended cylinder liner which is matched to an extended piston, having a circular quartz window in the piston crown for optical access into the combustion chamber and fitted with graphite piston rings, so that no liquid lubrication is required between the piston and the cylinder. Within the hollow extended piston, a fixed mirror (Figure 3.3 (b)) at 45° to the vertical is positioned that allows optical access via the piston window. Between the head and the cylinder liner is a ring assembly of 15mm thickness, which incorporates two rectangular quartz windows (Figure 3.3 (a)) for optical access from the side into the top part of the stroke. The entire head and extended cylinder are mounted on a Ricardo Hydra crankcase, motored by a regenerative dynamometer. The engine specifications are summarised in Table 3.1.

Table 3.1: Engine specifications

Engine type	Single cylinder, 4-valve engine
Fuel injection system	Port fuel injection
Displacement	498 cm^3
Bore x Stroke	83 mm x 92 mm
Compression Ratio	10.5
Combustion chamber	Pent-roof
Intake valves : . Valve timing . Maximum. valve lift	 -6° to 224° 9.45 mm

The spark plug and fuel injector are driven by a computer-controlled engine management system. A shaft-encoder producing 2880 electronic signals per engine revolution is fitted to the crankshaft, and a magnetic pick-up sensor attached to the camshaft detects the TDC position. These signals are fed to a counter-timer card installed in a PC which, using appropriate software, produces signals once per engine revolution that allow timing of both spark ignition and fuel injection. These signals are converted by an injector-ignition driver circuit into high power pulses which directly drive the injector solenoid and ignition coil. Thus, precise and flexible control of the injection and ignition timings can be achieved. In addition, these signals are used to trigger an analogue-digital (A/D) card, also installed in the PC, for acquisition of the in-cylinder pressure data and simultaneous triggering of the image acquisition equipment. The air/fuel ratio is monitored using an NTK UEGO lambda sensor and a digital display unit.

3.2.2 Experimental set-up

The gasoline delivery system incorporates a fuel reservoir connected via a pump, fuel filter and flexible hose to the rear of the injector. The fuel pressure is maintained at 3 bar and the fuel used is premium unleaded gasoline of octane rating 95.

CNG fuel is delivered to the injector via a dedicated CNG system (Figure 3.4), which houses bottled high pressure CNG in a storage vessel away from the experimental test cell. A regulator and a relief valve are fitted to the gas bottle. Within the test cell there is a second regulator to reduce the operating pressure from 150 bar to 5 bar, and the gas is delivered to the injector via a wire-mesh strengthened flexible hose. Also within the storage vessel and the test cell are methane sensors and alarms in case of a gas leak. Table 3.2 shows the composition of the natural gas used in this study:

Table 3.2: CNG Fuel Composition

Component	CH_4	C_2H_6	C_3H_8	C_4H_{10}	C_5 +	N_2	CO_2
Percentage by volume	93.5	3.5	0.7	0.22	0.065	1.5	0.5

* Data source from gas company

Fuel injection of both gasoline and CNG was achieved by injectors mounted in the intake manifold which direct fuel towards the back of the intake valves. For both gasoline and CNG single-jet Bosch fuel injectors were used with different flow rates and injection pressures. These injectors are operated when the solenoid valve is opened, as the 12-volt power supply is applied and controlled by the engine management system. Table 3.3 and Figure 3.5 show the comparison of the characteristics of the gasoline and CNG injectors.

Table 3.3: Technical specifications of injectors

	Gasoline injector	**CNG injector**
Static flow (l/min)	0.23	146.7
Injection hole diameter (mm)	0.5	2.5
Weight (g)	85	90
Injection pressure (bar)	3	5
Driver	Saturated type	Peak and hold type

The operation of the engine was controlled by a purpose-built electronic management system and Figure 3.6 schematically illustrates the details of the control circuitry, indicated in black, with the pressure acquisition in violet and the optical techniques,

such as LDV and PIV in blue. During the combustion analysis, the exhaust emissions of NOx (Cambustion fNOx 400) and hydrocarbons (Cambustion HFR 400) were recorded and are shown in red. The in-cylinder pressure was measured with a piezo-electric transducer (Kistler 6121) and associated charge amplifier and was monitored on an oscilloscope. Direct in-cylinder HC concentration in the vicinity of the spark plug, with at time resolution of a few degrees of crank angle, was measured using a fast FID (Cambustion HFR 400 with special spark plug kits) and is shown in orange in Figure 3.6.

The in-cylinder air flow velocity measurements were obtained using laser Doppler velocimetry (LDV), comprising an Argon-ion laser and a rotating diffraction grating-based optical unit which delivered the laser beams into the combustion chamber through the side window in the engine liner. Light scattered from silicone oil seeding particles, introduced into the intake manifold, was collected by a photo-multiplier using forward scattering. The resulting electrical signal, processed by a TSI 1990C counter, was interfaced to a personal computer and synchronised with the shaft encoder signal to allow the velocity information to be related to a crank angle index with a resolution of 0.5 degrees.

In this study, the two-dimensional in-cylinder flow field using a vertical plane was characterised using cross-correlation particle image velocimetry (PIV). This measurement plane, along the symmetry plane of the cylinder head, was used to observe the tumbling vortex just below the head; unfortunately, optical access was not available into the pent-roof chamber which prevented monitoring of the flow and mixture distribution in the close proximity of the spark plug. The laser sheet was produced in a vertical plane passing into the cylinder via a 45° mirror and piston window, while the PIV images were obtained through the side windows. For flow visualisation, copolymer-type microballons were used as seeding particles; these have a 50μm mean diameter and were introduced into the intake plenum chamber to allow time for uniform mixing. Due to the limited optical access, the field of view was rather narrow but sufficient to characterise the mean flow and turbulence under the spark plug and to identify the breakdown of the tumble as the piston approaches TDC. The cross-correlation PIV technique used here is based on the recording of two successive and separate images of the flow and the subsequent cross-correlation of these images.

Illumination in this case was provided by a pulsed copper-vapour laser of maximum output 15W and pulse frequency of 10kHZ, focused into a light sheet of 1mm minimum thickness through a system of two lenses and a slit. The images were taken using a Cordin Drum camera which incorporates a hollow drum rotating at speeds corresponding to around 150 Hz and an internal optical system that includes a shutter and a zoom lens (200mm) attached to the laser. On average, 70 consecutive images were recorded on the film rotating inside the drum camera. To convert negative film (Kodak Tmax 400) into positive digital images, the developed film was scanned using a Nikon scanner directly connected to a PC. The images were further processed to obtain the vector flow fields by commercial analysis software. The measurement plane and individual locations for the PIV and LDV measurement points are shown in Figure 3.7.

3.2.3 Engine operating conditions

The general engine operating conditions are outlined in Table 3.4.

Table 3.4: Engine operating conditions

Engine speed	1500 rpm
Manifold pressure	650 mbar
Fuel injection timing (ϕ=1) Closed valve injection Open valve injection	 400°-510° 50°-160°
Fuel	Gasoline (RON 95) and CNG (93% methane)
Injection pressure	Gasoline :3.0 bar CNG : 5.0 bar
Equivalence ratio	ϕ=1.0, 0.9, 0.8 and lean limit

Engine speed is set at 1,500 rpm constant level by the dynamometer controller. The intake manifold pressure is set at 650 mbar using the throttle valve upstream of the plenum chamber and measured by the vacuum gauge connected to the plenum chamber; this condition is one of the typical part load conditions in engine experiments. For this load condition, three equivalence ratios were initially examined:

stoichiometric, ϕ=0.9 and ϕ=0.8 and subsequently leaner mixtures were tested in order to find the lean operating limit of the engine. The equivalence ratio in each case was changed by altering the amount of fuel injected per cycle, and retaining a fixed throttle position. The coolant water and oil temperature were maintained at 80°C.

Four different configurations have been tested:

- Closed-valve injection with gasoline and CNG (conventional intake port).
- Modification of intake port geometry using sleeves for both gasoline and CNG.
- Open-valve injection with CNG (conventional and modified intake port).
- Increased compression ratio (CR:9.0 →11.5).

For each different equivalence ratio, intake port geometry and compression ratio, the ignition timing has been set to give maximum brake torque (MBT). MBT spark timing can be calculated by measuring the mean engine torque or IMEP over a number of cycles, at different spark timing positions, and selecting the crank angle which gives the highest torque value.

3.3 BASELINE COMPARISON OF GASOLINE AND CNG

3.3.1 Combustion characteristics

Figure 3.8 shows in graphical form a comparison in MBT ignition timing between gasoline and CNG combustion at the conditions tested. MBT ignition timing becomes more advanced with decreasing equivalence ratio, corresponding to the lower flame velocities associated with leaner mixtures. MBT ignition timing for CNG was approximately 2 - 5 degrees more advanced than for gasoline, since the laminar flame speed of CNG is lower than that of gasoline. Therefore, for the same turbulence levels, slower burning in the engine is expected with CNG and, therefore, advanced spark timing (Bradley et. al., 1996).

The difference in engine performance for the two fuels is demonstrated in Figure 3.9, in which IMEP and CoV of IMEP have been plotted against equivalence ratio. Figure 3.9

(a) shows the IMEP averaged over 150 cycles for gasoline and CNG at a range of equivalence ratios, ϕ = 1.0, 0.9, 0.8 and 0.76 (CNG only). The IMEP for gasoline is significantly greater than for CNG by between 6 and 24 %. This is due to a number of factors related to the properties of CNG, including its lower heating value and its gaseous state in the intake ports causing a reduction of volumetric efficiency compared to gasoline. The covariance of IMEP in Figure 3.9 (b) has lower values for CNG at all equivalence ratios tested and by considering a value of CoV of IMEP of 5% as the lean limit for stable engine operation, the lean limit for CNG is calculated to be equivalence ratio 0.76 compared to 0.78 for gasoline. This provides confirmation of the wider flammable air-fuel ratio limits for CNG combustion.

The mass fraction burned rates have been plotted for gasoline and CNG in Figure 3.10 for stoichiometric and lean conditions. Under stoichiometric conditions (Figure 3.10 (a)), the rate of mass fraction burned for gasoline is much higher than that of CNG, especially for the 10-80% burn duration, confirming the faster burning of gasoline. However, under lean mixture conditions (Figure 3.10 (b)), when compared to CNG, the 10-80% mass combustion period for gasoline was much longer. This result implies that when the equivalence ratio is approaching the lean limit, the combustion stability for gasoline is getting worse and the total burn duration increases.

24 images of the propagating flame were acquired for both gasoline and CNG at 7°, 12°, 17° and 22° after ignition, until the point at which the flame occupies the whole of the piston window. One of these cases has been selected to represent the flame development and the images are shown in Figures 3.11 and 3.12, with 4 images displayed at each crank angle position.

Analysis of the flame development as visualised at successive crank angle positions, confirms the faster flame propagation in the case of the gasoline fuel at stoichiometric mixture conditions. This is quantified by calculation of the notional enflamed area of each flame, shown for the different equivalence ratios in Figure 3.13 (a) and (b). It is evident that under lean mixture conditions (Figure 3.13 (b)), the growth of the flame area for CNG is much faster than that of gasoline due to the more stable combustion of CNG as the lean limit is approached. The early flame kernel development was also

faster with CNG, with the flame area being 40% larger than gasoline at 12° after ignition under lean mixture conditions.

3.3.2 Engine-out emissions characteristics

In a review of the mechanisms and pathways for engine-out unburned hydrocarbons in spark-ignition engines (Cheng et. al., 1993), six sources have been identified:

- Combustion chamber crevices,
- Absorption and desorption of fuel in oil layers,
- Absorption and desorption of fuel in deposits,
- Flame quenching (both wall quenching and bulk quenching)
- Liquid fuel present in the cylinder, and
- Exhaust valve leakage.

Using data from the literature, the contributions of the above sources to engine-out HC emissions were quantified. For a current production four-cylinder 2-liter engine at steady state under street cruise condition, the crevice mechanism was identified to have the largest contribution to the engine-out HC (~38 percent of the total). Crevices are narrow regions (2-3% of clearance volume) in various parts of the combustion chamber into which the flame cannot enter because of the significant heat transfer to the walls. When the cylinder pressure is increasing during compression and combustion, part of the charge which contains a significant amount of unburned fuel is forced into these crevices; On the other hand, when the cylinder pressure is decreasing during the expansion process, the crevice gas comes out. If the HCs in the crevice region are not oxidised during the expansion and exhaust strokes, they will contribute engine-out emissions. The most significant crevice is the piston-ring-liner crevice region which constitutes more than 75% of the total in-cylinder crevice volume (Kuo et al, 1989). Especially in the case of liquid fuels, when the engine is cold, fuel vaporisation is poor and the fuel tends to stick to the intake ports and the cylinder walls creating films. This makes the vapour mixture around the spark plug so lean that ignition and combustion can become unstable, thus giving rise to more unburned hydrocarbons emissions at cold start. Of particular interest in this project is comparison of the emission characteristics

between a liquid fuel (gasoline) and a gaseous fuel (CNG) in cold and hot phase engine conditions.

Cold start engine-out emissions -An experimental study of hydrocarbon emissions at cold-start was carried out in the single cylinder 4-valve spark ignition engine using both gasoline and CNG. A Cambustion HFR400 fast FID was used to sample the engine-out HC emissions. The FID was equipped with heated sampling lines to prevent condensation of exhaust gases. This system has enabled accurate measurements of HC during engine cold start (25°C) and subsequent warm-up; the engine speed was kept at 1,000 rpm and the intake manifold pressure at 550mbar. No fuel enrichment was used and the injected equivalence ratio (ϕ=1.0) remained constant throughout the experiment. The spark timing was kept at the steady state MBT timing and the in-cylinder pressure was measured in order to calculate IMEP and CoV of IMEP. The engine operating conditions for these tests are summarised in Table 3.5 below.

Table 3.5: Engine operating conditions during cold start fully warmed-up engine operation

Engine speed	1000 rpm
Intake manifold pressure	550 mbar
Coolant and oil temperature	.Cold phase engine : 25°C .Fully warmed-up engine : 80°C
Equivalence ratio	Stoichiometric fuel/air ratio(ϕ=1.0)
Spark timing	MBT

Figure 3.14 shows the HC emissions trace as a function of the number of cycles from start. Blue line represents cold start HC emissions and red line represents hot start HC emissions. When the engine is cold, the crevice volume is larger than that in a hot engine (Kapian and Heywood, 1991). Partly because of that reason, the unburned hydrocarbon engine-out emissions under cold start are high until the engine has warmed-up. In the gasoline case (Figure 3.14(a)), the engine-out HC emissions at cold start can reach 18,000 ppm C3, but fall rapidly after 5 cycles to levels of around 5,000 ppm C3, before gradually decreasing during the warm-up phase. During the early and warm-up phases of the gasoline engine, there are greater emissions of unburned/partially-burned HCs resulting from poorly mixed fuel preparation and a poor

vapour-phase air-fuel mixture. Under cold-start conditions, wall wetting through the intake ports into the cylinder may cause an appreciable amount of the injected fuel to drain into locations such as the piston top-land crevice, becoming a significant source of HC emissions. The importance of the piston top-land crevice to HC emissions is well understood and has been described by Cheng, 1993. Figure 3.14(b) shows engine-out HC emissions at cold start (blue line) and warm start (red line) with the engine fuelled by CNG. The level of engine-out HC emissions at cold and warm start conditions was not significantly different and in both cases much lower than gasoline. Since CNG is fully vaporised at injection, there is no chance of port wall wetting which is responsible for the higher HC emissions after fuel injection in a cold engine. Figure 3.15 shows 35 consecutive pressure traces of a cold and a fully warmed-up engine. In the case of cold gasoline engine (Figure 3.15 (a)), several misfired and partially burned cycles were detected due to a poor vapour-phase air-fuel mixture near the spark plug at the time of ignition. Evidence of this is the considerable mass of unburned hydrocarbons emitted during these cycles (Figure 3.15 (a)). Figure 3.15 (c) shows pressure traces of CNG engine at cold start. Comparing with the warm phase pressure traces (Figure 3.15 (d)), it is clear that cyclic variations are much higher in the cold phase CNG engine. This is may be due to piston expansion during engine warm-up. Kaplan and Heywood (1991) calculated the piston expansion rate during the engine warm-up time and concluded that there is a substantial decrease in the piston top land crevice volume. Depending on the test condition, the piston/liner clearance under warm conditions decreases rapidly up to 70% of the cold-start clearance. Table 3.6 below summarises the results of the pressure analysis.

Table 3.6: Comparison IMEP and CoV of IMEP between cold and warm conditions with gasoline and CNG

	Gasoline		**CNG**	
	Cold start	Warm start	Cold start	Warm start
IMEP (bar)	0.8	2.04	1.34	1.76
CoV of IMEP(%)	100.4	5.2	43	4.8
Mean Max. Pressure (bar)	11	19	12	14

Warmed-up engine-out emissions -Figure 3.16 shows engine-out emissions for both the natural gas and gasoline engine while varying the equivalence ratio at 1500 rpm part load condition. The test engine was fully warmed–up through the preheating process of the cooling water and oil temperature reaching to 80°C. Over the equivalence ratio range tested in the natural gas engine, UHC are lower and NO_x are lower. At the stoichiometric air-fuel ratio, the natural gas engine emits 33% lower UHC and 32% lower NO_x. The lower UHC emissions with natural gas are probably due to the high combustion efficiency associated with the fully vaporised fuel. On the other hand, the lower NO_x emissions in the natural gas engine are believed to be due to the lower peak cylinder pressures (Table 3.7). Lower peak cylinder pressures result in lower peak burned gas temperatures, and hence lower NO_x formation rates.

Table 3.7: Mean maximum pressure for gasoline and CNG

Equivalence ratio	Gasoline	CNG
	Mean maximum pressure (bar)	Mean maximum pressure (bar)
ϕ=1.0	27	22
ϕ=0.9	23	20
ϕ=0.8	20	18

3.4 Effect of intake port geometry

3.4.1 In-cylinder flow characteristics

The in-cylinder flow motion within internal combustion engines fundamentally affects engine performance and emissions. Modern spark-ignition engines with four valves per cylinder exhibit favourable characteristics with regard to power output and exhaust emissions and this has been attributed, in part, to the turbulence enhancement resulting from the break down of the tumbling motion generated during the induction stroke. As the piston approaches TDC, the large-scale tumble is believed to break down into

smaller structures and even into relatively homogeneous small-scale turbulence due to severe vortex distortion and shear. The enhanced turbulent flow field promotes rapid burn rate, improved flame propagation and reduced cyclic variations even under the high charge dilution condition required for fuel economy and emission control. In this section, the effects of introducing sleeves into the intake ports have been investigated through both LDV and PIV measurements.

Centre-line tumble - In order to quantify the effect of sleeved intake ports on the in-cylinder flow, the tumble flow velocity component has been measured during the induction and compression strokes using an LDV. At each point 2000 samples have been acquired within each crank angle window in order to calculate the respective mean and r.m.s. values. Figure 3.17 shows the temporal variation of the ensemble-averaged tumble velocity (Vt), with and without sleeves in the ports, at a location 11mm below the spark plug. During the induction stroke, the sleeved induction ports gave rise to higher tumble velocities with a peak value of 11.1Vp compared to 9.4Vp for the ports without sleeves, due to the blocking of the lower part of the inlet valve passage by the sleeves, which guides most of the flow towards the upper side of the inlet valve in the direction of the exhaust valve; this leads to a stronger tumbling vortex during induction. By BDC, the mean velocities diminish in magnitude but, during early compression, as the piston rises towards TDC, the mean tumble velocities increase again for both sleeved and non-sleeved ports due to vortex compression by the piston. After 240° CA, the mean velocities in the sleeved port case increase steeply to a maximum of about 2.2Vp at 290 ° CA. The reduction of the cylinder volume later in the stroke gives rise initially to higher tumble velocities and later on to lower velocities near TDC of compression, following the tumble vortex breakdown. For the case of the sleeved ports, by 330° CA which is the typical ignition timing for a port injected lean burn engine, the mean velocity reduces to about 1Vp with corresponding 0.9Vp turbulence levels, while for the non-sleeved ports, the mean velocity reaches levels as low as 0.5Vp with 0.7Vp turbulence. This corresponds at 330° CA to a turbulence enhancement of 28% induced by the sleeves, which can be very beneficial to the subsequent combustion process. Unfortunately, no data could be obtained after 330° aTDC due to interference of the piston with the laser beams. Thus, no definite information about the conditions at the spark plug closer to TDC exists, which are

important for consideration of early flame propagation, especially in terms of the comparison of the non-sleeved and sleeved ports. Thus, the rate of breakdown of the tumble vortex into turbulence near TDC and the presence or not of a significant bulk mean flow at the time of ignition capable of convecting the early flame have not been confirmed, offering little support to the observations on flame convection obtained from the flame images (for details see the results on flame development in section 3.4.2).

In-cylinder flow field - Measurements of the flow field in a vertical 2D plane below the spark plug were obtained for the non-sleeved and sleeved ports using the PIV technique. These measurements describe the flow field in a 42mm x 20mm area in the symmetry plane below the spark plug at 30° intervals between 180° to 330° and also at 340° to demonstrate the development of the instantaneous flow throughout the compression stroke. Figures 3.18-3.24 show the PIV results during the compression stroke for the two intake port configurations .

In general, the characteristics of the velocity field in the symmetry plane for the non-sleeved and sleeved ports are sufficiently different to be able to draw some conclusions. At BDC, it appears that the tumble velocities under the exhaust valves with the sleeved ports are higher than with non-sleeved ports, due to the deflection of the intake charge over the top of the valves by the inserted sleeves into the intake ports. After BDC when the inlet valves close, the axial intake air flow decays and the tumble structure starts dominating. During the compression stroke the upward movement of the piston helps to enhance the air motion on the inlet side. At 270° (Figure 3.21) the mean direction of the flow vectors for the non-sleeved ports is diagonally downwards towards the exhaust side, whereas for the sleeved ports the vectors are diagonally upwards again in the direction of the exhaust valves. The flow from the intake valve side of the piston crown is relatively strong, while in the exhaust side the mean flow exhibits small scale structures due to the interaction between the downward flow moving towards the piston and the rapid upwards motion of the tumbling vortex at about the instantaneous piston speed (Rouland and Buchou, 1997). This phenomenon is evident in the case of the sleeved ports. The development of the tumbling vortex after 300° CA shows that, as the aspect ratio of the combustion chamber decreases, the velocity gradients become steeper due to the compressive forces exerted by the moving piston, with associated

higher shear around the point of flow reversal and increased turbulence production. At 300° CA the mean direction of the upwards moving flow for the sleeved ports is inclined towards the intake side, but is separated into two different directions for the non-sleeved ports; one is towards the exhaust side and the other is inclined upwards. The latter weak tumble motion breaks down due to the piston movement at about this crank angle. Later on at 330° CA (Figure 3.23), there is a strong mean component of tumble still present in the case of the sleeved ports and lasting until 340° CA (Figure 3.24), thus creating appropriate charge motion at the time of ignition for flame initiation. These favourable initial conditions for flame development generated by the strong tumble induced by the sleeved ports, are expected to enhance the overall burn rate in the engine to levels approaching that of gasoline combustion.

3.4.2 Combustion characteristics

The previous sections have described the in-cylinder flow motion generated through modifications of the induction system. In this section, the effects of the increased in-cylinder tumble intensity on flame development were quantified by comparing the combustion characteristics of the engine with the non-sleeved and sleeved intake port configurations.

MBT ignition timing – Figure 3.25 shows MBT ignition timings for the non-sleeved and sleeved intake ports. As the equivalence ratio decreases and the mixture becomes leaner, the ignition timing for obtaining optimum engine performance is advanced from 30°CA bTDC to more than 40°CA bTDC. The high tumble configuration (sleeved ports) always required a smaller MBT ignition advance, indicating faster burning rates and reduced cyclic combustion variations. This is also confirmed by the cyclic variability in the IMEP values derived from the pressure measurements (Figure 3.26) and the pressure curves themselves (Figure.3.27 and 3.28).

Analysis of pressure – In order to quantify the effect of tumble strength on the performance of the engine, the indicated mean effective pressure (IMEP) and its coefficient of variation (CoV), defined as the standard deviation divided by the mean,

have been calculated as an average over approximately 150 cycles. Figure 3.26 shows values of the IMEP and CoV of IMEP at 5-6 different equivalence ratios. The results indicate that the IMEP values measured with the sleeved intake ports are consistently higher than those with the non-sleeved ports. This improvement is due to the reduced burning duration when using sleeved ports, which produces less variation in IMEP and allows the spark timing to be retarded thus reducing pumping losses and increasing efficiency (Heywood, 1988; Jeon et.al., 1998). Values of the CoV of IMEP in Figure 3.26 demonstrate that the sleeved ports generating strong tumble can improve significantly the combustion stability around the lean mixture limit. These results are summarised in Table 3.8.

Table 3.8: Comparison of combustion stability under very lean mixture conditions ($\phi = 0.76$)

Intake system	CoV of IMEP (%)
Non-sleeved ports	13.5
Sleeved ports	4.5

The extension of the lean operating limit achieved with the sleeved ports is mainly the result of the enhancement of the mean flow and turbulence by the stronger tumble generated by the sleeved intake ports. Mean flow at the spark plug at ignition has always been considered as the dominant factor for the initial flame developments, while the combined influence of the mean velocity and turbulence on the subsequent burn rate has been emphasised as an important factor in the development of high tumble, four-valve engines (Johansson, 1993; Hadded and Denbratt, 1991). These results have been confirmed through the additional analysis of mass fraction burned and flame image development (Figures 3.29 and 3.30).

A direct comparison of the in-cylinder pressures is presented in Figures 3.27 and 3.28 where there are two pairs of graphs; the in-cylinder pressure variation over 20 consecutive cycles and the mass fraction burned over the same 20 consecutive cycles. All data were obtained under stoichiometric and very lean mixture conditions corresponding to an equivalence ratio of 0.76, which was found to be very close to the lean operating limit of the engine when fuelled with CNG. The 20 in-cylinder pressure and mass fraction burned traces for the non-sleeved ports under lean mixture conditions

are widely spread, indicating poor stability. Closer inspection reveals that in the case of the non-sleeved ports there is a misfire in one cycle, but no misfires were observed in the sleeved ports where the pressure and mass fraction burned traces are closely grouped together. The mass fraction burned values obtained from averaged pressure data over 100 cycles are given in Figure 3.29 and Table 3.9.

Table 3.9: Comparison of mass fraction burnt in crank angle degrees under lean mixture conditions ($\phi = 0.76$)

Intake system	0-10% burnt (CA)	10-80% burnt (CA)
Non-sleeved ports	36°	47°
Sleeved ports	31°	36°

Considering the mass fraction burned rates under lean conditions, again the larger improvement appears to have taken place in the case of the sleeved ports.

Analysis of flame images - Direct flame images at 1,500 rpm, part load conditions for stoichiometric air-fuel (CNG) and lean mixtures (ϕ=0.8) are shown in Figure 3.12 and Figure 3.30 for non-sleeved and sleeved ports at 2°, 12°, 17° crank angle degrees after spark discharge. A comparison of the flame growth rate between the two different port configurations indicates that the faster flame growth occurs with the sleeved intake ports, confirming the anticipated link between charge motion and flame propagation. For both cases, the convection of the early flame is consistently towards the exhaust valves, caused by the prevailing tumble motion.

The qualitative observations about the flame position are supported by quantitative representation of the flame area temporal variation. Figure 3.31 shows the development of the enflamed area measured up to 22° after spark discharge; each area value represents an average over 24 separate flame images obtained from 24 consecutive cycles. There is a clear increase in the enflamed area at the same crank angle position for the case of the sleeved ports, independent of mixture conditions, in good agreement with the pressure analysis.

Overall, the stronger mean flow during flame kernel formation and the higher turbulence levels during flame propagation are jointly responsible for the faster and more stable combustion observed in the case of the sleeved intake ports.

Analysis of fuel concentration – The real-time fuel concentration in the vicinity of the spark plug was measured with a time resolution of a few degrees crank angle using a fast flame ionisation detector. The cycle-to-cycle variations of fuel concentration over 30 consecutive cycles at the spark plug for the non-sleeved and sleeved ports under lean mixture conditions are shown in Figure 3.32. The fuel concentration traces for the sleeved ports are closely grouped together, indicating good combustion stability at this lean mixture condition. The non-sleeved ports case gave rise to the relatively higher cycle-to-cycle variations compared to the sleeved port case at the time of ignition, implying poorer combustion stability under lean conditions. The enhanced tumble motion produced by the sleeved ports is broken down during the compression stroke into strong turbulence, which allows more uniform fuel concentration in the spark gap at the time of ignition, thereby improving combustion stability. Figure 3.33 show the averaged fuel concentration and air/fuel ratio over consecutive 100 cycles. The results show that there is no big difference of the local fuel concentration for the two cases, which implies that there is no charge stratification effect in the spark plug at the time of ignition using the sleeved ports.

3.4.2 Engine-out emissions

The engine-out emissions of unburned hydrocarbons and NO were measured with a fast FID and a NO analyser. Figure 3.34 (a) presents the HC emissions for combustion of CNG across a range of equivalence ratios on the lean mixture side. As the equivalence ratio decreases and the mixture becomes leaner, the HC emissions rise rapidly due to incomplete combustion and/or misfire in a fraction of the engine's cycles. In the case of the sleeved intake ports, the measured HC emissions were reduced significantly, confirming the improved the combustion stability even with leaner mixtures.

Figure 3.34 (b) presents the NO emissions for the combustion of CNG across a range

of equivalence ratios on the lean mixture side. Around the stoichiometric region the NO emissions are notably higher in the case of the sleeved ports, due to the higher in-cylinder pressures and temperatures associated with the faster burning observed under these flow conditions. However, with further extension of the lean operating limit through optimisation of the induction system, the benefits for fuel efficiency and engine-out emissions can be come even greater.

3.5 Effect of injection timing

In order to investigate ways to improve engine performance with CNG, the injection strategy was changed to allow the injection of CNG through open intake valves. The anticipated benefits are the effect on charge motion due to injection of the gas directly into the cylinder, and possible charge stratification effects especially with lean mixtures. In this section, the first part describes the optimisation of the fuel injection timing for improving the combustion characteristics of the lean mixture. The second part describes the improvements possible with lean mixtures, by employing the selected optimum open-valve injection strategy to enhance charge motion and stratification and sleeved ports to enhance the mean flow.

3.5.1 Optimising the fuel injection strategy

In a conventional spark-ignition engine fuelled with gasoline, the fuel is injected onto the back of the closed intake valves. This occurs a relatively long time before the valves open so that a significant fraction of the fuel vaporises before entering the cylinder to allow the nearly gaseous fuel to burn with air more efficiently than if in a liquid form. Since CNG is a gas at room temperature, it requires no such process for vaporisation, therefore it is possible to inject CNG through the open intake valves. It is anticipated that, in this case, the open valve injection can have a beneficial effect on in-cylinder large scale motion and turbulence which influence flame propagation.

Figure 3.35 shows schematically the open-valve injection scheme for the 1500 rpm part-load condition. Three injection timings are shown representing injection at early,

mid and late periods during the opening time of the intake valves. Early injection covers the time from the opening of the intake valves, around intake TDC (0°), to the time when the piston reaches its maximum speed. near 100° aTDC. Mid-stroke injection is approximately symmetrical with the opening of the intake valves–centred around the maximum valve-lift. Late injection ceases just before the intake valves close. Since the intake valves close approximately 50° after BDC, it is expected that at low engine load a significant back-flow from the cylinder into the intake manifold takes place in that period. Therefore at this injection timing, only part of the charge is injected directly into the cylinder, while the rest is residual fresh charge not inducted in the previous cycle. The injection timings are summarised in Table 3.10.

Table 3.10: Summary of injection strategies and timings at stoichiometric mixture condition

Injection strategy	Injection timing (°CA aTDC)
Close-valve injection	400-507
Early open-valve injection	1-108
Mid-stroke open-valve injection	50-157
Late open-valve injection	110-217

Preliminary measurements have been made using stoichiometric mixtures only, in order to analyse the effects on flame propagation and in-cylinder pressure. The use of open-valve injection to improve lean engine operation is subsequently investigated once the basic characteristics with the stoichiometric mixture are known.

Analysis of flame images - Analysis of flame propagation with open-valve injection was performed using the Imacon 468 high speed CCD camera, which is able to acquire up to six images of the propagating flame within a single engine cycle. This permits analysis of the flame throughout its development and investigation of the effects of in-cylinder charge motion on the shape and positioning of the flame. Figure 3.36 shows five such images from each of four cycles, each with different injection timing. The four sets of images demonstrate significantly different flame propagation for the four injection timings. For example, with closed-valve injection the initial convection of the

flame away from the spark plug is towards the exhaust valves (upwards), following the prevailing tumble motion, but with early open-valve injection the convection is towards the right hand side of the cylinder. This difference can be due only to the different charge motion produced by the fuel being injected through the open intake valves at higher-than-atmospheric pressure. Mid-stroke open-valve injection and late open valve injection also exhibit different direction of flame convection. For mid-stroke open-valve injection, early flame convection appears to be in the direction approximately 45° to the expected tumble direction, i.e. 'up and sideways' compared to the 'upwards' convection observed in the closed-valve injection case. The late-stroke injection demonstrates a different characteristic once again, this time the initial convection being in the direction of the exhaust valves, similar to closed valve injection. Complimentary information can be obtained from the position of the notional centre of the instantaneous flame (Figure 3.37) where, for closed-valve and for the three different open-valve injection timings, 20 points are plotted representing the flame centre position at the same crank angle over an equal number of engine cycles. At 7° after spark discharge, the four different injection timings demonstrate individual characteristics in agreement with the observations mentioned above. These results confirm that injection of CNG into the cylinder through open valves produces a significant change in the charge motion around TDC during the initiation and early propagation phase of the flame.

The qualitative observations about the flame position are supported by quantitative representation of the flame area development. Figure 3.38 shows the temporal variation of the enflamed area measured up to 17° after spark discharge; each area value represents an average over 24 separate flame images. There is a clear increase in the enflamed area at the same crank angle position for the case of early and mid-stroke open-valve injection case versus closed-valve late open-valve injection. This confirms that faster flame growth occurs with early and mid-stroke open-valve injection.

Analysis of fuel concentration – The in-cylinder measurement of the hydrocarbon concentration can give considerable insight to engine behaviour. Information of interest includes the A/F ratio of the charge (especially at the time of ignition), the variation of this ratio spatially within one cycle and temporally from cycle to cycle, and the residual

gas fraction of the charge. The post-flame HC signal signature can also be used to elucidate the in-cylinder storage and release HC mechanisms (Cheng *et.al.*, 1993).

Figure 3.39 shows the cycle-to-cycle variation of fuel concentration at the spark plug for altering the injection timing under very lean mixture condition (ϕ=0.76) which was found to be very close to the lean limit of the engine when fuelled with CNG. Figures 3.39 (a),(b),(c) and (d) show the fuel concentration under close- valve , early open-valve , mid-stroke open-valve and late open-valve injection strategies. The 30 consecutive fuel concentration traces of the close-valve case are widely spread, indicating poor stability of the lean mixture. Closer inspection reveals that there are many partial burning cycles in the case of close-valve injection and open-valve late injection. The associated incomplete burning decreases the combustion stability and increases the unburned hydrocarbon emissions during the exhaust stroke. In the case of early open-valve injection, several incomplete burning cycles are observed in Figure 3.39 (b). However, the fuel concentration traces of mid-stroke open-valve injection are closely grouped together, indicating good combustion stability even at lean mixture conditions. Figures 3.40 (a) and (b) show the averaged fuel concentration and air/fuel ratio over consecutive 50 cycles at the various injection timings under lean mixture condition (ϕ=0.76). With the mid-stroke open-valve injection, the average fuel concentration in the spark plug reached 26,330 ppm C3 (equivalent to an air/fuel ratio 21) at the time of ignition while with closed valve injection the averaged fuel concentration in the spark plug reached only 24,854 ppm C3 (equivalent to an air/fuel ratio of 23) at the time of ignition. The results summarised in Table 3.11.

Table 3.11: Cycle averaged fuel concentration and Air/Fuel ratio at the spark plug under lean mixture condition (ϕ=0.76, A/F=21.7)

Injection strategy	FID output (ppm C3)	Air/Fuel ratio
Close-valve injection	24,854	22.6
Early open-valve injection	26,243	21.3
Mid-stroke open-valve injection	26,330	21.2
Late open-valve injection	24,431	23.0

These results indicate that the early and mid-stroke open valve injection do lead to some charge stratification near the spark plug at the time of ignition relative to the close valve injection and late open-valve injection, especially near the lean limit condition. Although the effects of charge stratification are rather small, stable combustion has been realised even under extremely lean conditions.

Regarding the cycle-to-cycle variation and charge stratification effect, mid-stroke open valve injection was found to have the most consistent effect on engine performance comparing other injection strategies since the local air/fuel ratio remained nearly constant over a 30° window (310°-340°). So, from this section onwards, open-valve injection indicates the mid-stroke open valve injection strategy.

3.5.2 In-cylinder flow characteristics

Centre-line tumble - In order to quantify the effect of open valve injection on the in cylinder flow, the tumble flow velocity components have been measured during the induction and compression strokes using a LDV. Figures 3.41 (a) and (b) show the ensemble-averaged tumble velocities (Vt) with open and close valve injection strategies in the case of the non-sleeved ports and sleeved ports, at z=11mm from the spark plug. In general, open valve injection gave rise to higher tumble velocities and turbulence intensities than close valve injection. Especially, between 50° and 160° of the induction stroke, open valve injection with or without sleeved ports gave rise to higher tumble velocity and turbulence intensity compared to those of the close-valve injection case. This is probably due to the pressurised fuel (injection pressure of 5 bar) that is injected during the induction stroke, enhancing the air flow motion at that induction duration (50°-160°). As the piston moves up during the compression stroke, this enhanced flow motion persists to the time of ignition. After 320° CA, the velocity direction for open valve injection seems to change as a result of the centre of rotation shifting towards the apex of the combustion chamber above the measurement point.

These increased tumble velocities and turbulence intensities obtained with open-valve injection directly affect the burn rate during flame propagation. The LDV data are in reasonable agreement with the PIV and flame image analysis results.

In-cylinder flow field – Information about the flow field in a vertical plane below the spark plug was obtained for closed and open valve injection through the PIV measurements. These images describe the flow field in a 42mm x 20mm area in the symmetry plane below the spark plug at 30° intervals between 180° to 330° and also at 340°, to characterise the development of the instantaneous flow throughout the cycle. Figures 3.42 to 3.48 show the PIV measurement results during compression stroke for two different injection strategies.

In general, the results for open-valve injection demonstrate notable differences to those for closed-valve injection. On the other hand, the characteristics of the velocity field for the open valve injection and for the sleeved ports (Section 3.4.1) are similar in many aspects. The mean direction of the flow vectors at 270° CA for open valve injection is diagonally upwards, towards the exhaust valves side like in the sleeved ports case (Figure 3.21), whereas for close-valve injection it is diagonally downwards. The development of the tumbling vortex after 300° CA shows that, as the aspect ratio of the combustion chamber decreases, the velocity gradients become steeper due to the compressive forces exerted by the moving piston, with associated higher shear around the point of flow reversal and increased turbulence production. This trend is especially evident in the case of open-valve injection and sleeved ports. At 300° CA the mean direction of the upwardly moving flow for open-valve injection is slightly inclined towards the intake side, but it is separated into two different directions for the closed valve injection. This implies that the weak tumble motion breaks down due to the piston upward movement in the case of the closed valve injection at about this crank angle. At 330° CA, there is a strong mean component of tumble still present at least up to 340° CA, similar to that observed for the sleeved ports in Figure 3.23. This enhanced flow motion creates an appropriate charge motion and mixture strength at the time of ignition for flame initiation. Figure 3.49 summarises the flow patterns deduced from the LDV and PIV measurements for the four combinations of port configuration and injection strategy examined in this study.

Although the differences between the results for open-valve and closed-valve injection can be partly attributed to the cyclic variation in the flow field, the characteristics are sufficiently different to suggest that the injection of CNG through open valves

influences the charge motion to a degree which may have consequences for flame development, burn rate and engine performance.

3.5.3 Combustion characteristics

Analysis of pressure – Figure 3.50 (a) shows values of IMEP calculated from the in-cylinder pressure data, averaged over 150 cycles, for closed and open-valve injection with sleeved and non-sleeved intake ports. There is a small improvement in IMEP for open-valve injection, with both non-sleeved and sleeved intake ports, although most evident is the increase in IMEP achieved in the case of the sleeved ports. Figure 3.50 (b) shows the CoV of IMEP over 150 cycles. The CoV is reduced for open-valve injection across the whole range of equivalence ratios with lower values obtained in the case of sleeved ports. These results, which are summarised in Table 3.12, demonstrate that the open valve injection strategy can improve significantly the combustion stability around the lean mixture limit.

Table 3.12: Summary of CoV of IMEP under lean mixture condition (ϕ =0.76)

Close-valve injection		**Open-valve injection**	
Non-sleeved ports	Sleeved-ports	Non-sleeved ports	Sleeved-ports
13.5 %	4.0 %	6.3 %	1.8 %

The lean operating limit for stable combustion of the optical engine has been arbitrarily set at CoV of 5%; in production engines this limit is obviously lower (3%). Open valve injection alone allows extension of the equivalence ratio by 0.02 from 0.77 to 0.75 while sleeved ports alone allow extension of the limit by only 0.03 equivalence ratio, from 0.77 to 0.74; combination of the two allows extension of the lean limit by 0.05 equivalence ratio down to 0.72. This is a significant improvement achieved by only minor adjustments to the engine's induction geometry and injection strategy. These results are summarised in Table 3.13.

Table 3.13: Summary of lean operating limit under close- and open-valve injection

Close-valve injection		**Open-valve injection**	
Non-sleeved ports	Sleeved-ports	Non-sleeved ports	Sleeved-ports
0.77	0.74	0.75	0.72

It is interesting to note that the greater improvement in CoV of IMEP and in the lean operating limit is produced by open-valve injection and is due to two factors. The change in the in-cylinder charge motion between the two injection strategies is evident in the flame images, the increased turbulence intensity and the enhanced flame convection leading to better combustion. In addition, open-valve injection is able to produce some charge stratification which improves combustion especially with lean mixtures (Figure 3.40). The richer air/fuel ratio in the vicinity of the spark plug at the time of ignition complemented by the stronger mean flow during flame kernel formation and the higher turbulence levels during flame propagation, are jointly responsible for the faster and more stable combustion observed in the case of open-valve injection of CNG within sleeved intake ports. This charge stratification effect will be investigated in more detail later in the section by the in-cylinder direct HC sampling technique using the fast FID analyser.

A direct comparison of the in-cylinder pressure development during the various test cases is presented in Figure 3.51 (a). All data were obtained under very lean mixture conditions, at an equivalence ratio of 0.76, which was found to be very close to the lean operating limit of the engine when fuelled with CNG. The 20 in-cylinder pressure traces for the close-valve injection with non-sleeved ports are widely spread, indicating poor stability at this lean mixture condition. Closer inspection reveals that in the case of the close-valve injection with non-sleeved ports there is a misfire in one cycle, but no misfires were observed in the other three cases where the pressure traces are closely grouped together. The mass fraction burnt values obtained from averaged over 150 cycles pressure data are summarised in Table 3.14.

Table 3.14: Summary of ignition angle (mass fraction burnt) for four test cases under lean mixture conditions

Injection strategy	0-10% burnt (CA)	10-80% burnt (CA)
Close-valve injection with non-sleeved ports	36°	47°
Open-valve injection with non-sleeved ports	33°	42°
Close-valve injection with sleeved ports	32°	36°
Open-valve injection with sleeved ports	31°	34°

Considering the mass fraction burnt rates under lean conditions, the larger improvement appears again to take place in the case of open-valve injection with sleeved ports.

Analysis of flame images - Direct flame images at 1,500 rpm, part load conditions for a stoichiometric air-fuel (CNG) mixture are shown in Figure 3.52 for close- and open-valve injection with non-sleeved ports and sleeved ports, at 2°, 12°, 17° crank angle degrees after spark discharge. Initial inspection of the flame images for open-valve injection with non-sleeved ports identifies significant differences in the flame structure and flame development relative to the closed-valve injection case. A comparison of the flame growth rates between the various cases indicates that the faster flame growth occurs with open-valve injection and sleeved intake ports, confirming the anticipated link between charge motion and flame propagation. For closed-valve injection, the convection of the early flame is consistently towards the exhaust valves, caused by the prevailing tumble motion. For open-valve injection, on the other hand, early flame convection appears to be in a direction approximately 45° to the expected tumble direction, i.e. 'up and sideways' compared to the 'upwards' convection observed in the closed-valve injection case. These results confirm that injection of CNG into the cylinder through open valves can produce a significant change in the charge motion around TDC affecting the early propagation phase of the flame.

The qualitative observations about the flame position and development are supported by quantitative representation of the flame area temporal variation. Figure 3.53 shows the development of the enflamed area measured up to 17° CA after spark discharge; each area value represents an average over 24 separate flame images. There is a clear increase in the enflamed area at the same crank angle position for the case of open valve injection independent of the intake system configuration.

Analysis of fuel concentration – The cycle-to-cycle variations of fuel concentration over 30 consecutive cycles at the spark plug are presented in Figure 3.54 for open and closed valve injection with sleeved and non-sleeved port configurations under very lean mixture condition (ϕ=0.76). Fuel concentration traces of sleeved ports (c) are closely grouped together, indicating good combustion stability at this mixture condition

compared to the non-sleeved ports (a). This is due to the sleeved ports generating strong tumble which improves the combustion characteristics under lean mixture conditions. In the open valve injection cases (b) and (d) are closely grouped together and show the relatively higher mixture concentration compared to the close-valve injection cases (a) and (c). The open-valve injection case with sleeved ports (d) shows relatively higher mixture concentration and lower cycle-to-cycle variations compared to the other three cases. Figure 3.55 shows the averaged fuel concentration and air/fuel ratio over consecutive 50 cycles for the two injection timings and intake systems under lean mixture conditions. In the case of closed valve injection with non-sleeved ports, the average fuel concentration in the spark plug was 24,500 ppm C3 (equivalent to an air/fuel ratio 23) at the time of ignition while with open valve injection and sleeved ports the averaged fuel concentration in the spark plug reached 26,675 ppm C3 (equivalent to an air/fuel ratio of 21) at the time of ignition. These results are summarised in Table 3.15.

Table 3.15: Summary of successive cycles of fuel concentration at the time of ignition in the spark plug (overall A/F ratio: 22 ± 0.5)

Injection strategy	FID output (ppm C3)	Air/Fuel Ratio
Close-valve injection with non-sleeved ports	24,854	22.6
Open-valve injection with non-sleeved ports	26,330	21.2
Close-valve injection with sleeved ports	25,315	22.4
Open-valve injection with sleeved ports	26,950	20.6

These results reveal that the open-valve injection strategy does lead to some charge stratification near the spark plug at the time of ignition relative to the close-valve injection case independent of the intake system. The stratification is evidenced in the lower average air/fuel ratio (~20.9) obtained in the two open valve cases relative to the nominal air/fuel ratio of 22±0.5.

3.5.4 Engine-out emissions

In Figure 3.56 (a), the hydrocarbon emissions are shown for both closed and open-valve injection strategies and the two induction configurations as a function of equivalence ratio. In general, leaner homogeneous mixtures give lower HC emissions until combustion quality becomes poor (and eventually a misfire occurs), when HC emissions rise sharply and engine operation becomes erratic. In stoichiometric condition, open-valve injection shows higher hydrocarbon emissions compared to close-valve injection. That is probably due to the richer mixture near the spark plug at the time of ignition through the charge stratification induced by open-valve injection, resulting in higher hydrocarbon emissions. As the mixture becomes leaner, open-valve injection shows much lower levels of HC emissions relative to close-valve injection. In the case of open valve injection with sleeved ports, the measured HC emissions were reduced even further as a result of the combined effect of the limited charge stratification and enhanced flow motion in improving the combustion stability of leaner mixtures.

Figure 3.56 (b) presents the NOx emissions for combustion of CNG across a range of equivalence ratios on the lean mixture side. Around the stoichiometric region the NOx emissions are notably higher in the case of the sleeved ports, due to the higher in-cylinder pressures and temperatures associated with the faster burning observed under these flow conditions.

However, towards the lean operating limit, the NOx levels in the case of open-valve injection with sleeved ports drop significantly to levels similar to those for the non-sleeved ports. It is important also to note that the use of CNG allows extension of the engine's lean operating limit to about 0.72 with associated further reduction of the NOx engine-out emissions

3.6 Effect of compression ratio

Natural gas has a higher resistance to knock than gasoline and can operate at higher compression ratios. The increase in compression ratio gives higher torque and thermal efficiency, compensating to some extent for the loss in power resulting from decrease in fuel energy density and volumetric efficiency with the use of natural gas. However, this increase in compression ratio can have undesirable effects such as the increase in the exhaust oxides of nitrogen and hydrocarbon emission levels (Adam, 1985; Fleming and O'Neal, 1985).

In this study, a compression ratio investigation was carried out using natural gas as fuel to determine its potential for improving engine performance by taking advantage of the high octane number of natural gas. The in-cylinder pressure and NOx emissions for the 1500 rpm part load case were compared directly with results of the original compression ratio (10.5). In all cases, the ignition timing was adjusted to MBT at each equivalence ratio.

3.6.1 Variation of compression ratio

The compression ratio is defined as the ratio of the maximum to minimum cylinder volume:

$$Cr = \frac{Vd + Vc}{Vc} = 1 + \frac{Vd}{Vc}$$

Where,

Vd = Displacement volume

Vc= Clearance volume

In order to increase the compression ratio, the geometry of the engine was altered by reducing the clearance volume of the cylinder. This was achieved with little difficulty by removing the spacing shims of smaller thickness. The compression ratio of the engine could thus be increased from 10.5 to 11.5. On the other hand, the compression

ratio was decreased from 10.5 to 9.0 through introducing of an extra gasket between the cylinder head and block. Table 3.16 showed the comparison of clearance volume with varying compression ratio. The displacement volume of the experimental engine was 498 cc.

Table 3.16: Comparison of clearance volume with 3 different compression ratios

Compression ratio	Clearance volume (cc)
Cr 9.0	62
Cr 10.5	52
Cr 11.5	47

3.6.2 Combustion characteristics

Analysis of pressure – Figure 3.57 shows the motoring pressure variation for three compression ratios. The increase in motoring pressure with increasing compression ratio can be explained by the decreasing clearance volume. Engine performance, as measured in terms of IMEP for the three different compression ratios, is compared in Figure 3.58. Changing the compression ratio 9.0 to 11.5 resulted in part-load performance improvement by 21%. This result implies that if the compression ratio is optimised for natural gas, the performance of the engine does not necessarily have to be inferior to that of the equivalent gasoline engine.

Figure 3.59 shows the mass fraction burn rates. In increasing the compression ratio, there are a number of factors which contribute to an increase in the burn rate such as:

- Higher gas temperatures
- Smaller distance from spark plug to wall
- Reduced residual gases

Analysis of flame images – Figure 3.61 shows three sets of flame images at 1500 rpm part load for the three different compression ratios and a stoichiometric air-fuel

mixture. Analysis of the flame development, as visualised at successive crank angle positions, has revealed the faster burn rate achieved in the case of the higher compression ratio. This effect is quantified by calculation of the notional enflamed area of each flame in Figure 3.60 where the expected trend of faster flame propagation at the higher compression ratio is confirmed.

3.6.3 Engine-out emissions

NO is formed in the cylinder of the engine by the high temperature (>1800 K) reactions between oxygen atoms and nitrogen molecules present in the air and the few present in the fuel. The oxygen atoms are formed by thermal dissociation of oxygen containing species in the combustion gases, particularly oxygen. Within the combustion chamber, local gas temperature and oxygen concentration are the determining factors of NO formation.

Figure 3.62 shows NO and cylinder pressure for altering the equivalence ratio from stoichiometric to lean under part load at 1500 rpm, compression ratio 11.5:1. The cycle-to-cycle NO emissions can easily be seen following the exhaust gas pulsations recorded on the cylinder pressure trace. Only 23 engine cycles are displayed in Figure 3.62 but 100 cycles were recorded for statistical evaluation at this condition. As the equivalence ratio decreases and the mixture becomes leaner, the NO emissions decrease due to the lower gas temperature of the lean mixture. The peak NO production occurs somewhat lean of stoichiometric. That is explained by the increasing oxygen concentration that initially offsets the falling gas temperatures.

The emissions of oxides of nitrogen for all compression rates and all equivalence ratios tested are shown in Figure 3.62. The results of this study showed the dependence of NOx emissions on compression ratio. The increases in NO emissions with increasing compression ratio can be explained by the combined effect of reduced residual gas in the mixture, caused by the reduced the clearance volume, and higher temperature and pressure at the end of the compression stroke. Table 3.17 shows the comparison of the mean maximum pressure and mean NO emission over 100 cycles at the three different

compression ratios. This suggests strongly that higher peak cylinder pressures result in higher peak burned gas temperatures, and hence higher NO formation rates.

Table 3.17: Comparison of mean maximum pressure and mean NO emissions with varying compression ratio (ϕ=1.0)

Compression ratio	Mean maximum pressure (bar)	Mean NO emissions (ppm)
Cr 9.0	23	800
Cr 10.5	27	1380
Cr 11.5	34	1800

3.7 Conclusions

Investigation of the flow and combustion in a single-cylinder four-valve spark-ignition engine with port CNG injection revealed the following:

- In agreement with previous studies, combustion of CNG compared to gasoline gives rise to:
  - ♦ Advanced MBT ignition timing due to the lower flame speed of CNG.
  - ♦ Significantly lower IMEP, but improved cyclic variation in IMEP
  - ♦ Significantly lower HC and NOx emissions
  - ♦ Significantly lower cold start HC emissions

- The combination of sleeved intake ports with open-valve fuel injection increased the directional flow during early induction, generating a stronger tumble flow during compression and higher mean velocities and turbulence levels near the spark plug at the time of ignition.

- The enhanced tumble strength produced by the sleeved ports, which was assisted by the injection of CNG against open valves, achieved strong convection of the flame away from the spark plug during the early flame development and faster flame propagation in the direction of the mean flow during the main combustion period.

- The combination of sleeved intake ports with open-valve fuel injection strategy led to improved by 12% combustion stability (CoV of IMEP) under very lean mixture conditions (ϕ = 0.76) due to the combination of favourable flow conditions and modest charge stratification near the spark plug at the time of ignition.

- Although the use of sleeved intake ports and open-valve injection generated high NO emissions under stoichiometric conditions, as a result of the higher gas temperatures caused by fast burning, at the same time it allowed extension of the lean operating limit with associated lower NO emissions and fuel consumption. This approach offers promise for overall reduction of NO levels in engines fuelled with CNG.

- Due to the high octane number of natural gas, compression ratio could be increased to 11.5. Increase of the compression ratio from 9.0 to 11.5 resulted in part-load IMEP improvement by 21%. This result shows that if the compression ratio is optimised for natural gas, the performance of the engine can be comparable to that of gasoline engines.

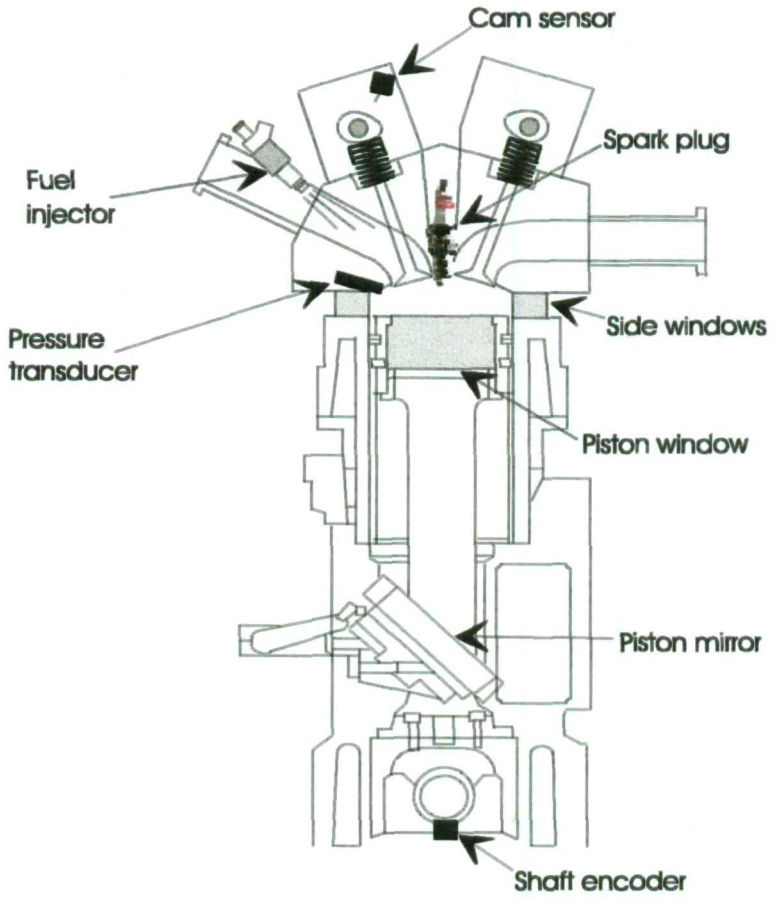

Figure 3.1: Schematic diagram of optical single cylinder engine

Figure 3.2: Photograph of optical single cylinder engine

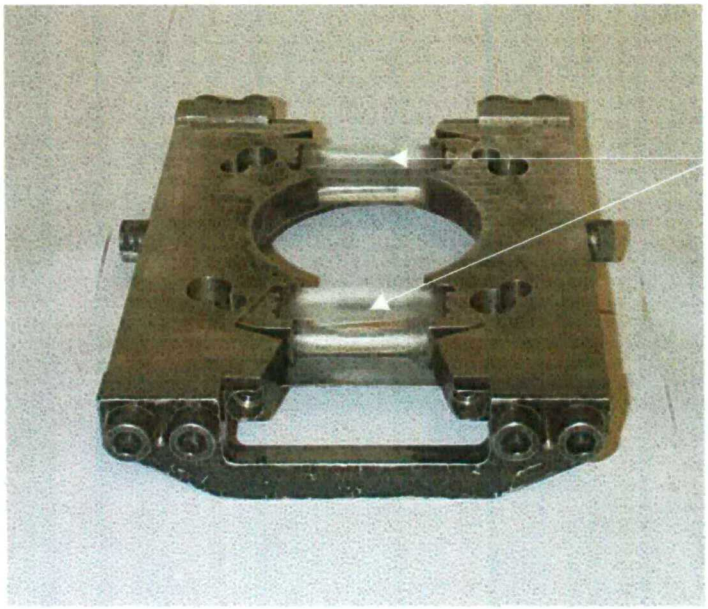

(a)

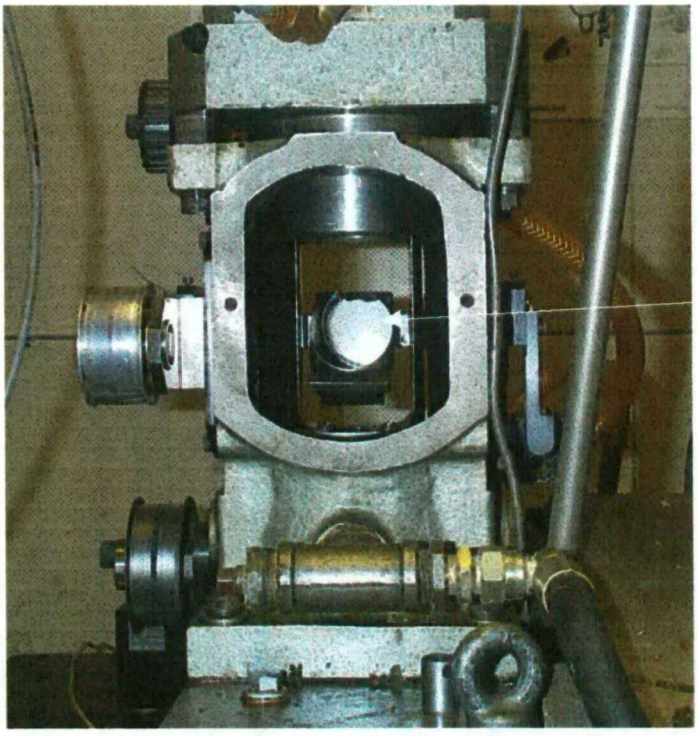

(b)

Figure 3.3: Photograph of the optical access assembly for the test engine

(a) Side window assembly (b) Bottom piston mirror

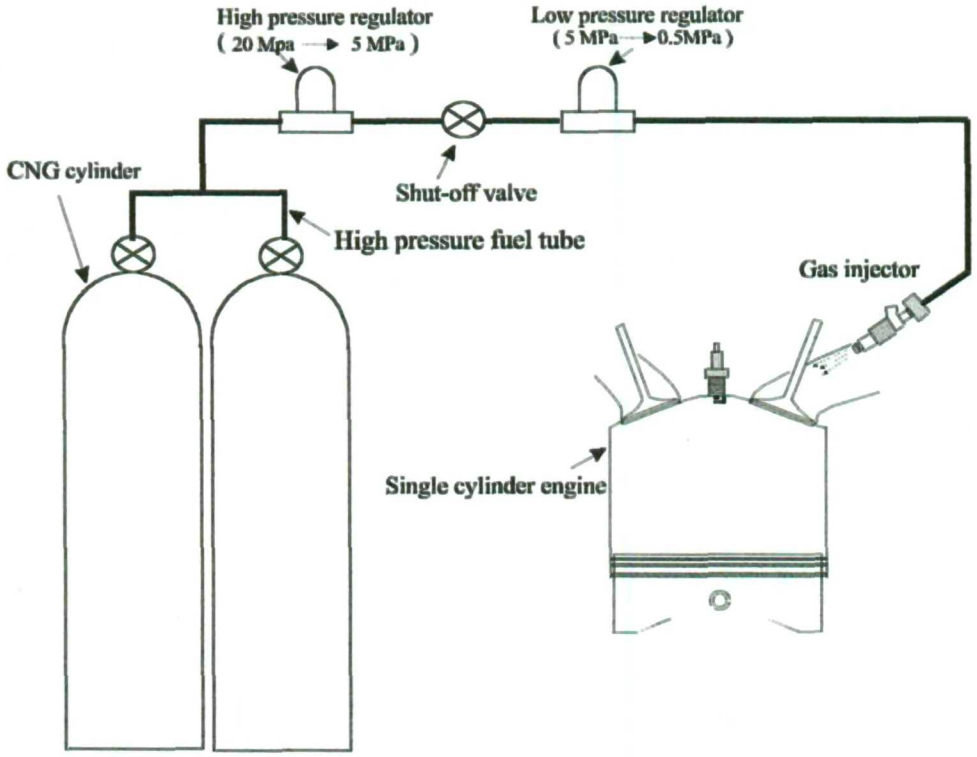

Figure 3.4: Schematic diagram of CNG fuelling system

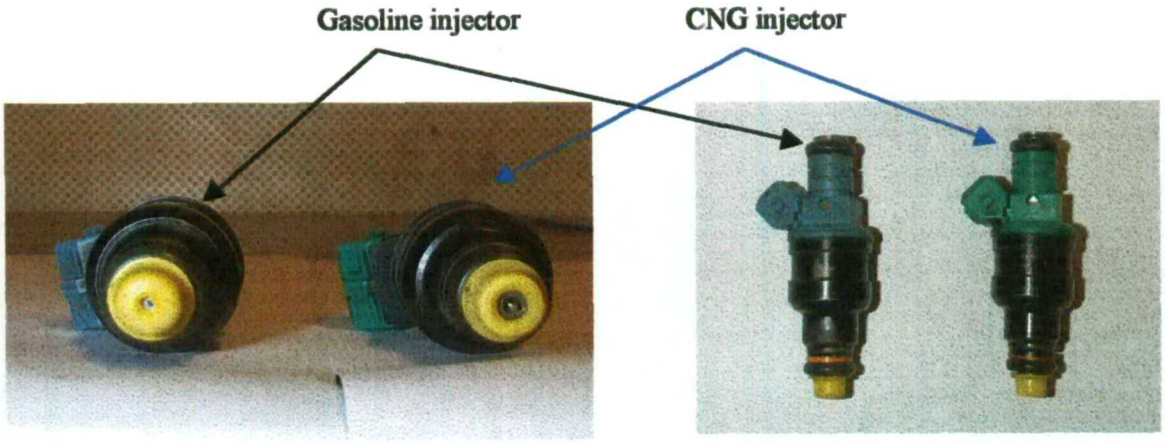

Figure 3.5: Photograph of CNG and gasoline injector

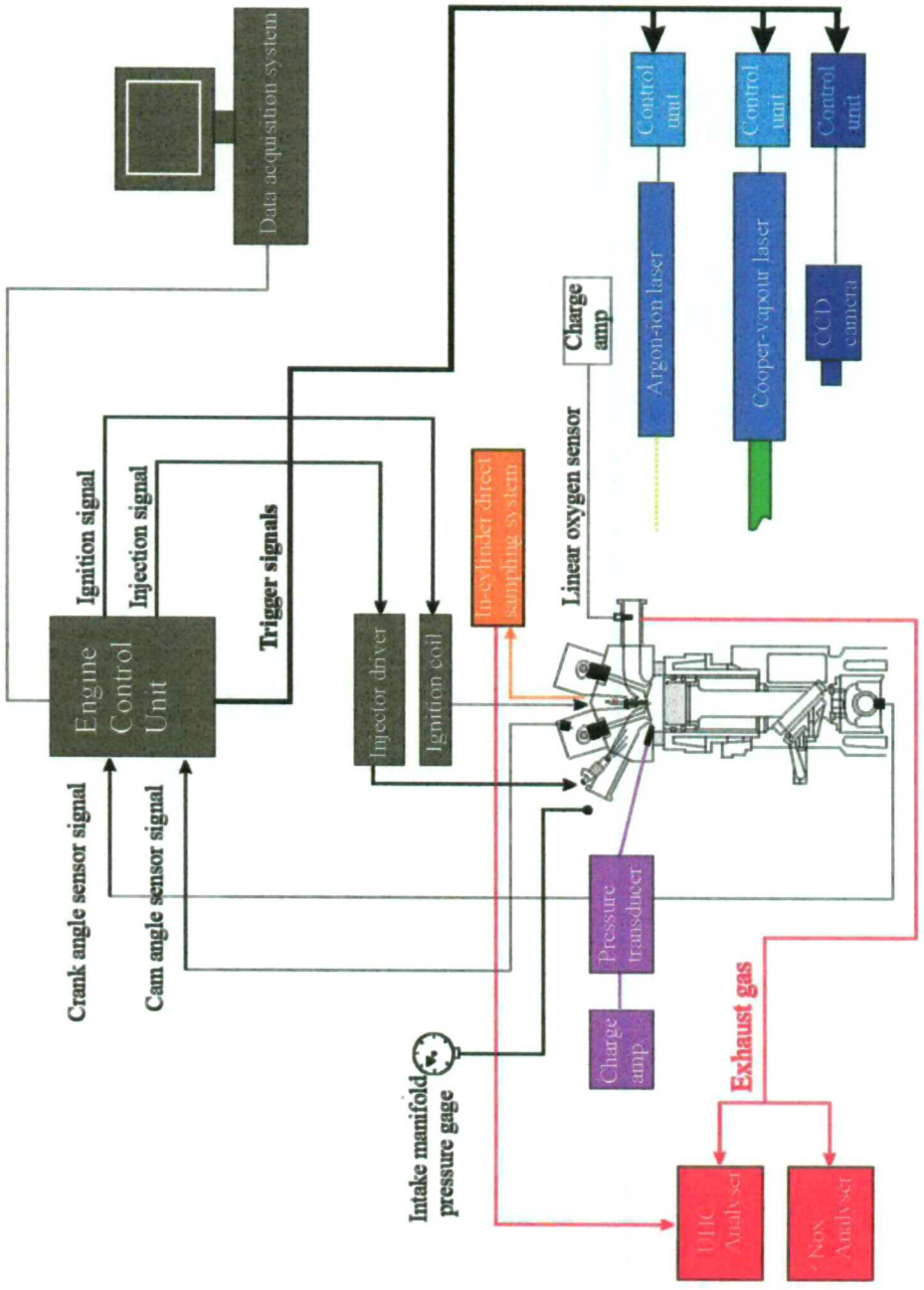

Figure 3.6: Schematic of experimental set-up

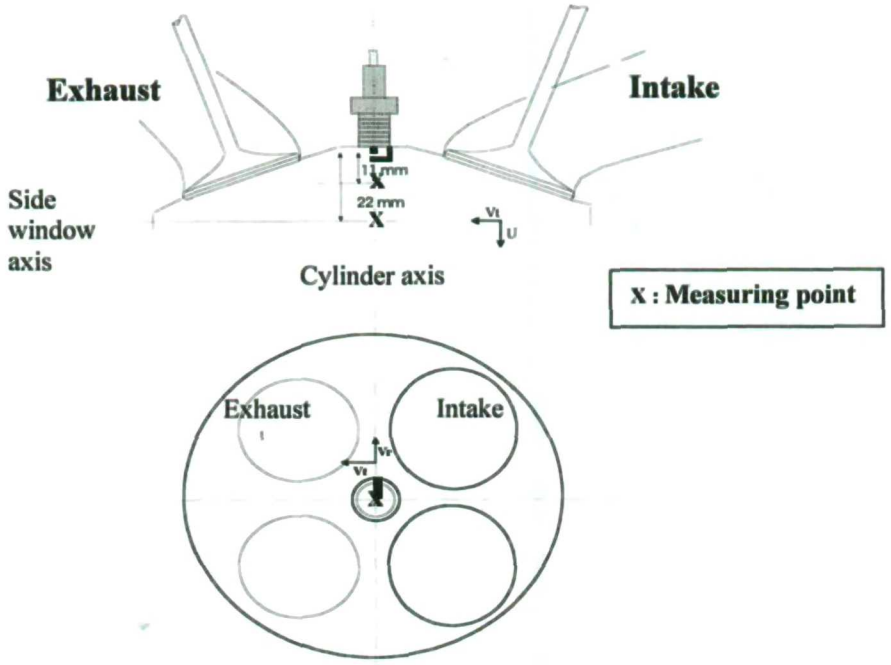

(a)

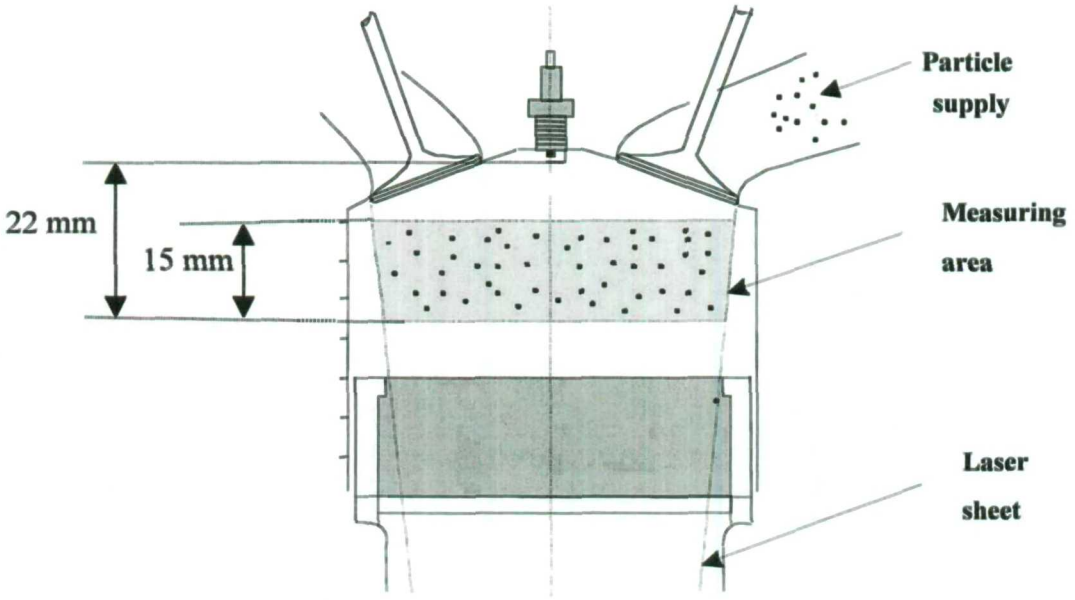

(b)

Figure 3.7: Locations of optical measurements

(a) LDV (b) PIV

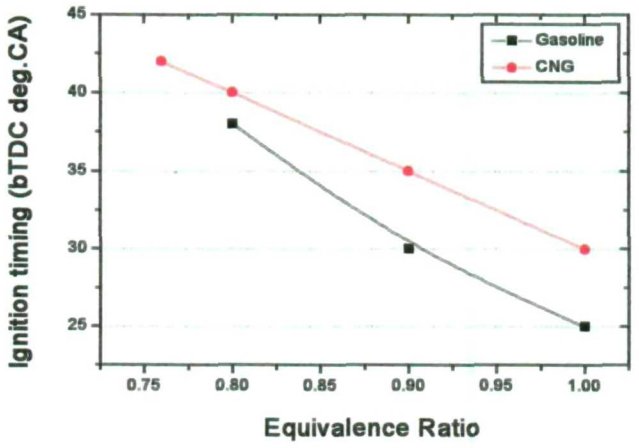

Figure 3.8: MBT ignition timing characteristics of gasoline and CNG

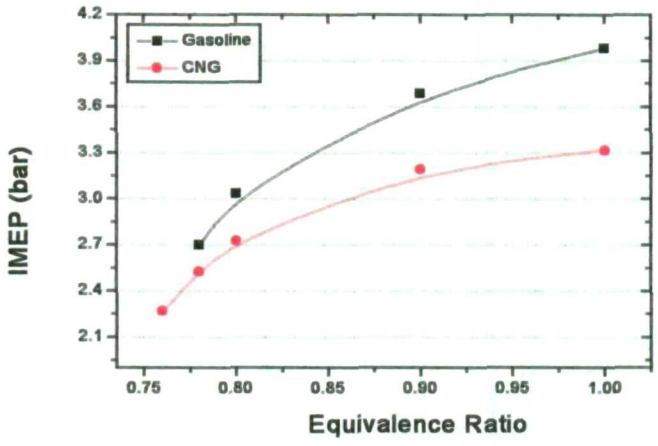

(a)

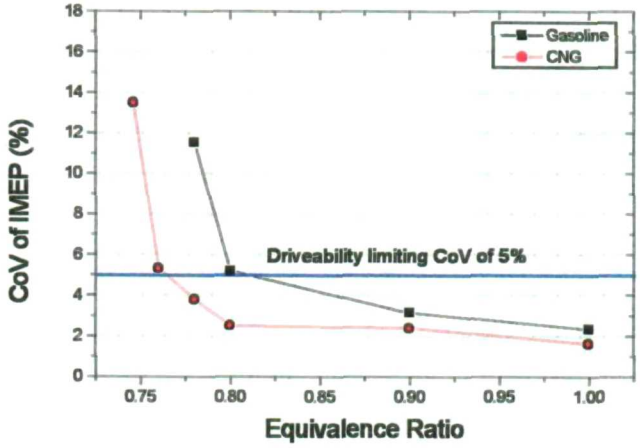

(b)

Figure 3.9: Comparison of IMEP and CoV of IMEP between gasoline and CNG

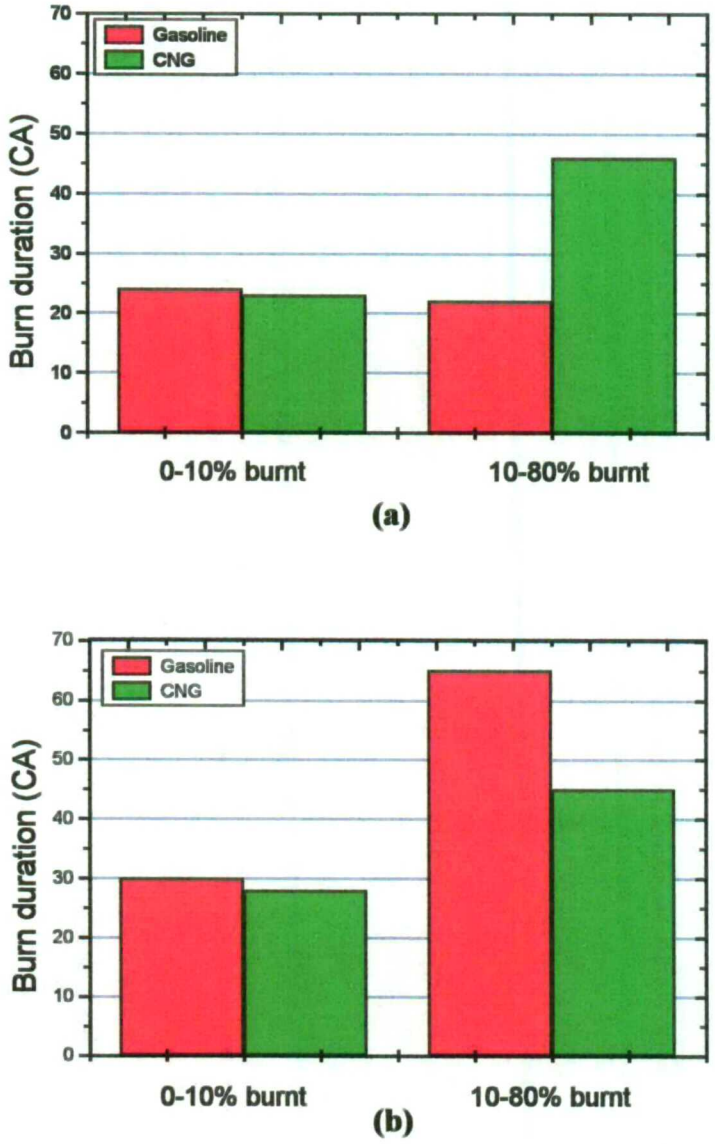

Figure 3.10: Comparison of mass fraction burnt for gasoline and CNG
(a) Stoichiometric condition ($\phi = 1.0$) (b) Lean condition ($\phi = 0.8$)

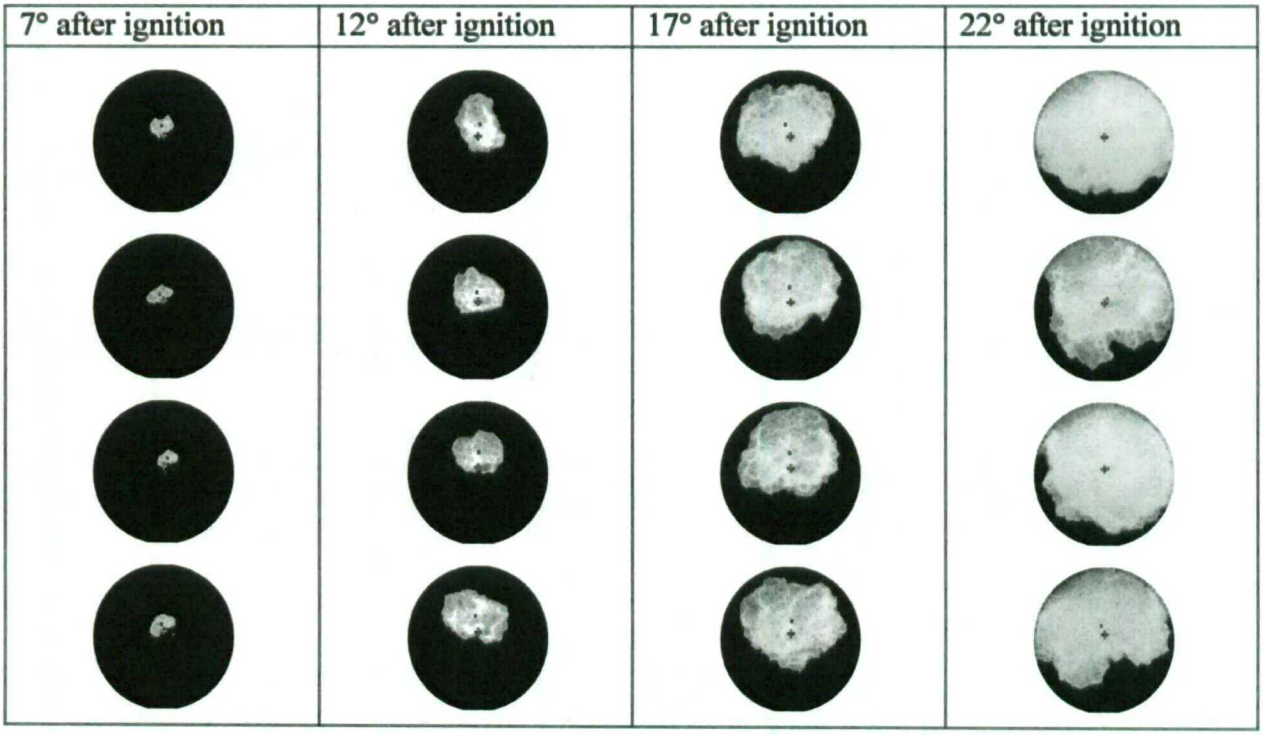

(a)

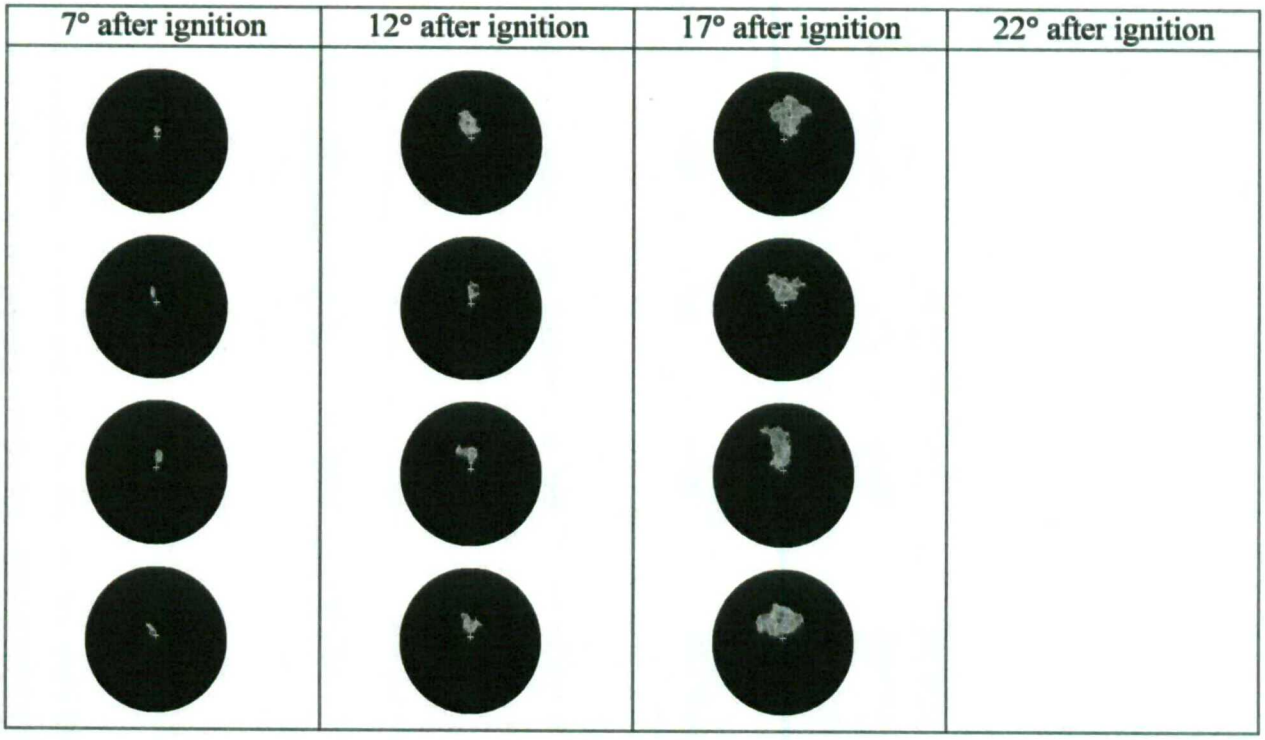

(b)

Figure 3.11: Flame images with gasoline fuel

(a) ϕ=1.0 (b) ϕ=0.8

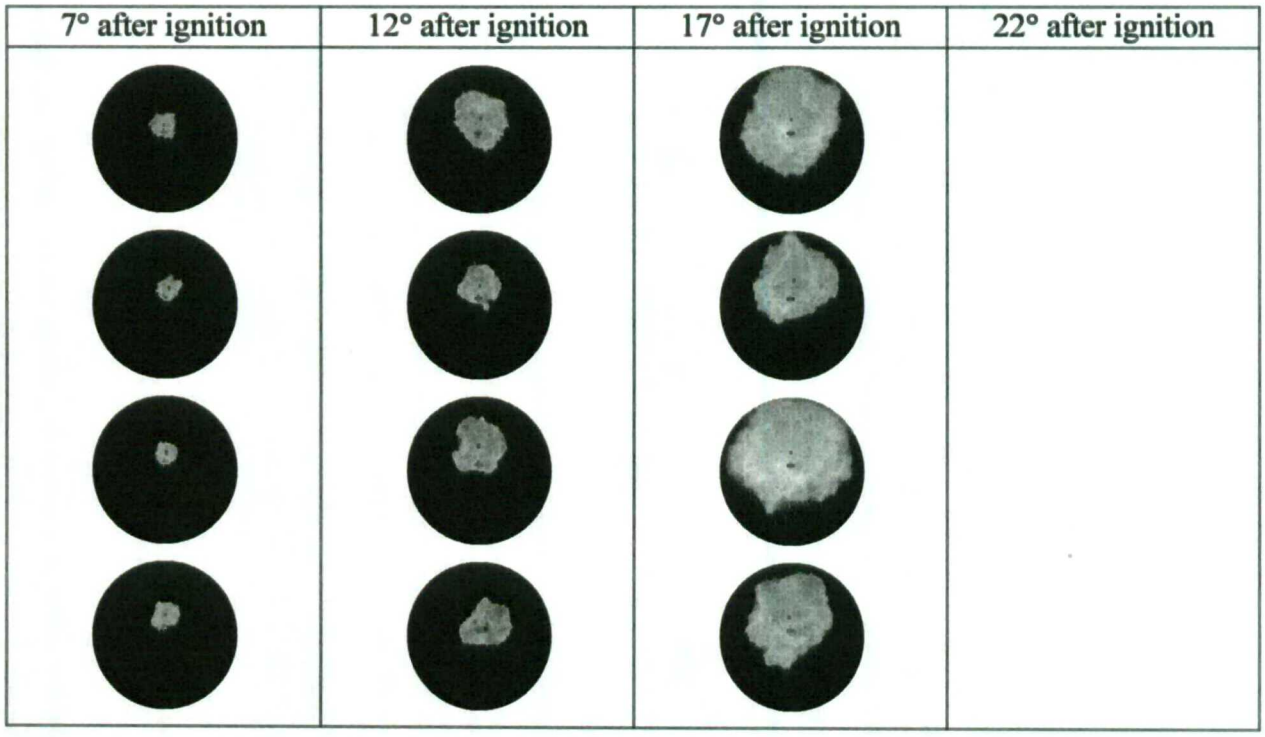

(a)

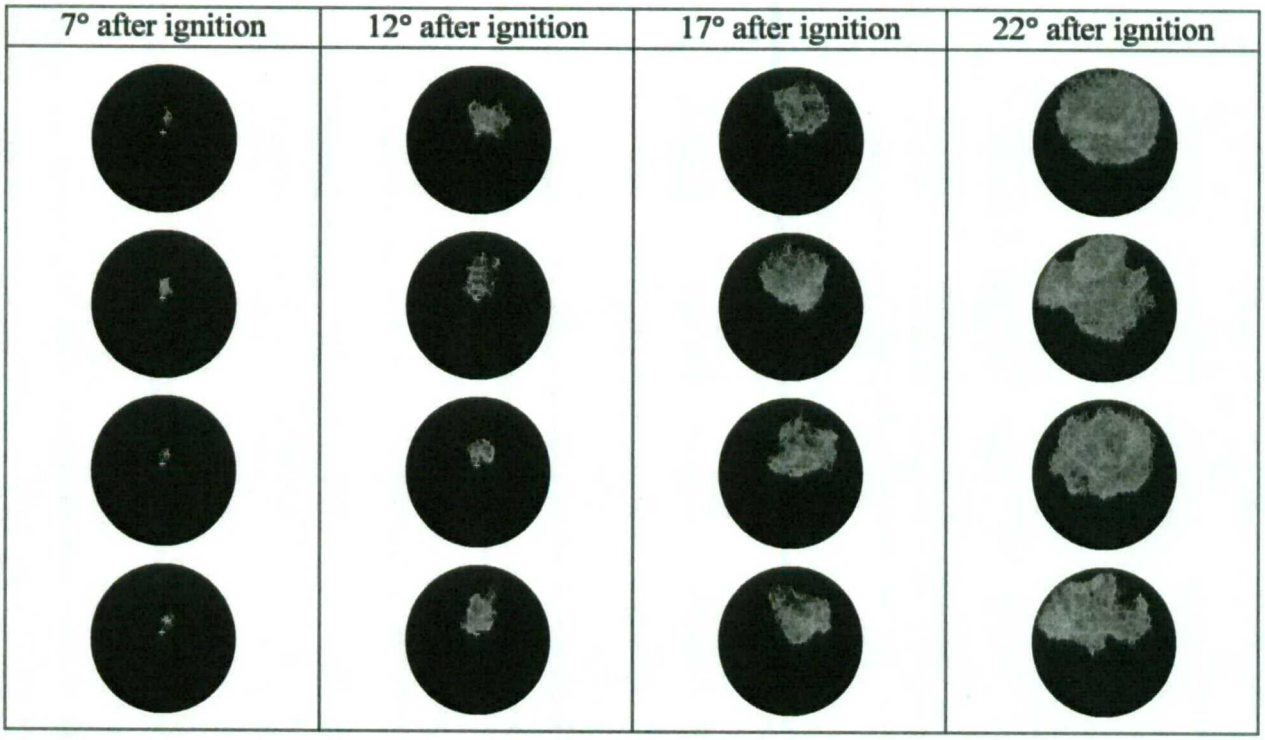

(b)

Figure 3.12: Flame images with CNG fuel

(a) ϕ=1.0 (b) ϕ=0.8

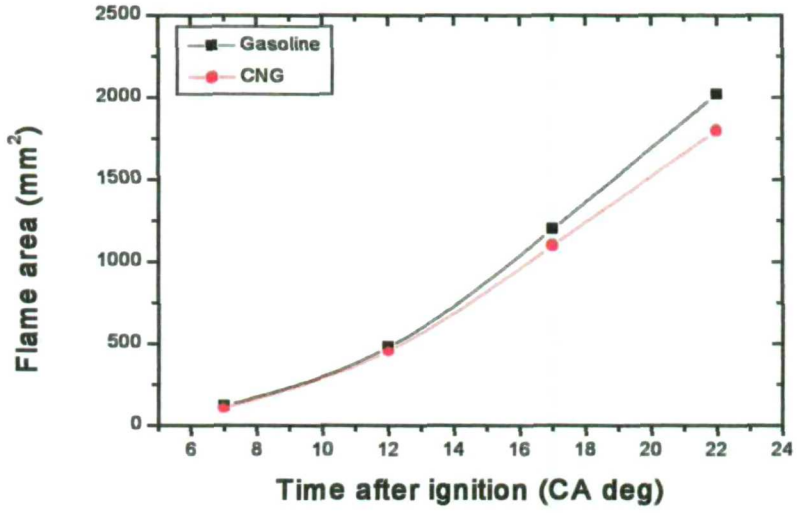

(a)

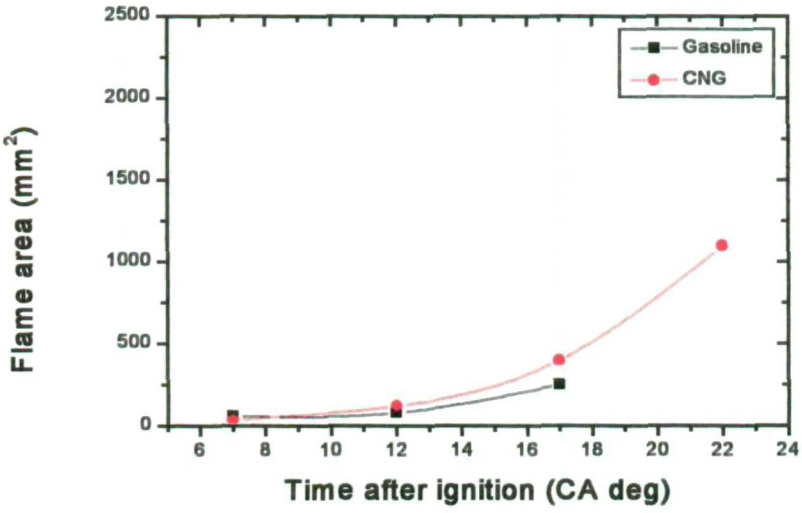

(b)

Figure 3.13: Flame area growth with gasoline and CNG
(a) Stoichiometric condition (ϕ=1.0) (b) Lean condition (ϕ=0.8)

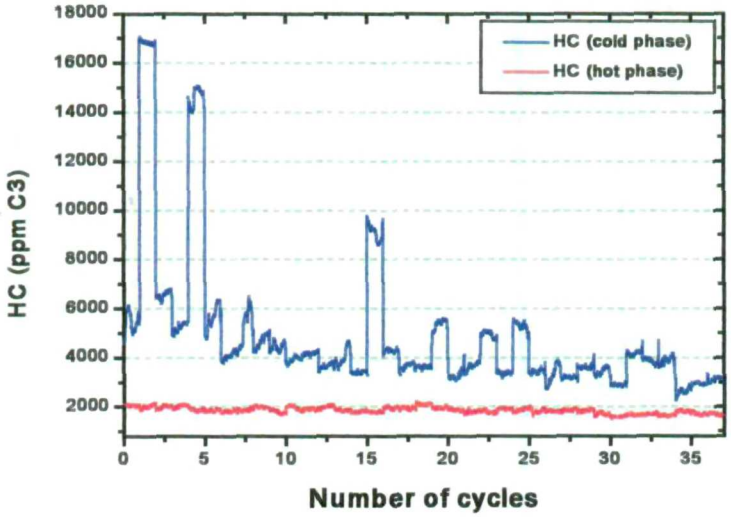

(a)

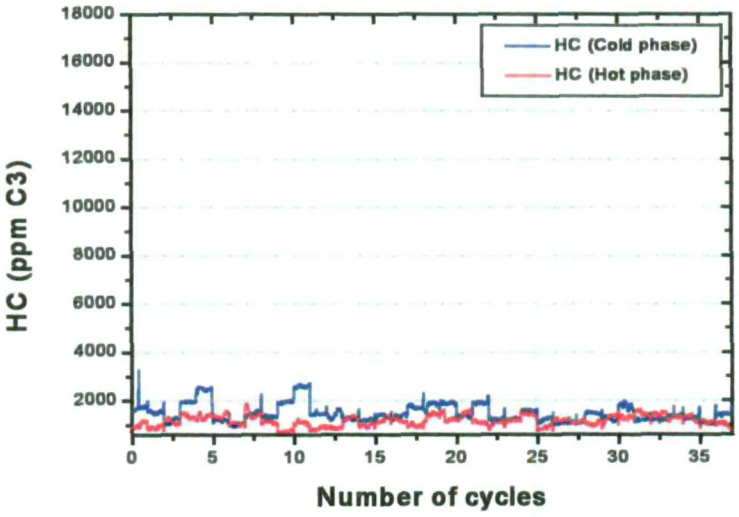

(b)

Figure 3.14: Engine-out HC emissions for cold and warm start engine operation

(a) Gasoline (b) CNG

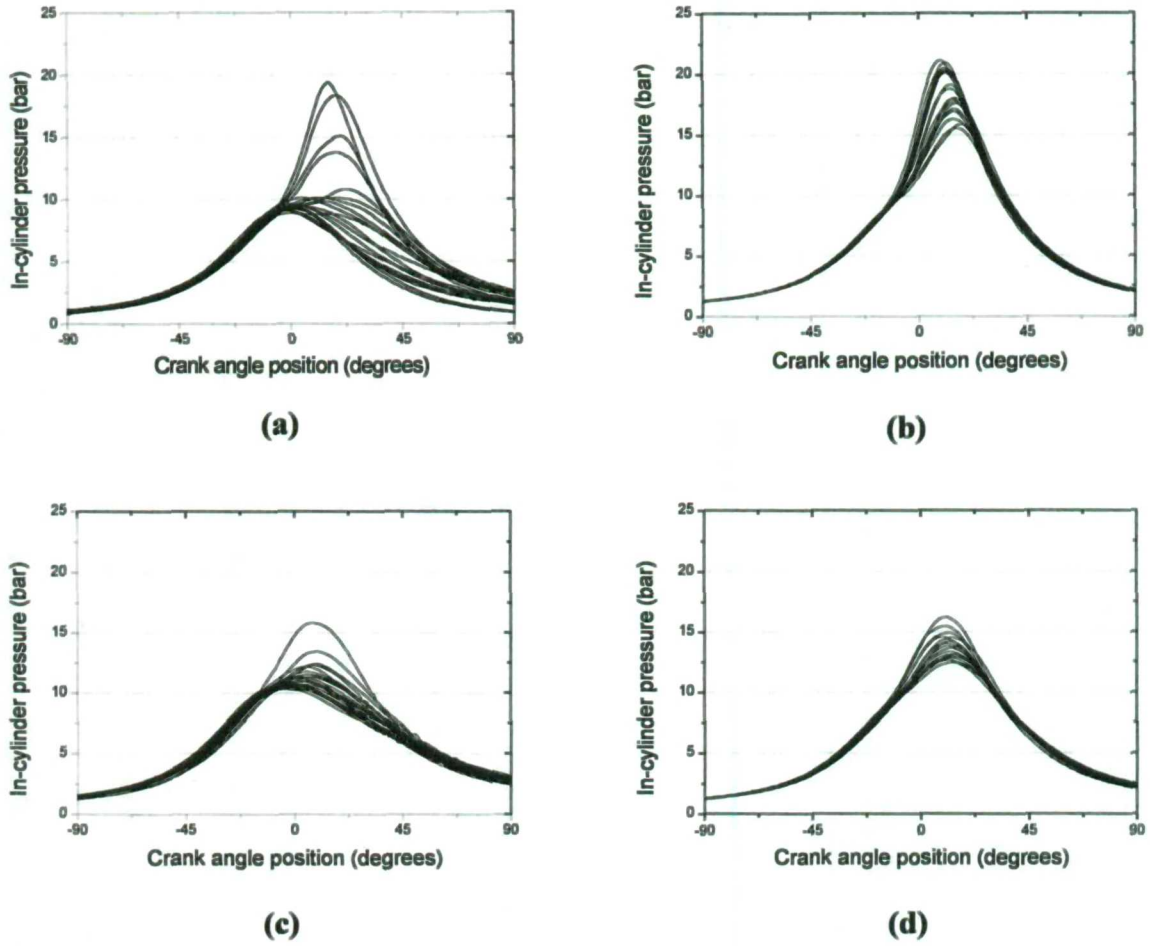

Figure 3.15: Comparison of in-cylinder pressures between cold start and warm start conditions

(a) Cold start with gasoline (b) Warm start with gasoline

(c) Cold start with CNG (d) Warm start with CNG

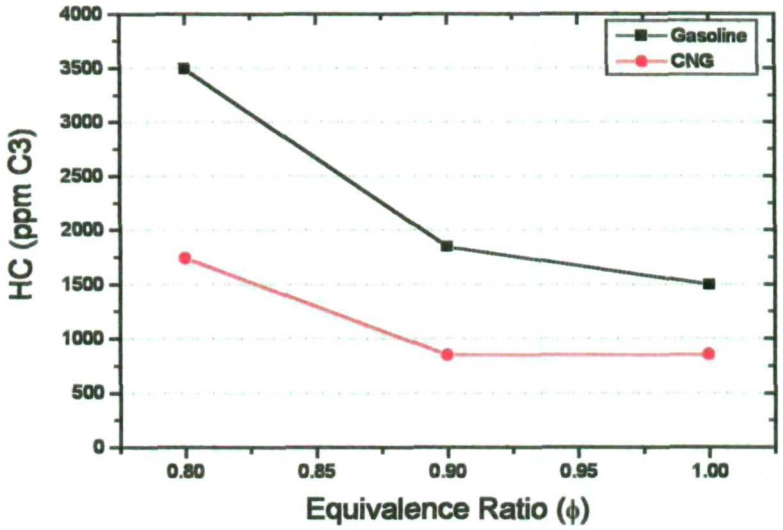

(a)

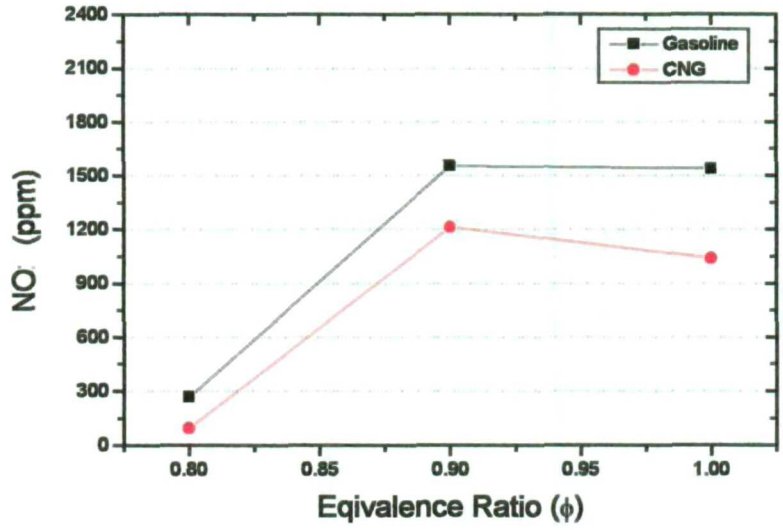

(b)

Figure 3.16: Comparison of engine out emissions between gasoline and CNG
(a) HC emissions (b) NO emissions

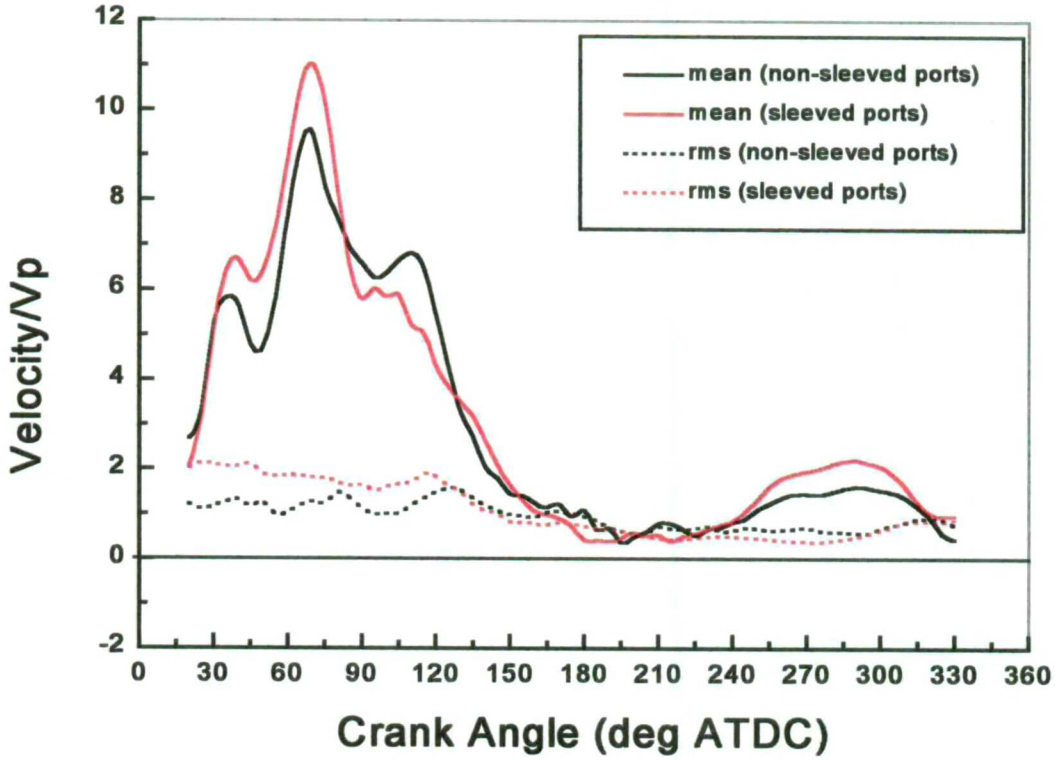

Figure 3.17: Comparison of the temporal variation of the tumble velocity component with the non-sleeved and sleeved ports below the spark plug (z=11mm)

CA=180° ATDC

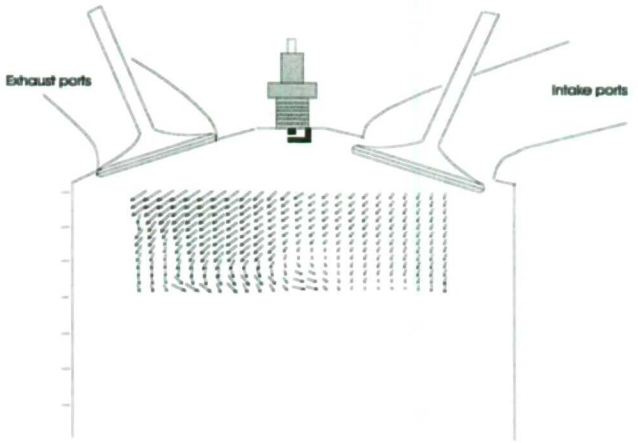

(a)

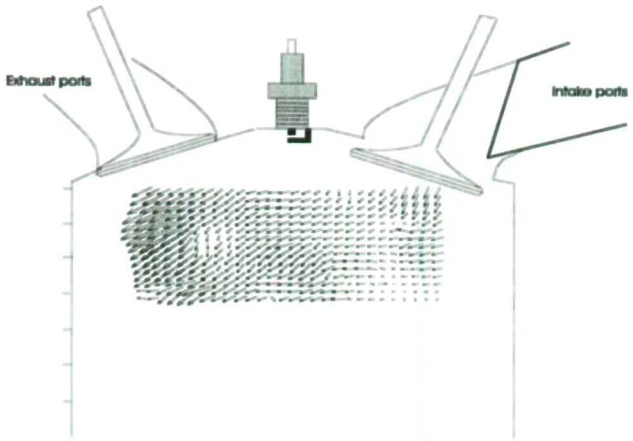

(b)

Figure 3.18: Comparison of in-cylinder flow motion using PIV with non-sleeves and sleeved ports at 180° ATDC

(a) Non-sleeved ports (b) Sleeved ports

CA=210° ATDC

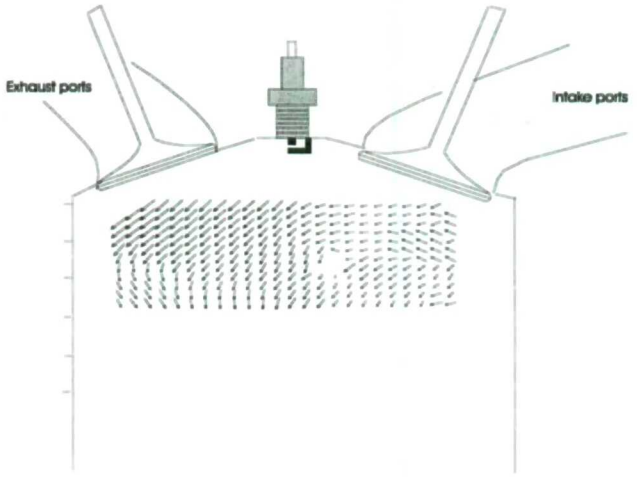

(a)

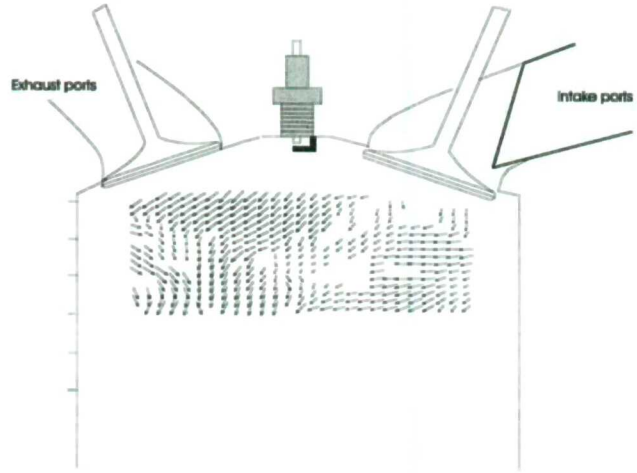

(b)

Figure 3.19: Comparison of in-cylinder flow motion using PIV with non-sleeves and sleeved ports at 210° ATDC

(a) Non-sleeved ports (b) Sleeved ports

CA=240° ATDC

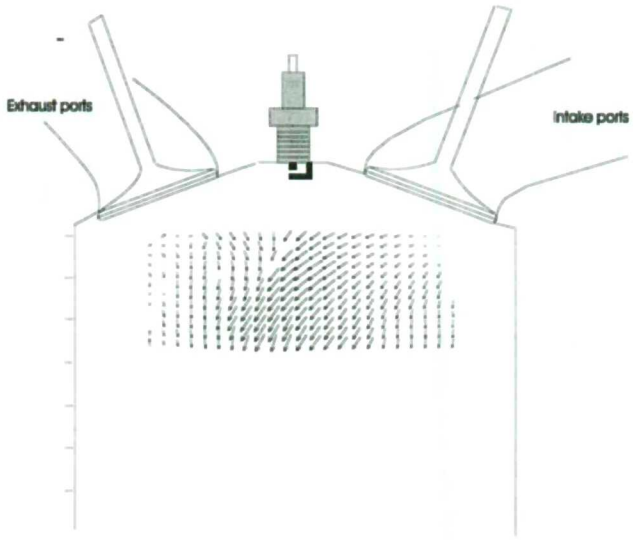

(a)

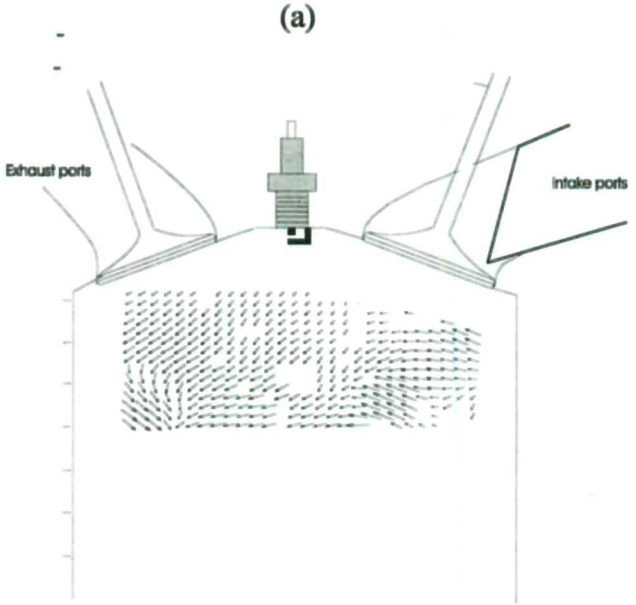

(b)

Figure 3.20: Comparison of in-cylinder flow motion using PIV with non-sleeves and sleeved ports at 240° ATDC

(a) Non-sleeved ports (b) Sleeved ports

CA=270° ATDC

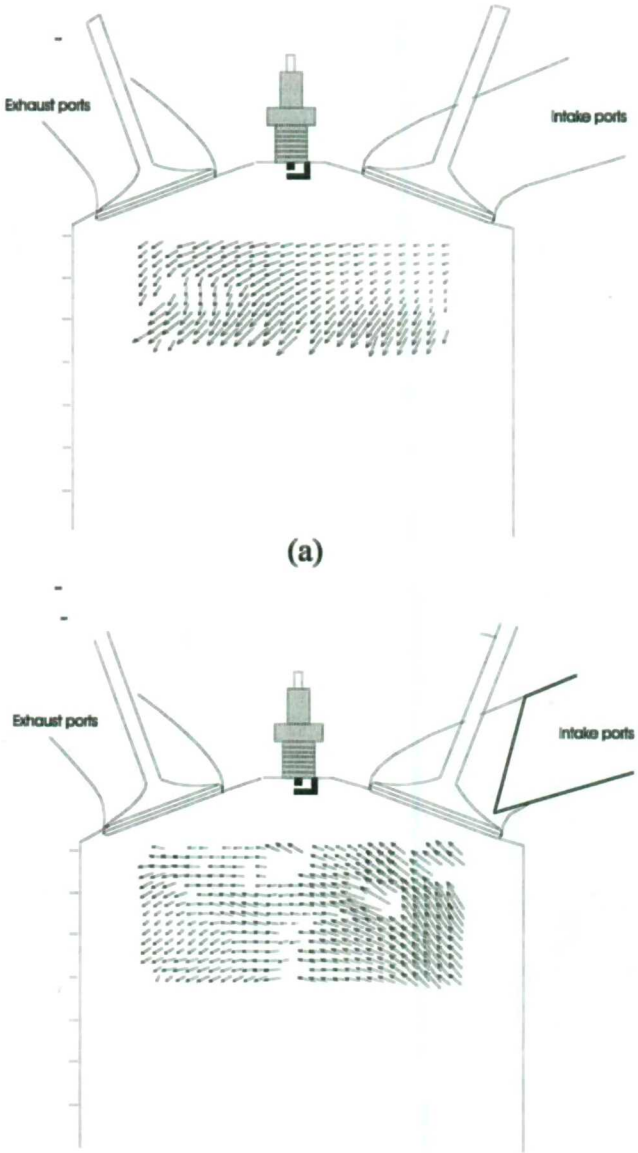

Figure 3.21: Comparison of in-cylinder flow motion using PIV with non-sleeves and sleeved ports at 270° ATDC

(a) Non-sleeved ports (b) Sleeved ports

CA=300° ATDC

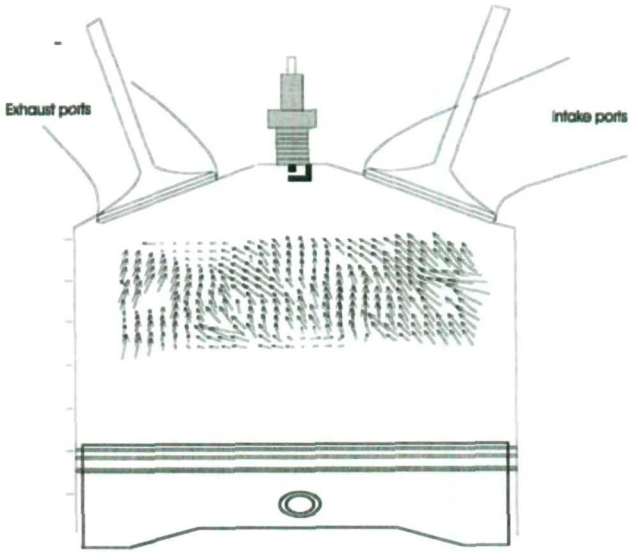

(a)

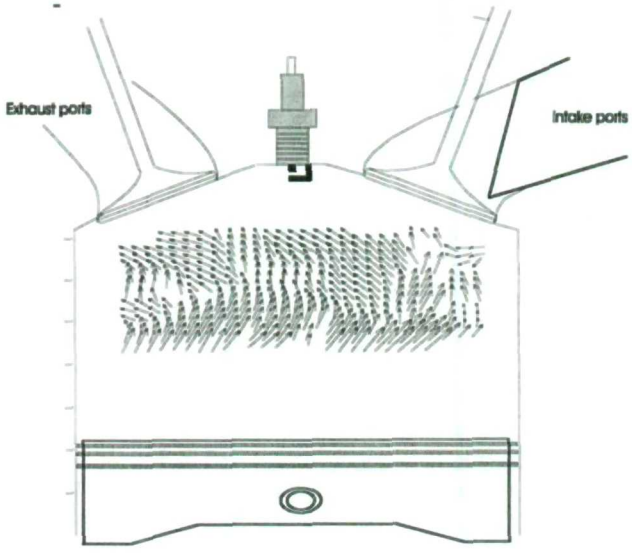

(b)

Figure 3.22: Comparison of in-cylinder flow motion using PIV with non-sleeves and sleeved ports at 300° ATDC

(a) Non-sleeved ports (b) Sleeved ports

CA=330° ATDC

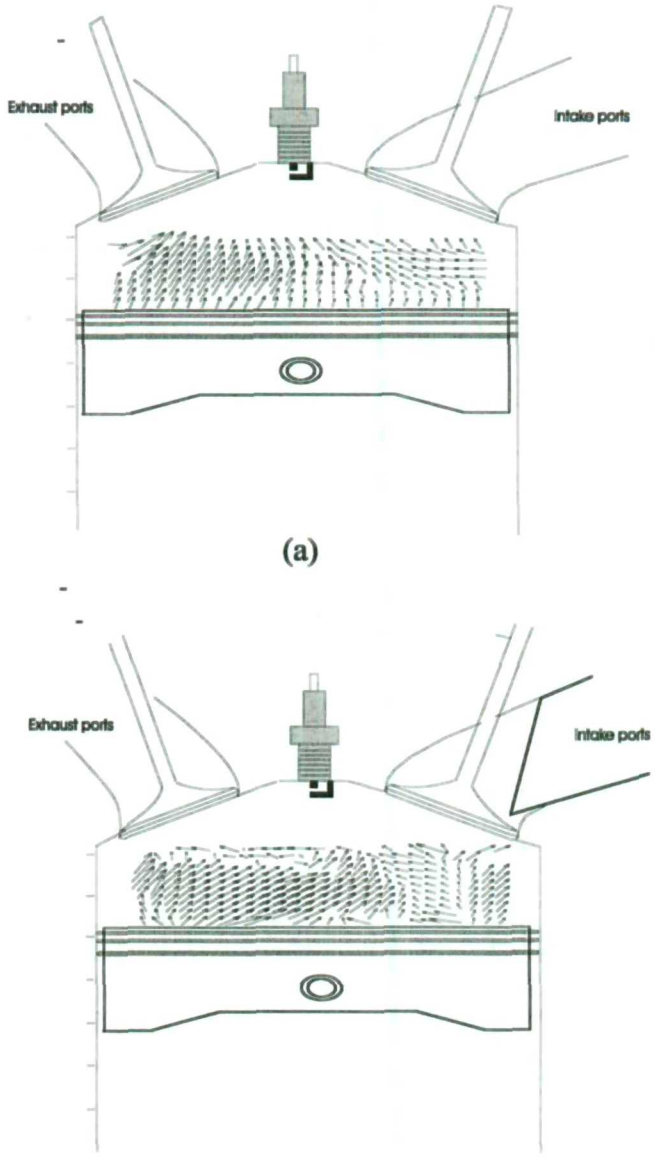

Figure 3.23: Comparison of in-cylinder flow motion using PIV with non-sleeves and sleeved ports at 330° ATDC

(a) Non-sleeved ports (b) Sleeved ports

CA=340° ATDC

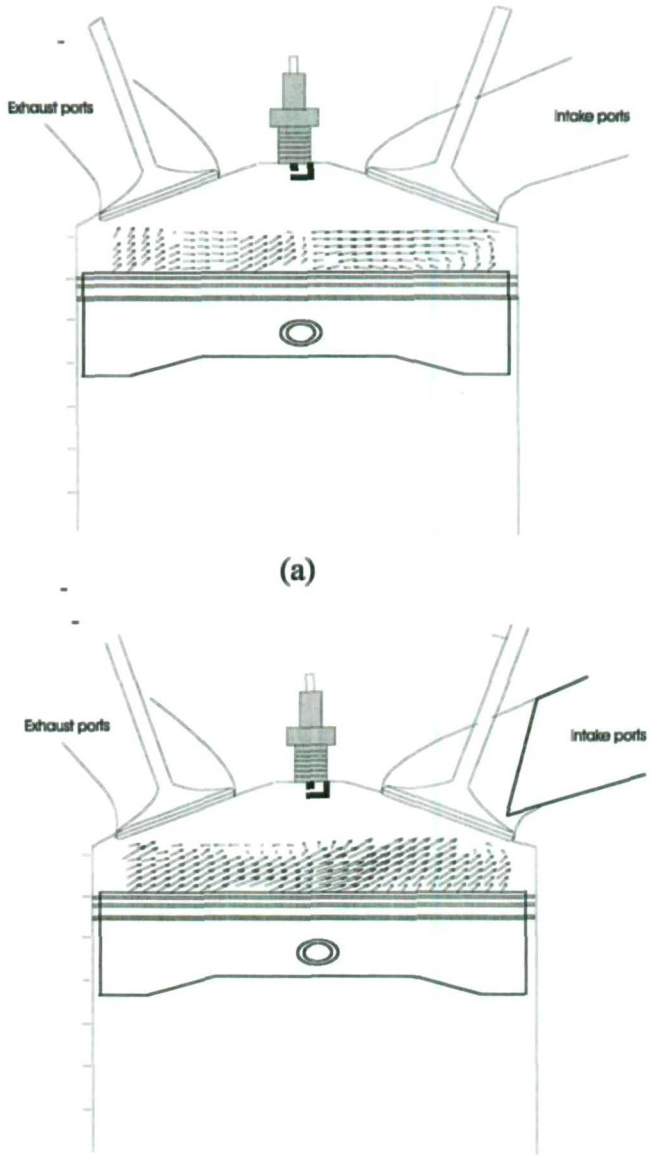

Figure 3.24: Comparison of in-cylinder flow motion using PIV with non-sleeves and sleeved ports at 340° ATDC

(a) Non-sleeved ports (b) Sleeved ports

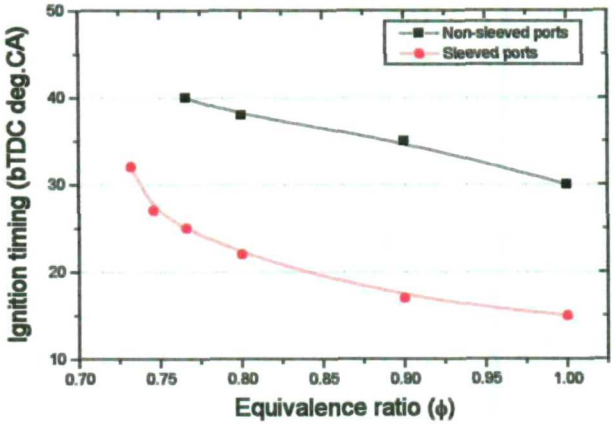

Figure 3.25: MBT ignition timing characteristics of non-sleeved and sleeved intake ports

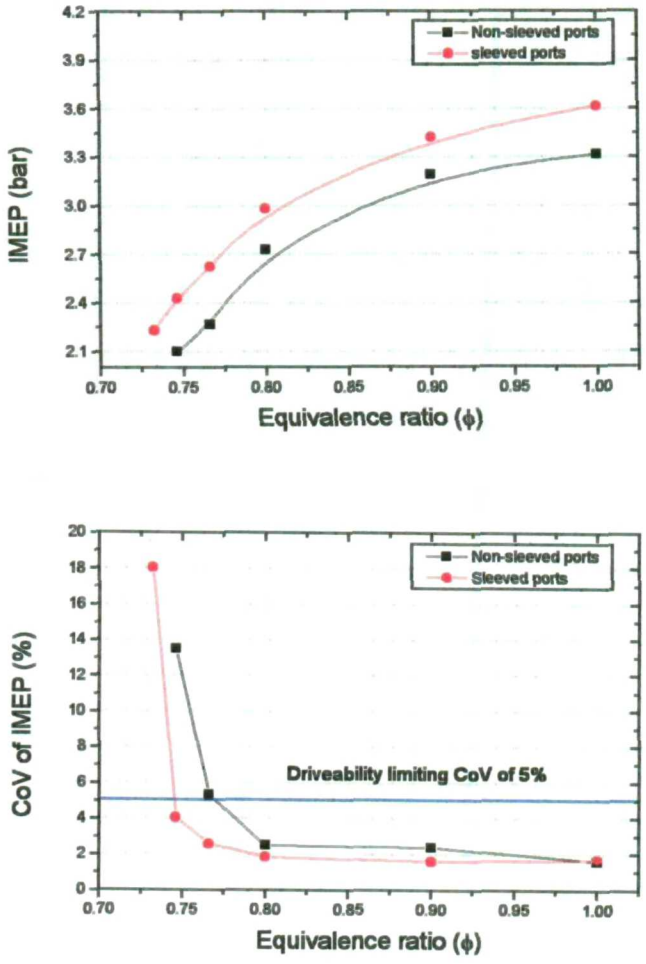

Figure 3.26: Comparison of IMEP and CoV of IMEP between non-sleeved and sleeved intake ports

ϕ =1.0

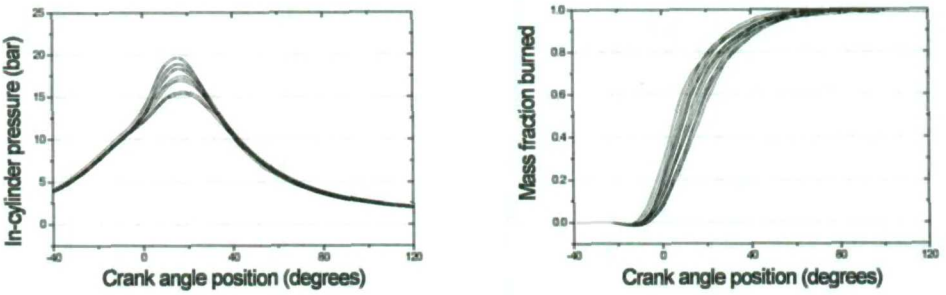

ϕ =0.76

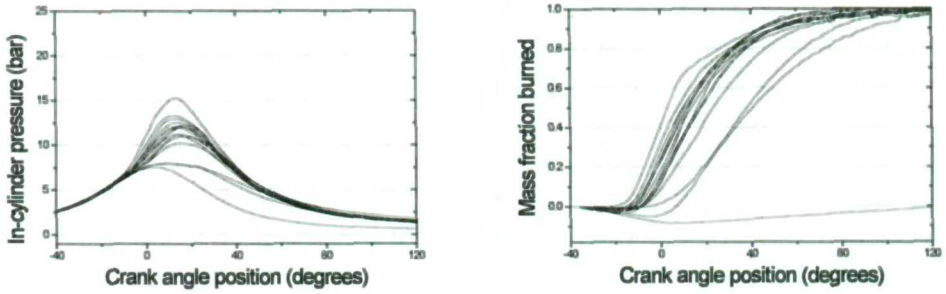

Figure 3.27: In-cylinder pressure and mass fraction burnt with non-sleeved ports

ϕ =1.0

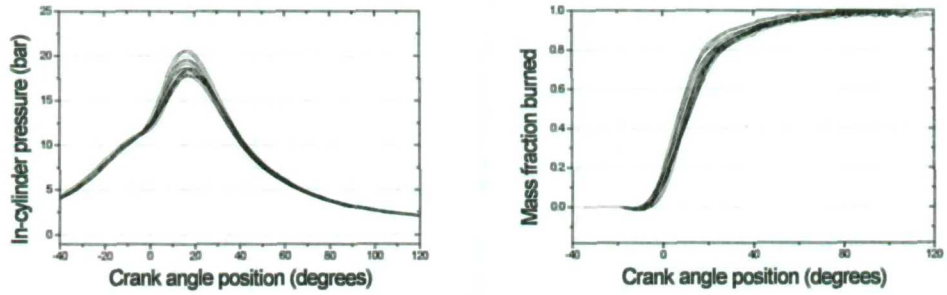

ϕ =0.76

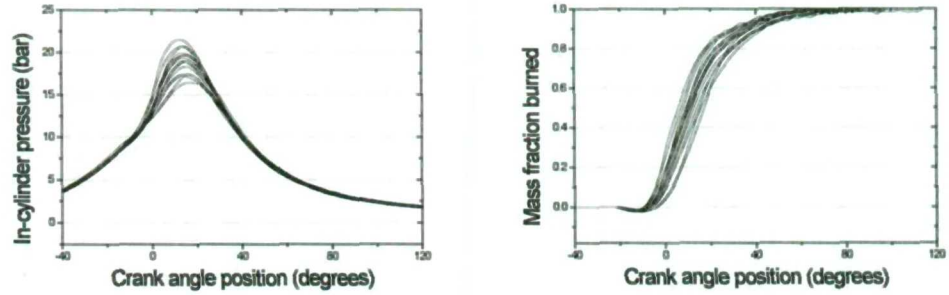

Figure 3.28: In-cylinder pressure and mass fraction burnt with sleeved ports

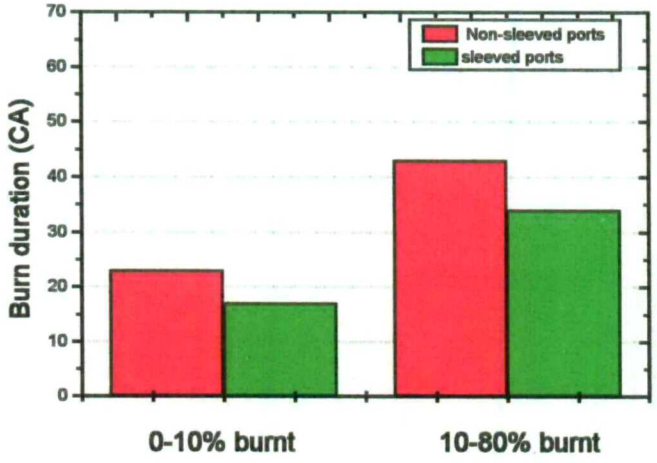

(a)

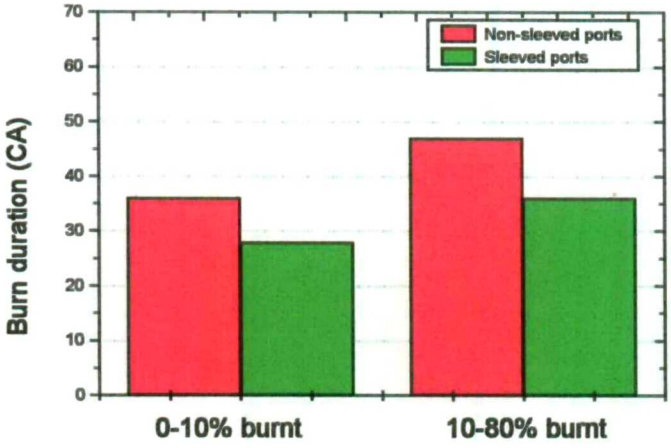

(b)

Figure 3.29: Comparison of mass fraction burnt for non-sleeved and sleeved ports

(a) ϕ=1.0 (b) ϕ=0.76

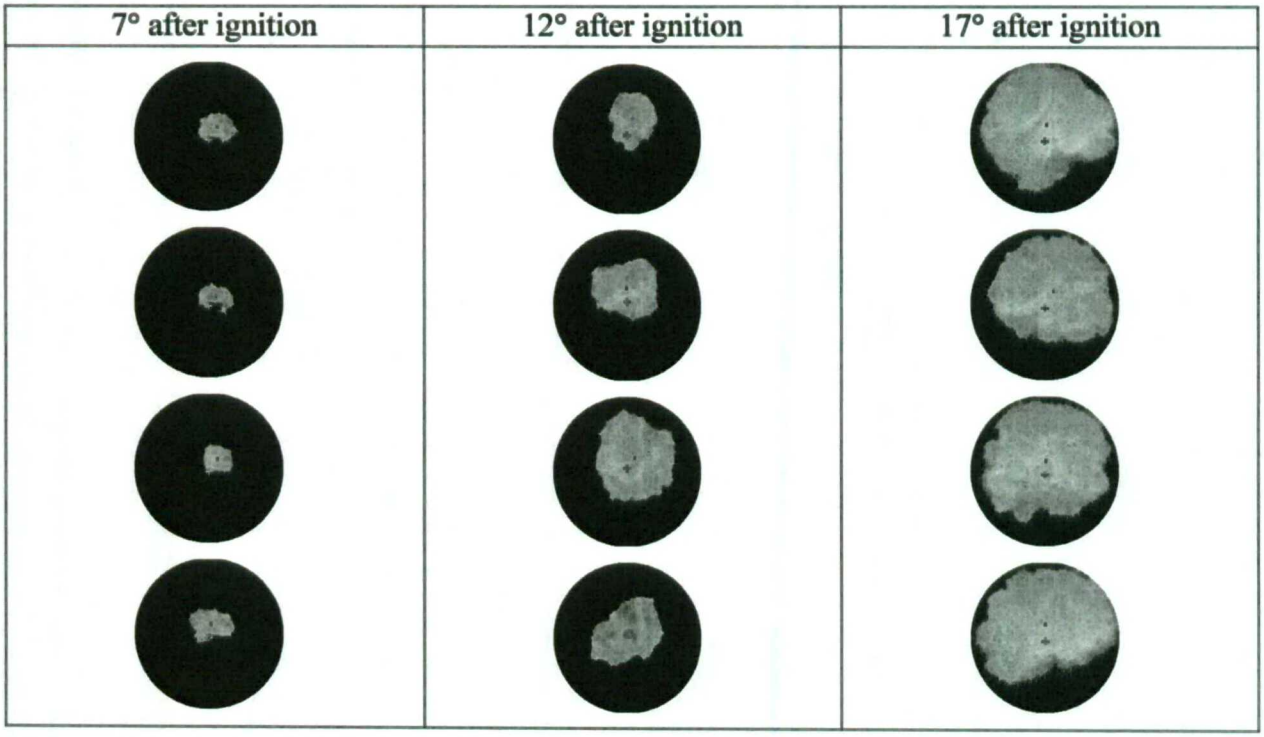

(a)

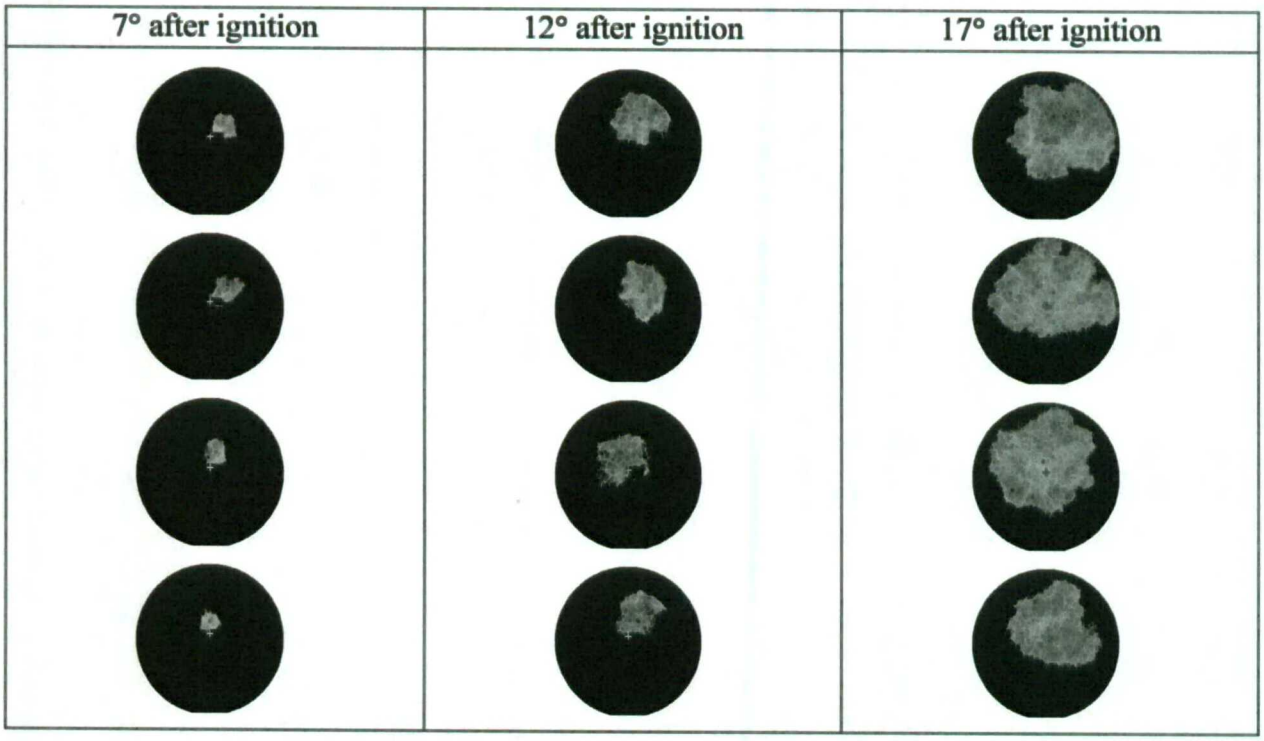

(b)

Figure 3.30: Flame images with sleeved ports

(a) ϕ=1.0 (b) ϕ=0.8

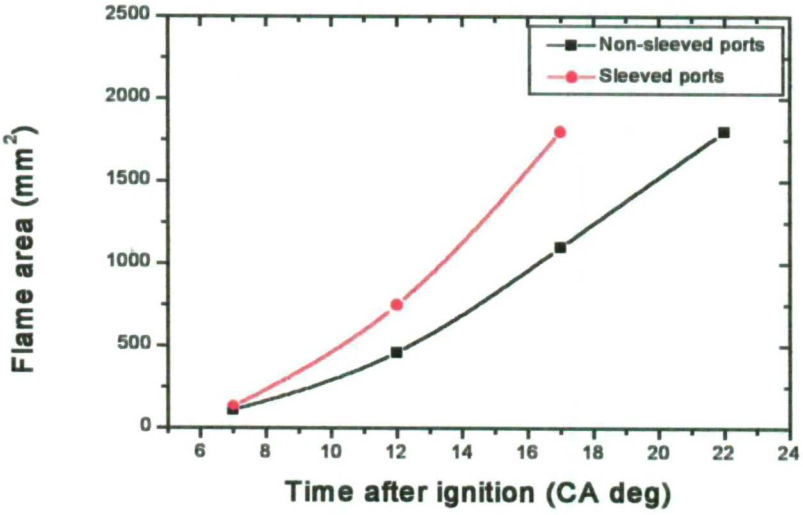

(a)

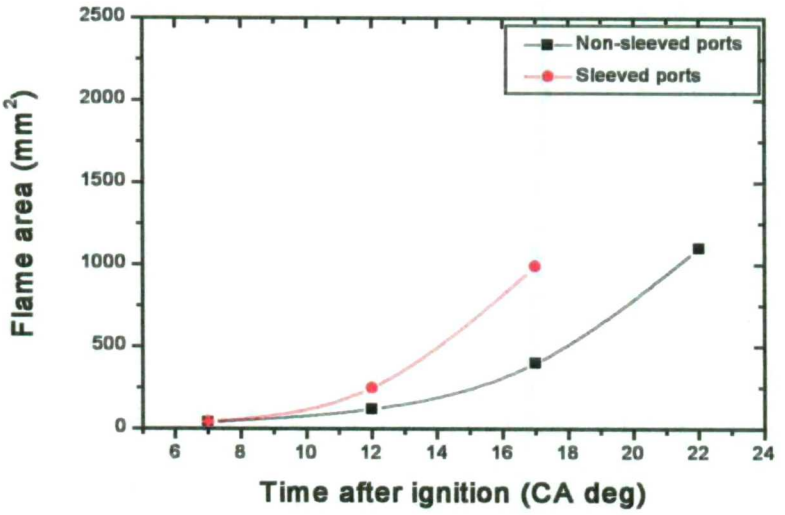

(b)

Figure 3.31: Flame area growth with non-sleeved and sleeved ports
(a) Stoichiometric condition (ϕ=1) (b) Lean condition (ϕ=0.8)

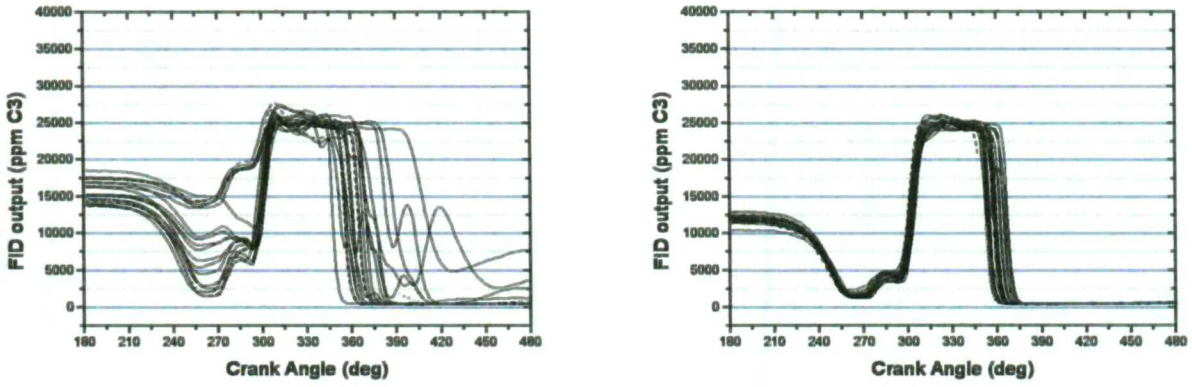

Figure 3.32: Cycle-to-cycle variation of fuel concentration at the spark plug for altering intake system under lean mixture (A/F=21.7 / ϕ=0.76)

(a) Non-sleeved ports (b) Sleeved ports

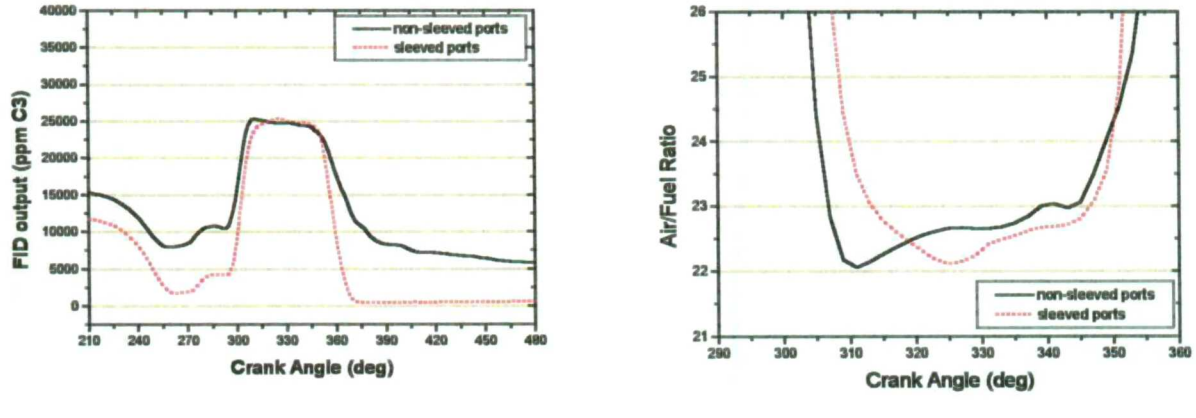

Figure 3.33: Averaged fuel concentration and Air/Fuel ratio over successive 100 cycles at the spark plug under lean mixture (A/F=21.7 / ϕ=0.76) conditions for sleeved and non-sleeved ports

(a) Fuel concentration (b) Air/Fuel ratio

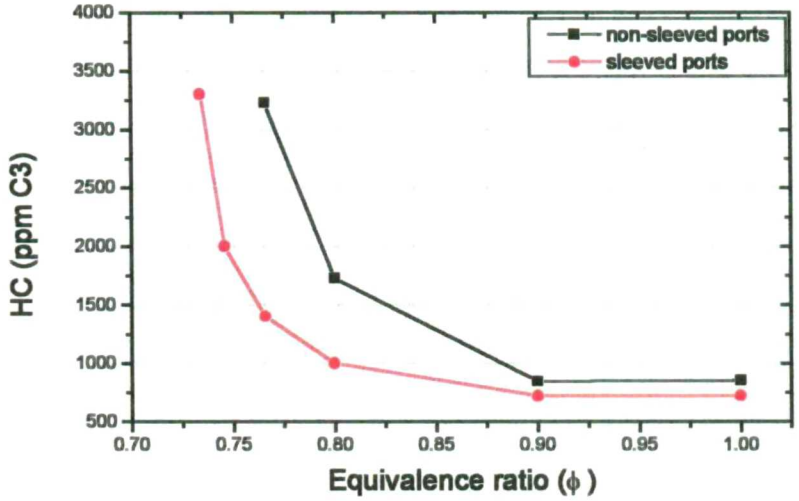

(a)

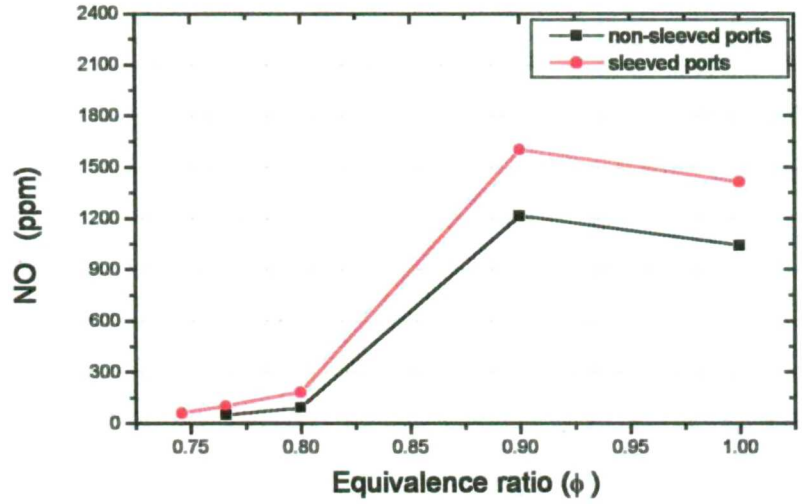

(b)

Figure 3.34: Comparison engine out emissions between non-sleeved ports and sleeved intake ports

(a) HC emission (b) NO emission

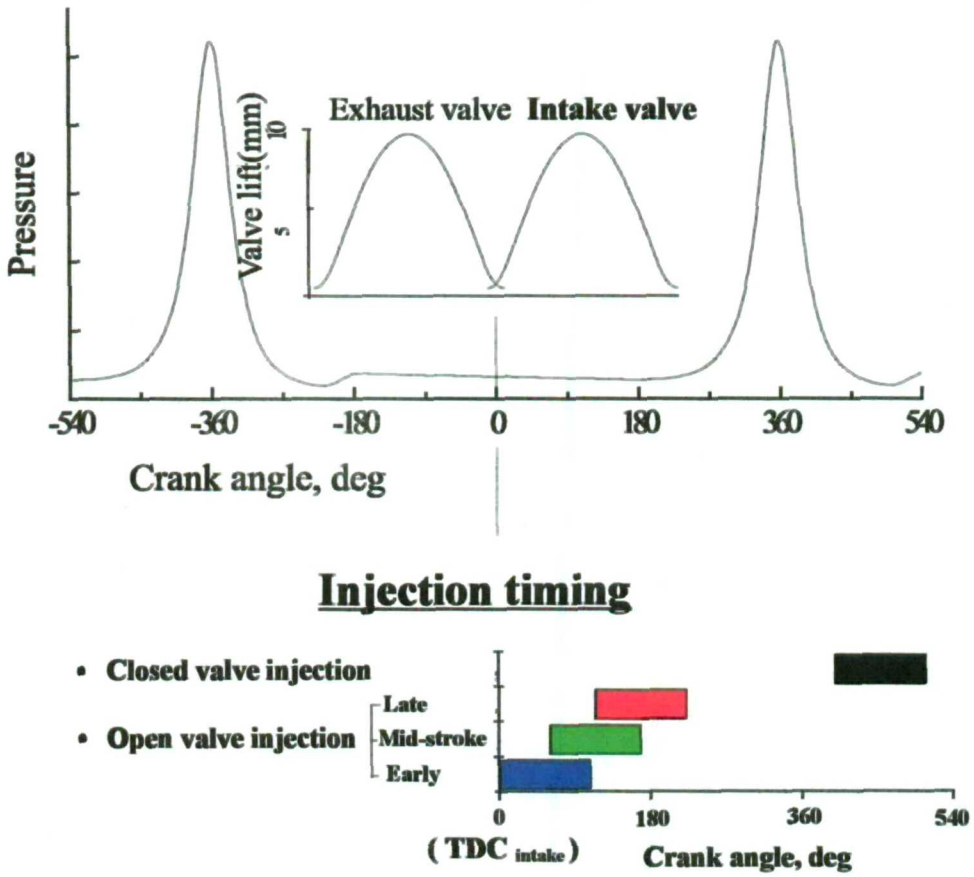

Figure 3.35: Summary of close- and open- valve injection timing strategies

	7°after ign.	11°after ign	16°after ign	19°after ign	24°after ign
Closed-valve injection					
Early open-valve injection					
Mid-stroke open-valve injection					
Late open-valve injection					

Figure 3.36: Comparison of consecutive flame images with close-valve injection and three different open-valve injection strategies (ϕ=1.0)

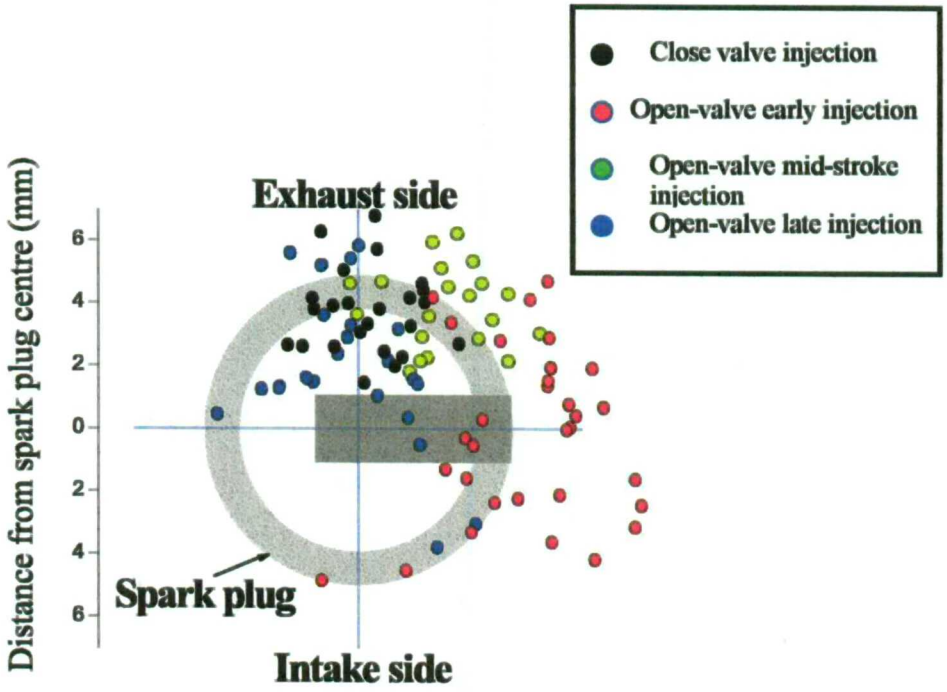

Figure 3.37: Comparison of notional flame centres at 7° after ignition with close valve injection and the three different open valve injection strategies

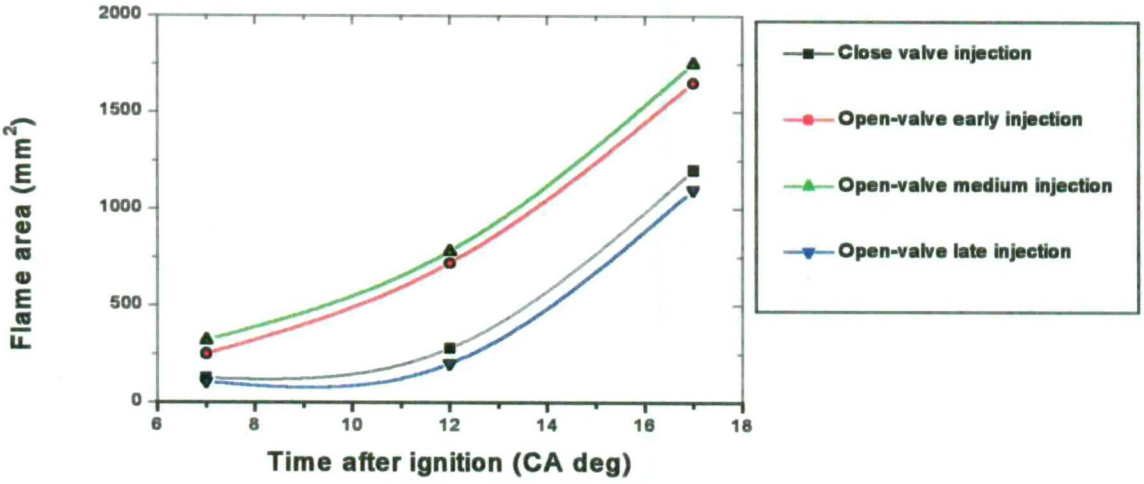

Figure 3.38: Flame area growth with closed-valve injection and the three different open valve injection strategies

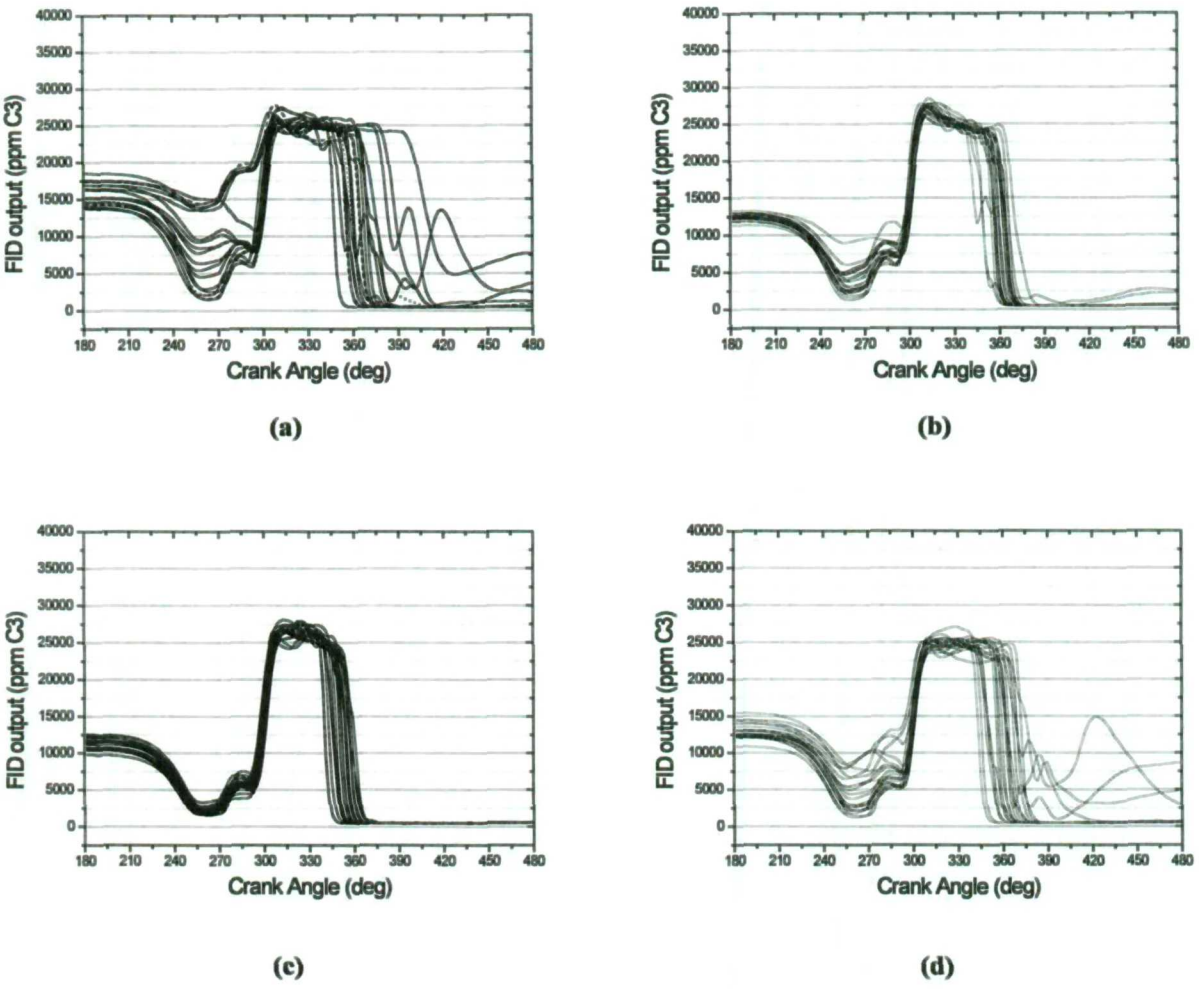

Figure 3.39: Cycle-to-cycle variation of fuel concentration at the spark plug for altering the injection timing under very lean mixture condition ($\phi = 0.76$)

(a) close- valve injection (b) open-valve early injection
(c) open-valve mid-stroke injection (d) open-valve late injection

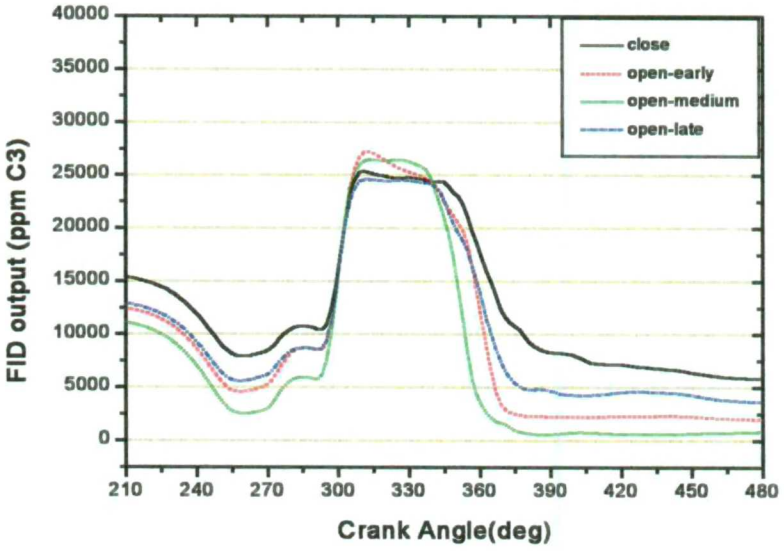

(a)

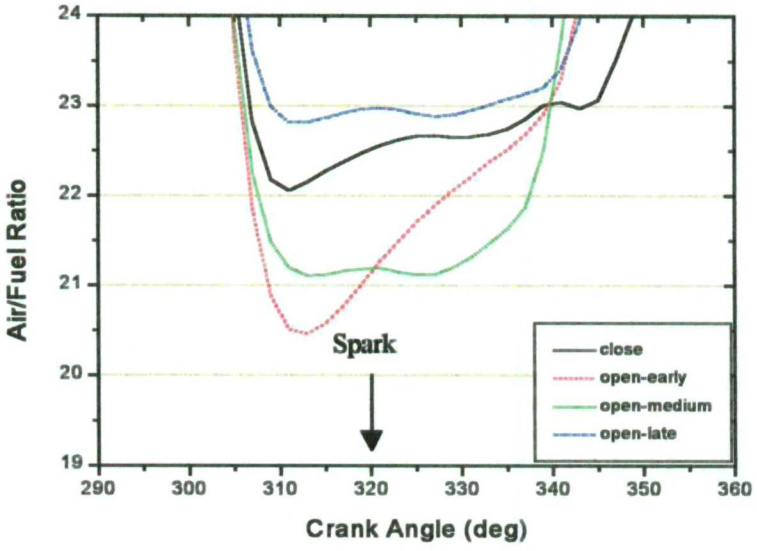

(b)

Figure 3.40: Averaged fuel concentration and Air/Fuel ratio for four different injection timings at the spark plug and lean mixture condition over successive 50 cycles (A/F=21.7 / ϕ=0.76)

(a) Fuel concentration (b) Air/Fuel ratio

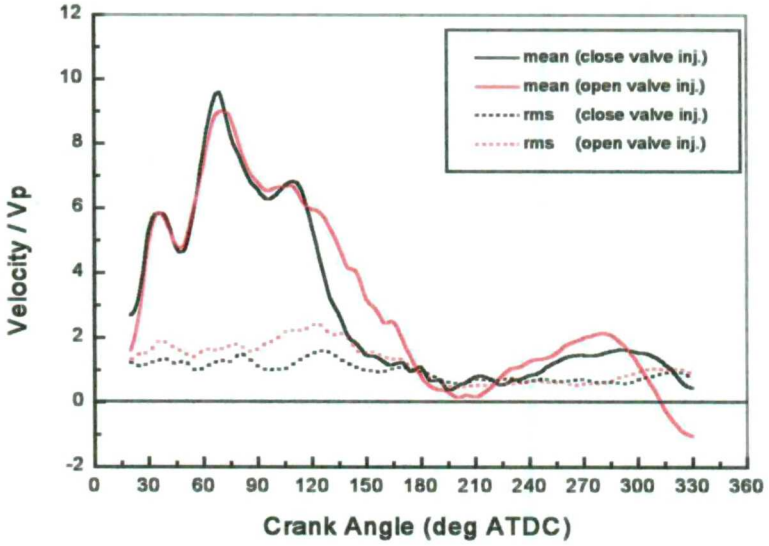

(a)

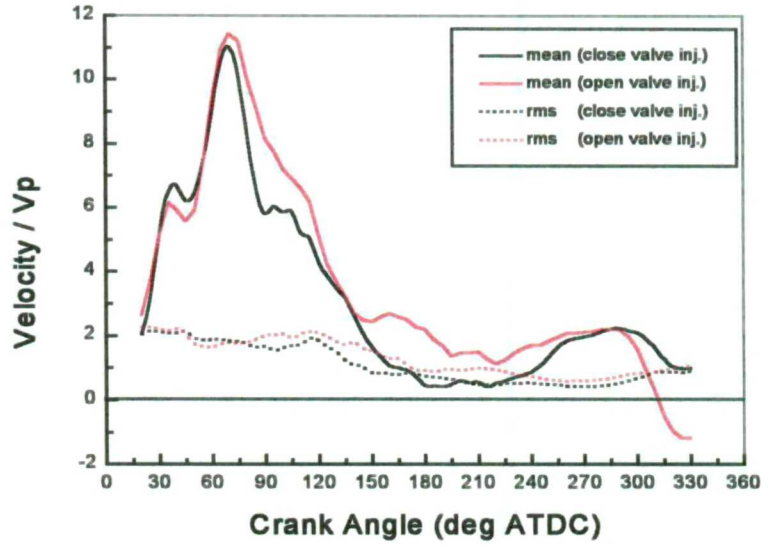

(b)

Figure 3.41: Effect of injection strategy on the mean and rms tumble velocities at a point below the spark plug (z=11mm) obtained by LDV

(a) Non-sleeved intake ports (b) Sleeved intake ports

CA=180° ATDC

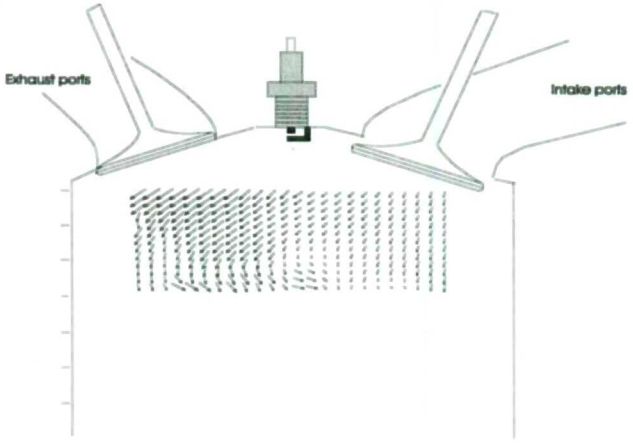

(a)

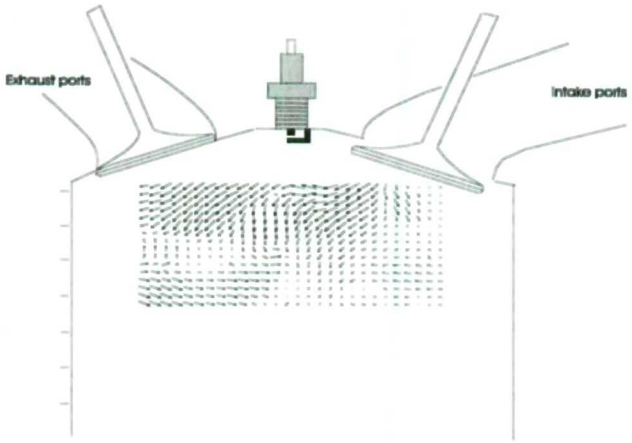

(b)

Figure 3.42: Comparison of in-cylinder flow motion using PIV with close-valve injection and open-valve injection at 180° ATDC

(a) Close- valve injection (b) Open-valve injection

CA=210° ATDC

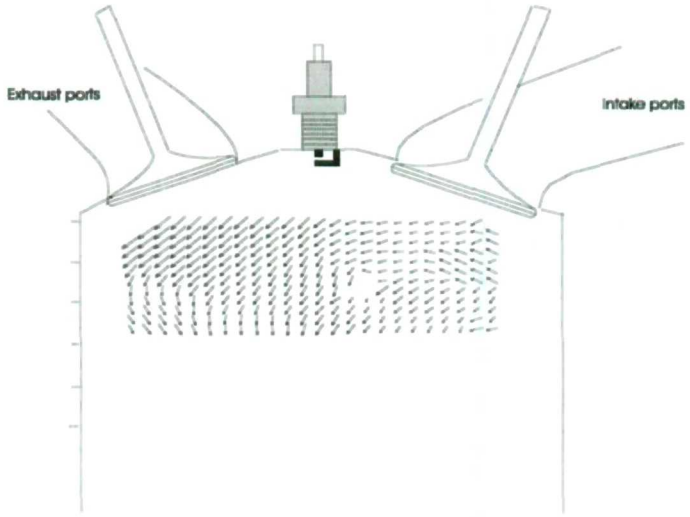

(a)

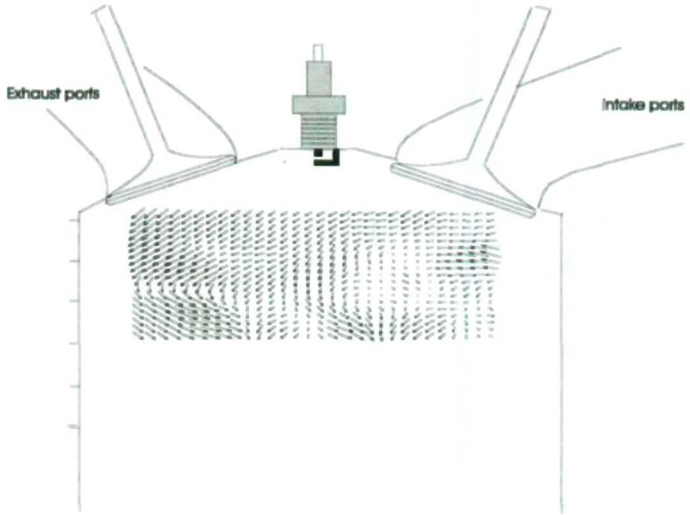

(b)

Figure 3.43: Comparison of in-cylinder flow motion using PIV with close-valve injection and open-valve injection at 210° ATDC

(a) Close-valve injection (b) Open-valve injection

CA=240° ATDC

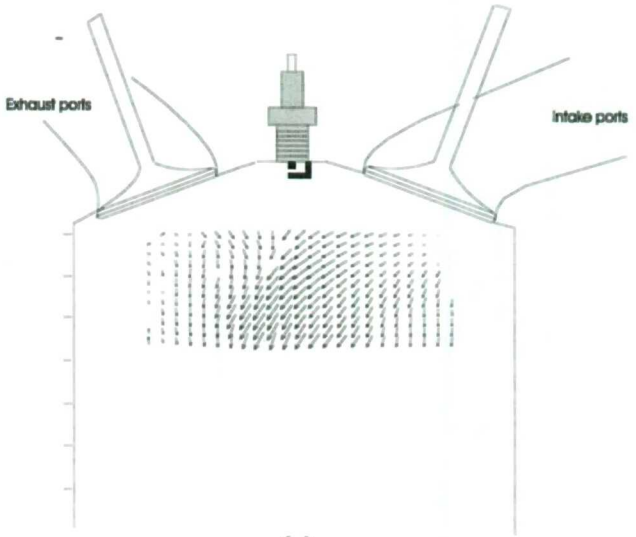

(a)

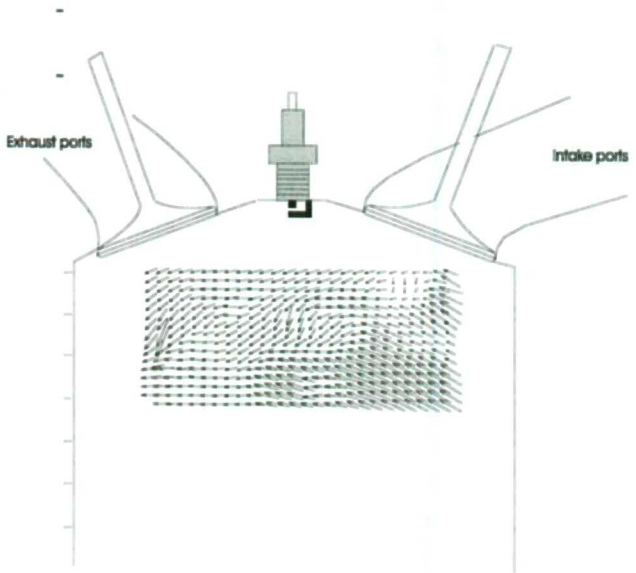

(b)

Figure 3.44: Comparison of in-cylinder flow motion using PIV with close-valve injection and open-valve injection at 240° ATDC

(a) Close-valve injection (b) Open-valve injection

CA=270° ATDC

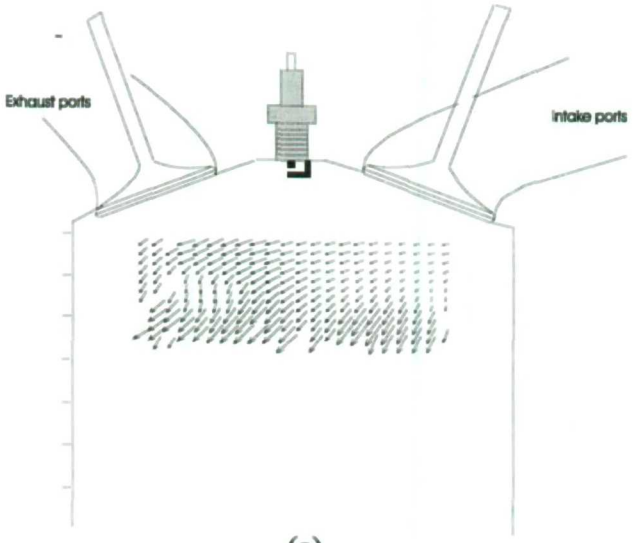

(a)

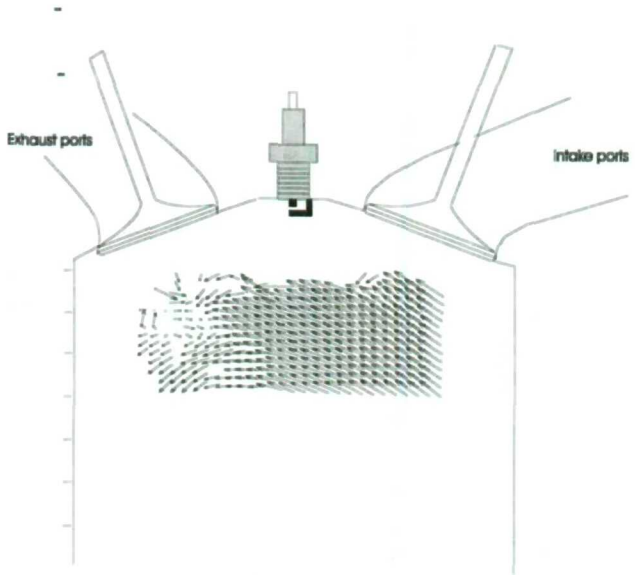

(b)

Figure 3.45: Comparison of in-cylinder flow motion using PIV with close-valve injection and open-valve injection at 270° ATDC

(a) Close-valve injection (b) Open-valve injection

CA=300° ATDC

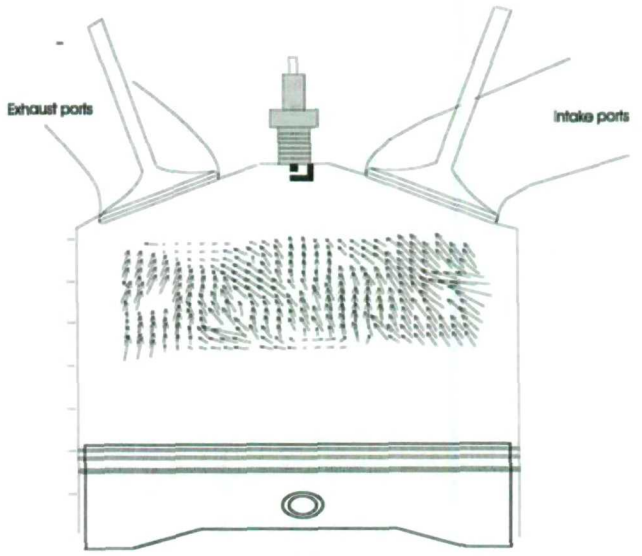

(a)

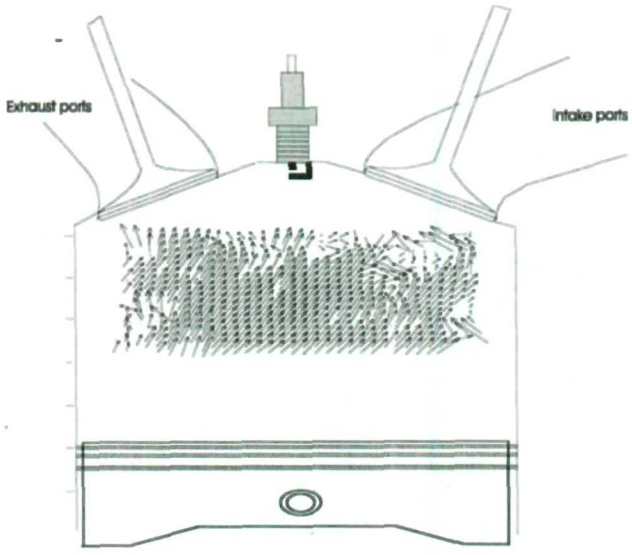

(b)

Figure 3.46: Comparison of in-cylinder flow motion using PIV with close-valve injection and open-valve injection at 300° ATDC

(a) Close-valve injection (b) Open-valve injection

CA=330° ATDC

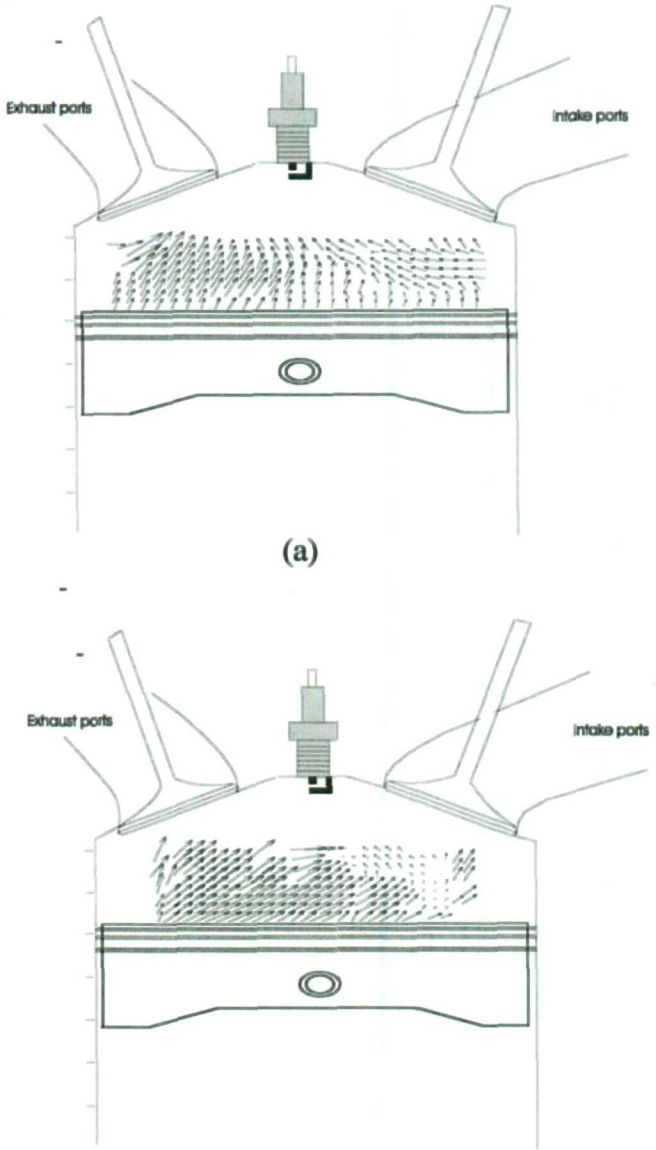

Figure 3.47: Comparison of in-cylinder flow motion using PIV with close-valve injection and open-valve injection at 330° ATDC

(a) Close-valve injection (b) Open-valve injection

CA=340° ATDC

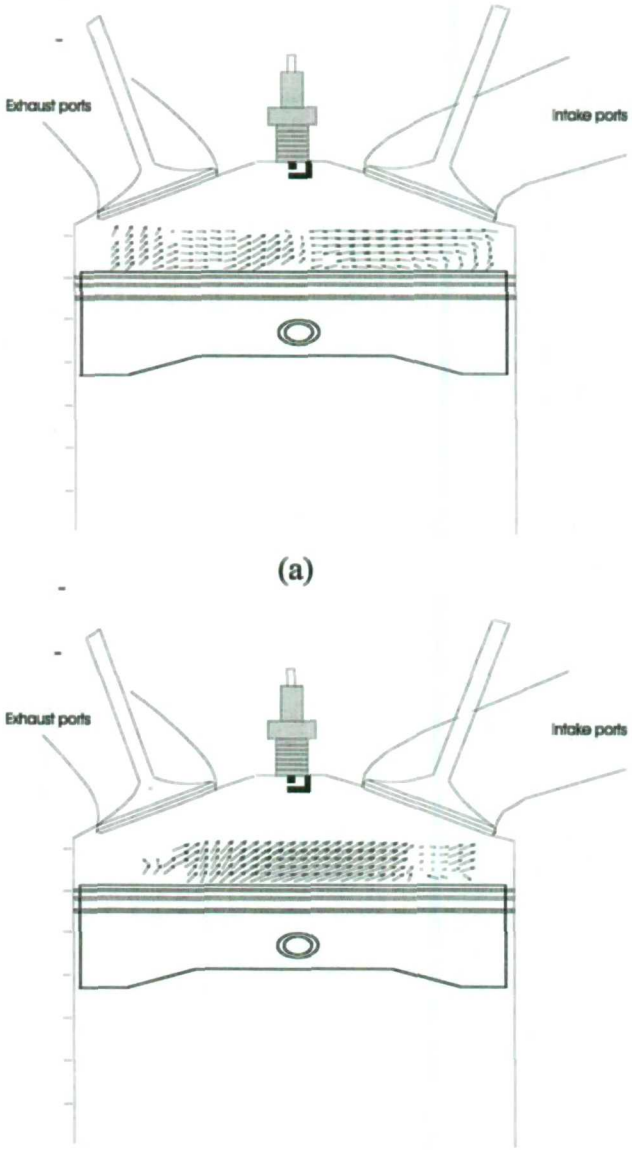

Figure 3.48: Comparison of in-cylinder flow motion using PIV with close-valve injection and open-valve injection at 340° ATDC

(a) Close-valve injection (b) Open-valve injection

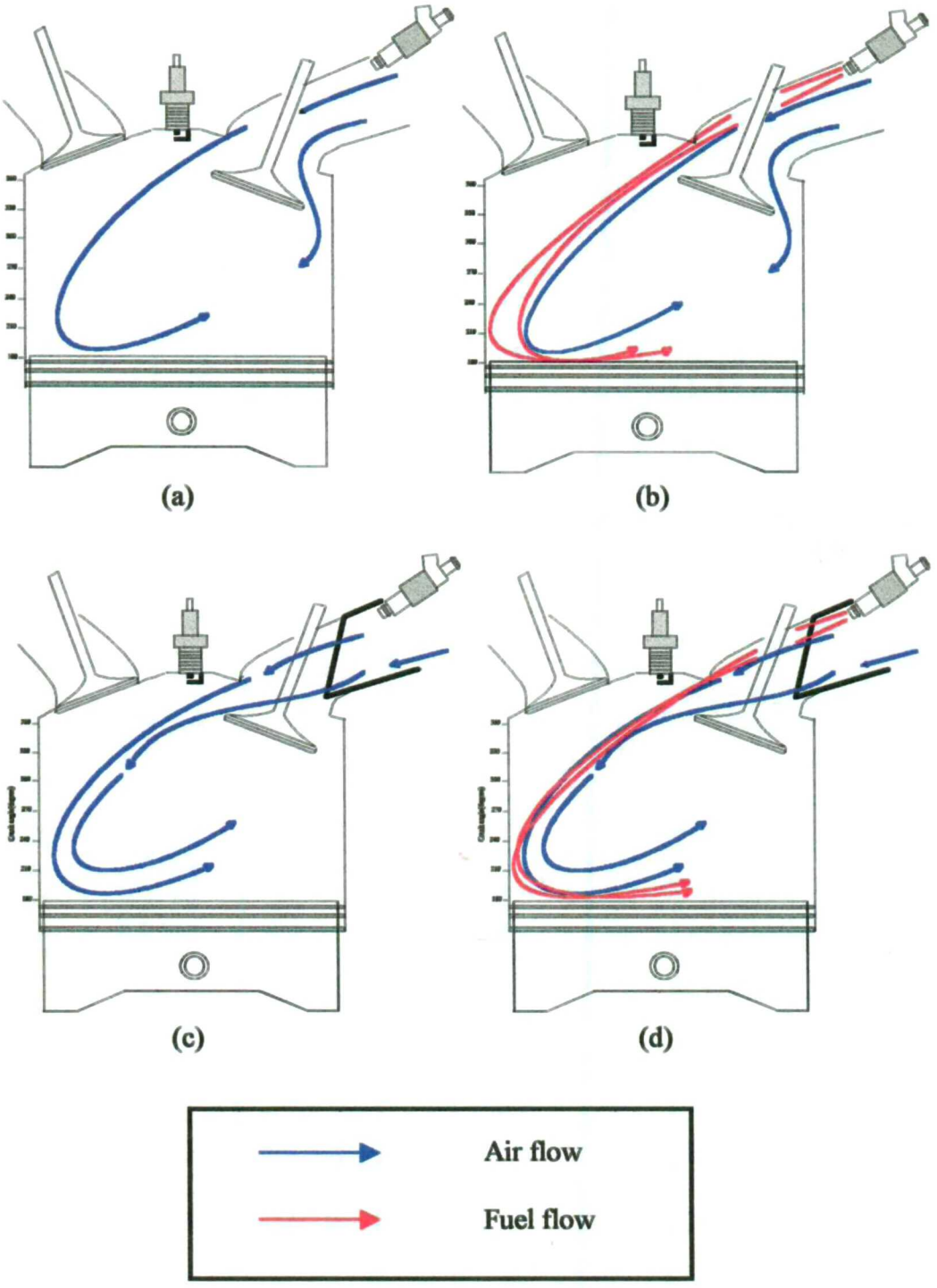

Figure 3.49: Concept of 4 different tumble flows

(a) Non-sleeved ports with close-valve injection (b) Non-sleeved ports with open-valve injection

(c) Sleeved ports with close-valve injection (d) Sleeved ports with open-valve injection

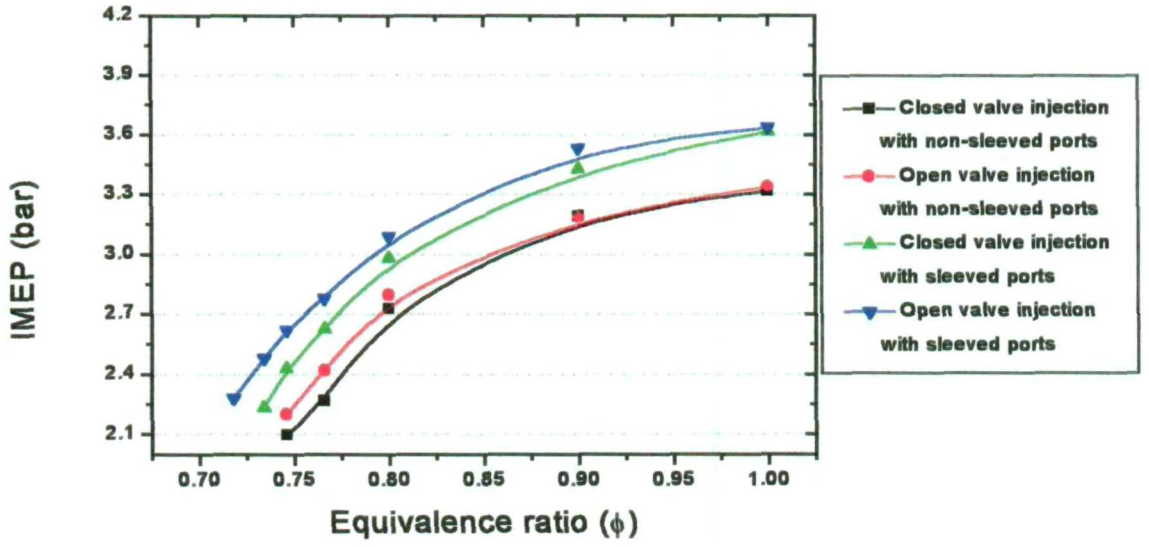

(a)

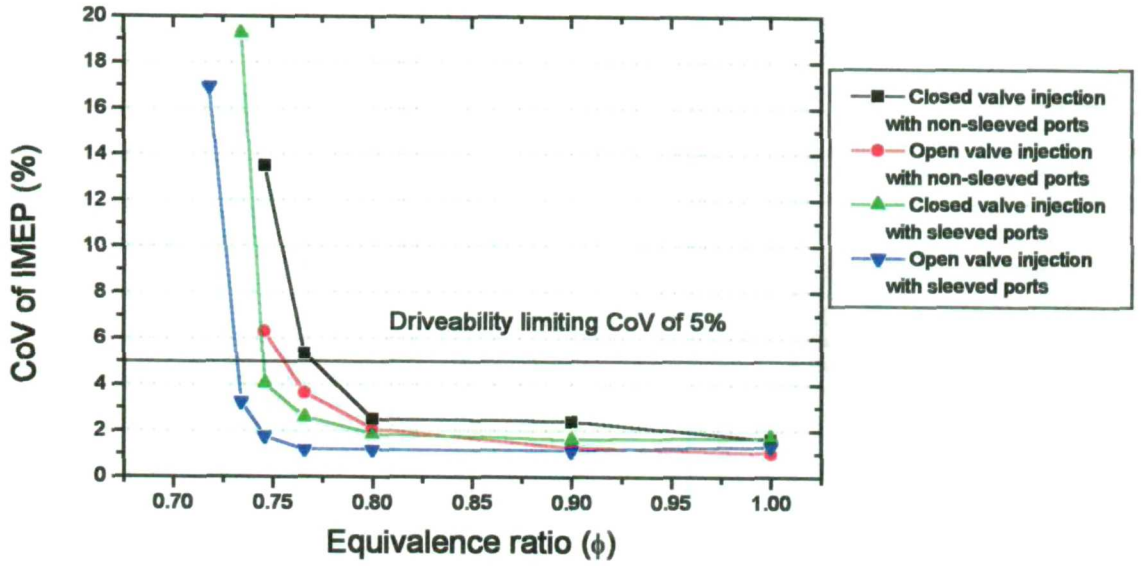

(b)

Figure 3.50: Effect of injection strategy on IMEP and CoV of IMEP with non-sleeved and sleeved ports

(a) IMEP (b) CoV of IMEP

(a) In-cylinder pressure

Close-valve injection with non-sleeved ports

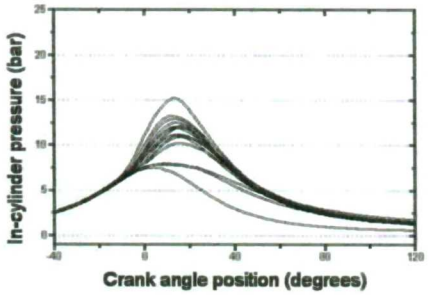

Open-valve injection with non-sleeved ports

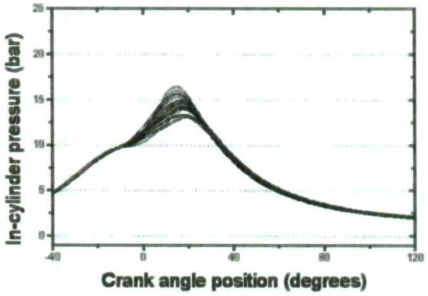

Close-valve injection with sleeved poers

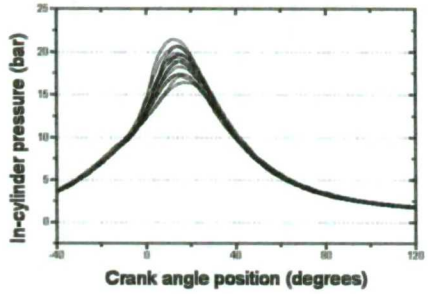

Open-valve injection with sleeved ports

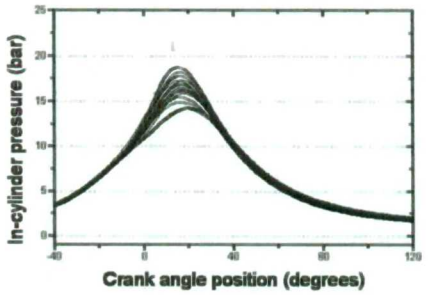

(b) Mass fraction burnt

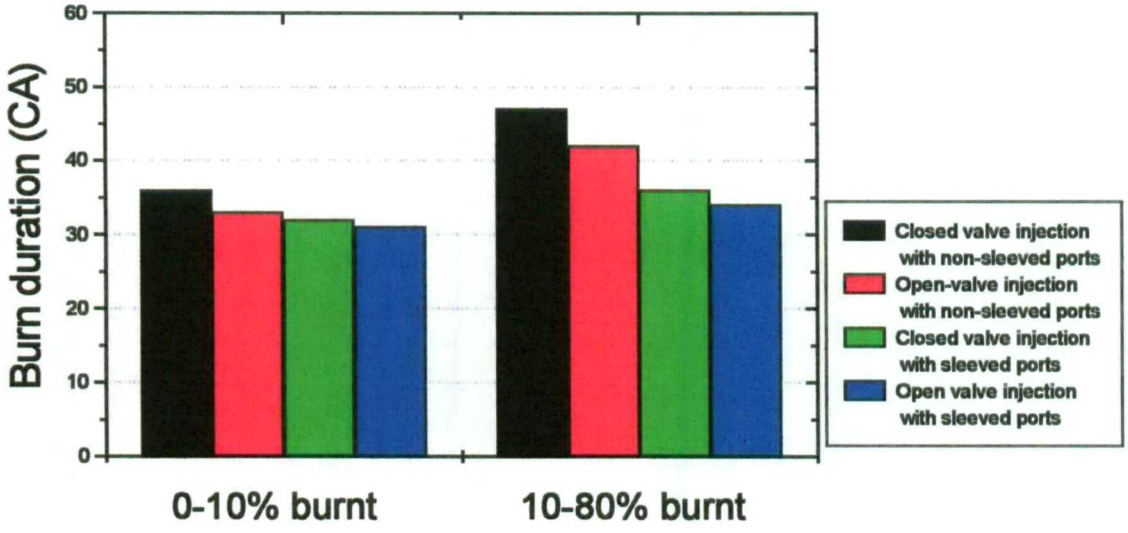

Figure 3.51: Comparison of in-cylinder pressure and mass fraction burnt for close-valve and open-valve injection strategies under very lean conditions (ϕ=0.76)

(a) In-cylinder pressure (b) Mass fraction burnt

	2° after ignition	7° after ignition	12° after ignition	17° after ignition
Non-sleeved ports with close-valve injection				
Non-sleeved ports with open-valve injection				
Sleeved ports with close-valve injection				
Sleeved ports with open-valve injection				

Figure 3.52: Comparison of flame images with different intake system and injection timing (ϕ=1.0)

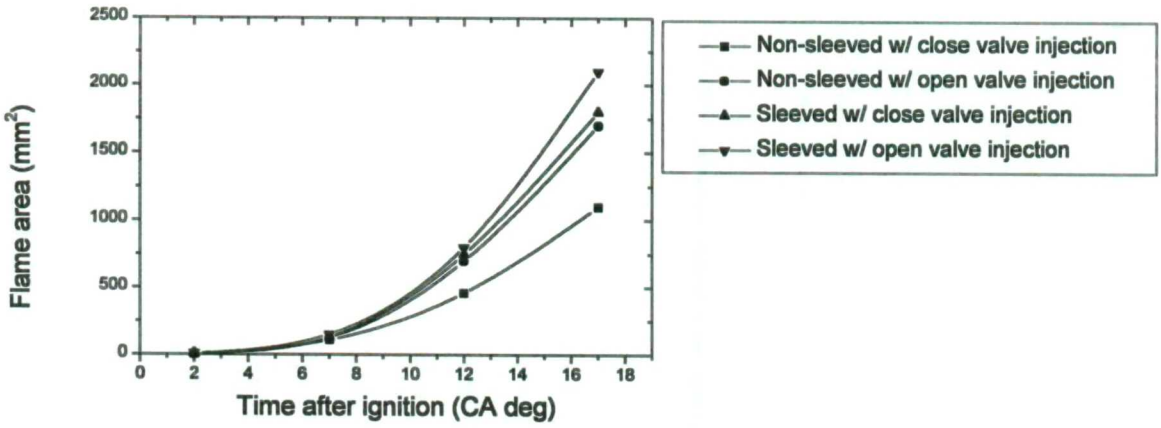

Figure 3.53: Flame area growth with different intake system and injection timing (ϕ=1.0)

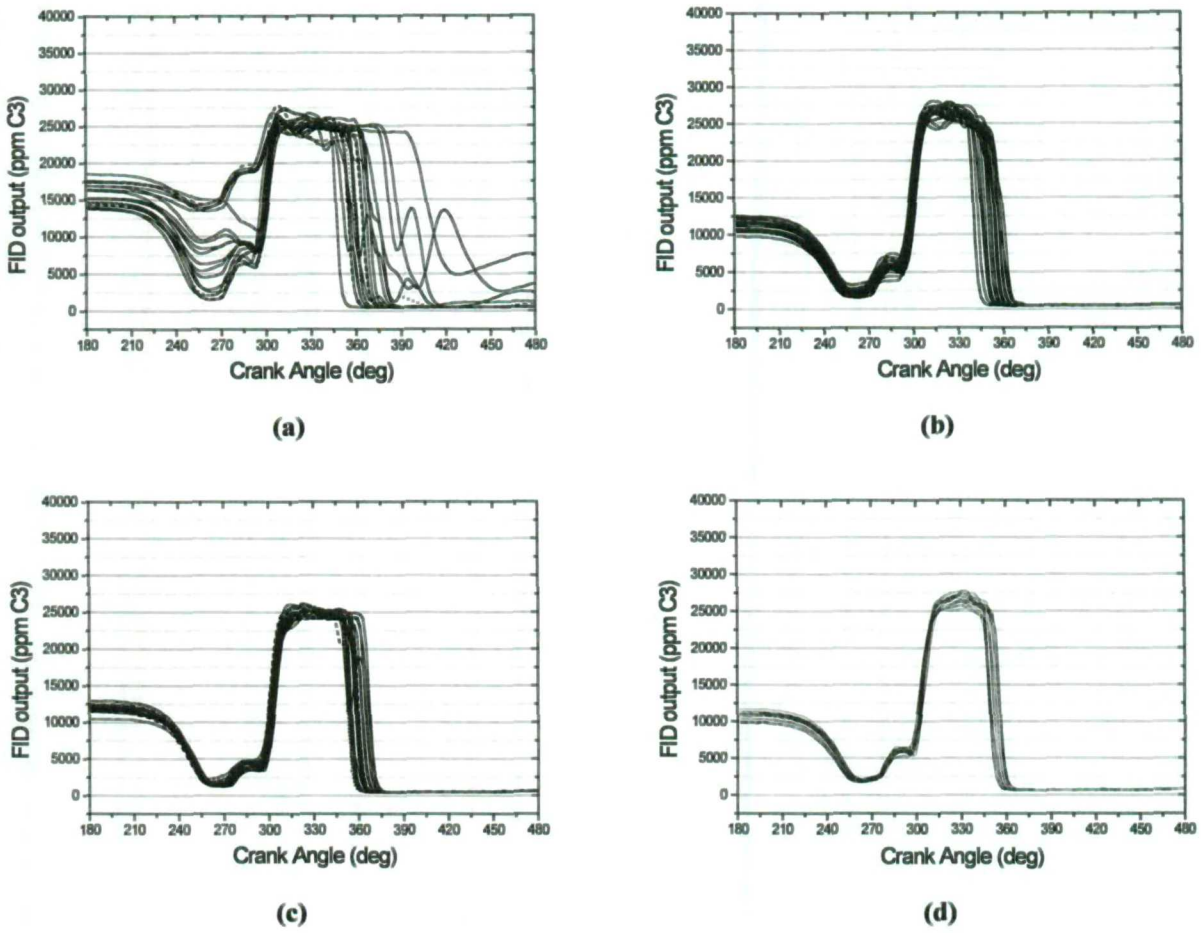

Figure 3.54 Cycle-to-cycle variation of fuel concentration at the spark plug for altering both Intake system and injection timing at the spark plug under very lean mixture condition (ϕ=0.76)

(a) non-sleeved ports with close-valve injection (b) non-sleeved ports with open-valve injection
(c) sleeved ports with close-valve injection (d) sleeved ports with open-valve injection

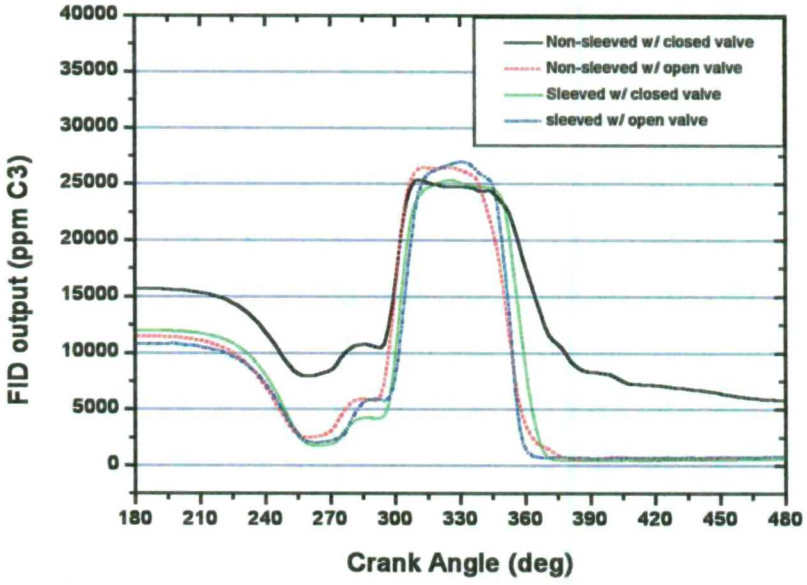

(a)

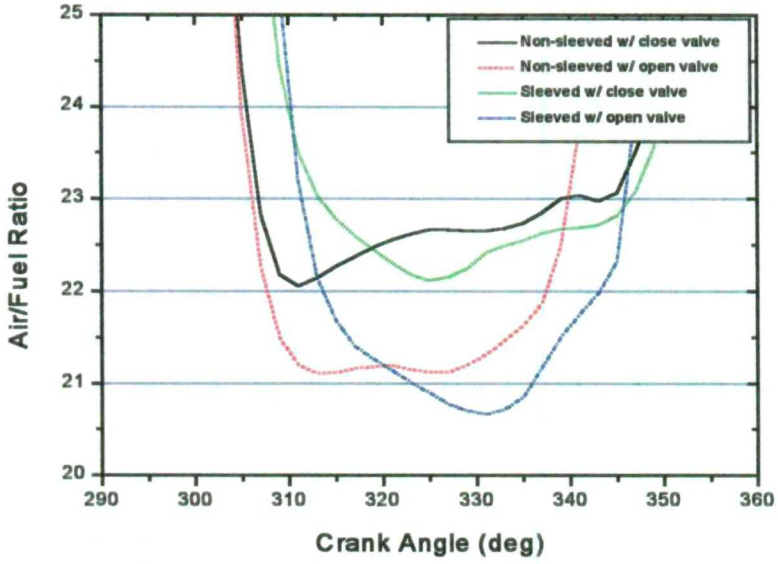

(b)

Figure 3.55: Averaged fuel concentration and air/fuel ratio over successive 50 cycles for different injection timing and intake port geometry at the spark plug under very lean mixture condition (A/F=21.7 / ϕ=0.76)

(a) Fuel concentration (b) Air/Fuel ratio

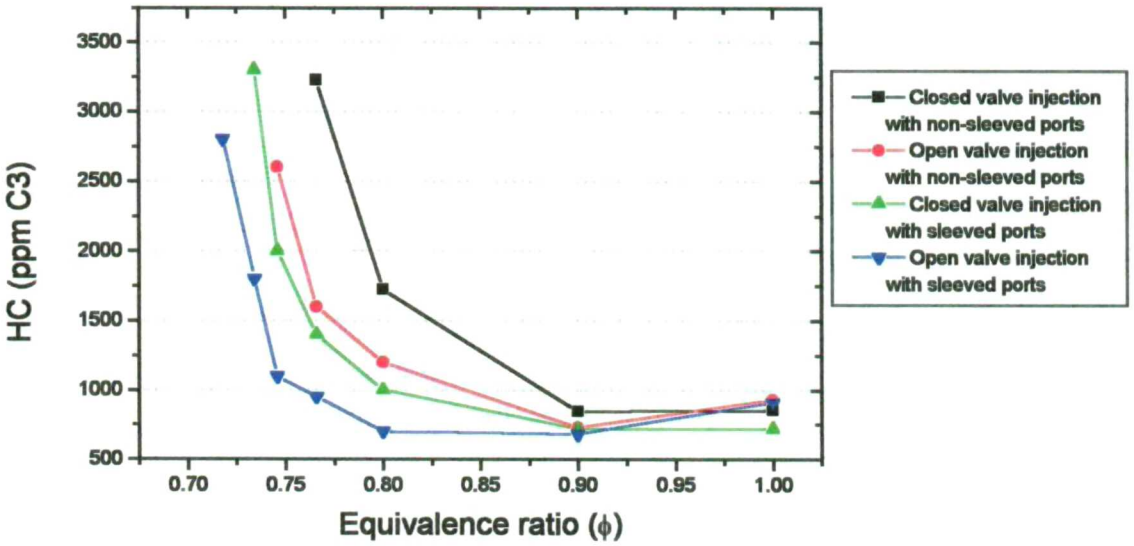

(a)

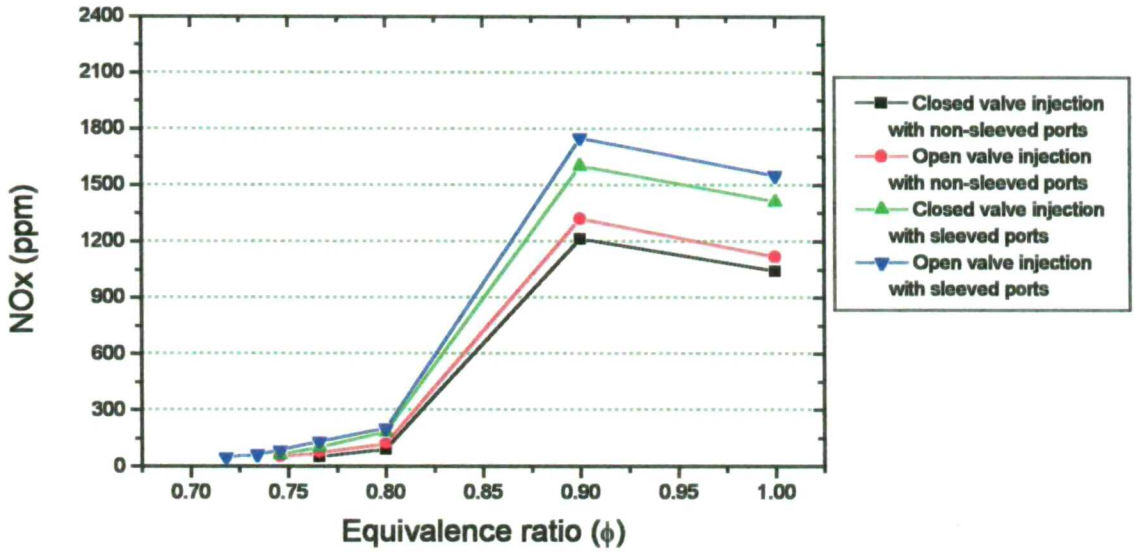

(b)

Figure 3.56: Comparison of engine-out emissions between close-valve and open -valve injection strategies for the two induction systems

(a) HC (b) NOx

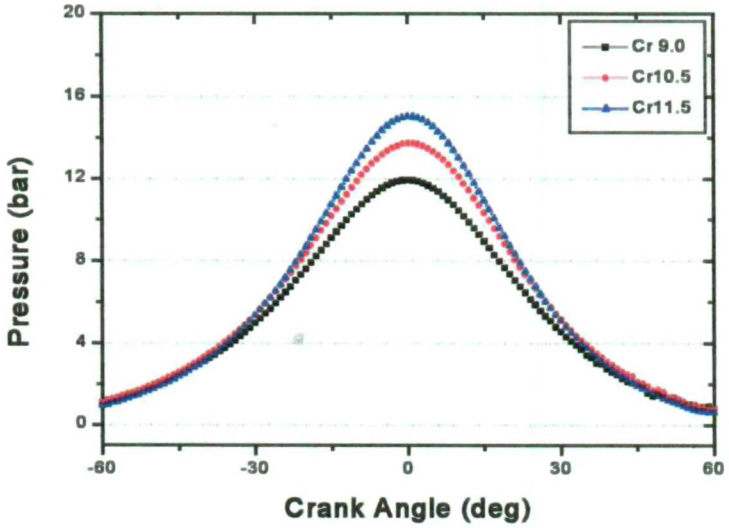

Figure 3.57: Comparison of motoring pressure for three compression ratios

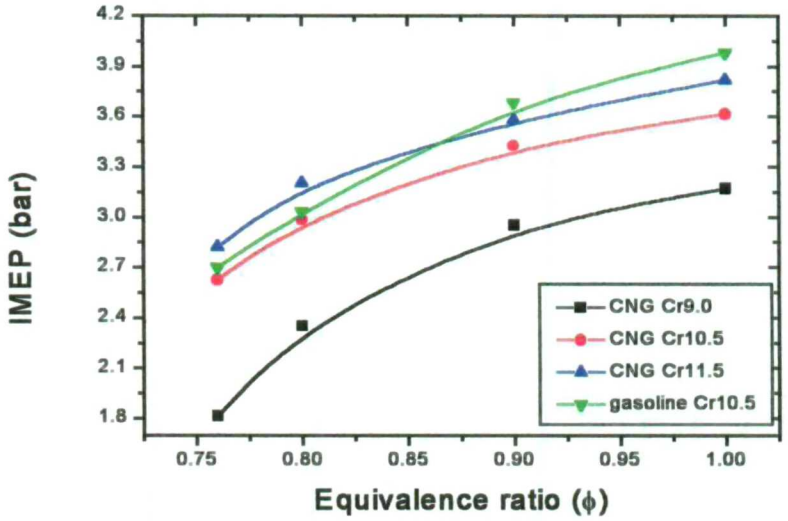

Figure 3.58: Variation of IMEP as a function of equivalence ratio for three compression ratios

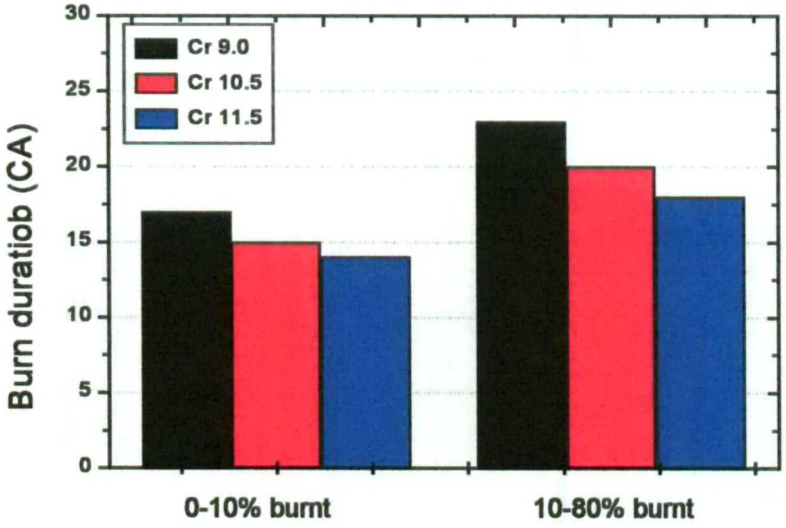

Figure 3.59: Comparison of mass fraction burnt rates with varying compression ratio (ϕ=1.0)

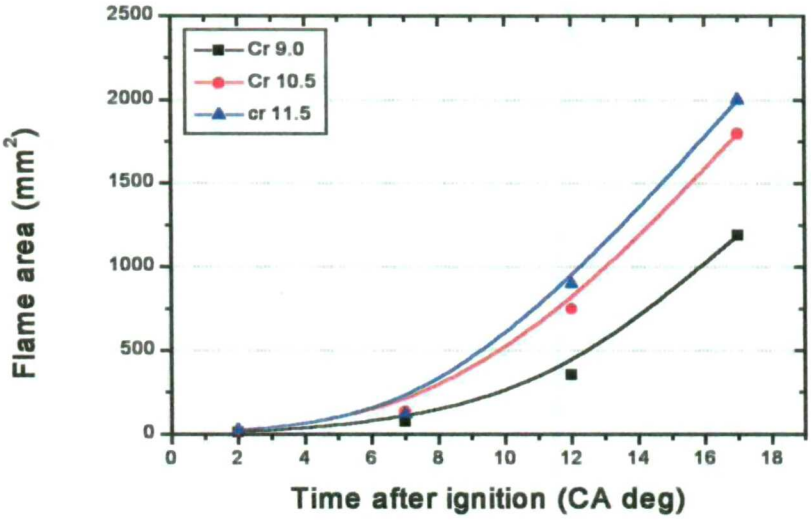

Figure 3.60: Comparison of flame areas with varying compression ratio (ϕ=1.0)

	7° after ignition	12° after ignition	17° after ignition
Cr 9.0			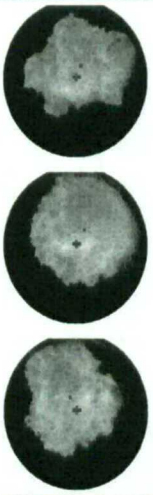
Cr 10.5			
Cr 11.5			

Figure 3.61: Comparison of flame images with varying compression ratio (ϕ=1.0)

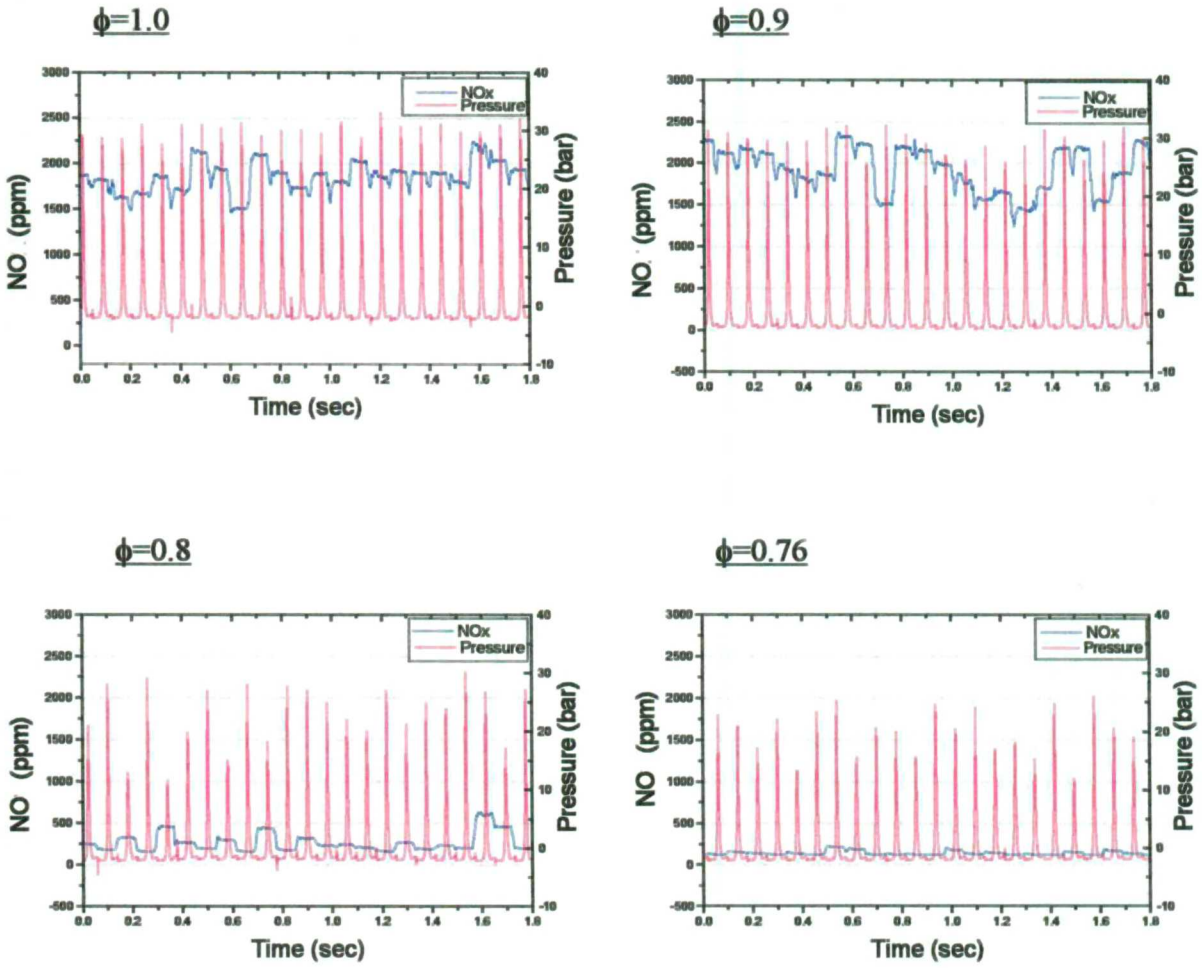

Figure 3.62: Comparison of NO emissions with varying equivalence ratio at compression ratio of 11.5 :1

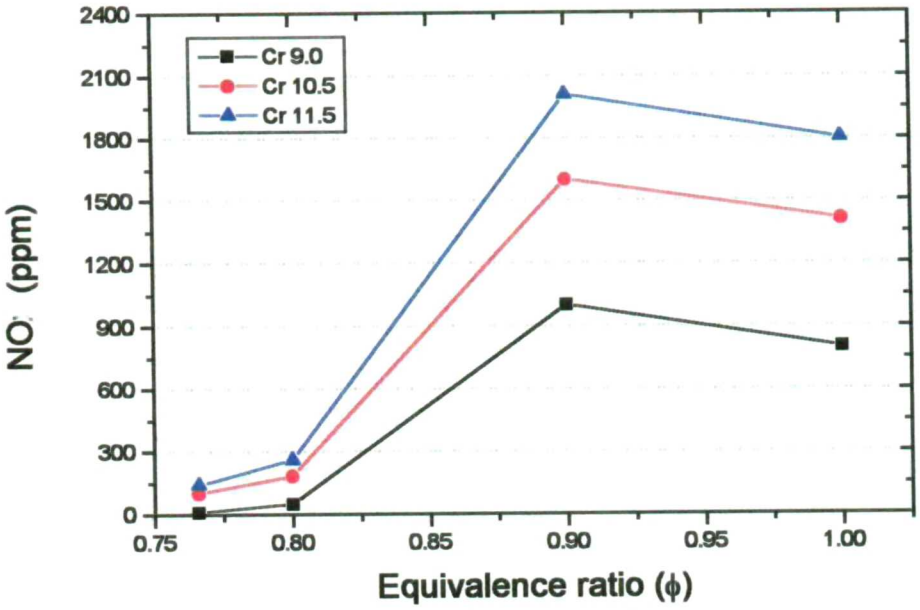

Figure 3.63: Comparison of NO emissions with varying compression ratio

CHAPTER 4

DIRECT INJECTION CNG ENGINE

4.1 Introduction

As already discussed in Chapter 3, a convenient way to improve the fuel economy and reduce the exhaust emissions of CNG-fuelled vehicles is to operate the engine with lean air/fuel mixtures. Unfortunately, these are associated with increased cycle-to-cycle variations and hydrocarbon emissions as well as reduced flame initiation and propagation rates. The most practical approach for improving engine stability under lean mixture conditions is to shorten combustion duration through enhanced in-cylinder mean flow and turbulence combined with stratification of the local mixture near the spark plug at the time of ignition. The gas direct-injection spark ignition engine has been considered to be the most promising solution for achieving this aim due to the ability to control both the fluid mechanics and mixture strength at the spark plug independent of the in-cylinder pre-injection flow motion.

It is well known that the rate of combustion in SI engines is strongly influenced by turbulence and charge motion. Because of the much lower density of natural gas compared to gasoline, the flow through the nozzle of a gas injector attains the speed of sound with a few bar over-pressure. In gas direct injection, turbulent mixing and diffusion of the fuel greatly influence the in-cylinder motion and combustion and, thus, require careful control.

The aim of this chapter is to explore the concept of direct-injection of CNG as means for improving combustion, emissions and performance relative to manifold injection engines. The experimental work has concentrated on a four-cylinder optical spark-ignition engine, with emphasis placed on evaluating the benefits of direct injection against the baseline arrangement where the CNG/air mixture is prepared in the intake

manifold. The high pressure gas injector made by Magneti Marelli was tested in a constant-volume chamber with various ambient and injection pressures and subsequently installed in one of the four engine cylinders. Measurements of engine performance with manifold and direct injection of CNG were obtained respectively, in terms of IMEP, COV of IMEP, flame propagation (CCD imaging), fuel concentration at the spark plug around the time of ignition by means of a sampling probe, and exhaust emissions (HC and NO). Following the description of the experimental systems and techniques in the next section, the results are presented and discussed with conclusions summarised at the end of the chapter.

4.2 Test engine and experimental system

4.2.1 Engine modifications

For doing experiments in an engine that is as close as possible to a production engine while at the same time having optical access for visualisation of flow and combustion, it was decided that the best line of action was to convert into spark-ignition an existing four-cylinder research Diesel engine which has a number of useful features, including an extension between the block and the existing cylinder head that allows optical access through the base of any of the four extended pistons; the bore and stroke of this research engine are 79.5 and 95.5 mm, respectively. Thus, one of the main additions required was a cylinder liner inserted within each of the bores on the extended block. Concerning the cylinder head, it was decided to use the four-valve pent-roof cylinder head from a production 1.8 litre spark-ignition VW engine having a bore of 81 mm which is very close in dimensions to the bore (and stroke) of the existing diesel engine, thus allowing the cylinder spacing and stud positions to remain the same.

To match the cylinder head to the block, a number of the water and oil passages had to be blocked or restricted, with attention being paid to those remaining, in order to ensure that they were able to provide adequate cooling. New extended studs were designed and manufactured to replace the bolts of the original engine.

Before the cylinder head could be installed, a number of modifications were made. Access had to be provided for the CNG injectors as well as for a cylinder pressure transducer, the correct size drive pulley had to be used and a position sensor for the ignition system had to be installed. The injectors were positioned in a way as to direct gas towards the tumbling motion of the charge air, in the direction of the spark plug. Due to space limitations, a hole was drilled through the side of the cylinder head below the exhaust ports and through the water jacket. A sleeve was then manufactured which was screwed through the hole, sealing the water jacket and providing a mount for the injector. Details of the installation are shown in Figure 4.1.

Further machining was required to bore through the top of the cylinder head into the combustion chamber, between the inlet and exhaust valves, next to the spark plug, for a Kistler type 6121 pressure transducer to be installed. This also required provision for the pressure transducer lead to exit through the rocker cover. The cam position was monitored using a Hall effect sensor installed within the standard distributor body, which provided a signal that, when conditioned, was suitable for the ignition system. With the correct drive pulley mounted on the front of the engine, the drive belt tensioner was provided by an arrangement of the pulley that was mounted to the front of the block extension.

The cylinder head was centred on the block using split dowels positioned at the top of the block and machined specially for this purpose. Although provision for the dowels existed within both the cylinder head and the block and at the correct position, the holes were unfortunately of different size.

In order to fit the extended block, special extended pistons had to be manufactured. These were designed to utilise the existing connecting rod from the HSDI engine, and to have a hollow extension between the base and crown of the piston in order to provide optical access through a quartz window inserted in the crown. The quartz window was sized and positioned to provide the maximum possible optical access into the combustion chamber without compromising the strength and durability of the piston. The chosen design of the piston enabled easy removal of the quartz window for cleaning or repair purposes from the space within the piston extension, without a need for the piston removal. Aluminium blanks were also manufactured to replace the

expensive quartz windows, as most of the tests carried out with the engine required optical access to only one cylinder, thus reducing the risk of damage to the other three. The length of the piston was such as to provide a compression ratio of 10.4:1 with the engine cold. The base of the piston was fitted with the standard piston ring pack, with lubrication provided through the oil ring and sealing within the original engine block. The top of the piston was fitted with two dry sealing rings to provide adequate seal within the extended block. Wet lubrication was not provided to this part of the piston, as any oil present at the top of the piston would foul the optical windows within only a small number of motored engine cycles. Thus, dry lubrication was achieved by coating the liner within the extended block with a molybdenum disulphide based spray providing a dry, low friction surface on the liner. The piston design also accounted for thermal expansion/distortion and elongation of the piston immediately before TDC due to deceleration, both effects exaggerated with such a long piston. The design also took into account the potential impact between the piston crown and the inlet valves under normal operating conditions, thus cut outs were machined into the piston crown. A drawing and photograph of the extended piston can be seen in Figures 4.2 and 4.3.

With the addition of a new liner to the existing extended block, small ports were machined through the liner of cylinder #4 in line with the ports already existing in the block extension, so that small quartz windows could be fitted within the ports to both seal the hole and provide optical access into the combustion chamber from the side at all times except when the piston was very close to or at TDC (Figure 4.4). In addition to this, a four-two-one exhaust manifold was fabricated to accommodate the engine design.

Due to the 'top heavy' nature of the engine with the block extension, an additional engine mount was installed, from the engine cradle to near the top of the side face of the block extension. A rubber mount was used to damp any vibrations that occurred, as it was not considered necessary to rebalance the crankshaft to suit the forces introduced by the new pistons.

4.2.2 Test engine

The four-cylinder optical research engine is based on a VW 1.9 L diesel engine and was modified to accommodate a production 1.8 L spark ignition cylinder head of four-valve pent-roof geometry. Figures 4.5 and 4.6 show the modified optical engine used in the present tests, which incorporates a production cylinder head and an extended piston, with windows in the cylinder liner and piston crown made of quartz for providing optical access into the combustion chamber. The engine specifications are summarised in Table 4.1.

Table 4.1: Engine specifications

Engine type	4 cylinder, 4 valve pent-roof cylinder head
Bore x Stroke	79.5 x 95.5 (mm)
Displacement	1.9 l
Compression ratio	10.4
Ignition system	Dynalco Starfire 800
Injection system	Intake manifold injection

The engine was coupled to a 37 kW dynamometer (Thriege-Scott) providing engine motoring and firing capability with automatic switching between positive and negative torque.

Two different fuel injection systems were used in these experiments. The first is manifold injection and the other is a high pressure direct injection system. In the case of manifold injection, the inlet manifold was fitted with a throttle, and upstream of the throttle the CNG supply was connected via a rotameter to the inlet air supply. This enabled the engine to be run under firing conditions with a pre-mixed fuel/air mixture of known equivalence ratio. In the high pressure direct injection system, the injectors were positioned to direct gas, towards the spark plug for inducing charge stratification. Figure 4.7 show the comparison of two different gas injectors for manifold and direct injection. The throttle was fitted with a digital reference and the air mass flow rate was calibrated against throttle setting for a range of engine speeds using an air flow meter (Lucas Dawes 1641). In addition, the fuel mass flow rate was estimated using a fuel flow meter (Micro motion RTF 9726 and D6-D12).

A commercial ignition system (Dynalco Starfire 800) was connected to an inductive ignition coil on each spark plug, and it was fully programmable from a PC link. The system was provided with two reference signals, a magnetic pick-up which detected the 125 teeth on the flywheel and a Hall effect sensor attached to the camshaft which provided a marker pulse every firing cycle. To accommodate the limited sensor inputs, the ignition system was configured to assume that the engine was a 2-stroke, so that the number of flywheel teeth the unit would count per revolution could be doubled; this eliminated the requirement for another reset sensor.

Data acquisition was performed using a multi-channel data logging system with a resolution of 1/8 crank angles relative to the engine shaft-encoder and the camshaft position sensor. A shaft-encoder producing 2880 pulses per engine revolution was fitted to the crankshaft and a magnetic pick-up sensor attached to the camshaft detects the TDC position. These signals are used for acquisition of the in-cylinder pressure and simultaneous triggering of the image acquisition equipment. The air-fuel ratio was monitored using an NTK UEGO lambda sensor (NGK type TL-7111-W1) which was fitted to the exhaust pipe.

4.2.3 Experimental set-up and engine operating conditions

Figure 4.8 schematically illustrates the interconnection between the control circuitry, indicated in black, the pressure acquisition system in violet and the flame imaging with the CCD camera in green. During the combustion analysis, the exhaust emissions of NOx and hydrocarbons were recorded using Cambustion fNOx 400 and Cambustion HFR 400 and are shown in red. The cylinder pressure was measured with a piezo-electric transducer (Kistler 6121) and associated charge-amplifier and monitored on an oscilloscope, while the digitised signal was integrated with the data acquisition system. The in-cylinder HC concentration in the vicinity of the spark plug, with a time resolution of a few degrees crank angle, was measured using a fast FID (Cambustion HFR 400) with a special spark plug kit which is shown in orange.

There are two main operating conditions examined in this experimental programme. The first is fixed throttle position and the second is fixed load. Fixed throttle maintains

the intake manifold pressure at 650 mbar using the throttle valve which is positioned upstream of the plenum chamber and a vacuum gauge connected to it; this setting corresponds to typical part-load conditions in engine testing and is used here as the baseline case for comparing engine performance. Fixed-load condition, on the other hand, corresponds to fixed amount of fuel and air; in both cases, the engine speed is set at 1,600 rpm using the dynamometer controller. For these load conditions, three equivalence ratios were examined: stoichiometric, ϕ=0.9 and ϕ=0.8, with subsequently leaner mixtures tested in order to identify the lean operating limit of the engine. The coolant water and oil temperature were in all cases maintained at 80°C. The general engine operating conditions are outlined in Table 4.2.

Table 4.2: Engine operating conditions

Engine speed	1600 rpm
Load conditions	• Fixed throttle • Fixed load
Test fuel	CNG (93% methane)
Injection pressure	• Manifold injection : 10 bar • Direct injection : 80 bar
Equivalence ratio	ϕ=1.0, 0.9, 0.8 and lean limit
Spark timing	MBT
Coolant water and oil temperature	80° C

The ignition timing has been set in all cases to give maximum brake torque. This MBT ignition timing was calculated by measuring the average engine torque or IMEP over a number of engine cycles at different spark timing positions, and then selecting the crank angle degree that produces the highest torque/IMEP value.

4.3 Gas jet imaging

Prior to the engine tests, an experimental study was performed to investigate the gaseous jet characteristics of high-pressure fuel injection systems appropriate for use in direct–injection CNG engines. The global jet development process was visualised using Schlieren photography; this technique is one of the most effective means of

determining the penetration and structure of a gaseous jet. The constant-volume chamber described in Chapter 2 was used to characterise the gaseous jet injected from the prototype high-pressure injector provided by Magneti Marelli under different chamber and injection pressure conditions.

4.3.1 Effect of ambient pressure

Figure 4.9 shows a sequence of photographs taken in the constant-volume chamber at various times after the start of injection, ranging between 2.0 and 3.0 ms, at a fuel injection pressure of 80 bar and an ambient pressure of 2 bar. The injection jet angle which was experimentally determined from the Schlieren photographs, depends on the geometry of the nozzle and the axial jet velocity. The jet penetration has been defined as the maximum distance from the exit of the injector at a given time after the start of injection. The obtained images confirmed that the gas emitted from the injector propagates in the form of a straight jet and is symmetric in structure. After 2ms, the jet reaches the far side of the chamber and begins to form wall jets towards both sides. After 3 ms it can be seen that the jet bounces back from the bottom of the chamber wall and reaches the top of the chamber around the injector. The momentum of the deflected jet is closely related to the injection pressure. When the chamber pressure increases to 8 bar, as shown in Figure 4.10, although the gas jet develops in a similar fashion, unlike the low chamber pressure case the gas jet does not reach the bottom of the chamber at the time of 2ms after injection implying reduced penetration. With an increase in ambient pressure, the cone angle seems also to decrease from 28° to 24°. Thus, an increase of the chamber pressure leads, maybe surprisingly, to a decrease of both the jet penetration and cone angle; the test results are summarised in Table 4.3.

Table 4.3: Comparison of jet cone angle and penetration as a function of chamber pressure.

Chamber pressure	Cone angle	Penetration
2 bar	28°	48 mm
8 bar	24°	34 mm

4.3.2 Effect of injection pressure

Figure 4.11 shows the Schlieren images at injection pressures between 20 and 80 bar at 2ms after injection and at 8 bar ambient pressure. The Schlieren technique provides images of the first derivative of the refractive index of the gas jet which is proportional to the gas density gradient. As a result, the jet image at the low-pressure injection is not as clear as that at higher pressures. With increasing injection pressure, the cone angle decreases slightly from 26° to 24°. As expected, increasing the injection pressure also leads to an increase in jet penetration; the test results are summarised in Table 4.4.

Table 4.4: Comparison of cone angle and penetration as a function of injection pressure

Injection pressure	Cone angle	Penetration
20 bar	26°	31 mm
80 bar	24°	34 mm

4.4 Comparison between manifold and direct injection

The most likely cause of the lower power output of port-injected CNG engines when compared to gasoline engine is the reduction in volumetric efficiency (η_v). Compared to gasoline that is supplied to the engine's intake port in liquid form, in the case of CNG the fuel injection system injects gas which accounts for 10% of the intake air volume. The end result is that the actual amount of inducted air into the cylinder is reduced.

In order to investigate ways to improve the performance of engines fuelled with CNG, the injection strategy has been changed to allow injection of CNG directly into the cylinder. The anticipated benefits are the effect on charge motion due to injection of highly pressurised gas directly into the cylinder, and possible charge stratification effects especially with lean mixtures. In this section, first the optimisation of the fuel injection timing in terms of the combustion characteristics is described, followed by the improvements achieved with lean mixtures when the selected optimum injection strategy for enhancing charge motion and stratification is employed.

4.4.1 Effect of fuel injection timing

In a conventional spark-ignition engine fuelled with gasoline, fuel is injected onto the back of the closed intake valves. This occurs a relatively long time before the valves open so that a significant fraction of the fuel vaporises before entering the cylinder to allow the nearly gaseous fuel to mix with air efficiently prior to combustion. Since CNG is a gas at room temperature, it requires no time for vaporisation which makes it possible to inject the fuel directly into the cylinder even late in the compression stroke. It is anticipated that, in this case, direct injection can have a beneficial effect on volumetric efficiency and in-cylinder large-scale motion and turbulence which, in influence flame propagation. In addition, it makes easier to induce charge stratification at the time of ignition which improves combustion under overall lean mixture conditions. However, high pressure injection is required to overcome the chamber pressure late during the compression stroke and achieve adequate gas penetration towards the spark plug.

Figure 4.12 shows the injection strategies for the manifold and direct injection schemes at 1600 rpm part-load conditions. In the case of manifold injection, during the expansion stroke, the injector was installed upstream of the throttle which enabled the engine to run under firing conditions with a pre-mixed air/fuel mixture. Two direct-injection timings are shown in the diagram representing early and late injection during the induction and compression stroke, respectively. In the case of the early injection strategy during the induction stroke, CNG is required to mix with air providing a homogeneous charge of either stoichiometric or lean composition. In the case of the late injection strategy during compression, a high degree of charge stratification is required with a rich mixture near the spark plug at the time of ignition and the rest of the mixture being very lean. Table 4.5 summarises the three different injection timings used in the present research programme.

The early injection timing is symmetrically arranged relative to the opening of the intake valves, i.e. it is centred on the maximum valve-lift. Late injection corresponds to the time from just before the closing of the intake valves, around intake BDC, to 30° before ignition. This implies that in this case accurate start of injection and careful

synchronisation with the time of ignition is required to achieve optimum charge stratification and flame initiation conditions.

Table 4.5: Summary of manifold and direct injection timings for stoichiometric engine operation

Injection strategy	Injection timing
Manifold injection	330-230 (°CA bTDC)
Direct injection (early)	50 -155 (°CA aTDC)
Direct injection (late)	188 -310 (°CA aTDC)

4.4.2 Combustion characteristics

MBT ignition timing – Figure 4.13 shows MBT ignition timings for three different injection strategies. As the equivalence ratio decreases and mixture becomes leaner, the ignition timing for obtaining optimum engine performance is advanced from 25° CA bTDC to 50° CA bTDC. Since CNG has a high octane rating, it is possible to set ignition timing at MBT at all engine speeds without knocking. On the other hand, MBT timing was retarded in the case of direct injection due to the faster burning rates achieved relative to the manifold injection case. As the equivalence ratio decreases, the difference in the retarded timing required between manifold injection and direct injection becomes larger. There are several reasons for the faster burning rates achieved with direct injection relative to manifold injection which include enhanced mean flow and turbulence, charge stratification and increased volumetric efficiency. Generally, enhanced in-cylinder flow motion (tumble or swirl) requires a smaller MBT ignition advance, indicating faster burning rates and reduced cyclic combustion variations (Kalghatgi, 1987).

Pressure analysis – In order to quantify the effect of direct injection on the performance of the engine, the indicated mean effective pressure (IMEP) and its coefficient of variation (CoV), defined as the standard deviation divided by the mean, have been calculated as an average over approximately 150 cycles. Figure 4.14 shows the variation of IMEP and CoV of IMEP with equivalence ratio.

The results indicate that the IMEP measured in the case of direct injection is consistently higher than that with manifold injection. For example, the IMEP for the late and early direct-injection strategies is higher by between 9 and 15% than that for manifold injection; this is mainly due to the increased volumetric efficiency achieved through direct injection of CNG into the cylinder. Figure 4.15 shows the comparison of air and fuel flow rates for three different injection timings at a fixed throttle condition (engine speed of 1600 rpm; intake manifold pressure of 650 mbar). The air-flow rates for late and early direct injection are higher by between 9 and 14% than for manifold injection. This represents a significant improvement achieved by simply altering the injection strategy which allows enhanced performance of the engine fuelled with CNG.

Figure 4.14(b) shows the CoV of IMEP over 100 cycles. The CoV is reduced for direct injection across the whole range of equivalence ratios. These results, which are summarised in Table 4.6, demonstrate that the direct-injection strategy can improve significantly the combustion stability around the lean operating limit, bringing it within the driveability range of production engines.

Table 4.6: Comparison of combustion stability under very lean mixture conditions with fixed throttle (n=1600 rpm, P_I=0.65 bar, ϕ=0.72)

Injection system	CoV of IMEP (%)
Manifold injection	23.7
Direct injection (early)	4.0
Direct injection (late)	1.6

The lean operating limit for stable combustion in the optical research engine has been arbitrarily set at CoV of IMEP of 5%; in production engines this limit is even lower (3%). Direct injection (early) allows only a slight extension of the lean limit from 0.73 to 0.72, contrary to late direct injection which results to a more substantial extension from 0.73 to 0.67. These results are summarised in Table 4.7.

Table 4.7: Summary of the lean operating limit for manifold and direct injection with fixed throttle (n=1600 rpm, P_I=0.65bar)

Injection system	Lean limit (ϕ)
Manifold injection	0.73
Direct injection (early)	0.72
Direct injection (late)	0.67

It is surprising to see what a significant improvement in the CoV of IMEP and lean operating limit has been produced by direct injection which may be due to several factors. The increased volumetric efficiency associated with direct injection leads to more stable combustion than manifold injection while the enhanced in-cylinder charge motion generated by high pressure injection during the induction and compression strokes gives rise to increased turbulence intensity and, thus, enhanced flame convection and overall burn rate. This is confirmed by the flame image analysis later in this section. Most important, the direct injection of CNG can induce some degree of charge stratification which improves combustion especially with lean mixtures. The richer air/fuel ratio in the vicinity of the spark plug at the time of ignition complemented by the stronger mean flow during flame kernel formation and the overall higher turbulence levels during flame propagation, are jointly responsible for the faster and more stable combustion observed in the case of open-valve injection of CNG within sleeved intake ports. This charge stratification effect will be discussed further in a later section in conjunction with the in-cylinder direct sampling of HC using a fast FID analyser.

To further investigate the reasons for the observed extension of the lean limit with direct injection, the fixed load test condition was also examined. By maintaining the same amount of air and fuel between direct and manifold injection, the effect of the increased volumetric efficiency associated with direct injection can be eliminated, allowing the effects of charge stratification and enhanced flow motion generated by fuel injection into the cylinder to be highlighted.

Figure 4.16(a) shows the variation of IMEP with equivalence ratio for the manifold and two direct injection cases under fixed load condition. For stoichiometric mixtures, there is an improvement in IMEP for early and late direct injection, relative to manifold

injection, attributed to the increase in the air flow rates under fixed load condition; the effect is more pronounced for lean mixtures.

Figure 4.16(b) shows the CoV of IMEP over 100 cycles. Despite the increase of the air-flow rate for early and late direct injection, the improvement in combustion stability with manifold and early direct injection is still lower compared to that of late direct injection. So, there should be some additional effects for the extension of the lean limit and improvement of combustion stability in the case of late direct injection ; such effects will be investigated in more detail later when the flame image analysis and the in-cylinder HC sampling will be discussed. Table 4.8 summarises the results of the combustion stability analysis under lean mixture condition (ϕ=0.72).

Table 4.8: Comparison of combustion stability under very lean mixture condition at fixed load (n=1600 rpm, air flow rate =242 g/min, fuel flow rate=10.5g/min, ϕ=0.72)

Injection system	CoV of IMEP (%)
Manifold injection	8.6
Direct injection (early)	3.5
Direct injection (late)	1.6

Direct comparison of the in-cylinder pressure distribution for the various test cases is presented in Figure 4.17. All data were obtained under very lean mixture conditions, at an equivalence ratio of 0.72 which was found to be close to the lean operating limit of the engine when fuelled with CNG. The in-cylinder pressure traces for the manifold injection case are widely spread, indicating poor stability at this operating condition. Closer inspection reveals that there is partial burning in one cycle, but no partial burning was observed in the direct injection cases where the pressure traces for the various cycles are closely grouped together. The mass fraction burnt values obtained over 100 cycles are given in Figure 4.18 and Table 4.9 where it is clear that the larger improvement appears again to take place in the case of late direct injection.

Table 4.9: Summary of mass fraction burnt for 3 different injection strategies at fixed load condition and lean mixture.(n=1600 rpm, air flow rate =242 g/min, fuel flow rate=10.5 g/min, ϕ=0.72)

Injection strategy	0-10% burn (CA)	10-80% burn (CA)
Manifold injection	36°	41°
Direct injection (early)	26°	30°
Direct injection (late)	21°	24°

Analysis of flame images - Direct flame images for 1,600 rpm part-load and a stoichiometric air-fuel mixture are shown in Figure 4.19 for the manifold and the two direct injection cases over the range 6°-31° crank angle degrees after spark discharge and for 5° degree intervals. Initial inspection of the flame images for the direct injection case has identified significant differences in the flame structure relative to the manifold injection case. Comparison of the flame growth rate between the various cases indicates that faster flame growth occurs with direct injection. For manifold injection (Figure 4.19(a)), the convection of the early flame is consistently towards the exhaust valves, caused by the prevailing tumble motion, but with early direct injection (Figure 4.19(b)) the direction of flame convection is quite different, this time towards the left hand side of the cylinder. For late direct injection (Figure 4.19(c)), on the other hand, early flame convection appears to be in a direction approximately 30° to the fuel jet direction, i.e. 'up and sideways' compared to the 'upwards' convection observed in the manifold injection case. These results confirm that direct injection of CNG at high injection pressure (80 bar) produces a significant change in the charge motion around TDC during the early propagation phase of the flame.

Complementary information can be obtained from the position of the notional centre of the instantaneous flame (Figure 4.20) where, for manifold injection and for the two direct injection timings, 12 points are plotted representing the flame centre position at the same crank angle over an equal number of cycles. On the basis of the images obtained, at 6° and 11° after spark discharge, it can be concluded that injection of CNG into the cylinder produces a significant change in the charge motion and strength around TDC that is evident during the early propagation phase of the flame. A comprehensive representation of the general in-cylinder flow motion for both early and late direct injection strategies is given in Figures 4.21 and 4.22. The injector was

inclined 15° relative to the centre of the spark plug, in the direction of the tumbling motion of the air, towards the spark plug.

In the late direct-injection case, the gaseous jet impinges on the cylinder wall and then spreads out in both down wards and upwards directions. The downwards moving jet impinges on the top of the piston, which moves upwards during the compression stroke and also collides with the induction-driven air flow, losing part of its momentum as it mixes with air. On the other hand, the upwards moving wall jet is directed towards the exhaust side close to the tip of the spark plug, but without any interaction with the upwards moving piston. The upwards injected gas is re-circulated around the upper part of the combustion chamber giving rise to charge stratification as it entraining air during its penetration. This charge stratification effect achieved with late direct injection will be confirmed in the next section through the spark plug sampling experiments.

In the early-direct injection case, during the induction stroke, the high pressure jet interacts with the induction-driven air flow which moves down the exhaust side of the chamber and also impacts on the edge of the intake valve at early injection timings. So, this jet might be deflected to different directions compared to that of late injection enhancing mixing with air. The qualitative observations about the flame position are supported by quantitative representation of the flame area temporal variation. Figure 4.23 shows the development of the enflamed area measured up to 31° after spark discharge; each area value represents an average of over 12 separate flame images. There is a clear increase in the enflamed area at the same crank angle position for the cases of early and late direct injection relative to that of manifold injection, confirming the advantages of the direct injection concept in flame development.

Analysis of fuel concentration - Figure 4.24 shows the cycle-to-cycle variations of the fuel concentration at the spark plug for the three different injection timings under very lean mixture conditions (ϕ=0.72), closely corresponding to the lean limit of the engine when fuelled with CNG. The 12 consecutive fuel concentration traces for the case of manifold injection are widely spread, indicating poor combustion stability. Closer inspection reveals that there are several partial burning cycles in the case of manifold injection. This incomplete burning decreases the combustion stability and increases the

unburned hydrocarbon emissions during the exhaust stroke. However, fuel concentration traces for early and late direct injection are more closely grouped together, indicating better combustion stability. In particular, with late direct injection, the average fuel concentration in the spark plug reached 32,500ppm C3 (equivalent to an air/fuel ratio of 17.3) at the time of ignition, i.e. richer that the rest of the mixture, while with manifold injection the averaged fuel concentration in the spark plug reached only 25,000 ppm C3 (equivalent to an air/fuel ratio of 23) at the time of ignition. These results are summarised in Table 4.10. Figure 4.25 shows averaged air/fuel ratio traces for the three injection timing under lean mixture conditions (A/F ratio=22.8).

Table 4.10: Cycle-averaged fuel concentration and Air/Fuel ratio at the spark plug under lean mixture conditions (A/F ratio=22.8)

Injection strategy	FID output (ppm C3)	Air/Fuel ratio
Manifold injection	25,000	22.3
Direct injection (early)	26,500	22.0
Direct injection (late)	32,500	17.3

These results confirm that late direct injection does lead to some charge stratification near the spark plug at the time of ignition relative to both manifold and early direct injection, especially near the lean limit. It is thus clear that, through charge stratification, stable combustion can be realised even at extremely lean conditions. It should be noted that this approach is more promising with gas rather than with liquid fuel injection where electrode wetting can be a serious problem with late direct injection, necessitating careful control of injection timing and spray characteristics.

4.4.3 Engine-out emissions

In Figure 4.26(a), the hydrocarbon emission measurements are shown for manifold and the two direct injection cases as a function of equivalence ratio. In general, leaner mixtures give lower HC emissions until the combustion quality becomes poor (leading eventually to misfire), and HC emissions rise sharply, while engine operation becomes erratic. Under stoichiometric conditions, late direct injection shows higher hydrocarbon emissions relative to manifold injection and early direct injection. This is due to the

relatively rich mixture near the spark plug at the time of ignition as a result of charge stratification induced by late direct injection, that gives rise to higher hydrocarbon emissions. Previous results have shown (Arcoumanis *et.al.*,1998; Arcoumanis and Kim.,1999) that, as the mixture becomes leaner than equivalence ratio of 0.8, open-valve port injection results in lower HC emissions compared to close-valve injection. In the case of direct injection, the measured HC emissions were reduced significantly compared to manifold injection near the lean limit. As already said, this is due to the combined effect of charge stratification and enhanced flow motion which allows improved combustion stability even under leaner mixture conditions. It should be mentioned, however, that better control of gas jet penetration and timing of ignition relative to the time arrival of the fuel jet at the spark plug can reduce the HC emissions significantly.

Figure 4.26(b) shows the NOx emissions for combustion of CNG across a range of equivalence ratios on the lean mixture side. Around the stoichiometric ratio the NOx emissions are higher in the case of late direct injection, due to the higher in-cylinder pressures and temperatures associated with the faster burning observed under these flow and mixture conditions. However, towards the lean operating limit, the NOx levels in the case of the late direct injection drop significantly to levels similar to those of manifold injection. It is important to note that the use of direct injection allows extension of the engine's lean operating limit to about 0.67 with associated further reduction of the NOx engine-out emissions. Overall, it can be argued that careful control of fuel jet orientation, jet structure with associated air entrainment, and ignition timing relative to stratified charge can lead to simultaneous reduction of HC and NOx engine-out emissions. Using CNG it is also possible to reduce particulate emissions to insignificant levels which is now becoming an important emission issue in gasoline engines running at high loads and speeds.

4.5 Conclusions

Investigation of the possible advantages offered by direct injection of CNG into the cylinder of a four-valve spark-ignition engine revealed the following:

- The gas injected from a high-pressure production injector was in the form of a symmetric solid-cone jet with an average cone angle of ~25 degrees. Increase of the ambient pressure in the constant volume chamber led to a decrease of the gas jet penetration and cone angle. Increase of the injection pressure, on the other hand, gave rise to slightly smaller jet cone angle and increased tip penetration.

- Direct injection of CNG offers advantages in terms of power output, extension of lean limit and UHC emission levels relative to the baseline case of manifold injection.

- Direct injection of CNG has a significant effect on flame propagation. Different injection timings (early and late injection) produced different flame propagation rates, with different initial flame convection, and different levels of charge strength.

- Late injection provides more benefits than early injection. In-cylinder sampling at the spark plug has indicated that the local mixture concentration at the time of ignition was close to stoichiometric, although the overall mixture was very lean.

- For the fixed throttle case, direct injection increased the IMEP by 18-35% compared to manifold injection, while the MBT timing was retarded by 7-22 CAD. Lean limit was extended from an air/fuel ratio of 22 with manifold injection to 23 and 26 for early and late injection, respectively; the corresponding cycle-by-cycle variations of combustion in terms of CoV of IMEP were reduced from 23.7% to 4% and 1.6%, respectively, at ϕ=0.72.

- For the fixed load case, an increase in IMEP was also evident for direct injection while the CoV of IMEP was reduced from 8.6% for manifold injection to 3.5% and 1.6 % for early and late injection, respectively. A study of the combustion process

using heat release analysis has indicated that, for the same nominal equivalence ratio in the cylinders, the burning rate of the initial 10% of the mixture was shortened by 10 CAD and 15 CAD with the two direct-injection strategies, while similar reductions were identified at the later stage of combustion.

- Visualisation of combustion by means of digital imaging has confirmed the faster combustion obtained with late direct injection. The initiation and propagation of the flame were affected by fuel injection due to the modification of the large scale flow in the cylinder by the high-speed gaseous jet. The enhanced mean flow and turbulence seemed to be responsible for the increased flame speed, while the distribution of the mixture played an equally important role in the stability of combustion observed with very lean overall mixtures.

- Although the use of direct injection of CNG into the engine cylinder generated high UHC and NO emissions under stoichiometric conditions, it allowed at the same time extension of the lean operating limit with associated lower UHC and NO emissions and better fuel consumption. This approach offers promise for overall reduction of UHC and NO levels in engines fuelled with CNG while maintaining comparable performance to that of gasoline engines of equal capacity. The key to reducing exhaust emissions is the optimisation of the fuel jet penetration and air entrainment relative to the time of ignition and the air flow generated by the intake ports.

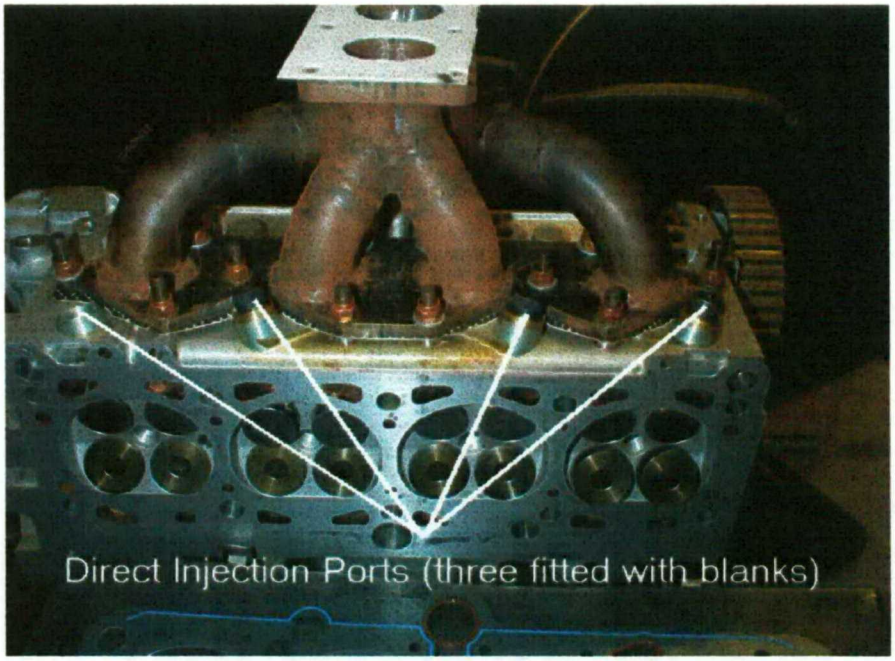

Figure 4.1: Under side of cylinder head showing direct injection ports

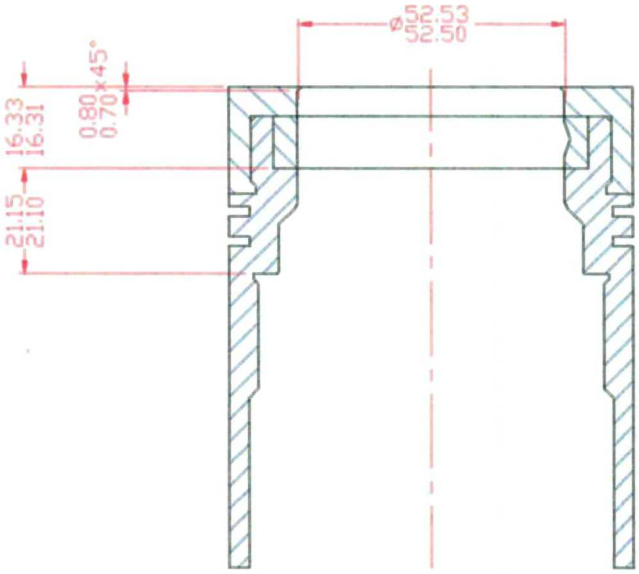

Figure 4.2: Drawing of optical quartz piston

Figure 4.3: Optical piston protruding from original block

Figure 4.4: Side window in cylinder liner

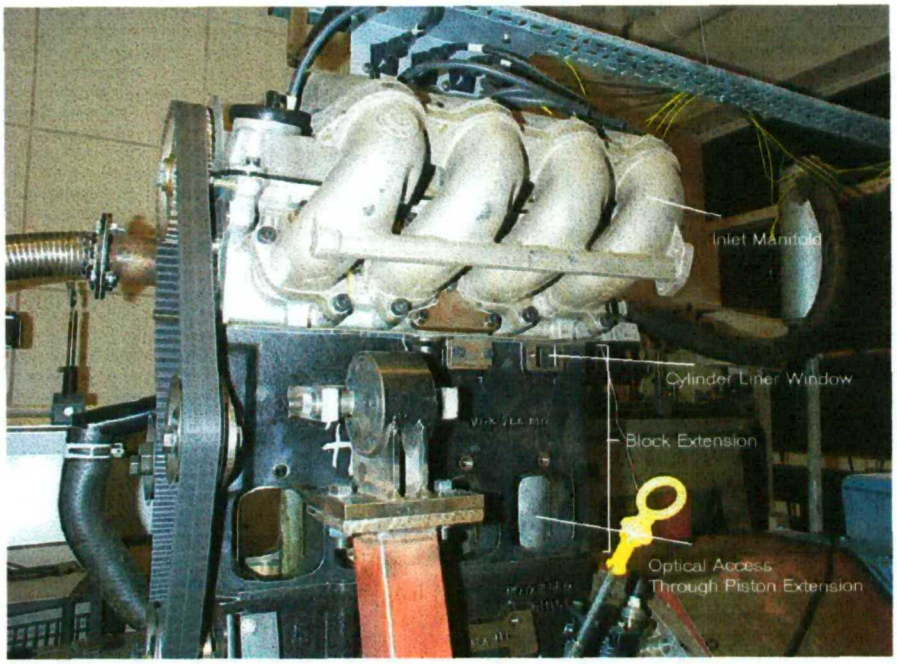

Figure 4.5: Inlet port view of the engine

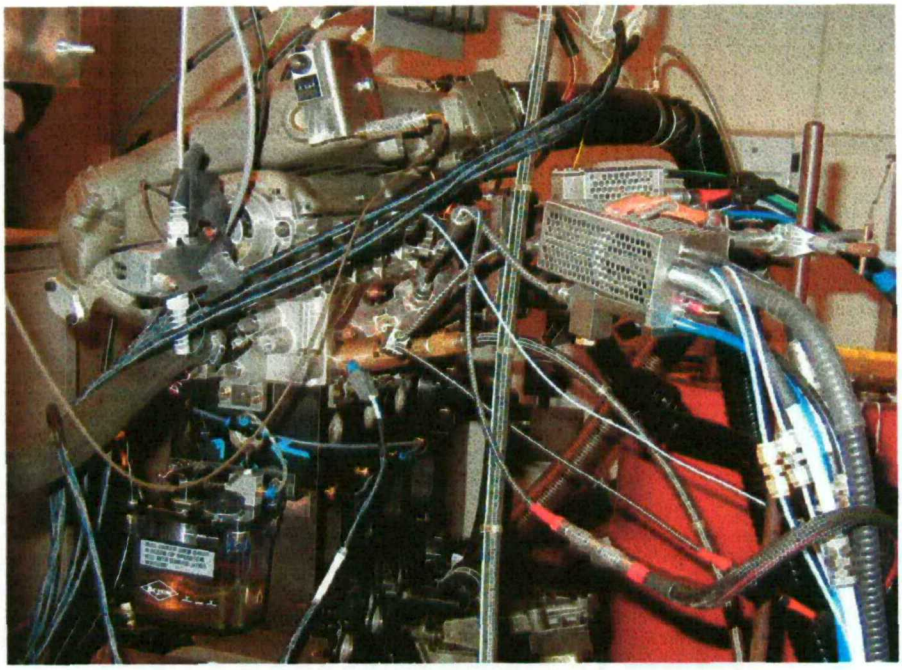

Figure 4.6: Exhaust port view of the engine

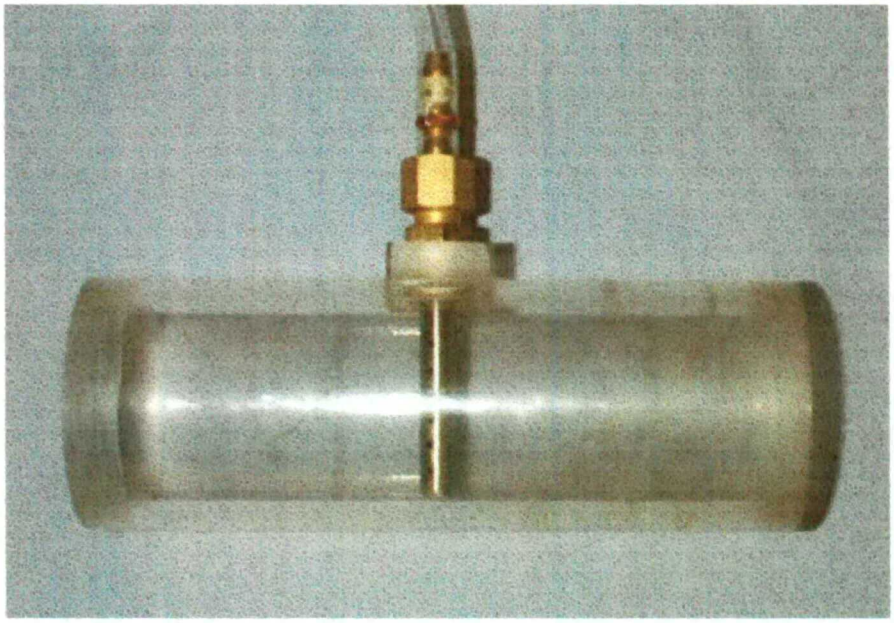

(a)

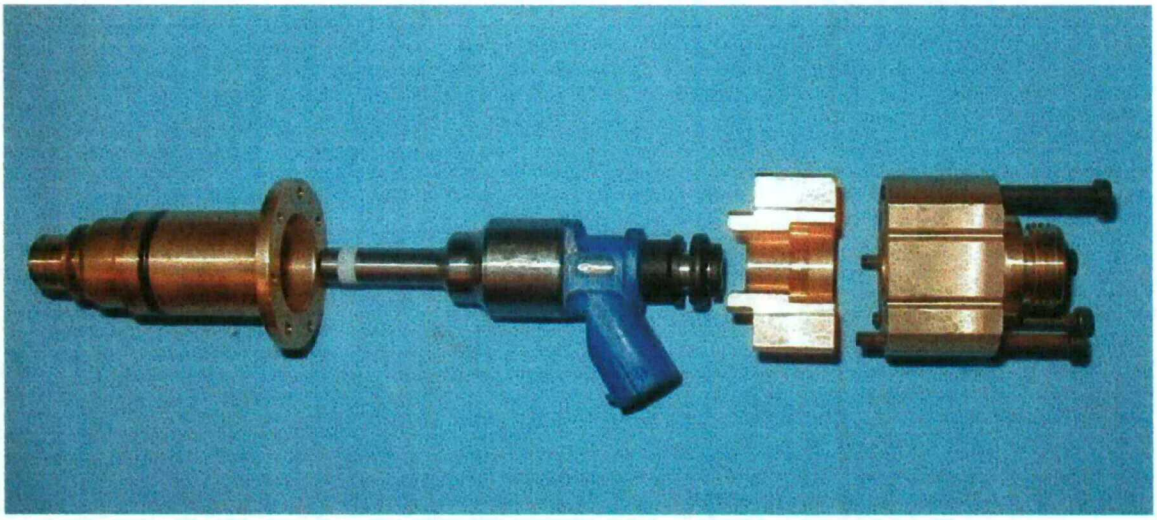

(b)

Figure 4.7: Photograph of two different gas injectors

(a) Low pressure manifold injector with adapter

(b) High pressure direct injector with adapter

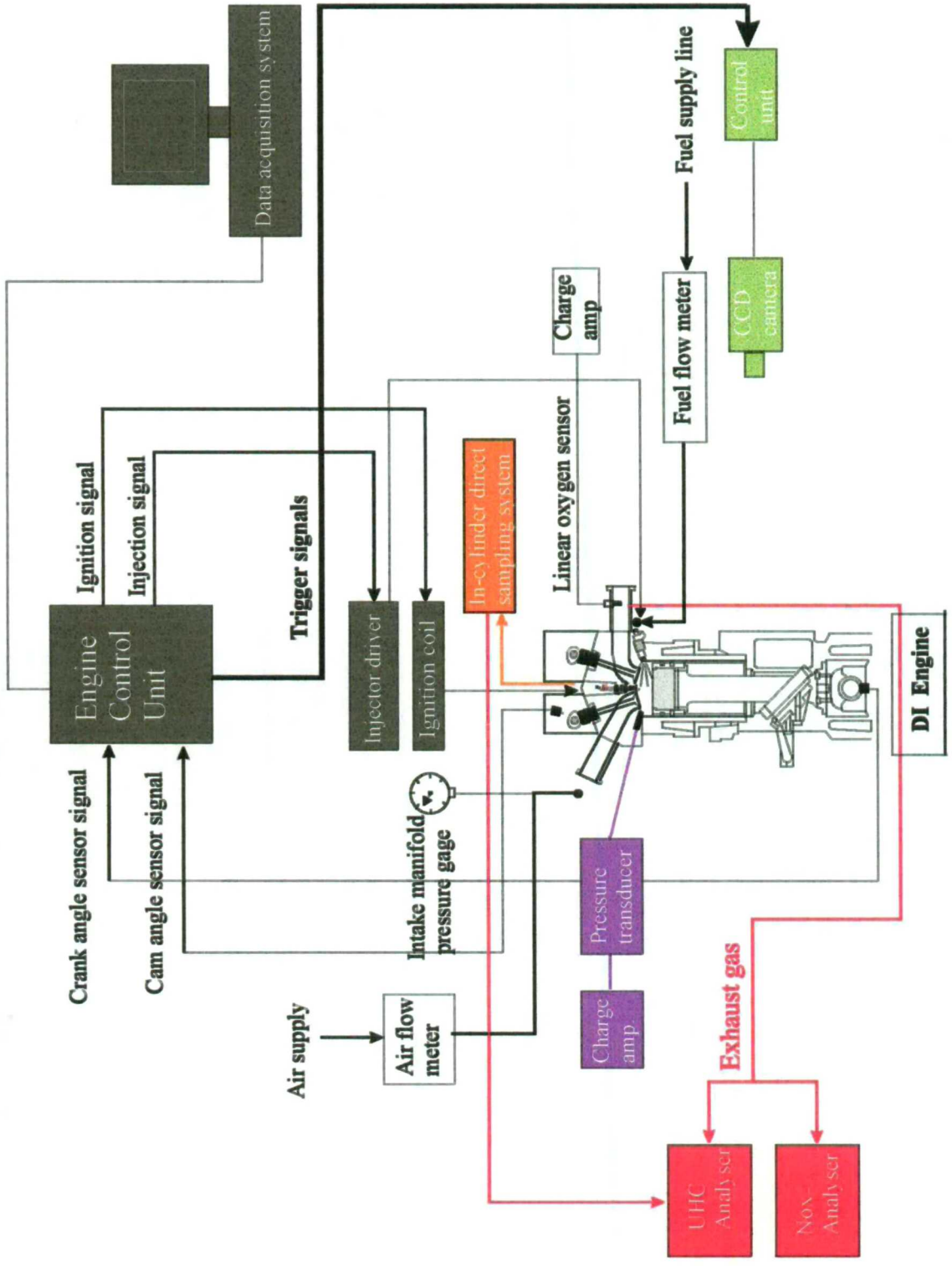

Figure 4.8: Schematic of experimental set-up

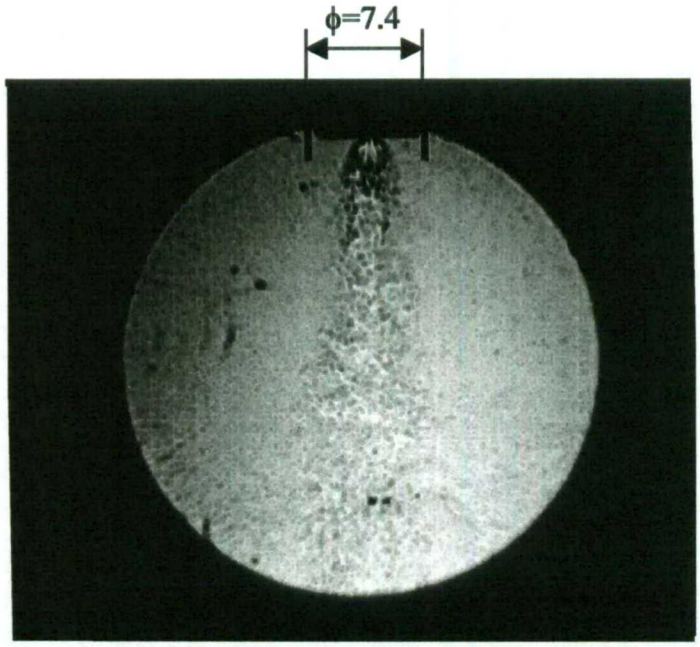

Cone angle : 28°

(a)

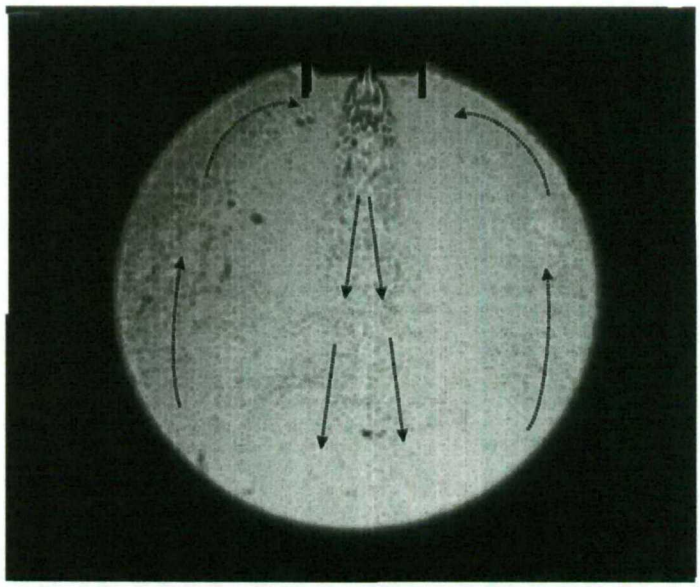

Cone angle : 28°

(b)

Figure 4.9: Schlieren images of CNG spray at different moments after injection start (P_l=80 bar, P_a=2 bar)

(a) 2.0 ms after injection (b) 3.0 ms after injection

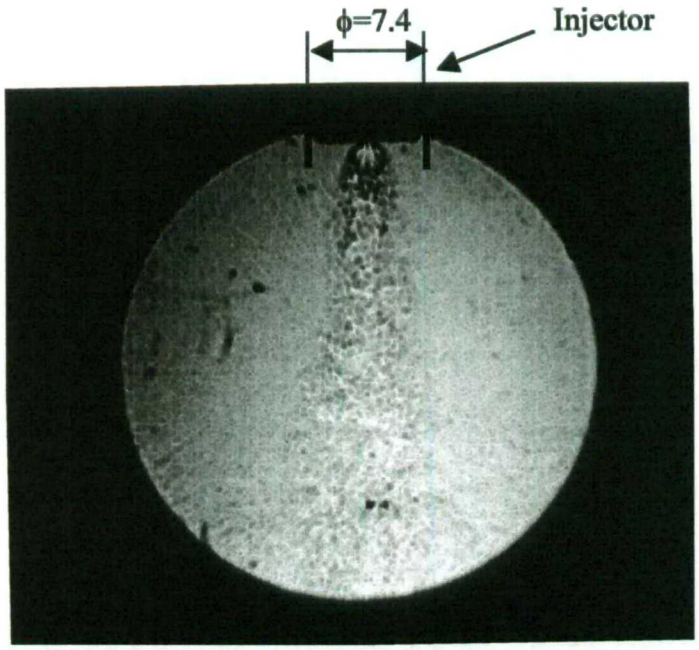

Cone angle : 28°

(a)

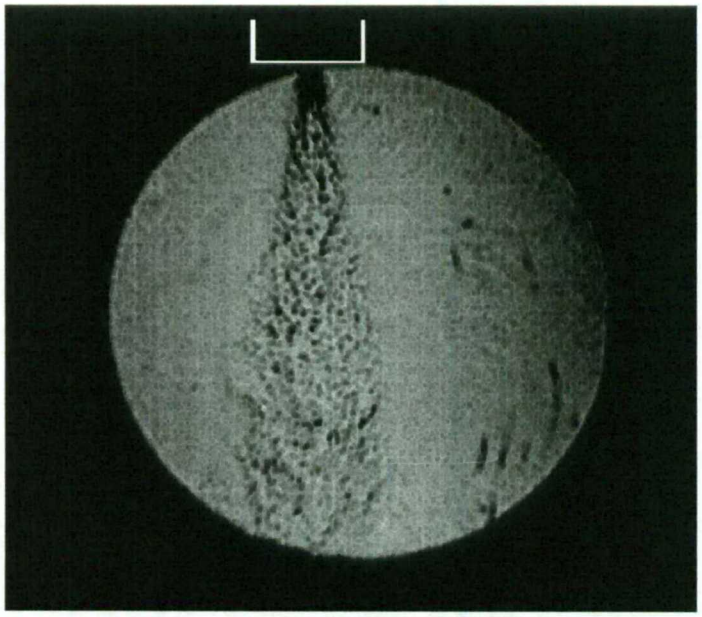

Cone angle: 24°

(b)

Figure 4.10: Schlieren images of CNG at 2.0 ms after injection (P_i=80 bar)

(a) 2 bar ambient pressure (b) 8 bar ambient pressure

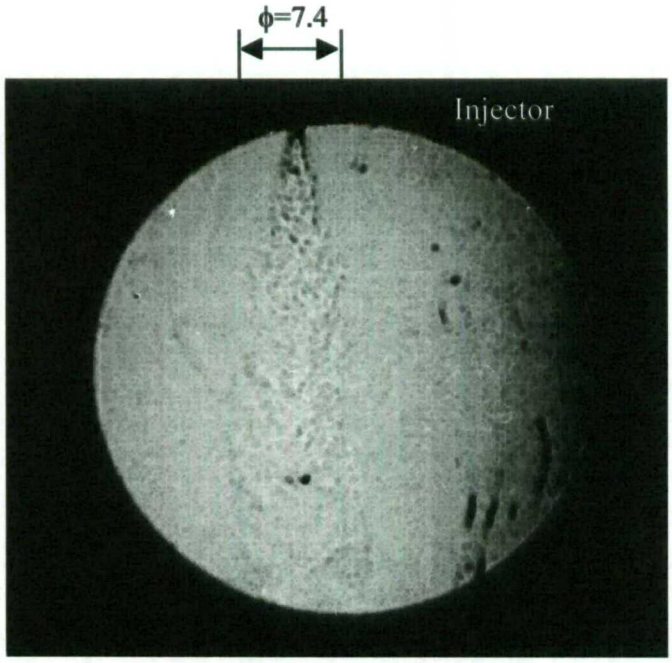

Cone angle: 28°

(a)

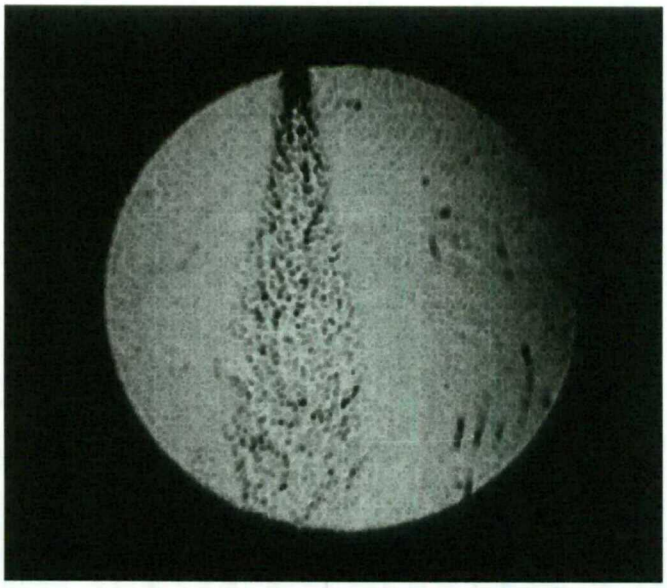

Cone angle: 24°

(b)

Figure 4.11: Schlieren images of CNG at 2.0 ms after injection into the constant volume chamber at 8 bar chamber pressure

(a) 20 bar injection pressure (b) 80 bar injection pressure

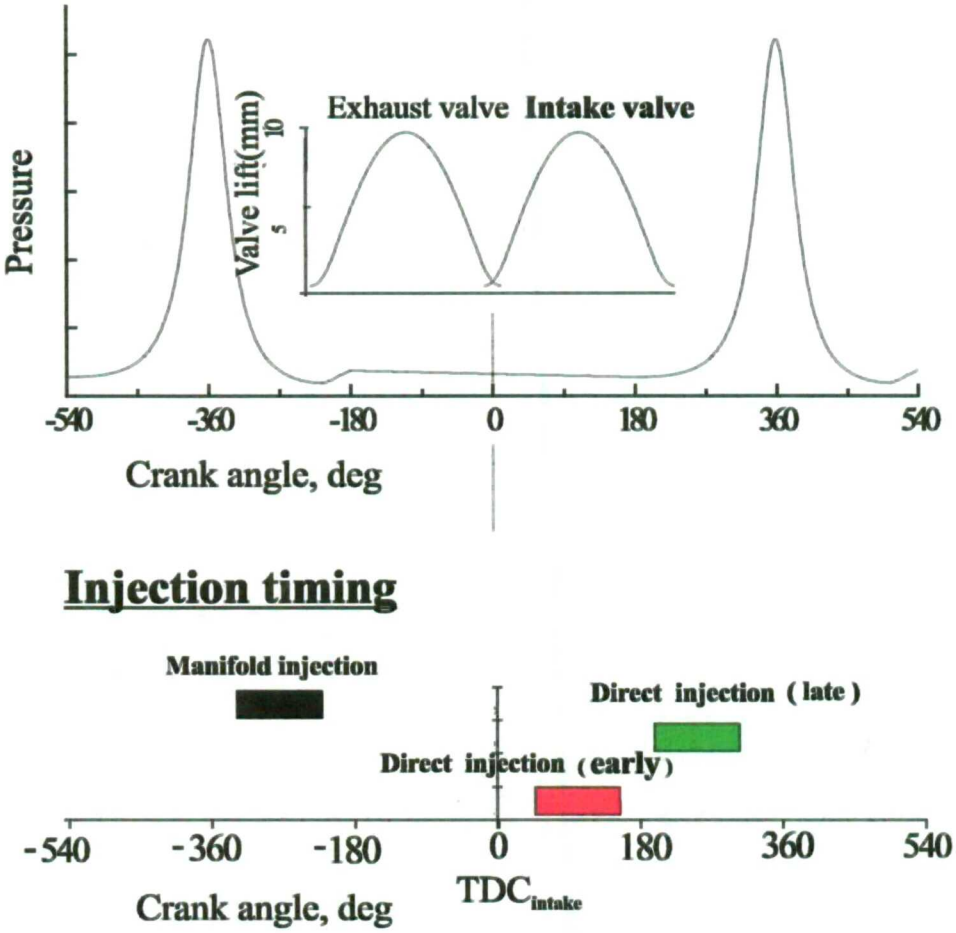

Figure 4.12: Diagram of manifold and direct injection timings

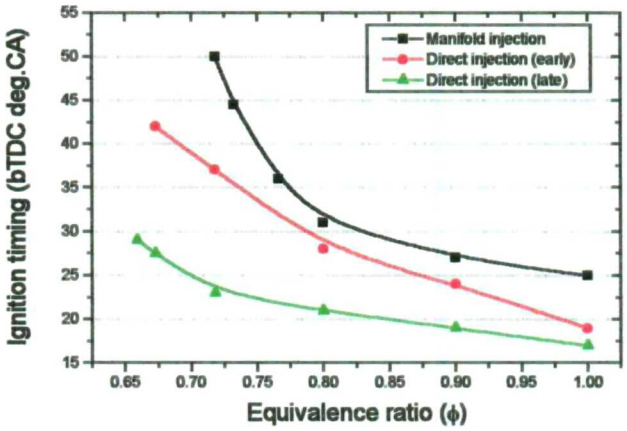

Figure 4.13: MBT spark timing characteristics for three different injection system at fixed throttle condition (n =1600 rpm, P_I = 0.65 bar)

(a)

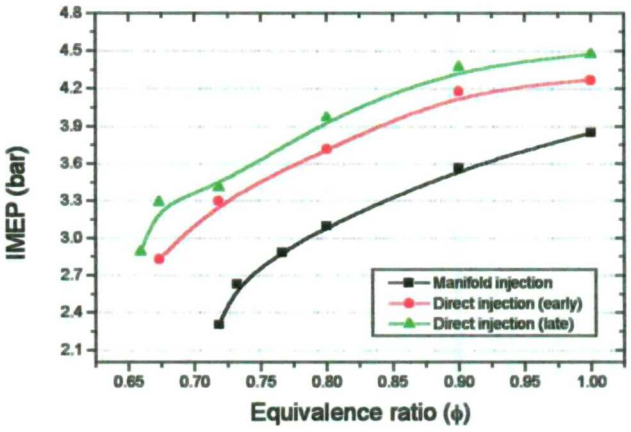

(b)

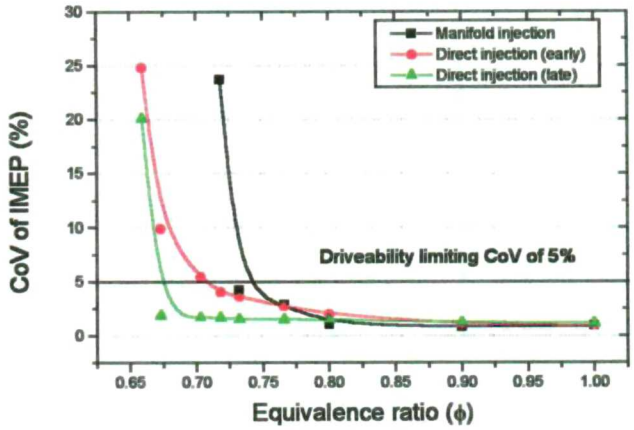

Figure 4.14: Comparison IMEP and CoV of IMEP of three different injection strategies at fixed throttle condition (n=1600 rpm, P_I = 0.65 bar)

(a) IMEP (b) CoV of IMEP

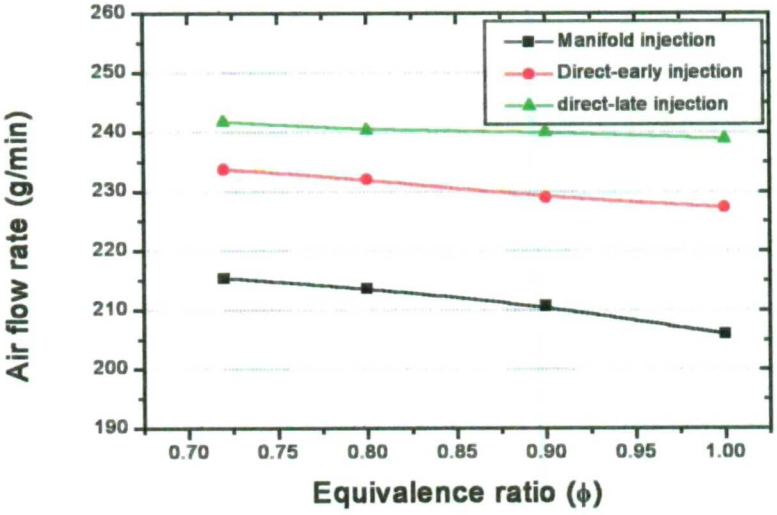

(a)

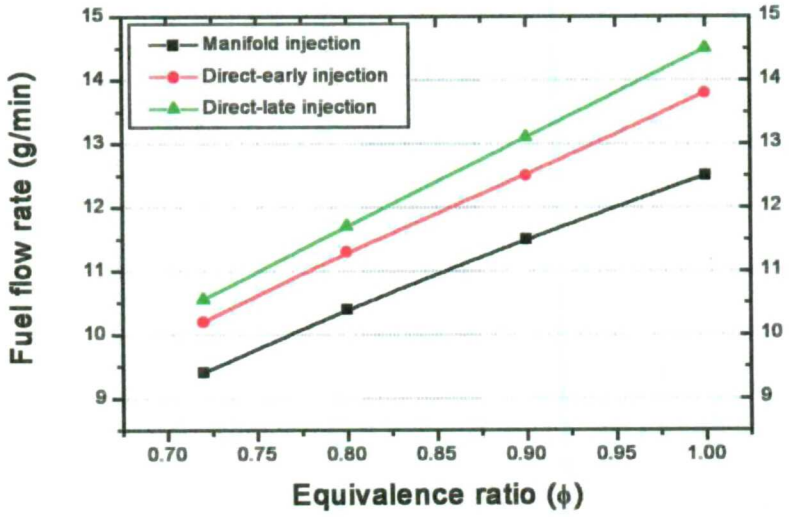

(b)

Figure 4.15: Comparison of air and fuel flow rates for three different injection timings at fixed throttle condition (n= 1600 rpm, P_I = 0.65 bar)

(a) Air flow rate (b) Fuel flow rate

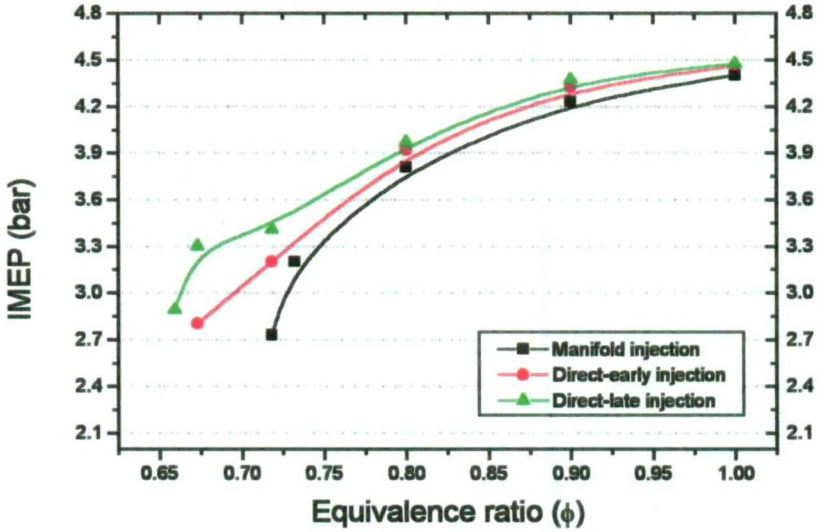

(a)

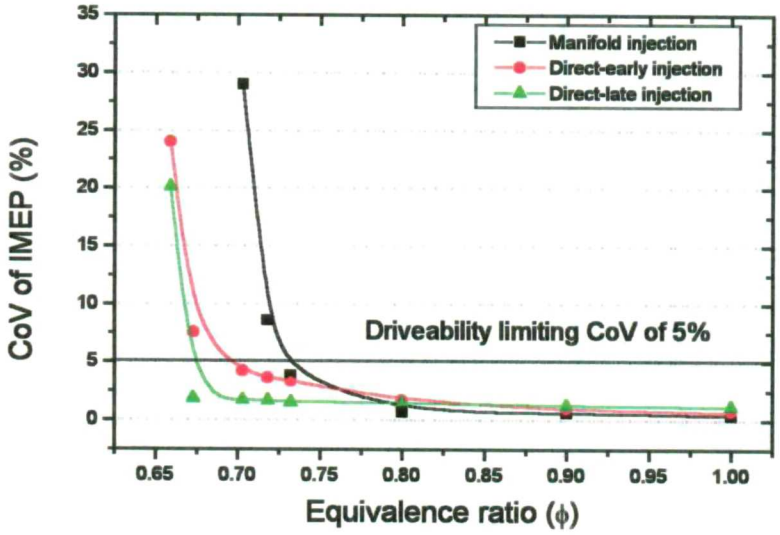

(b)

Figure 4.16: Comparison of IMEP and CoV of IMEP for three different injection strategies at fixed load condition based on air flow rate of direct-late injection case (n= 1600 rpm)

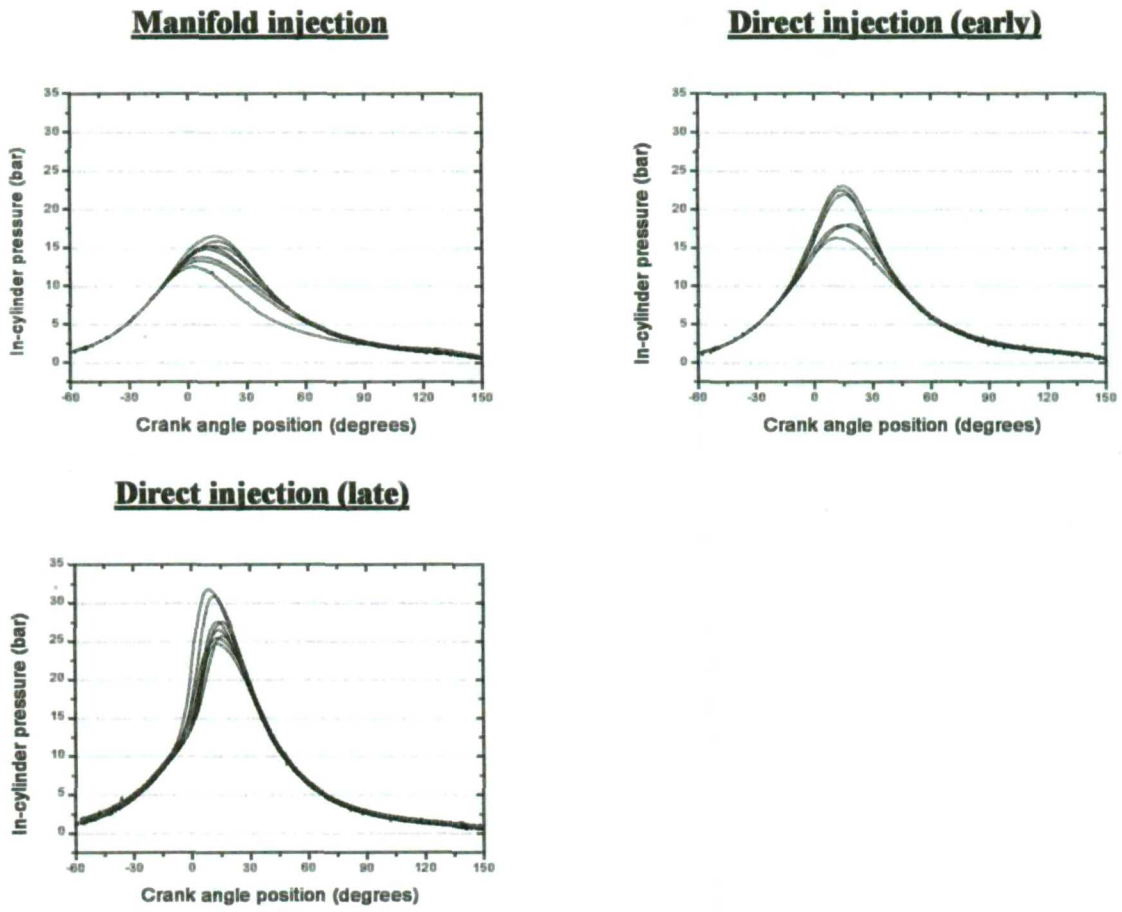

Figure 4.17: Cycle-to-cycle variations of in-cylinder pressure for three different injection strategies at fixed load condition and lean mixture (n = 1600 rpm, ϕ=0.72)

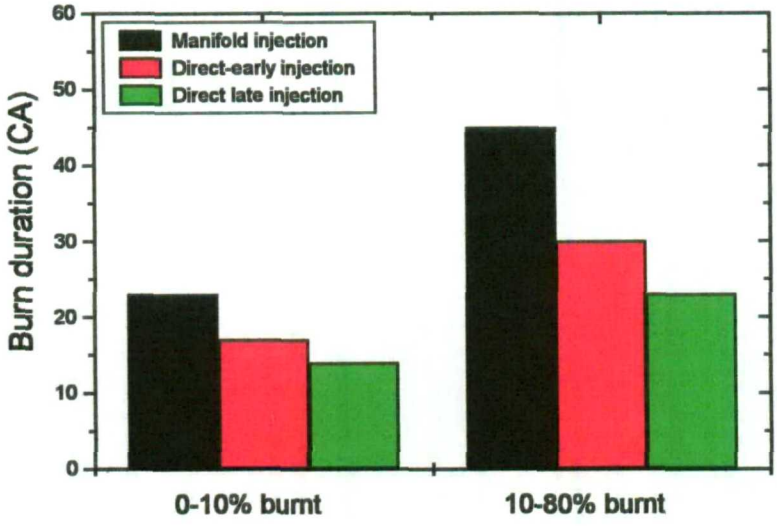

Figure 4.18: Comparison of mass fraction burnt for three different injection strategies at fixed load condition and lean mixture (n = 1600 rpm, ϕ = 0.72)

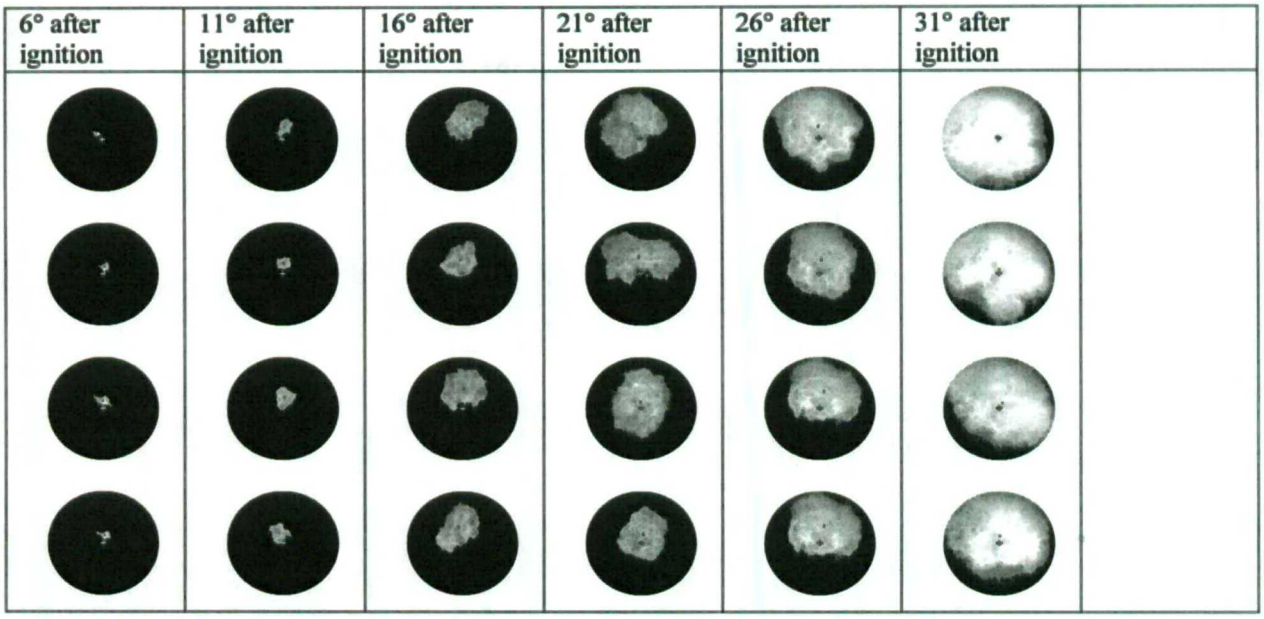

(a)

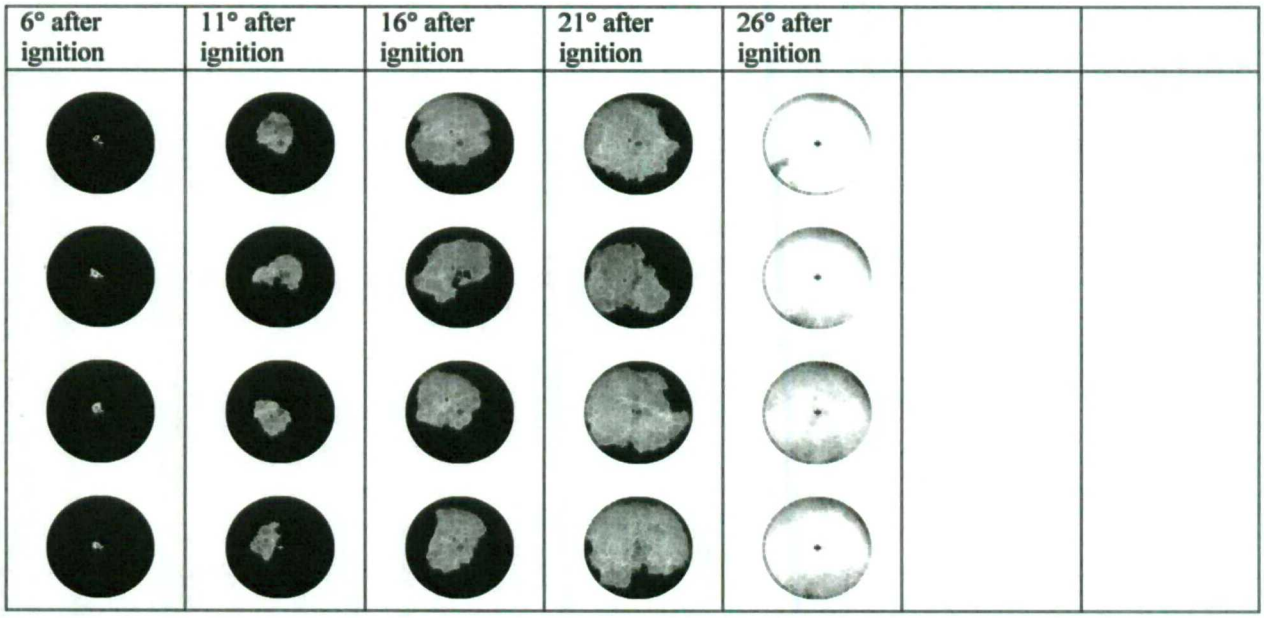

(b)

Figure 4.19: Flame images of three different injection strategies at fixed load condition (n = 1600 rpm, ϕ=1.0)

(a) Manifold injection (b) Direct injection (early)

6° after ignition	11° after ignition	16° after ignition	21° after ignition	26° after ignition		
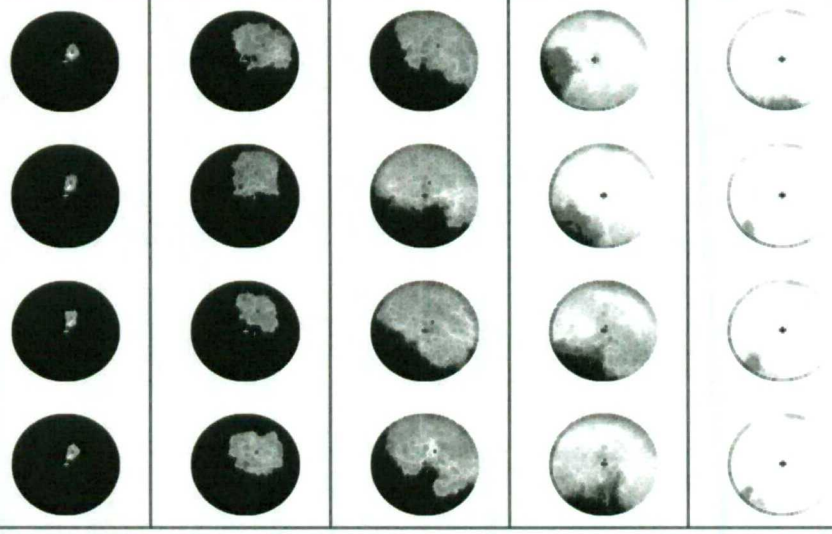						

(c)

Figure 4.19: (Continued)
Flame images of three different injection strategies at fixed load condition
(n = 1600 rpm, ϕ=1.0)

(c) Direct injection (late)

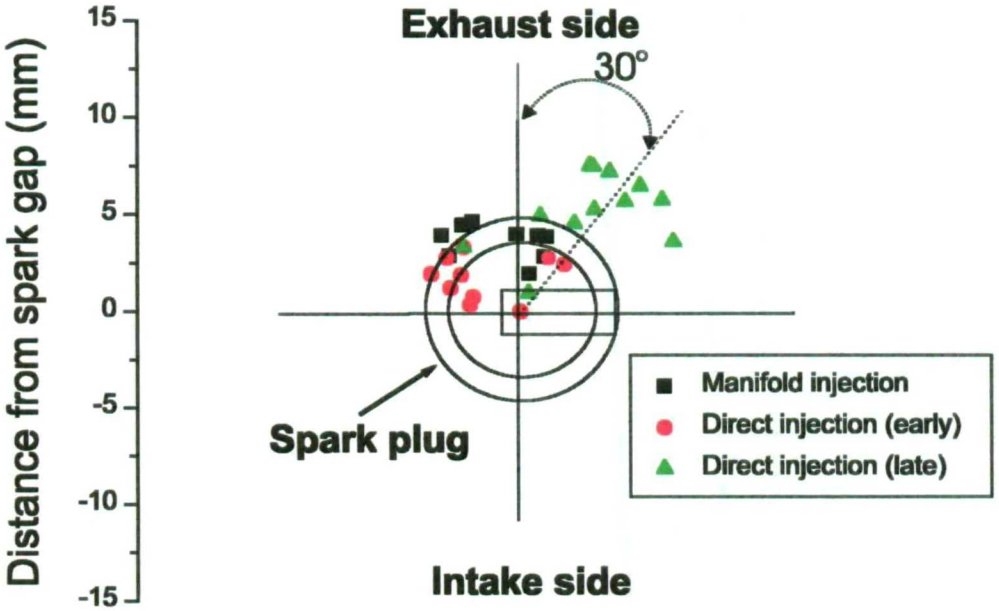

(a)

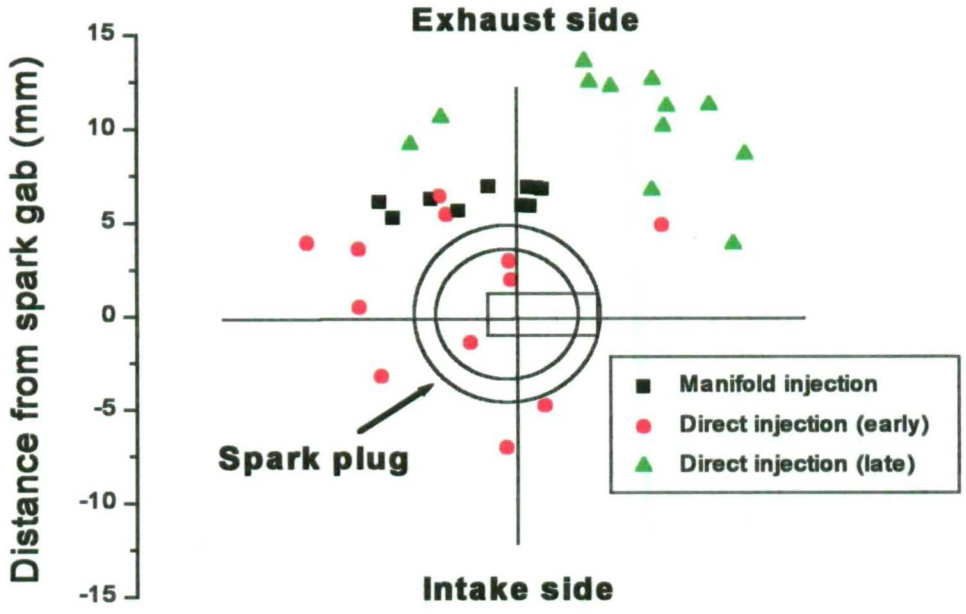

(b)

Figure 4.20: Comparison of notional flame centres with three different injection strategies at fixed load condition (n = 1600 rpm, ϕ = 1.0)

(a) 6° CA after ignition (b) 11° CA after ignition

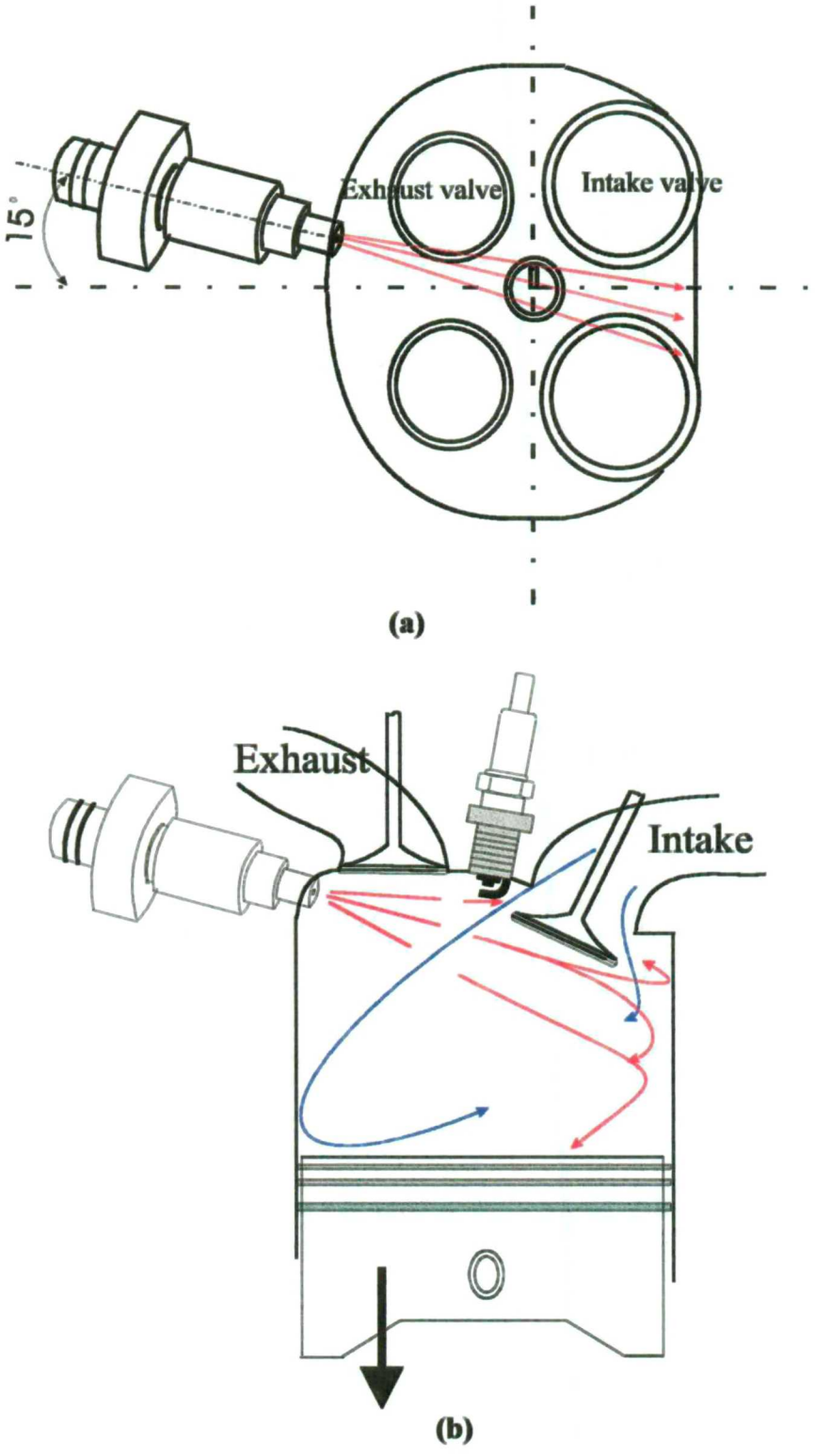

Figure 4.21: Schematic diagram of direct–early injection concept

(a) Bottom view (b) Side view

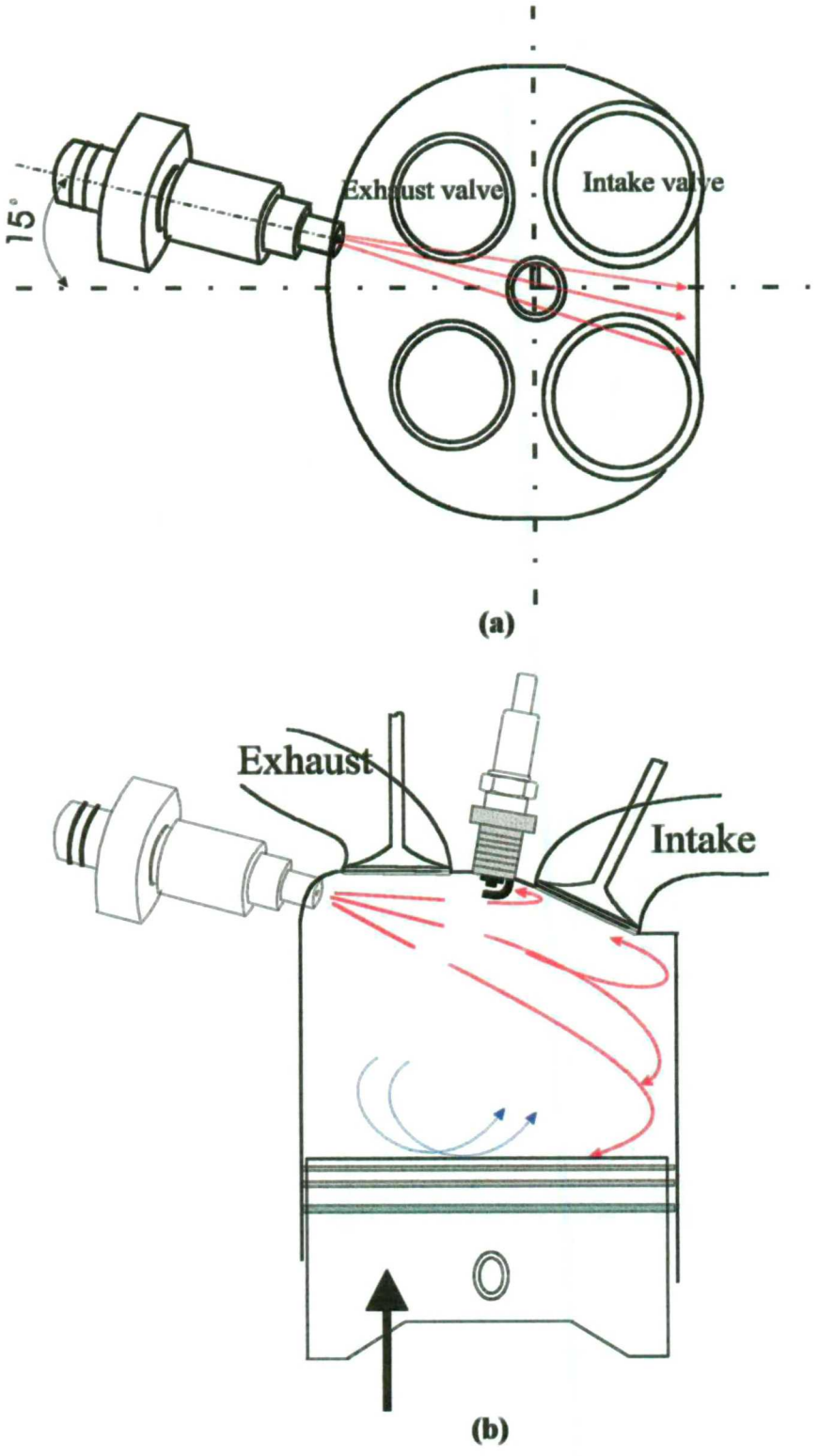

Figure 4.22: Schematic diagram of direct–late injection concept

(a) Top view (b) Side view

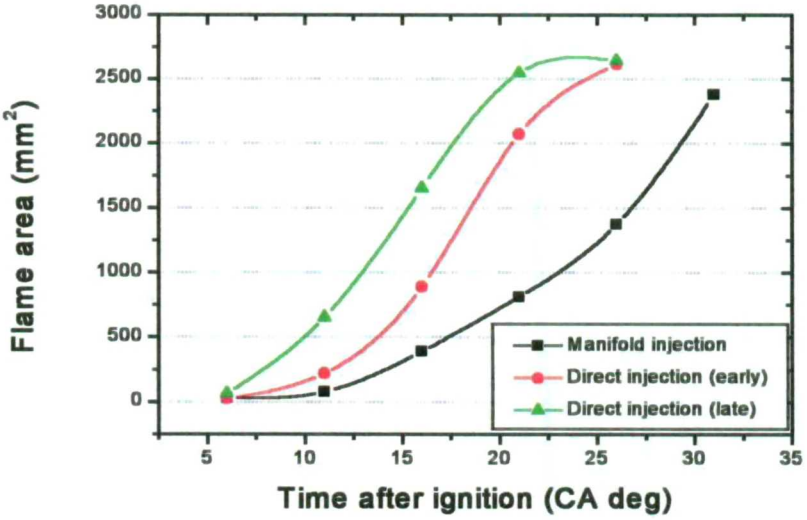

(a)

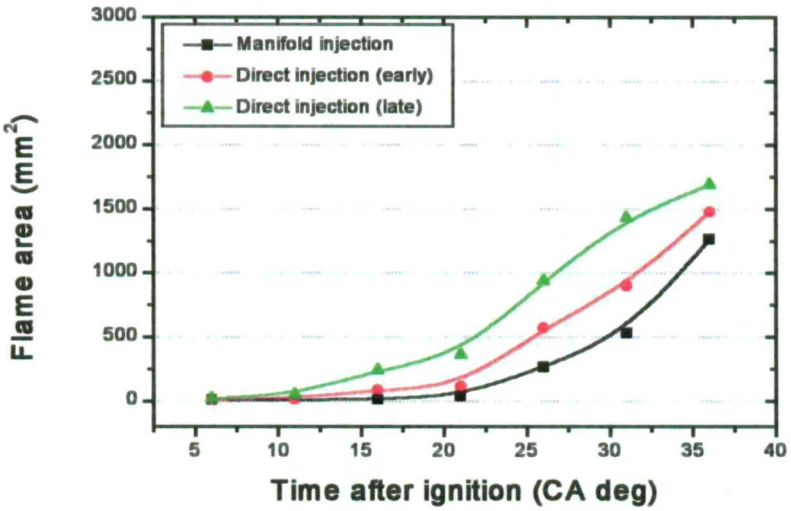

(b)

Figure 4.23: Flame area growth for three different injection strategies at fixed load condition (n = 1600 rpm)

(a) Stoichiometric condition (ϕ=1.0) (b) Lean condition (ϕ=0.72)

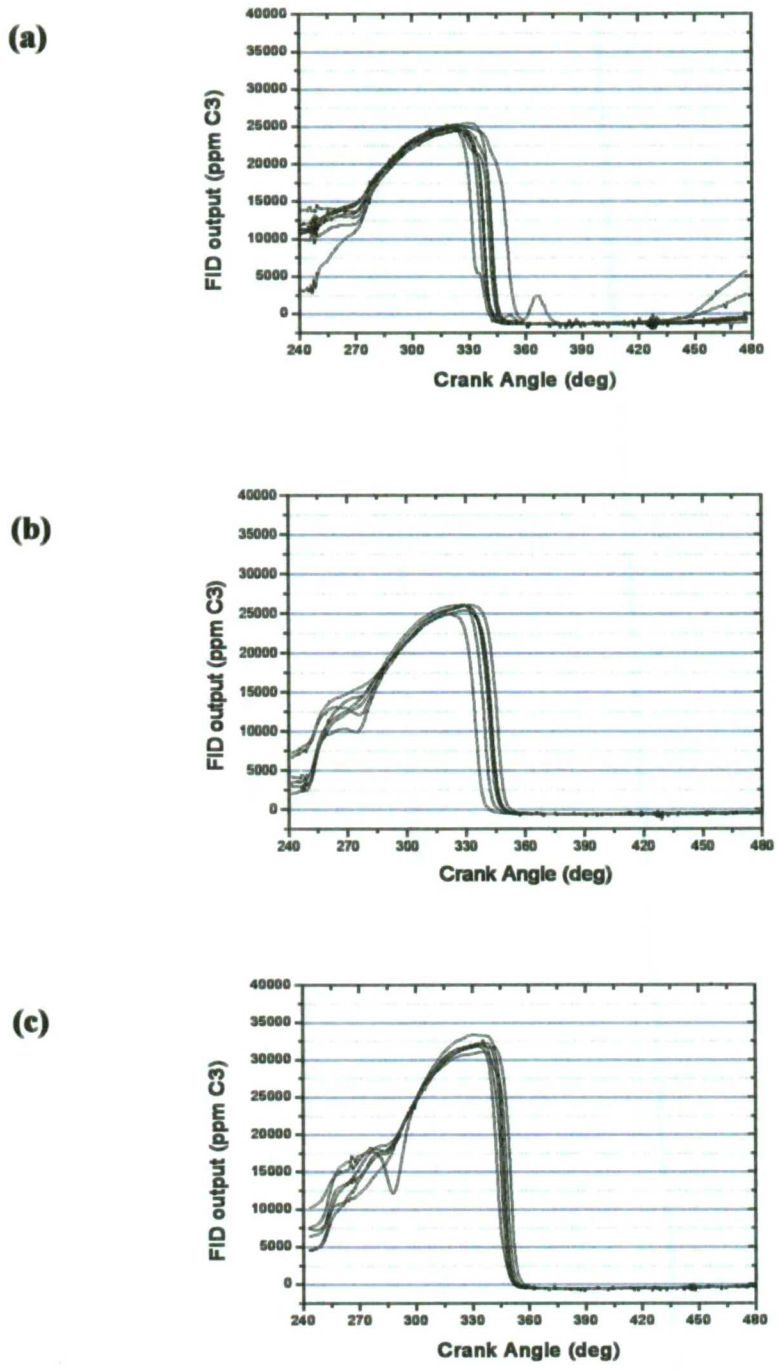

Figure 4.24: Cycle-to-cycle variation of fuel concentration at the spark plug for three different injection timings under fixed load condition (n=1600 rpm, ϕ=0.72)

(a) Manifold injection (b) Direct-early injection (c) Direct-late injection

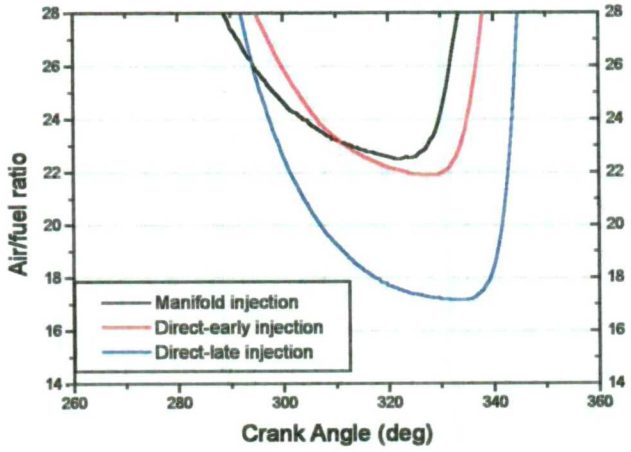

Figure 4.25: Averaged over successive 50 cycles air/fuel ratio at the spark plug under fixed load condition (n = 1600 rpm, A/F=22.8/ϕ=0.72)

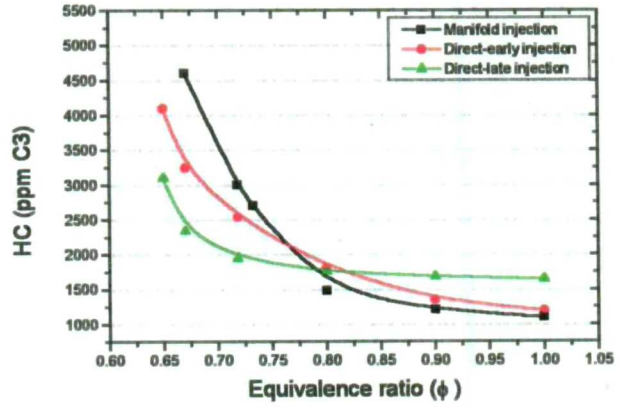

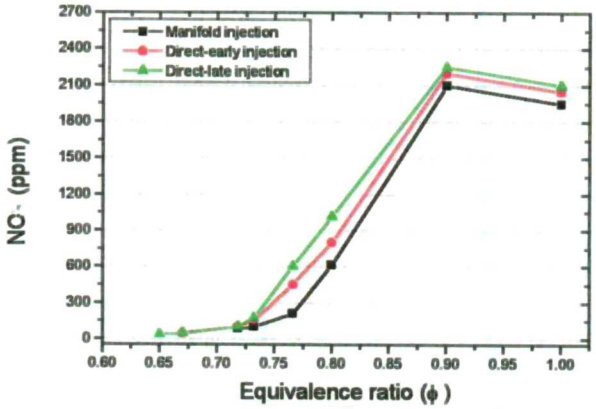

Figure 4.26: Engine-out emission characteristics for three different injection systems at fixed load condition (n=1600 rpm)

(a) HC emissions (b) NO emissions

CHAPTER 5

CONCLUSIONS AND RECOMMENDATION FOR FURTHER WORK

5.1 Summary of conclusions

Experiments in two four-valve spark-ignition engines fuelled by compressed natural gas (CNG) have been performed using in-cylinder flow measurements, combustion analysis, in-cylinder fuel concentration measurements and engine-out emissions analysis. The investigation was divided into two projects involving port and direct fuel injection.

During the first experiment, the effects of intake port geometry, injection timing and compression ratio were investigated in a single-cylinder engine with port fuel injected CNG. The results of this investigation have revealed that the enhanced tumble strength produced by the sleeved ports achieved strong convection of the flame away from the spark plug during the early flame development and faster flame propagation in the direction of the mean flow during the main combustion period. Measurements using LDV and PIV indicated that with sleeved ports higher tumble velocities are generated during induction which persist to the compression stroke until at least 330° aTDC.

Open-valve injection has a significant effect on in-cylinder flow and flame propagation. Different open-valve injection timings produce different flame propagation rates, different magnitude and direction of initial flame convection and therefore different engine performance. The results also revealed that open valve injection does lead to some charge stratification near the spark plug at the time of ignition relative to close valve injection, especially near the lean operating limit. Through mainly the effect of charge stratification, stable combustion can be realised even at extremely lean conditions.

The combination of sleeved intake ports with open-valve fuel injection strategy led to improved by 12% combustion stability (CoV of IMEP) under lean mixture conditions (ϕ=0.76) due to the combined effect of favourable flow conditions and modest charge stratification near the spark plug at the time of ignition.

In principle, optimised natural gas engines can be more efficient than gasoline engines. Methane, the principal constituent in natural gas, has a research octane number (RON) of 130, which allows the compression ratio to be increased significantly, producing an increase in engine performance and thermal efficiency. Increasing the compression ratio from 9.0 to 11.5 resulted in part load improved performance by 21%.

Unfortunately, even a dedicated port-injection CNG engine may not achieve any significant overall improvements, in view of the inherent power loss through reduced volumetric efficiency, unless it is turbocharged or supercharged. The best way to compensate for this problem is to inject the gas directly into the cylinder following the recent approach of the Japanese automotive manufacturers in introducing direct injection gasoline engines for passenger cars. For this reason, during the second experiment, an investigation of the possible advantages offered by direct injection of CNG into the cylinder of a multi-cylinder four-valve spark-ignition engine was performed. Direct injection of CNG offers advantages in terms of power output and extension of lean limit relative to the baseline case of manifold injection. Direct injection of CNG has a significant effect on flame propagation. Different injection timings (early and late injection) produced different flame propagation rates, with different initial flame convection; late injection provides more benefits than early injection. In-cylinder sampling at the spark plug has indicated that the local mixture concentration at the time of ignition was close to stoichiometric, although the overall mixture was very lean. This charge stratification generated by the direct injection of CNG towards the spark plug was probably responsible for the extension of the lean limit of the CNG engine relative to its operation with gasoline.

For the fixed throttle case, direct injection increased the IMEP by 18-35% compared to manifold injection. Lean limit was extended from an air/fuel ratio of 22 with manifold injection to 23 and 26 for early and late injection, respectively. The corresponding cycle-by-cycle variations of combustion in terms of CoV of IMEP were reduced from

23.7% to 4% and 1.6%, respectively, at ϕ=0.72. For the fixed load case, an increase in IMEP was also evident while the CoV of IMEP was reduced from 8.6% to 3.5% and 1.6 % for manifold injection, early and late injection, respectively. Visualisation of combustion by means of digital imaging has confirmed the faster combustion obtained with late direct injection. The initiation and propagation of the flame were affected by fuel injection due to the modification of the global flow in the cylinder by the high-speed gaseous jet. The enhanced mean flow and turbulence seemed to be responsible for the increased flame speed, while the distribution of the mixture played an equally important role in the stability of combustion observed with very lean overall mixtures.

Direct gas injection leads to much better mixture control while at the same time allowing homogeneous stoichiometric or lean mixtures to be formed by simply injecting the gas early during the induction stroke and by varying the fuel quantity to correspond to different air/fuel mixtures. Late direct injection does lead to charge stratification near the spark plug at the time of ignition relative to both manifold and early direct injection, allowing extension of the lean limit.

Although the use of direct injection of CNG into the engine cylinder generated high UHC and NO emissions under stoichiometric conditions, it allowed at the same time extension of the lean operating limit with associated lower UHC and NO emissions and better fuel consumption. This approach offers promise, through optimisation of jet characteristics and ignition timing, for overall reduction of UHC and NO levels in engines fuelled with CNG while maintaining comparable performance to that of gasoline engines of equal capacity.

Overall, direct injection natural gas engines offer greater promise relative to gasoline engines for increasing the power output through increased volumetric efficiency and reducing the fuel consumption and exhaust emissions through enhanced in-cylinder flow and charge stratification under lean mixture conditions.

5.2 Recommendations for further work

There are a number of follow-up experiments that are recommended to advance the understanding of the mixing and combustion characteristics in CNG engine.

To enhance charge motion and fuel stratification effectively, the injector should be repositioned from its present exhaust side location to the intake side, so that the gas jet is in the same direction with the intake air flow. This would be expected to have a stronger effect on the in-cylinder flow motion and charge stratification relative to its positioning on the exhaust side. To analyse the effect of the enhanced charge motion in the region of the spark plug, LDV and PIV measurements are necessary in the optical engine. To verify the charge stratification at the spark plug, direct sampling in the spark plug region with the fast FID should be used together with laser-induced fluorescence. To optimise the direct injection position, modification of the research engine will be necessary to provide optical access into the pentroof of the cylinder head which has been a limiting factor in the investigation presented in this thesis.

Natural gas can be stored as compressed gas at 200 bar in a high-pressure gas bottle in a natural gas vehicle. The injectors which were used in the previously discussed experiments were originally made for gasoline direct injection engines. To meet the required flow rate of the CNG engine, the injection pressure was increased to 80 bar. In this case, if the storage bottle pressure falls below 80 bar, the injector can not match the required flow rate in the engine and the storage bottle should be refilled with gas. Thus, this system is not desirable on practical grounds. Therefore, the development of new gas injectors with increased fuel passage area for achieving the required flow rates in CNG engines is essential to allow reduction of the injection pressure to under 20 bar. It should be noted that, due to the gaseous state of CNG, high injection pressures are not required. Using this low-pressure injector, tests in the multi-cylinder engine and optimisation of the air/fuel mixing for improved stratification, combustion and lower fuel consumption and exhaust emissions should be repeated in order to explore the advantages of CNG over the widest possible range of engine operation.

Finally, natural gas engines require dedicated catalysts with high loading of active catalytic components to maximise methane oxidation and able to operate within a very

narrow air/fuel ratio window. Methane represents about 80% of the total hydrocarbon emissions in CNG engines, although there may be a slight variation depending on the original composition of the fuel. Among all hydrocarbons, methane has been excluded from the regulations of the California Air Resources Board because it has the lowest photochemical reactivity, although it still contributes to the ozone layer when hydrocarbons react with the ultra-violet sun rays. Unfortunately, methane is known to be also a contributor to the greenhouse effect. For this reason, minimisation of methane emissions becomes vital to the development of clean CNG engines. It is thus necessary to study the optimisation of precious metal loading of emerging catalysts to reduce the methane and NMHC emissions under various engine-operating conditions.

References

"Gasoline Reformulation and Vehicle Technology Effects on Exhaust Emissions", 1995, Technical Bulletin No 17, Auto/Oil Air Quality Improvement Research Programme, August 1995

Anon. (1995), "Exhaust emissions of compressed natural gas (CNG) vehicles compared with gasoline vehicles", Technical Bulletin No. 15, Auto/Oil Air Quality Improvement Research Programme.

Arcoumanis, C., Hu, Z., Vafidis, C. and Whitelaw, J. H. (1990), "Tumbling Motion: A Mechanism for Turbulence Enhancement in Spark-Ignition Engines", SAE Technical Paper Series No. 900060.

Arcoumanis, C and Contogoulas, C (1993), "Knock Characteristics of Methanol/Petrol Blends", Paper C462/5/062, Autotech'93

Arcoumanis, C., Hu, Z., and Whitelaw, J. H. (1993), "Steady flow characterisation of tumble-generating four-valve cylinder heads", Proc. Inst. Mech. Eng. Vol. 207 Part D, pp. 203-210, 1993.

Arcoumanis, C., Bae, C.-S. and Hu, Z. (1994), "Flow and combustion in a four-valve spark-ignition engine", SAE Technical Paper Series No. 940475.

Arcoumanis, C., Hull, D. and Whitelaw J. H. (1994), "An Approach to Charge Stratification in Lean-Burn Spark-Ignition Engines", SAE Technical Paper Series No. 941878.

Arcoumanis, C. and Bae, C.-S (1995), "Flame Image Processing in a Four Valve Spark Ignition Engine", Paper Presented at the 3rd International Conference of The Institute of Mechanical Engineers, 9-10 January 1996, IMechE HQ, London.

Arcoumanis, C., Gold, M. R., Whitelaw, J. H., Xu, H.-M., Gaade, J. E. and Wallace, S (1998), "Droplet velocity/size and mixture distribution in a single-cylinder four-valve spark-ignition engine", SAE Technical Paper Series No. 981186.

Arcoumanis, C (1998), "Research Issues in Passenger Car Engines", 4th International Symposium COMODIA 98, pp 1-15, Japan

Arcoumanis, C., Godwin, S.N. and Kim, J. W (1998), "Effect of Tumble Strength on Combustion and Exhaust Emissions in a single-cylinder, Four-Valve, Spark-Ignition Engine", SAE Technical Paper Series No. 981044.

Arcoumanis, C. and Kim, J. W (1999), "Flow and Combustion Characteristics in a Four-Valve Spark-Ignition Engine Fuelled by CNG", 4th International Conference, ICE99, Internal Combustion Engines: Experiments and Modeling, pp. 267-275, Capri, September, 1999

Black, F (1991), " An Overview of the Technical Implication of Methanol and Ethanol as Highway Motor Vehicle Fuels", 1991 SAE 912413

Bae, C.S. (1993), "Flow and Flame Interaction in Spark-Ignited Premixed Mixtures", PhD. Thesis, Imperial College, London.

Baker, P., Benjamin, S. F., Girgis, N. S., Newman, A. W. and Seeley, W. A. (1995), "Characterisation of Barrel Swirl Motion Under Steady Flow Conditions", SAE Technical Paper Series No. 950729.

Berckmüller, M., Tait, N. P., and Greenhalgh, D. A. (1996), "The Time History of the Mixture Formation Process in a Lean Burn Stratified Charge Engine", SAE Technical Paper Series No. 961929.

Bradley, D., Lawes, M., Sheppard, C. G. W. and Woolley, R. (1996), "Methane as an engine fuel", Proc. Inst. Mech. Eng. S410/002 pp. 9-15.

Carabateas, N. E, Taylor, A. M. K. P., Whitelaw, J. H., Ishii, K., Yoshida, K. and Matsuki, M. (1996), "The Effect of Injector and Intake Port Design on In-Cylinder Fuel Droplet Distribution, Airflow and Lean Burn Performance for a Honda VTEC-E Engine", SAE Technical Paper Series No. 961923.

Church, W. and Farrell, P.V. (1998), "Effect of Intake Port Geometry on Large Scale In-cylinder Flows", SAE Technical Paper Series No. 980484.

Cheng, K., Hamrin, D., Heywood, J.B., Hochgreb, S., Min, K. and Norris, M. (1993), "An Overview of Hydrocarbon Emissions mechanisms in Spark-Ignition Engines", SAE Technical Paper Series No. 932708

Cheng, K., Summers, T. and Collings, N. (1998), "The Fast-Response Flame Ionization Detector", Prog.Energy Combust. Sci. Vol. 24, pp. 89-124.

Chun, K. M. and Heywood, J. B. (1987), "Estimating Heat-Release and Mass-of-Mixture Burned from Spark-Ignition Engine Pressure data", Combust. Sci. and Tech., Vol. 54, pp133-143.

Church, W. and Farrell, P. V. (1998), "Effects of Intake Port Geometry on Large Scale In-Cylinder Flows", SAE Technical Paper Series No. 980484.

Endres, H., Neußer, H.-J. and Wurms, R. (1992), "Influence of Swirl and Tumble on Economy and Emissions of Multi-Valve SI Engines", SAE Technical Paper Series No. 920516.

Evans, R. I. and Blaszczyk, J (1997), "A comparative study of the performance and exhaust emissions of a spark ignition engine fuelled by natural gas and gasoline", Proc. Inst. Mech. Eng. Vol. 211 Part D, pp. 39-47.

Fleming, R. D. and O'Neal, G. B. (1985), "Potential for Improving the Efficiency of a Spark Ignition Engine for Natural Gas Fuel", SAE Technical Paper Series No. 852073.

Floch, A., Van Frank, J. and Ahmed, A. (1995), "Comparison of the Effects of Intake-Generated Swirl and Tumble on Turbulence Characteristics in a 4-Valve Engine", SAE Technical Paper Series No. 952457.

Gambino, M., Corbo, P., Iannacone, S. and Unich,A. (1994), "Low emission stoichiometric CNG engine with EGR", Int. Comb. Eng.-Vol. 24, Natural Gas and Alternative Fuels for Engines, ASME.

Geiss, R. O., Burkmyre, W. M., and Lanigan, J. W. (1992), "Technical Highlights of the Dodge Compressed Natural Gas Ram Van/Wagon", SAE Technical Paper Series No. 921551.

Goto, Y and Narusawa, K (1996), "Combustion stabilisation of a spark ignition natural gas engine", JSAE 9631669

Goto, Y , Sato, Y. and Narusawa, K (1998), "Combustion and emissions Characteristics in Direct Injection natural gas Engine Using Multiple Stage Injection", Forth International Symposium COMODIA 98, pp 543-548, Japan

Drain, L.E. (1980), "The laser Doppler technique", John Wiley and Sons.

Green, H. G., Whitelaw, J. H. and Wong, K. Y. (1987), "Air Fuel Mixture Characteristics of Reciprocating Engines", Comb. Sci. Tech., Vol. 59, pp225-246.

Gupta, M., and Bell, S. R. (1994), "An investigation of lean combustion in a natural gas fueled spark ignited engine", Int. Comb. Eng.-Vol. 21, Natural Gas and Alternative Fuels for Engines, ASME.

Durst, F.; Melling A. and Whitelaw J.H. (1976), "Principles and Practice of laser Doppler Anemometry," Academic Press Inc.(London) Ltd.

Hadded, O. and Denbratt, I. (1991), "Turbulence Characteristics of Tumbling Air Motion in Four-Valve S.I. Engines and their Correlation With Combustion Parameters", SAE Technical Paper Series No. 910478.

Hall, M. J. (1989), "The Influence of Fluid Motion on Flame Kernal Development and Cyclic Variation in a Spark Ignition Engine", SAE Technical paper Series No. 890991.

Harada, J., Tomita, T., Mizuno, H., Mashiki, Z. and Yasushi, I. (1997), "Development of Direct Injection Gasoline Engine", SAE Technical Paper Series No. 970540.

Heywood, J. B. (1988), "Internal Combustion Engine Fundamentals", McGraw-Hill Automotive Technology Series.

Hilliard, J.C (1984), "Fuel Economy in Road vehicles powered by Spark Ignition Engines", Plenum Press

Horie, K., Nishizawa, K., Akazaki, S. and Miura, K. (1992), "The Development of a High Fuel Economy and High Performance Four-Valve Lean Burn Engine", SAE Technical Paper Series No. 920455.

Hu, Z., Whitelaw, J. H. and Vafidis, C. (1992), "Flame Propagation Studies in a Four-Valve Pentroof-Chamber Spark Ignition Engine", SAE Technical Paper Series No.922321..

Inoue, T., Matsushita, S., Nakanishi, K. and Okano, H. (1993), "Toyota Lean Combustion System – The Third Generation System", SAE Technical Paper Series No. 930873.

Iwamoto, Y., Noma, K., Nakayama, O., Yamauchi, T. and Ando, H. (1997), "Development of Gasoline Direct Injection Engine", SAE Technical Paper Series No. 970541.

Jääskeläinen, H. E. and Wallace, J. S. (1993), "Effect of Increasing Compression Ratio in Light-Duty Natural Gas Fueled Engine on Efficiency and Emissions", SAE Technical Paper Series No. 932746.

Jackson, NS (1997), " Development Trends in Gasoline Engines", Lecture notes, Course on Direct Injection Engines (Lecture 6), Imperial College, London

Janach, W., Zuber, P and Heini, K (1998),"High Speed Pulsed Injection of natural Gas", Forth International Symposium COMODIA 98, pp 531-535, Japan

Jeon, C.-H., Chang, Y.-J., Cho, K.-B. and Kang, K.-Y. (1998), "Effects of Intake Ports on In-Cylinder Flow and Lean Combustion in a 4-Valve Engine", SAE Technical Paper Series No. 981048.

Johanssen, B. (1993), "Influence of the Velocity Near the Spark Plug on Early Flame Development", SAE Technical Paper Series No. 930481.

Kano, M., Basaki, M., Matsushita, S. and Gohno, T. (1998), "Analysis of Mixture Formation of Direct Injection Gasoline Engine", SAE Technical Paper Series No. 980157.

Kaplan, J.A. and Heywood, J.B (1991), " Modeling the Spark Ignition Engine warm-up process to Predict Component Temperatures and Hydrocarbon Emissions", SAE Technical Paper Series No. 910302.

Keck, J. C, Heywood, J. B and Noske, G. (1987), "Early Flame Development and Burning Rates in Spark Ignition Engines and Their Cyclic Variability", SAE Technical Paper Series No. 870164.

Khalighi, B. (1990), "Intake generated in-cylinder tumbling flow - a flow visualisation study", SAE Technical Paper Series No. 900051.

Kim, J.-W., Park, S.-H., Jeong, C., Yoo, S.-J. and Park, P. (1994), "Development of the Daewoo Dedicated Light Duty NGV II", EV25, Fourth Biennial International Conference and Exhibition on Natural Gas Vehicles, Toronto, Canada

Kiyota, Y., Akishino, K. and Ando, H. (1992), "Concept of Lean Combustion by Barrel-Stratification", SAE Technical Paper Series No. 920678.

Kudou, H., Yamamoto, H and Lida, Y (1992), " A Study About In-Cylinder Flow and Combustion in a 4-valve S.I. Engine", SAE 920574

Kuwahara, K., Watanabe, T., Takemura, J., Omori, S., Kume, T. and Ando, H. (1994), "Optimisation of In-Cylinder Flow and Mixing for a Centre-Spark Four-Valve Engine Employing the Concept of Barrel Stratification", SAE Technical Paper Series No. 940986.

Lapetz, J., Beitler, J., Fulton, B., LeRoux, M., Locke, J., Peters, E., Roman, L., Walsh, R. and Wolff, W (1995), "Ford's 1996 Crown Victoria Dedicated Natural Gas Vehicle", SAE Technical Paper Series No. 952743.

Le Coz, J. F. (1992), "Cycle-to-Cycle Correlations Between Flow Field and Combustion Initiation in an S.I. Engine", SAE Technical Paper Series No. 920517.

Matsura, H., Otaka, A., Kato, A., Yamashiro, M. and Fujii, I. (1996), "Honda Dedicated CNG Passenger Vehicle", Honda R&D Co. Ltd.

Matsushita, S., Inoue, T., Nakanishi, K., Kato, K. and Kobayashi, N. (1985), " Development of Toyota Lean Combustion system", SAE Technical Paper Series No 850044

Min, K., Cheng, K. and Heywood, J.B. (1994), "The Effect of Crevices on the Engine-Out Hydrocarbon Emissions in SI Engines", SAE Technical Paper Series No. 940306

Moriyoshi, Y. and Muroki, T. (1995), "'Proposition of a Stratified Charge System by Using In-Cylinder Gas Motion'", SAE Technical Paper Series No. 952455.

Moriyoshi, Y., Nomura, H. and Saisyu, Y. (1998), "Evaluation of a Concept for DI Gasoline Combustion Using Enhanced Gas Motion", SAE Technical Paper Series No. 980152.

Poulsen, J. H. and Wallace, J. S. (1994), "Operating Parameter Effects on the Speciated Hydrocarbon Emissions from a Natural Gas Fueled Engine", SAE Technical Paper Series No. 942007.

Queenan, B. and Nightingale, C. (1997), "Charge Stratification in a 4-valve SI Engine Through Injection into One intake Port with Induced Axial Swirl Within the Cylinder", SAE Technical Paper Series No. 972875.

Reavell, K. St., Collings, N., Peckham, M., and Hands, T. (1997), " Simultaneous fast response NO and HC Measurements from a spark Ignition Engine" SAE Technical Paper Series No. 971610.

Reeves, M., Garner, C. P., Dent, J. C. and Halliwell, N. A. (1996), "Particle image velocimetry measurements of in-cylinder flow in a multi-valve internal combustion engine", Proc. Inst. Mech. Eng. Vol. 210 Part D, pp. 63-70.

Richardson, D and Cains, T. (1999), "Fast Response HC measurement for DI Gasoline Engine Development" Paper C575/15, Autotech '99

Rönnbäck, M., Le, W. X. and Linna, J.-R. (1991), "Study of Induction Tumble by Particle Tracking Velocimetry in a 4-Valve Engine", SAE Technical Paper Series No. 912376.

Rouland, E. and Trinite, M (1997), " Particle Image velocimetry Measurements in a high Tumble Engine for In-cylinder Flow Structure Analysis" SAE 972831

Russ, S., Peet, G. and Stockhausen, W. (1997), "Measurements of the Effect of In-Cylinder Motion on Flame Development and Cycle-to-Cycle Variations Using an Ionization Probe Head Gasket", SAE Technical Paper Series No. 970507.

Sadler, M., Stokes, J., Edwards, SP., Zhao, H. and Ladommatos, N. (1997), " Optimisation of the combustion System for a Direct Injection Gasoline Engine, using a High Speed In-cylinder Sampling Valve", EURO IV CHALLENGE – Future Technologies and Systems, IMechE HQ, London

Stone, C. R., Mendis, K. J. S., and Daragheh, M. (1996), "Measurements and modelling of a lean-burn gas engine", Proc. Inst. Mech. Eng. Vol. 210 Part A, pp. 449-462.

Subramanian, S., Kudia, R. J. and Chattha, M. S. (1993), "Treatment of Natural Gas Vehicle Exhaust", SAE Technical Paper Series No. 930223.

Takagaki, S. S. and Raine, R. R. (1997), "The Effects of Compression Ratio on Nitric Oxide and Hydrocarbon Emissions from a Spark-Ignition Natural Gas Fuelled Engine", SAE Technical Paper Series No. 970506.

Takagi, Y., Itoh, T., Muranaka, S., Iiyama, A., Iwakiri, Y., Urushihara, T. and Naitoh, K. (1998), "Simultaneous Attainment of Low Fuel Consumption, High Output Power and Low Exhaust Emissions in Direct Injection SI Engines", SAE Technical Paper Series No. 980149.

Thiagarajan, S., Midkiff, K. C., Bell, S. R. and Greeen, M. N. (1994), "Investigation of Fuel Composition Effects on a Natural Gas Fueled Spark-Ignited Engine", Int. Comb. Eng., Vol. 24, Natural Gas and Alternative Fuels for Engines, ASME.

Vafidis, C., Vorropoulos, G. and Whitelaw, J. H. (1993), "Effects of Intake Port and Combustion Chamber Geometry on In-Cylinder Turbulence in a Motored Reciprocating Engine", Thermofluids Section, Internal Report, Dept. of Mech. Eng., Imperial College, London.

Varde, K. S, Cherng, J. C., Bailey, C. J. and Majewski, W. A. (1992), "Emissions and Their Control in Natural Gas Fueled Engines", SAE Technical Paper Series No. 922250.

White, J. J., Carroll, J. N., Liss, W. E., Brady, M. J., Burkmyre, W. M. and Church, M (1993), "Natural Gas Converter Performance and Durability", SAE Technical Paper Series No. 930222.

Wirth, M., Piock, W. F., Fraidl, G. K., Schoeggl, P. and Winklhofer, E. (1998), "Gasoline DI engines: the Complete System Approach by Interaction of Advanced Development Tools", SAE Technical Paper Series No. 980492.

Witze, P. O. and Vilchis, F. R. (1981), "Stroboscopic Laser Study of the Effect of Swirl on Homogeneous Combustion in a Spark-Ignition Engine", SAE Technical Paper Series No. 810226.

Yamamoto, Y., Sato, K., Matsumoto, S. and Tsuzuki, S. (1994), "Study of Combustion Characteristics of Compressed Natural Gas as Automotive Fuel", SAE Technical Paper Series No. 940761.

Young, M. B. (1981), "Cyclic dispersion in the homogeneous-charge spark-ignition engine - a literature survey", SAE Technical Paper Series No. 810020.

Zhao, F., Yoo, J.H., Liu, Y. and Lai, M. (1996), " Spray Dynamics of High Pressure Fuel Injectors for DI Gasoline Engines", SAE Technical Paper Series No. 961925